Mechanistic and structural studies of the MHC I peptide loading complex

Dissertation

zur Erlangung des Doktorgrades

der Naturwissenschaften

vorgelegt beim Fachbereich 14

Biochemie, Chemie und Pharmazie

der Johann Wolfgang Goethe-Universität

in Frankfurt am Main

von

Alexander Domnick

aus Lübeck

Frankfurt am Main, 2022

(D30)

Vom Fachbereich 14 Biochemie, Chemie und Pharmazie der Johann Wolfgang Goethe-Universität als Dissertation angenommen.

Dekan: Prof. Dr. Clemens Glaubitz

1. Gutachter: Prof. Dr. Robert Tampé
2. Gutachter: Prof. Dr. Inga Hänelt

Teile der vorliegenden Arbeit wurden veröffentlicht in:

Mavridis G, Arya R, **Domnick A**, Zoidakis J, Makridakis M, Vlahou A, Mpakali A, Lelis A, Georgiadis D, Tampé R, Papakyriakou A, Stern LJ, Stratikos E (2020) *A systematic re-examination of processing of MHCI-bound antigenic peptide precursors by ER aminopeptidase 1,* Journal of Biological Chemistry **295**, 7193 - 7210

Domnick A*, Winter C*, Sušac L, Hennecke L, Hensen M, Zitzmann N, Trowitzsch S, Thomas C, Tampé R (2022) *Molecular basis of MHC I quality control in the peptide loading complex,* Nature Communications **13**, 4701

Winter C*, **Domnick A***, Cernova D, Tampé R (2022) *Semisynthetic viral inhibitor for light control of the MHC I peptide loading complex*, Angewandte Chemie Int. Ed., **61**, e202211826

* authors contributed equally

Table of contents

I. Declaration 7
II. Summary 8
III. Zusammenfassung 11
1. Introduction 16
1.1. MHC I antigen presentation 16
1.2. The peptide loading complex (PLC) 19
1.2.1. Transporter associated with antigen processing (TAP) 20
1.2.2. Tapasin and ERp57 21
1.2.3. MHC I / β_2m 22
1.2.4. Calreticulin 24
1.2.5. ERAP1/2 25
1.2.6. GluII 26
1.2.7. Viral immune evasion and PLC purification strategy 26
1.3. Cryogenic electron microscopy 28
1.4. Reconstitution of membrane proteins 29
2. Aims 33
3. Material and methods 34
3.1. Chemicals 34
3.1.1. Antibodies 34
3.1.2. Chemicals and reagents 34
3.1.3. Devices and accessories 35
3.1.4. Peptides 36
3.2. Cell culture 37
3.2.1. Raji cell culture 37
3.3. Protein biochemistry 37
3.3.1. Expression and purification of ICP47^{SBP}, ICP47^{His6}, and ICP47^{AF647} 37
3.3.2. Production of pc-ICP47^{SBP} 38
3.3.3. Expression and purification of MSP2N2 40
3.3.4. Expression and purification of Saposin A 40
3.3.5. Expression and purification of ERAP1 and ERAP2 40
3.3.6. Expression and purification of GluII 41
3.3.7. Processing of mammalian spleen for PLC purification 41
3.3.8. Purification of PLC 42
3.3.9. PLC reconstitution in MSP2N2 (on beads) 42

3.3.10. PLC reconstitution in Peptidisc (on beads) 42
3.3.11. PLC reconstitution in Saposin A (on beads) 43
3.3.12. PLC reconstitution in liposomes 43
3.3.13. PLC solubilization with SMA/DIBMA 43
3.3.14. ERAP1/2 peptide loading complex pulldown assay 43
3.3.15. Size exclusion chromatography 44
3.3.16. Size exclusion analysis of ERAP1/2 – PLC interaction 44
3.3.17. Peptide synthesis – DG057 44
3.3.18. Peptide binding assay 45
3.3.19. Thermostability assay 45
3.3.20. SDS-PAGE 45
3.3.21. SDS-PAGE silver staining 46
3.3.22. SDS-PAGE Coomassie staining 46
3.3.23. Immunoblotting 46
3.3.24. ATP binding assay 47
3.3.25. ATP hydrolysis assay 47
3.3.26. LC-MS analysis of intact proteins under denaturating conditions 47
3.3.27. LC-MS analysis for protein identification 48
3.3.28. PNGase treatment 49
3.3.29. GluII treatment 49
3.3.30. Liposome size determination 49
3.3.31. Flow cytometry of liposomes 50
3.3.32. Protease protection assay 50
3.3.33. Flow cytometry of microsomes 50
3.3.34. Peptide transport assay – liposomes 50
3.3.35. Peptide transport assay – microsomes 51
3.3.36. pc-ICP47 cleavage 51
3.3.37. $ICP47^{AF647}$ binding after $pc\text{-}ICP47^{SBP}$ cleavage 51

3.4. Electron microscopy 52

3.4.1. Negative stain electron microscopy 52
3.4.2. Cryo-EM: Sample preparation and image collection 52
3.4.3. Cryo-EM data analysis of PLC::MSP2N2 52
3.4.4. Model building 53

4. Results and Discussion 54

4.1. Isolation and characterization of PLC from primary mammalian tissue 54
4.2. Reconstitution of human PLC in membrane mimetics 59

4.2.1. Purification of human PLC after SMA/DIBMA solubilization not possible 59
4.2.2. Reconstitution in MSP2N2 nanodiscs 62

4.2.3. Reconstitution in Saposin A and Peptidiscs 64
4.3. Mass spectrometric analysis of human PLC 65
4.3.1. MHC I glycosylation 68
4.3.2. Tapasin glycosylation 69
4.3.3. Identification of an alternative tapasin isoform in human PLC 70
4.4. Structural analysis of MHC I editing in the PLC 72
4.4.1. Negative-stain electron microscopy 72
4.4.2. Cryo-EM analysis of PLC::MSP2N2 73
4.5. Allosteric coupling of peptide loading and MHC I glycan processing 80
4.6. No kinetically stable interaction between human PLC and ERAP1/2 85
4.7. Reconstitution of human PLC in liposomes 88
4.8. Photocleavable ICP47^{SBP} as tool for functional and structural studies 92
5. Conclusion 97
6. References 99
IV. Appendix 113
6.1. Figures 113
6.2. Tables 121
V. Abbreviations 127
VI. List of figures 131
VII. List of tables 133

I. Declaration

Except where stated otherwise by reference or acknowledgement, the work presented was generated by myself under the supervision of my advisor during my doctoral studies. All contributions from colleagues are explicitly referenced in the thesis.

Whenever a figure, table, or text is identical to a previous publication, it is stated explicitly in the thesis that copyright permission and/or co-author agreement have been obtained.

Following parts of the thesis have been previously published as open access publications under Creative Commons Attribution (CC BY 4.0) allowing the use for this thesis:

Chapter 4.6 in Journal of Biological Chemistry **295**, 7193 - 7210 as "*A systematic re-examination of processing of MHCI-bound antigenic peptide precursors by ER aminopeptidase 1."* by Mavridis G, Arya R, **Domnick A**, Zoidakis J, Makridakis M, Vlahou A, Mpakali A, Lelis A, Georgiadis D, Tampé R, Papakyriakou A, Stern LJ, Stratikos E (2020) Figure 4.6-1, Figure 4.6-2, Figure 4.6-3, and material and methods 3.3.5, 3.3.14, 3.3.16, 3.3.17.

Chapters 4.2.2, 4.3, 4.4, and 4.5 in Nature Communications **13**, 4701 as "*Molecular basis of MHC I quality control in the peptide loading complex"* by **Domnick A***, Winter C*, Sušac L, Hennecke L, Hensen M, Zitzmann N, Trowitzsch S, Thomas C, Tampé R (2022), including Figure 4.2-4, Figure 4.3-1**,** Figure 4.3-2, Figure 4.3-3, Figure 4.3-4, Figure 4.4-2, Figure 4.4-3, Figure 4.4-4, Figure 4.4-5, Figure 4.4-6, Figure 4.4-7, Figure 4.5-1, Figure 4.5-2, Figure 4.5-3, Figure 4.5-4, Figure 6.1-4, Figure 6.1-5, Figure 6.1-6, and Figure 6.1-7 and Table 6-2, Table 6-4, and Table 6-5, and material and methods 3.2.1, 3.3.6, 3.3.8, 3.3.9, 3.3.18, 3.3.26, 3.3.28, 3.3.29, 3.4.2, 3.4.3, and 3.4.4.

Chapters 4.8 in Angewandte Chemie Int. Ed., **61**, e202211826 as "*Semisynthetic viral inhibitor for light control of the MHC I peptide loading complex"* by Winter C*, **Domnick A***, Cernova D, Tampé R (2022) including Figure 4.8-1, Figure 4.8-2, Figure 4.8-3, Figure 4.8-4, Figure 6.1-10, Figure 6.1-11, Figure 6.1-12, and Figure 6.1-13, and material and methods 3.3.2, 3.3.24, 3.3.25, 3.3.32, 3.3.33, 3.3.35, 3.3.36, and 3.3.37.

II. Summary

The peptide loading complex (PLC) is a central machinery in adaptive immunity ensuring antigen presentation by major histocompatibility complex class I (MHC I) molecules to immune cells. If nucleated cells present foreign antigenic peptides from various origins (e.g., viral infected or cancer cells) on their cell surface they are targeted and eliminated by effector cells of the immune system to protect the organism against the hazard. The antigen presentation process starts with proteasomal degradation. Peptide loading and quality control of most, if not all, MHC I is performed by the PLC. Despite the main components, architecture, and general functions of this labile and multi-subunit assembly have been described[1–3], knowledge about the inner mechanics of MHC I loading and quality control in the PLC is limited. Detailed structural insights into the interactions and functions of key elements are lacking. In this PhD thesis, structural and functional aspects of the PLC in peptide loading and quality control of MHC I are unraveled, and the PLC was analyzed from an evolutionary perspective.

First, composition and architecture of native PLC isolated from different mammalian species was analyzed. Comparison of detergent-solubilized PLC from cow and sheep spleens with PLC isolated from human source showed a compositional conservation in mammals, with the central components TAP, ERp57, tapasin, calreticulin, and the MHC I heterodimer were conserved in these species. Negative-stain electron microscopy (EM) analyses revealed an identical overall architecture of PLCs from human, sheep, and cow with two major densities at opposing sides of the plane of the detergent micelle corresponding to endoplasmic reticulum (ER) luminal and cytosolic domains. Interestingly, the glucose-regulated protein 78 (GRP78) was associated only with the PLC from sheep and cow as revealed by mass spectrometry. This ER chaperone is involved in initial folding steps of MHC I but was not co-purified with human PLC, rendering it an interesting target for future functional and in-depth structural studies.

The human PLC was stabilized by reconstitution in membrane mimicking systems that replace the detergent, which is necessary to solubilize the complex. This stabilization allowed detailed structural analysis by single-particle cryogenic electron microscopy (cryo-EM). The structure of the MHC I editing module in the PLC, composed of tapasin, ERp57, calreticulin, MHC I, and β-2-microglobulin (β_2m), was solved at an overall resolution of 3.7 Å. Within the structure, two important features were visualized: (i) the editing loop of tapasin, which is directly involved in peptide proofreading of MHC I; (ii) the A-branch of the Asn86 tethered N-linked glycan on MHC I. Both features are crucial elements in the quality control and peptide editing process on MHC I. The editing loop interacts with the peptide binding groove in MHC I. It disturbs the interaction between a cargo peptide C terminus and the F-pocket in the binding groove by displacing Tyr84 and the helices α1 and α2. The helix displacement

widens the F-pocket which allows a faster peptide exchange on MHC I. The glycan is bound in its monoglucosylated form ($Glc_1Man_9GlcNAc_2$) by the lectin domain of calreticulin. The A-branch of this glycan is stretched between MHC I Asn86 and the lectin domain, leading to the hypothesis that the glycan will be released from calreticulin once MHC I is loaded with a favored peptide (pMHC I).
For investigation of the glycan status of MHC I, intact protein liquid chromatography coupled mass spectrometry (LC-MS) was performed under denaturating conditions. An allosteric coupling between peptide loading and removal of the terminal glucose by α-Glucosidase II (GluII) was discovered. In addition, the PLC remained fully intact after peptide loading, which demonstrated GluII action on the PLC once MHC I is loaded.
With establishing GluII as transient interaction partner, this work deepens the knowledge of the molecular sociology of the PLC and how the PLC is involved in the endoplasmic reticulum quality control (ERQC). Further investigation of the ER aminopeptidases ERAP1 and ERAP2 showed that these enzymes neither alone nor together stably interact with the PLC. In contrast, both work independent from the PLC on free peptides in the ER[4].

LC-MS analysis of the PLC components revealed a very unusual glycosylation pattern of tapasin. Tapasin was observed with N-linked glycans ranging from the full glycan ($Man_9GlcNAc_2$) to heavily trimmed glycans, where only a single GlcNAc remained attached to Asn233. In the PLC, tapasin is probably shielded from degradation by ERQC and can remain functional and intact without a full N-linked glycan.
In addition, this PhD thesis describes the identification of an additional tapasin isoform in the PLC. The additional isoform 5 is 1,077 Da heavier than the canonical isoform 1. We discovered that the exon eight is skipped in the isoform 5. Exon 8 skipping results in a frameshift and a shifted stop codon, leading to an 11 amino acid longer tapasin variant and a variation of the C terminus.

Functional studies on PLC often require isolation of the PLC. Detergent solubilization of the PLC is required to obtain isolated PLC from Raji cells. The membrane surrounding the PLC is removed during the solubilization. Furthermore, current purification strategies utilize viral TAP inhibitors which partially inhibit the PLC function. In this PhD thesis two complementary strategies are described which facilitate the investigation of fully functional PLC in a membrane environment. PLC was reconstituted in liposomes, which provide an intact and unrestricted lipid system for the PLC, allowing to study peptide transport by the PLC. Also, dissociation of pMHC I from the PLC can be studied in liposomes, as demonstrated by pMHC I detection after peptide loading. Furthermore, a photocleavable analog of the viral TAP inhibitor ICP47 (pc-ICP47^{SBP}) was established as tool for TAP reactivation by light. pc-ICP47^{SBP} can be used for PLC preparation like ICP47^{SBP}. After photocleavage of pc-ICP47^{SBP}, TAP function in peptide binding, peptide-coupled ATP

hydrolysis, and peptide transport were demonstrated. These major advancements will facilitate detailed structural and mechanical studies of the PLC in a fully intact membrane.

This PhD thesis advanced the understanding of MHC I loading and quality control in the PLC by providing structural and functional insights. In addition, reconstitution of fully functional PLC in liposomes will facilitate future studies unraveling the interplay of TAP with the editing modules.

III. Zusammenfassung

Der menschliche Körper ist ständig inneren und äußeren Bedrohungen ausgesetzt. Daher ist er auf ein effizientes System zur Abwehr dieser Bedrohungen angewiesen. Dabei spielt das adaptive Immunsystem eine wichtige Rolle, da es sich flexibel an eine Vielzahl von Erregern und Bedrohungen anpassen kann, um diese anschließend zu neutralisieren. Der Haupthistokompatibilitätskomplex Klasse I (MHC I) ist ein elementarer Bestandteil der adaptiven Immunantwort und erlaubt Effektorelementen des Immunsystems alle kernenthaltenden Zellen zu überwachen und Bedrohungen zu identifizieren. MHC I wird innerhalb der Zellen mit kurzen Proteinbruchstücken – Peptiden – beladen und repräsentiert so den aktuellen Zustand der Zelle. Sind in der Zelle Gefahren für Zelle und Organismus (z.B. Krebs, Viren) vorhanden, so werden auch Bestandteile dieser Bedrohungen mittels MHC I auf der Zelloberfläche präsentiert. Anschließend kann das Immunsystem Zellen, die eine Bedrohung präsentieren, identifizieren und eliminieren und so den gesamten Organismus schützen. Körpereigene Bestandteile werden nicht als Gefahren erkannt, da Effektorelemente des Immunsystems einer strengen Kontrolle unterliegen. Zusätzlich muss jede individuelle Zelle sicherstellen, dass sie ihren aktuellen Zustand repräsentativ auf der Zelloberfläche wiedergibt. Der MHC I *Peptide Loading Complex* (PLC) ist ein zentraler Bestandteil der Antigenpräsentation durch MHC I und ist entscheidend in die Beladung und Qualitätskontrolle von MHC I involviert. Dadurch ist er direkt an adaptiven Immunprozessen zur Bekämpfung interner oder externer Gefahren beteiligt. Trotz dieser wichtigen Funktionen ist das Wissen über die innere Mechanik der MHC I-Beladung und der Qualitätskontrolle im PLC begrenzt. Die Hauptkomponenten, Architektur und die allgemeinen Funktionen dieses labilen Multi-Proteinkomplexes wurden bereits beschrieben[1–3]. Es fehlen jedoch detaillierte strukturelle Einblicke in die Interaktionen und Funktionen einiger Schlüsselelemente. In dieser Doktorarbeit wurden verschiedene Analysen durchgeführt, um strukturelle und funktionelle Aspekte des PLC, der Peptidbeladung und der Qualitätskontrolle von MHC I aufzuklären.

Der PLC wurde erstmals von anderen Säugetierspezies als dem Menschen gereinigt und analysiert. Dazu wurde PLC aus Milzen von Schaf und Rind mithilfe des viralen TAP Inhibitors ICP47^{SBP} und Affinitätschromatographie, analog zur Reinigung von humanem PLC, isoliert. Die Reinigung von PLC aus Kuh- und Schafsmilz ergab, dass der PLC in diesen Spezies ähnlich zusammengesetzt ist wie menschlicher PLC. Die Identität der isolierten Proteine wurde durch Vergleiche in SDS-PAGE, sowie direkter Analyse per Massenspektrometrie bestätigt. Dieses Ergebnis deutet auf eine konservierte Zusammensetzung des PLC in Säugetieren hin. Die anschließende strukturelle Analyse der Architektur dieser PLCs mittels Elektronenmikroskopie (EM) ergab eine ähnliche räumliche Architektur wie beim menschlichen PLC. Beide Merkmale machen den PLC der untersuchten Spezies zu einem interessanten Ziel für zukünftige funktionelle und strukturelle Studien.

Zusätzlich wurde das Glukose-regulierte Protein 78 (GRP78) mit dem PLC aus Schaf und Rind isoliert. Dieses Chaperon ist an den ersten Faltungsschritten von MHC I im ER beteiligt, wurde bisher aber nicht als Interaktionspartner des menschlichen PLC identifiziert. Zukünftige Studien müssen zeigen, ob dieser Befund eine Funktion von GRP78 im PLC darstellt.

Um das Wissen über die Funktion des menschlichen PLCs zu vertiefen, wurde in dieser Dissertation ein Fokus auf die Strukturaufklärung gelegt. Bisher musste der labile PLC für die Strukturaufklärung mittels chemischer Quervernetzung stabilisiert werden, um die Architektur mittels kryogener Einzelpartikel-Elektronenmikroskopie (Cryo-EM) aufzuklären. Daher wurde der humane PLC zunächst durch Rekonstitution in membrannachbildenden Systemen stabilisiert, die das Detergens ersetzten, das zum Solubilisieren des Komplexes verwendet wurde. Das hier verwendete System heißt *Nanodisc* und schließt innerhalb eines Rings aus amphiphilen Proteinen Lipide und den PLC ein. Durch Rekonstitution des PLC in diesem System konnte der PLC stabilisiert werden. Diese Stabilisierung ermöglichte eine detaillierte Strukturanalyse mittels Cryo-EM, wobei die erreichte Auflösung deutlich verbessert werden konnte. Für den gesamten PLC bestehend aus zwei Editiermodulen (jeweils bestehend aus Tapasin, ERp57, Calreticulin, MHC I hc und β_2m) und einem Membrananteil (bestehend aus TAP1, TAP2, sowie Transmembranhelices von Tapasin und MHC I) wurde eine gemittelte Auflösung von 4.0 Å erreicht. Allerdings zeigte sich, dass die beiden Editiermodule und der in der Membran enthaltene Anteil zueinander flexibel sind. Daher konnten die Membranbestandteile des PLCs strukturell nicht aufgelöst werden. Des Weiteren stellte sich in einer intensiven Analyse heraus, dass immer ein Editiermodul im PLC komplett assembliert ist und alle oben genannten Proteine enthält. Das zweite Editiermodul liegt in verschiedenen Assemblierungszuständen vor. Diese reichen von einem ebenfalls vollständig assemblierten Modul bis zu einer vollständigen Abwesenheit dieses Moduls. Dabei ist aktuell unklar, ob es sich bei allen Zuständen um natürliche Assemblierungen handelt oder ob diese durch Beschädigung während der Cryo-EM-Probenpräparation der hoch-fragilen PLCs entstanden sind. Durch Fokussierung der Strukturaufklärung auf eines der vollständig assemblierten Editiermodule konnte dieses mit einer Auflösung von 3.7 Å gelöst werden.
Neben der Verbesserung der Auflösung konnten innerhalb der Struktur zwei wichtige, bisher ungelöste, Merkmale aufgeklärt werden: (i) die Editierschleife von Tapasin, die direkt an der Peptid-Editierung am MHC I beteiligt ist; (ii) der A-Zweig des an Asn86 gebundenen N-Glykans an MHC I. Die Editierschleife interagiert direkt mit der MHC I-Peptidbindungstasche. Dabei kontaktiert diese Schleife die Oberseite der Peptidbindungstasche und stört die Interaktion zwischen dem C-Terminus eines Peptids und der F-Tasche der MHC I-Peptidbindungstasche. Dazu taucht Leu18 des Tapasins in die Bindungstasche ein und verhindert den Kontakt des MHC I Tyr84 mit dem C-Terminus des Peptides. Außerdem werden die α1- und α2-Helices verschoben. Diese Verschiebung

erweitert die Peptidbindetasche, was einen Peptidaustausch am MHC I katalysiert. Die schwere Kette (hc) des MHC I trägt ein N-Glykan am Asn86. Dieses wird co-translational durch die Oligosaccharyltransferase (OST) angefügt und ist ein wichtiger Marker für den Faltungs- und Beladungszustand von MHC I im ER. Zunächst trägt das Glykan drei Glukose-Reste ($Glc_3Man_9GlcNAc_2$). Diese werden schrittweise durch die Enzyme α-Glukosidase I und α-Glukosidase II entfernt. Nach der Entfernung von zwei Glucose-Resten liegt das Glykan in seiner monoglukosylierten Form ($Glc_1Man_9GlcNAc_2$) vor und wird von der Calreticulin-Lektindomäne gebunden und anschließend in den PLC rekrutiert. Der A-Zweig dieses Glykans wurde in dieser Arbeit erstmals strukturell aufgelöst und befindet sich zwischen Asn86 und der Lektindomäne von Calreticulin. Die Analyse des gestreckten Glykans im unbeladenen Zustand von MHC I führte zu der Hypothese, dass das Glykan von Calreticulin freigesetzt wird, sobald MHC I mit einem Peptid beladen ist (pMHC I) und anschließend die terminale Glucose durch α-Glukosidase II ebenfalls entfernt werden kann.
Zur Untersuchung des Glykanstatus von MHC I wurde eine Flüssigchromatographie mit Massenspektrometrie-Kopplung (LC-MS) des intakten Proteins unter denaturierenden Bedingungen durchgeführt. Dabei wurde zunächst der Glykanstatus des unbeladenen MHC I in der monoglucosylierten Form nachgewiesen. War kein geeignetes Peptid vorhanden, konnte die α-Glukosidase II das Glykan ($Glc_1Man_9GlcNAc_2$) nicht erreichen und die verbliebene Glukose nicht abspalten. Nach der Zugabe von hoch-affinen MHC I-bindenden Peptiden wurde das Glykan allerdings für die α-Glukosidase II zugänglich und MHC I lag deglukosyliert vor ($Man_9GlcNAc_2$). Mit dieser Analyse wurde die allosterische Kopplung zwischen der Peptidbeladung und Entfernung der terminalen Glukose durch Glukosidase II nachgewiesen. Darüber hinaus bleibt der PLC nach der Peptidzugabe vollständig assembliert, was darauf schließen lässt, dass α-Glukosidase II innerhalb des vollständig assemblierten PLC deglukosylieren kann, sobald MHC I beladen wurde. Allerdings verhindert Rekonstitution in *Nanodisc*, dass eine Dissoziation von pMHC I vom PLC stattfinden kann.

Bei der LC-MS-Analyse der weiteren PLC-Komponenten wurde ein sehr ungewöhnliches Glykosylierungsmuster von Tapasin festgestellt. Tapasin trägt ein N-gebundenes Glykan an Asn233. An dieser Stelle wurden Glykane verschiedener Länge gefunden. Diese reichten vom vollständigen Glykan ($Man_9GlcNAc_2$) bis zu sehr reduzierten Glykanen, bei denen nur ein einziges GlcNAc an Asn233 gebunden war. Teile des Glykans konnten in der Strukturanalyse dargestellt werden, allerdings nur die Grundstruktur des Glykans ($ManGlcNAc_2$). Die hohe Varianz der Glykanmodifizierung, sowie eine große Flexibilität des Glykans erschwerten die vollständige strukturelle Auflösung. Wahrscheinlich ist Tapasin im PLC vor dem Abbau durch die ER-Qualitätskontrollmechanismen (ERQC) geschützt und kann auch ohne ein vollständiges N-gebundenes Glykan intakt und funktionsfähig bleiben.
Mittels Massenspektrometrie wurde zudem eine alternative Tapasin-Isoform 5 beschrieben, die zusammen mit dem PLC aus Raji-Zellen isoliert wurde. Diese Isoform ist 1,077 Da schwerer als die kanonische Isoform 1, die ebenfalls im PLC vorhanden ist. Etwa ein Drittel

der Tapasine im PLC aus humanen Raji Zellen liegt in dieser Isoform 5 vor. Durch massenspektrometrische Analyse von tryptischen Peptidfragmenten wurde festgestellt, dass das Exon 8 in der Isoform 5 übersprungen wird. Dies führt zu einer Verschiebung des Leserasters und einem alternativen Stopcodon. Die Tapasin Isoform 5 ist dadurch um elf Aminosäuren verlängert und besitzt einen anderen C-Terminus als die Isoform 1. Die Funktion von Tapasin im ER ist jedoch wahrscheinlich nicht beeinträchtigt und Integration in den PLC ist weiterhin möglich. Jedoch könnte es sein, dass die alternative Tapasinvariante das ER verlassen kann. Im Gegensatz zur Isoform 1 ist hier das ER-Retentionssignal (KKXX) nicht mehr vorhanden.

Mit der Identifizierung der α-Glukosidase II als transientem Interaktionspartner vertieft diese Arbeit das Wissen über die molekulare Soziologie des PLC und darüber, wie der PLC in die Qualitätskontrolle der ER-Glykoproteine eingebunden ist. Aufgrund seiner zentralen Rolle im Prozess der MHC I-Beladung und Qualitätskontrolle wurde spekuliert, dass weitere Proteine den PLC als Interaktionsplattform nutzen. Besonders bei verschiedenen Proteinen, die indirekt mit der Beladung von MHC I befasst sind, wurde eine Interaktion vermutet. Daher wurde in dieser Arbeit die Interaktion der Aminopeptidasen ERAP1 und ERAP2 mit dem PLC untersucht. Beide Enzyme sind in der Prozessierung von potenziellen Klienten-Peptiden beteiligt und eine räumliche Nähe zu MHC I wäre daher von Vorteil. Untersuchungen beider Aminopeptidasen im Zusammenhang mit dem PLC ergaben allerdings, dass weder diese Enzyme allein noch ERAP1/2 zusammen eine stabile Interaktion mit dem PLC eingehen. Sie wurden nicht mit dem PLC zusammen aus humanen Zellen isoliert. Auch nach Zugabe von ERAP1, ERAP2 oder einem Gemisch beider Enzyme zu isoliertem PLC konnte keine kinetisch stabile Interaktion festgestellt werden. Im Gegensatz dazu arbeiten beide Enzyme unabhängig vom PLC an freien Peptiden im ER[4].

Bisherige Untersuchungen am PLC haben entweder an isoliertem PLC oder in intakten Zellen stattgefunden. Beide Ansätze haben Vor- aber auch Nachteile. Die Untersuchung des PLC innerhalb von Zellen reduziert die Wahrscheinlichkeit essenzielle Bestandteile seiner Umgebung während der Isolierung zu entfernen. Allerdings können viele Messungen aufgrund eines starken Hintergrundsignals nicht oder nur eingeschränkt durchgeführt werden. Auch sind direkte Manipulationen am PLC hier nicht möglich, da dieser innerhalb der Zelle nicht direkt zugänglich ist. Assays bei denen eine direkte Manipulation des PLC notwendig ist, sind mit isoliertem PLC realisierbar. Nach einer Reinigung des PLC mittels des viralen Inhibitors $ICP47^{SBP}$ ist der PLC monodispers nach Gelfiltration (SEC) und weitestgehend frei von Verunreinigungen. Allerdings werden bei der Isolierung des PLC die Lipidmembran sowie weitere, möglicherweise transient interagierende, Partner entfernt. Aufgrund der fehlenden Lipidmembran und fehlender Kompartimentierung kann der Peptidtransport von isoliertem PLC nicht untersucht werden. Dies gilt für isolierten PLC in Detergenzien, aber auch für PLC stabilisiert in Rekonstitutionssystemen wie in den oben genannten *Nanodiscs*.

Zudem ist die Bindung des Inhibitors ICP47^{SBP} an TAP, aufgrund einer sehr hohen Affinität, faktisch irreversibel und erschwert funktionale Untersuchungen am PLC, da auch durch diesen Inhibitor die Transportfunktion von TAP blockiert wird.
In dieser Arbeit wurden zwei, sich ergänzende Strategien etabliert, die es ermöglichen, den PLC vollständig funktional in Lipidvesikeln zu untersuchen. Dafür wurde der PLC erstmals in Liposomen rekonstituiert. Liposomen bieten eine geschlossene Lipidmembran, in der sich außer dem Zielproteinkomplex keine weiteren Proteine befinden. Die Liposomen ähneln dabei Mikrosomen und sind komplett geschlossen. Dadurch werden nun sowohl Transportprozesse über die Membran als auch laterale Diffusion von Membranproteinen des PLC für Untersuchungen zugänglich. Die laterale Diffusion einzelner PLC Komponenten ist von besonderem Interesse, da pMHC I nach erfolgreicher Beladung mit einem Peptid und Qualitätskontrolle im PLC aus dem PLC entlassen wird um an die Zelloberfläche zu gelangen.
Um die TAP-Aktivität nach PLC-Isolierung wieder zu reaktivieren, kommt die zweite Strategie zum Tragen. In dieser Arbeit wurde eine Variante des bisher verwendeten TAP-Inhibitors ICP47^{SBP} etabliert. Diese Variante ist zusätzlich zum SBP-tag, für die Affinitätsreinigung des PLC, mit einer photospaltbaren Aminosäure ausgestattet (pc-ICP47^{SBP}). Nach erfolgreicher Reinigung des PLCs mittels pc-ICP47^{SBP} soll TAP durch Belichtung mit UV-Licht reaktiviert werden, da pc-ICP47^{SBP} in zwei Bruchstücke zerfällt, die eine deutlich geringere Affinität zu TAP haben als vollständiges pc-ICP47^{SBP}. Die Ergebnisse dieser Doktorarbeit zeigen, dass pc-ICP47^{SBP} analog zur bisherigen Variante von ICP47^{SBP} zur Isolierung des PLC genutzt werden kann. Zusätzlich wurde demonstriert, dass Peptidbindung und peptidabhängige ATP-Hydrolyse von TAP reaktiviert werden. Durch Kombination der Reinigung des PLC mit pc-ICP47^{SBP}, Rekonstitution dieses PLCs in Liposomen und anschließender Aktivierung durch Licht, konnte außerdem erfolgreich Transportaktivität in PLC-enthaltenden Liposomen gezeigt werden. Besonders die Kombination von pc-ICP47^{SBP} mit Liposomenrekonstitution wird zukünftig wichtige funktionale Erkenntnisse zum PLC ermöglichen. Zusätzlich wird es nach Reaktivierung von TAP im isolierten PLC möglich sein, alternative Strategien zur Stabilisierung der Transmembrandomänen des PLC durchzuführen. Beispielsweise wurden in dem funktionellen TAP homolog TmrAB verschiedene ATP-Analoga verwendet, um unterschiedliche strukturelle Zustände unter Transportbedingungen zu charakterisieren[5]. Diese Strategien können nun auch auf den humanen PLC übertragen werden, um Informationen über die Organisation der Transmembrandomänen zu erhalten und so eine funktionelle Verknüpfung zwischen Peptidtransport durch TAP und Peptidbeladung in den Editiermodulen darzustellen.

1. Introduction

1.1. MHC I antigen presentation

Every nucleated cell in the human body presents its current translational status on the cell surface. Here, cluster of differentiation 8 positive ($CD8^+$) effector cells can sample the status of the cell. Major histocompatibility complex class I (MHC I) molecules present the transcriptional status of each cell by carrying small protein fragments (peptides) (pMHC I). pMHC I loaded with foreign peptides can activate $CD8^+$ T cells if foreign or unusual proteins are detected. Activated $CD8^+$ cells induce apoptosis of the cell carrying the foreign peptide. However, T cells do not recognize pMHC I carrying peptides that originate from a legit source, because self-recognizing T cells are eliminated during T cell selection in the thymus. If cells fail to present pMHC I or no MHC I on the cell surface, the "missing-self" response is activated, and the respective cell is also eliminated[6,7]. Therefore, each healthy cell needs to ensure presentation of stable pMHC I complexes on the cell surface.

MHC I is a heterodimeric complex formed by the highly polymorphic MHC I heavy chain (hc) and the invariant light chain β-2-microglobulin (β_2m)[(ref. 8)]. Because of the critical function of MHC I in the detection of pathogens and infections, its folding and loading process is facilitated by several chaperones and quality controlled at different stages during the loading process (Figure 1.1-1). The hc is co-translationally inserted into the endoplasmic reticulum (ER) membrane and initially stabilized by immunoglobulin binding protein (BiP) and calnexin[9,10]. hc molecules are intrinsically labile until they have engaged with β_2m and bound a high-affinity cargo peptide. Afterwards, they are stable up to several days[11–14]. After engaging with calnexin, the hc binds β_2m and calreticulin. In this form, MHC I can engage with the peptide loading complex (PLC) for loading with a high-affinity cargo peptide[1,15,16]. The PLC is a multi-protein machinery located in the ER membrane, which is dedicated to perform peptide loading and quality control on MHC I. The cornerstone of the PLC is the heterodimeric ABC transporter associated with antigen processing (TAP) which transports peptides from the cytosol into the ER lumen. Furthermore, TAP interacts with tapasin, a main peptide exchange facilitator for MHC I[17]. Putative antigenic cargo peptides are generated in the cytosol by the proteasome. Sources are defective ribosomal products (DRiPs)[(ref. 18,19)] and peptides from degradation of ubiquitinated proteins[20]. TAP selectively transports a fraction of the generated peptides into the ER[21–23]. Here, the peptides are further processed by the aminopeptidases ER-aminopeptidase 1 and 2 (ERAP1 and ERAP2, respectively) to a length of 8-10 amino acids[24–27], which is optimal for MHC I[8]. The PLC facilitates peptide binding of MHC I and catalyzes the exchange to peptides with high affinity to MHC I. Afterwards, loaded pMHC I leave the PLC towards the Golgi-apparatus and the cell surface.

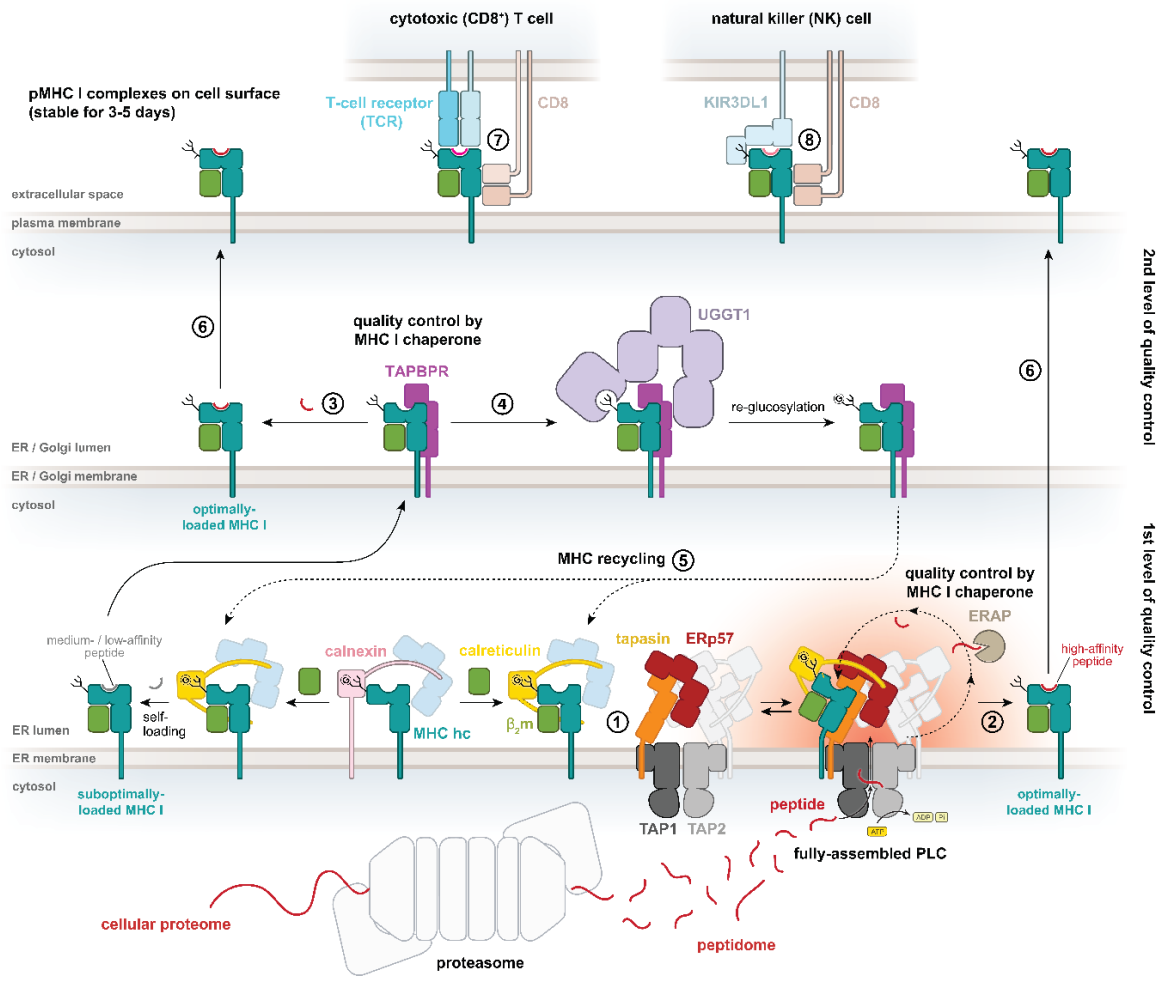

Figure 1.1-1: MHC I loading and quality control. Unfolded hc is chaperoned by calnexin after transport into the ER. Upon engagement of MHC I hc with β_2m, calnexin is replaced by calreticulin and this complex can engage with the PLC (1). Here, MHC I is loaded with high-affinity cargo peptides (2). TAP1/2 transport putative cargo peptides into the ER and create a peptide rich environment in proximity to empty MHC I (red cloud). TAPBPR is a homolog of tapasin and realizes a second level of quality control in the ER or Golgi apparatus. Here peptide exchange is facilitated outside the PLC (3). Without suitable cargo peptides for MHC I, TAPBPR promotes reglucosylation of MHC I by UGGT1 (4). The monoglucosylated MHC I can re-engage with calreticulin and the PLC for peptide loading (5). MHC I loaded with a high-affinity peptide (pMHC I) can travel to the cell surface after the terminal glucose has been removed (6). On the cell surface can pMHC I interact with the TCR of T cells (7) or with NK cells via the KIR3DL1 receptor (8). The figure was adapted from[16].

The tapasin homolog TAP-binding protein related (TAPBPR) acts outside of the PLC and performs the second level of MHC I quality control[16,28]. It also functions as peptide-exchange catalyst if pMHC I is loaded with low or medium affinity peptide (>500 nM) in the ER or Golgi.

Besides the peptide exchange-catalysts tapasin and TAPBPR, which assure high-affinity loading of pMHC I, MHC I is under surveillance by other proteins during maturation and loading. N-linked glycosylation is a very important quality marker. The glycan is attached to Asn86 on MHC I by the oligosaccharyltransferase (OST)[ref. 29]. The OST transfers a $Glc_3Man_9GlcNAc_2$ glycan tree onto the target protein (Figure 1.1-2). After initial removal of two glucoses on the A-branch by α-Glucosidases I and II (GluI and GluII, respectively), monoglucosylated MHC I is recognized by calreticulin[15,16]. The chaperone binds specifically to N-linked glycans with a single glucose residue remaining on the A-branch[30]. After peptide loading of MHC I, the remaining glucose is removed by GluII to allow the export of pMHC I to the Golgi apparatus. Here, TAPBPR can facilitate reglucosylation of MHC I via the UDP-glucose:glycoprotein glucosyltransferase 1 (UGGT1) if it is present without a high-affinity peptide binding partner[31,32]. Glucosylated MHC I is re-cycled back to the ER and MHC I can interact with the PLC again. If no high-affinity binding partner for MHC I has been found or the folding process stalled, ER-α1,2-mannosidase I (ERmanI) removes the terminal mannoses on the B- or C-branch[33]. This flags MHC I for ubiquitination and subsequent degradation in the ER associated protein degradation (ERAD) pathway.

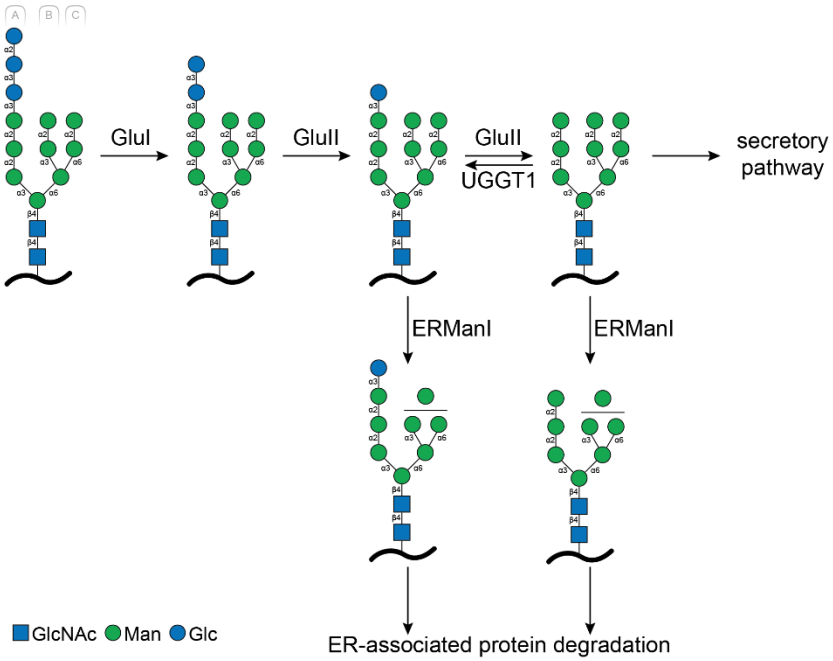

Figure 1.1-2: Schematic overview of N-linked glycan processing in the ER and Golgi. A $Glc_3Man_9GlcNAc_2$ glycan is linked to an asparagine residue of proteins in the ER destined to enter the secretory pathway and the associated quality control. GlucI and GluII remove single glucose moieties on the A-branch allowing proteins to advance towards the secretory pathway which requires removal of all three glucoses. UGGT1 can reattach a single glucose residue, triggering either ER retention or transport from the Golgi back into the ER. Removal of a single mannose on the B- or C-branch by ERmanI tags proteins as substrates for degradation by the ERAD pathway.

1.2. The peptide loading complex (PLC)

MHC I peptide loading and quality control in the ER is performed by the PLC. This is a dynamic multi-protein assembly, centered around the ATP-binding cassette (ABC) transporter TAP (Figure 1.2-1). TAP binds tapasin with its transmembrane domains 0 (TMD0) and thereby anchors the PLC in the ER membrane. Tapasin is the main scaffold protein in the PLC and interacts with all protein components of the PLC. However, its main function in the PLC is to chaperone MHC I and catalyze peptide exchange on MHC I. The oxidoreductase ER protein 57 (ERp57) is covalently bound to tapasin via an intermolecular disulfide-bridge and serves as a structural protein in the PLC. However, the inherent oxidoreductase function of ERp57 is not used in the PLC[34]. The MHC I heterodimer of the hc and β_2m is bound by tapasin via several interactions. Further, MHC I is chaperoned by calreticulin which binds to the monoglucosylated A-branch of the N-linked glycan of MHC I. Calreticulins P-domain is binding ERp57 and tapasin with its C-terminal acidic helix. The architecture of the assembly was solved by cryogenic electron microscopy (EM)[1]. However, many critical aspects of peptide loading and quality control have not been described sufficiently.

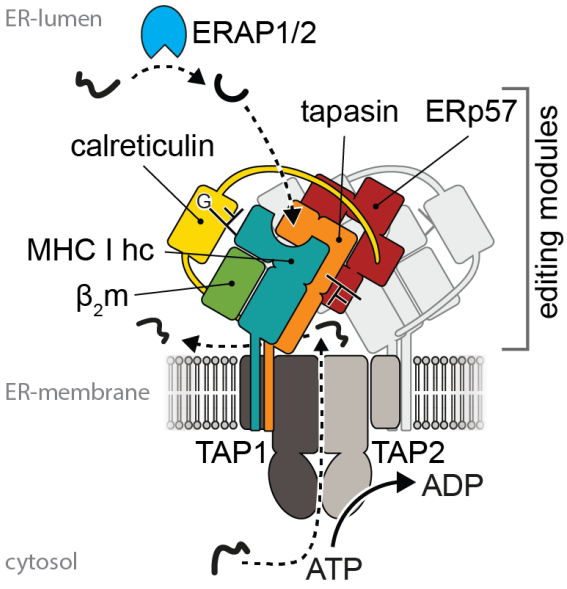

Figure 1.2-1: Schematic depiction of the PLC. The PLC contains two editing modules, centered around the peptide transporter TAP1/2 (dark/light grey). Each editing module consists of tapasin (orange), calreticulin (yellow), ERp57 (red), MHC I hc (petrol), and β_2m (green). ERAP1 processing peptides is depicted in blue. For better visualization, one of the two editing modules is shown in light grey. TAP peptide transport and ATP hydrolytic functions are indicated, as well as peptide binding by MHC I.

The PLC is suspected to be a main interaction hub for proteins involved or associated with MHC I peptide loading or quality control. Examples are ERAP1 and ERAP2(ref. 27). These proteins serve as peptide editors and trim putative cargo peptides to a suitable length for

MHC I binding. GluII is also a suspected PLC interaction partner. It catalyzes the removal of the terminal glucoses in the ER and on MHC I once a high-affinity binder has been bound and pMHC I is supposed to travel towards the cell surface[35–37]. However, for these proteins it is unknown whether stable interaction with the PLC occurs to perform their tasks.

1.2.1. Transporter associated with antigen processing (TAP)

TAP is a heterodimeric transporter, which belongs to the family of ABC transporters and is formed by the proteins ABCB2 (TAP1) and ABCB3 (TAP2). ATP is consumed as energy source for peptide transport from the cytosol into the ER lumen, but peptide binding is ATP independent[21,38,39]. TAP1 and TAP2 have a similar overall fold, and both are required and sufficient for efficient peptide transport[40–43]. Both transporter proteins have the same topology with ten membrane spanning helices, N and C terminus in the cytosol, and a C-terminal nucleotide-binding domain (NBD)[(ref. 44)]. Six of these helices form the core transporter, while the four N-terminal helices assemble in the TMD0, which is the interaction platform to assemble the PLC by binding tapasin[2]. This interaction depends on an intermembrane salt bridge[17].

TAP preferentially transports short peptides (8-10 amino acids) which are the supply for MHC I loading (Figure 1.1-1)[(ref. 21–23,45)] but can also transport much larger peptides or peptides carrying fluorophores[46–48]. After peptide binding, the binding of ATP to the NBDs induces a conformational change from the inward open conformation to the outward open conformation. Thereby the peptide is transported across the membrane. The system is reset to the inward open conformation by ATP hydrolysis and release of ADP and inorganic phosphate[5,41,42,49]. TAP1 and TAP2 form two composite, asymmetric NBDs. Both NBDs are competent in ATP binding. ATP-binding site II (composed by Walker A and B motive of TAP2 and C-loop of TAP1) is canonical and competent in ATP hydrolysis, while ATP binding site I is degenerate, lacking catalytic residues in the Walker A and B motives of TAP1, as well as mutations in the C-loop of TAP2, which results in very low ATP hydrolysis rates[50,51].

The overall structure of inward-facing core TAP has been solved by cryo-EM[52,53]. However, the transporter was in a disrupted, non-transport confirmational state, while the TMD0s have not been resolved. For the TAP homolog TmrAB, the full functional cycle has been delineated by a series of eight cryo-EM structures[5].

1.2.2. Tapasin and ERp57

Tapasin links all proteins and functions of the PLC. It establishes proximity between MHC I and the pool of putative cargo peptides by binding both, TAP and MHC I (Figure 1.2-1)[ref. 1]. However, the role of tapasin is not limited to a structural function but it is also a major facilitator of peptide exchange on MHC I and thereby directly involved in the quality control of MHC I loading[54–56]. ERp57 is a member of the protein disulfate isomerase (PDI) family[57,58]. These proteins can form, break, or rearrange intra- and inter-molecular disulfide bonds. However, ERp57 in the PLC is limited to a structural function, bridging tapasin and the P domain of calreticulin[1,34]. Tapasin and ERp57 occur in the ER almost exclusively as heterodimer linked by an intermolecular disulfide bridge between tapasin Cys95 and ERp57 Cys57[ref. 59].

Tapasin adopts an L-shaped conformation in complex with ERp57 and in the PLC (Figure 1.2-2). The short C-terminal tail and membrane helix (not shown) are preceded by the C-terminal/membrane-proximal immunoglobulin (Ig) domain and a N-terminal Ig domain. The N-terminal Ig domain is elongated by a 7-stranded β-barrel. From the β-barrel emerges the editing loop and the mixed disulfide bridge between tapasin and ERp57 is in this region. MHC I interacts with all three ER-lumenal domains of tapasin. Tapasin utilizes these interfaces to stabilize MHC I and facilitate peptide editing and proofreading. Most prominent, but not structurally described for tapasin, is the editing loop. In the tapasin homolog TAPBPR, this loop is directly involved in peptide editing and "dives" into the peptide binding groove of MHC I, widens the peptide binding groove and facilitates peptide exchange on MHC I[28].

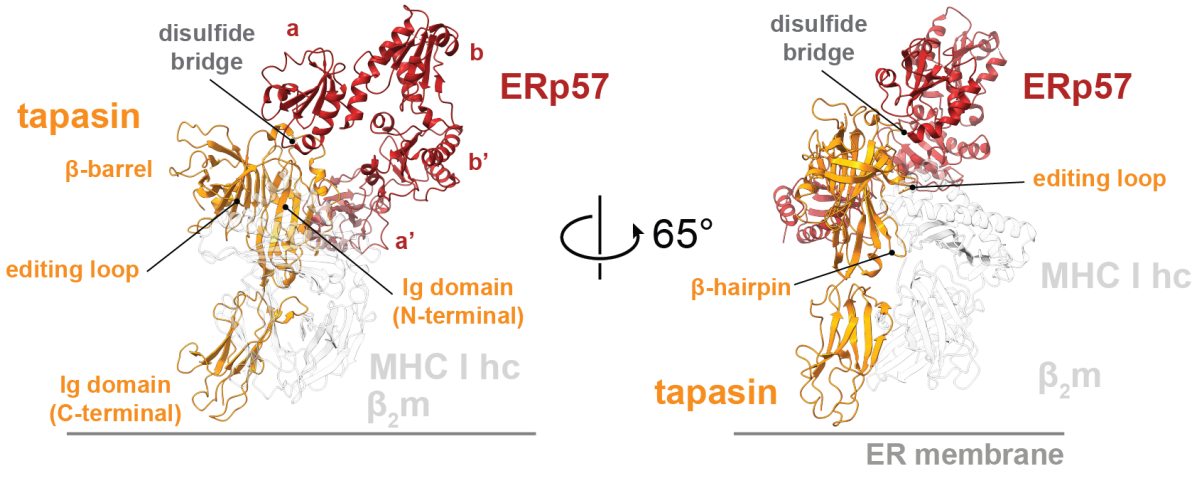

Figure 1.2-2: Structure of the tapasin and ERp57 heterodimer in the PLC. Ribbon diagram of Tapasin (orange) and ERp57 (red) as arranged in the PLC (front view on MHC I and rotated side view). The domains of both proteins are indicated, as well as the editing loop, β-hairpin of tapasin, and the position of the intermolecular disulfide bridge (tapasin Cys95 – ERp57 Cys57). The position of MHC I and β_2m are indicated in light grey. PDB: 6ENY

ERp57 adopts a U-shaped conformation, when in complex with tapasin[60]. The interaction surface of ERp57 with tapasin is in the a and a' domains, while the b' domain binds the P-domain of calreticulin. The a and a' prime domains harbor the thioredoxin-like motives (CxxC), which can form disulfide bridges with client proteins, including tapasin. Typically, ERp57 disengages from the client by utilizing an 'escape pathway' by forming an intramolecular disulfide bridge within the CxxC motive. However, for the tapasin-ERp57 dimer, this has not been observed and the dimer seems to be a stable entity[59].

1.2.3. MHC I / β_2m

MHC I hc genes are encoded in three distinct human leucocyte antigen (HLA) loci in the genome, named A, B, and C. Several thousand different alleles of HLA molecules have been described, making them the most polymorphic genes in the human genome[15,61]. Each HLA allele encodes an MHC I molecule, which differ in their preference for different sets of cargo peptides. With up to six different HLA alleles (two for each locus due to diploidy) a broad peptide repertoire can be presented by each individual cell[15].

The MHC I heterodimeric protein complex is formed by the highly variant and membrane anchored MHC I hc and the invariant and soluble light chain β_2m (Figure 1.2-3). This dimer is intrinsically instable and requires chaperones for stabilization. However, after loading of MHC I with a high-affinity cargo peptide, pMHC I is stable for up to several days on the cell surface, still undergoing constant turnover to represent the current state of the cell[11–14].

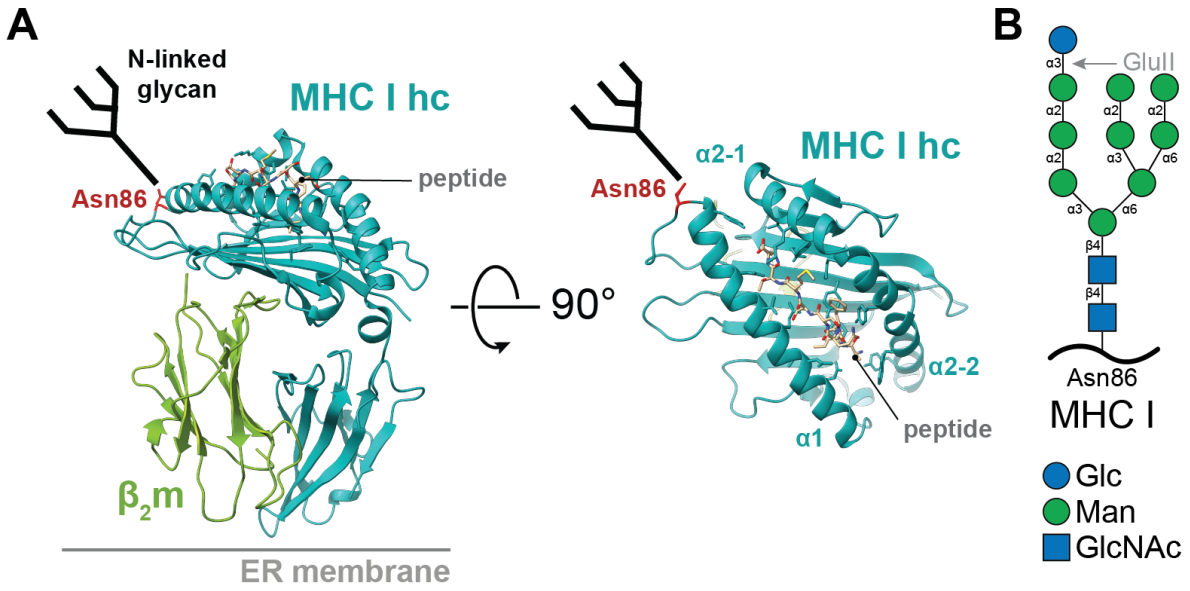

Figure 1.2-3: Structure of the peptide loaded MHC I dimer. (**A**) Structure of the peptide loaded MHC I HLA-A*03:01 (petrol)/β_2m (green) heterodimer in complex with a cargo peptide (sand). The Asn86, which carries the N-linked glycan is highlighted in red. The glycan is not resolved in the crystal structure but schematically depicted in black. PDB: 3RL1 (**B**) Schematic depiction of the N-linked glycan on MHC I hc when MHC I is engaged in the PLC. The terminal glucose is removed by GluII once MHC I is peptide loaded.

Loading of MHC I with peptides occurs in the ER lumen and occasionally in the Golgi. MHC I is chaperoned by either calnexin or calreticulin until a stable pMHC I complex has formed (Figure 1.2-3). While MHC I is chaperoned by calreticulin, it can enter the PLC. Here, tapasin engages as chaperone and promotes peptide binding and exchange[54,62–64]. Binding of calreticulin is dependent on the N-linked glycan of the MHC I hc, which carries a glycosylation on Asn86. This glycan ($GlcNAc_2Man_9Glc_3$) is attached cotranslationally by the OST[65,66] and is trimmed during maturation of MHC I. After initial trimming of the glycan by GluI and GluII to $Glc_1Man_9GlcNAc_2$, calreticulin can interact with MHC I[67]. Once a stable pMHC I complex has been formed, the terminal glucose is removed by GluII. pMHC I can now travel along the secretory pathway towards the cell surface[67,68]. The glycan therefore serves both as marker for stability and as indicator of the MHC I loading status.

The hc of MHC I is organized in three domains (Figure 1.2-3). The domains α1 and α2 form the peptide binding groove with two prominent α-helices on each side and a β-sheet floor[8]. The α3 domain has an Ig-like fold and forms the main interaction surface with β_2m, which also appears in an Ig-like fold. The peptide binding groove is flexible and can adapt to different cargo peptides but has strong, allotype specific peptide preferences[69]. A peptide receptive status of the hc and peptide exchange is supported by several ER chaperones[70,71] (Figure 1.2-4). Typical cargo peptides have a length of 9-12 amino acids and are stretched in the peptide binding groove. Specific interactions of the N and C terminus of the cargo peptide stabilize it in the binding groove. These anchor points are called A- and F-pocket, interacting with the N and C terminus of the cargo peptide, respectively. Further interactions between cargo peptide and side chains of MHC I are localized in further pockets B, C, D, and E and are denominated relative to the terminii of the cargo peptide. The nature of the pockets define the peptide specificity of a MHC I allomorph and dictate sidechains, which are necessary for stable binding[69].

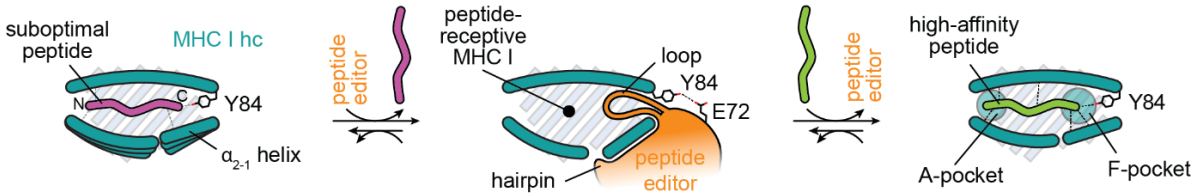

Figure 1.2-4: MHC I peptide binding groove and editing by tapasin/TAPBPR. Mechanistic model of the peptide editing process on MHC I. MHC I loaded with suboptimal peptides are recognized by tapasin or TAPBPR due to increased flexibility on the $\alpha_{2\text{-}1}$-helix. The peptide editors induce peptide exchange by disruption of peptide – MHC I interaction in the F-pocket region, widening of the binding groove by interactions via the hairpin and loop. Furthermore, Tyr84 is displaced and stabilized by a conserved Glu in tapasin/TAPBPR. By these actions the peptide editors lower the activation energy for peptide exchange towards high-affinity peptides. Figure was adapted from[15].

During peptide editing, the chaperones tapasin or TAPBPR act mainly on the F-pocket region[28,72]. Here, the pocket is widenened by pulling on the $\alpha_{2\text{-}1}$ helix by which the interaction between the suboptimal cargo peptide and the F-pocket is disturbed. Mainly the hydrogen bond between Tyr84 and the C terminus of the peptide is weakened and the Tyr84 is stabilized by a conserved Glu on tapasin (Glu72) and TAPBPR (Glu105)[(ref. 28,60,73)]. A structure of this interaction in the tapasin-ERp57-MHC I heterotrimer has been solved recently[72]. For TAPBPR these interactions are similar[28]. Both chaperones sense the peptide loading status of their MHC I client by several contacts. One major interaction is performed by the editing loop, which disrupts peptide-MHC I interactions directly. Second, both proteins use a β-hairpin, which interacts with the floor of the binding groove from below[28,60,74,75]. These interactions are most likely similar in the fully assembled PLC but have not been resolved at high resolution[1]. Additional interactions of the N-linked glycan with calreticulin occur, which have not been resolved in structural experiments.

1.2.4. Calreticulin

Calreticulin is a versatile protein which is involved in the maintenance of Ca^{2+} levels by binding ~50% of the cellular calcium[76], protein folding and quality control in the ER[77,78], and is even considered important in cell death[79]. It can interact transiently with many proteins in the ER and cytosol and changes its function depending on the cellular localization. In the ER, the 46 kDa chaperone calreticulin is involved in the calnexin/calreticulin cycle where it acts together with ERp57[80]. A similar role is adopted during MHC I loading and quality control, where calreticulin is a part of the PLC[1,81]. Here, all three domains of calreticulin are involved in interactions with PLC components (Figure 1.2-5 A). Several low-affinity interactions stabilize calreticulin in the PLC. The P domain of calreticulin binds ERp57 with low affinity

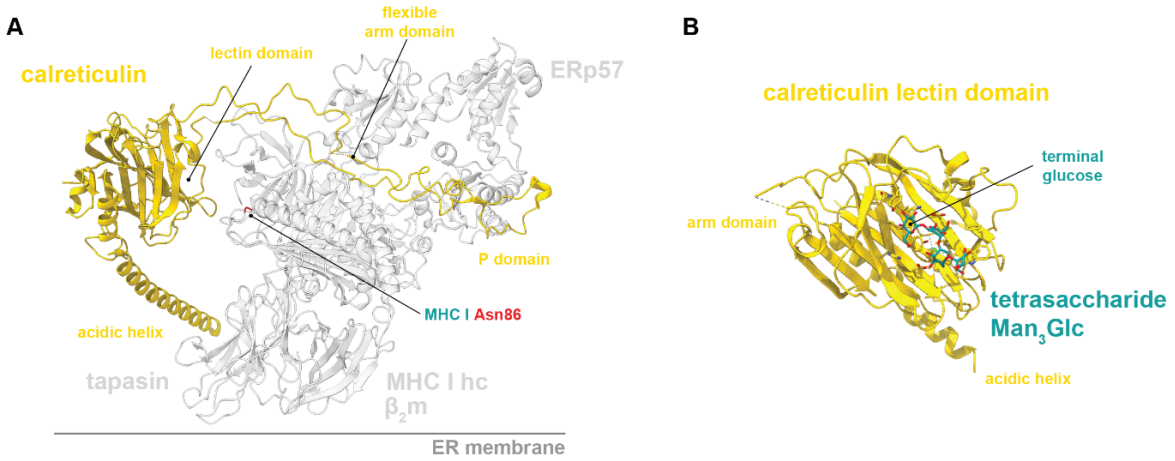

Figure 1.2-5: Structure and interactions of calreticulin in the PLC. (**A**) Position and structure of calreticulin in the PLC. Calreticulin contacts both, tapasin by the C-terminal acidic helix, and ERp57 with its P domain. The lectin domain is in spatial proximity of the putative position of the MHC I glycan on MHC I Asn86 (red). PDB: 6ENY. (**B**) Crystal structure of the calreticulin lectin domain in complex with the Man_3Glc tetrasaccharide which resembles the A-branch of N-linked glycans after Glu trimming by GluI and GluII, respectively. PDB: 3O0W.

($K_d \approx 20$ µM)[ref. 82]. Additionally, the acidic C-terminal helix binds not only Ca^{2+} but is also in contact with the C-terminal Ig domain of tapasin[1,77,83]. Third, the central lectin domain of calreticulin binds specifically to monoglucosylated A-branches of N-linked glycans (Glc_1Man_3) with micromolar affinity ($K_d \approx 1$ µM) (Figure 1.2-5 B)[ref. 30]. All three interactions keep the calreticulin stably interacting with MHC I and the PLC. Due to the different functions, calreticulin is involved in both protein chaperoning and protein quality control in the ER.

1.2.5. ERAP1/2

MHC I molecules preferably bind peptides with a length of nine to 12 amino acids. The first length restriction for peptides imported in the ER is peptide transport by TAP which preferably transports peptides with a length of eight to 12 amino acids[21,46]. Afterwards, peptides can be loaded on MHC I but could require trimming for optimal interaction. Most peptides generated by the proteasome already contain a suitable C terminus for MHC I interactions[84]. However, the N terminus is optimized for MHC I binding by proteases[85]. The ER-resident zinc-metallopeptidases ERAP1 and ERAP2 perform this task and trim peptides to a length of eight to nine amino acids[24–26]. ERAP1 and ERAP2 are structurally related and share ~50% sequence identity[86,87]. Especially ERAP1 has been described as an important factor for antigen presentation in the ER. In addition to peptide trimming, it also curates the peptide pool by removing a fraction of this pool by trimming the peptides below MHC I preferences[85,88,89]. A study demonstrated a reduction of pMHC I number and stability on the cell surface if ERAP1 is depleted in the cell[90]. However, ERAP1 seems to act only on a selection of potential cargo peptides. While some antigens are poorly presented in absence of ERAP1, others are not affected[91–94]. ERAP2 shows a distinct trimming pattern compared to ERAP1 and selects a different length of peptides[86,87,95]. This complementary effect is reflected in some antigens that require both enzymes for efficient cell surface presentation[86,96]. Because of the distinct function, proposed synergistic effects of a dimerization of ERAP1 and ERAP2, and experimental findings, a heterodimeric assembly of ERAP1 and ERAP2 was proposed[86,97,98]. However, this heterodimer has not been observed to date, indicating that additional protein-protein interactions might be necessary for ERAP1 and ERAP2 dimerization[27]. The PLC was proposed as an interaction partner supporting dimerization or close association of ERAP1 and ERAP2.

The trimming properties of ERAP1 and ERAP2 in solution have been described in detail[24,99]. However, it remained unclear whether ERAP1/2 act only on peptides in solution or whether it could also act on peptides already associated with MHC I[100,101]. The PLC has been suggested to be involved as mediator between partly loaded pMHC I complex and the trimming function of ERAP1 and/or ERAP2[27].

1.2.6. GluII

Proteins that are glycosylated with N-linked glycans undergo a strict quality control regime in the ER lumen, which is established by the ER glycoprotein quality control (ERQC)[ref. 102–105]. In this regime, the glycan serves as a marker for the progress of protein maturation within the ER. Initially, a full N-linked glycan ($Glc_3Man_9GlcNAc_2$) is transferred to Asn residues of glycoproteins by the OST (Figure 1.1-2)[ref. 29]. Afterwards, the terminal glucose residues are subsequently cleaved by GluI and GluII. GluI removes the initial glucose, resulting in $Glc_2Man_9GlcNAc_2$[ref. 106,107]. This event triggers the entry of a protein into the ERQC. Subsequent removal of the second glucose by GluII generates the monoglucosylated glycan $Glc_1Man_9GlcNAc_2$[ref. 108–110]. GluII is a dimeric protein with a catalytic α-subunit and an accessory β-subunit[108,111,112]. The β-subunit likely mediates contact with the client glycoprotein and retains GluII in the ER[113]. Monoglucosylated glycoproteins can engage with calnexin and calreticulin, which recruit different effector proteins involved in folding of the glycoprotein (e.g. ERp57)[ref. 114,115]. After successful folding, the glycosylated protein is released from the calnexin/calreticulin cycle and fully deglucosylated[35–37]. Again, this task is performed by GluII. The glycoprotein can then leave the ER towards the Golgi apparatus.

MHC I is a subject of this quality control process, too. After two deglucosylation events by GluI and GluII, respectively, MHC I engagement with calreticulin triggers association with the PLC, where peptide loading and editing occurs[15]. Eventually, pMHC I molecules are deglucosylated by GluII, leave the PLC, and need to disengage from calreticulin. However, the order of these events is currently unclear. Like for ERAP1 and ERAP2 it is possible that the PLC links the functions of chaperoning and loading of MHC I to the deglucosylation function of GluII by providing an interaction hub for the several interaction partners.

1.2.7. Viral immune evasion and PLC purification strategy

Viruses must hide from the adaptive immune system to mount a persistent infection in the human body. To do so, viruses evolved several different disguise strategies. One target of viruses from the *Herpes*- and *Poxviridae* is the antigen presentation pathway and especially the PLC[15,16,116]. Several viral factors have evolved to target antigen presentation in different steps (Figure 1.2-6). The large number of viral factors that directly target TAP and the PLC underline the fundamental function of peptide transport and MHC I loading in antigen presentation. Loss of TAP or the PLC function is linked to lower MHC I presentation on the cell surface and therefore detection of a viral infection is less likely[117–119]. Viruses directly targeting TAP or the PLC produce effector proteins that bind one or several components of the PLC and inhibit its functions or lead to degradation of the complex.

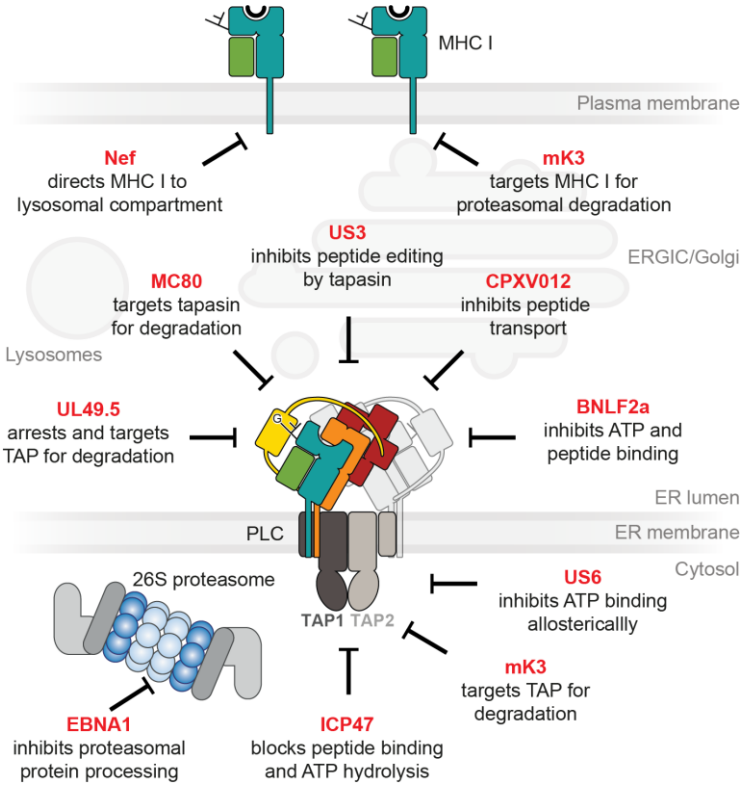

Figure 1.2-6: Viral immune evasins. Points of action for several viral immune evasion proteins in the antigen presentation pathway. Several proteins directly target TAP (dark/light grey) as centerpiece of the PLC. The herpes simplex virus (HSV) protein ICP47 blocks peptide transport by preventing peptide binding while the cytomegalovirus (CMV) protein US6 inhibits peptide transport by blocking ATP binding with its ER luminal domain. Further TAP inhibitors are BNLF2a (Ebbstein-Barr virus (EBV)), UL49.2 (HSV), and CPXV012 (cowpox virus). Other inhibitors block functions of other components of the PLC or label them for degradation. US3 (CMV) blocks the peptide editing function of tapasin while MC80 (Molluscum contagiosum virus) induces the degradation of tapasin. Similarly, mK3 (murine gammaherpesvirus 4) acts on pMHC I and TAP, and targets them for degradation by ubiquitination. The human immune deficiency virus (HIV) protein Nef redirects MHC I into lysosomal compartments instead of the cell surface. Peptide production is altered, too. The EBV protein EBNA1 inhibits the function of the proteasome. The PLC components are color coded as labeled in Figure 1.2-2. The figure is adapted from[15].

The first viral TAP inhibitor discovered was the infected cell protein 47 (ICP47) from herpes simplex virus (HSV)[(ref. 120–122)]. The protein is 88 amino acids (aa) long and the only known soluble high-affinity inhibitor of TAP ($K_d \approx 50$ nM)[(ref. 74,123,124)]. It is an unstructured protein in solution, but adopts a helix-turn-helix motive when in proximity of a membrane[125–127]. ICP47 blocks the peptide binding and transport function of TAP as well as ATP hydrolysis, while ATP binding is not impaired[121,123]. It freezes the transporter in an inward facing state and thermally stabilizes TAP[52,53,128]. The active domain has been mapped on the first 34 amino acids[124,129]. However, also the tail is involved in assisting TAP stabilization and inhibition[128,130]. The stabilizing function, as well as the soluble nature of ICP47, led to its use

as bait protein for PLC purification from Raji cells by combining it with a streptavidin binding peptide (SBP) tag for affinity purification[1,131].

Several other proteins directly interfere with TAP function and all these inhibitors are membrane embedded or anchored proteins. Human cytomegalovirus (HCMV) expresses the protein unique short sequence 6 (US6), which is a TAP inhibitor; blocking peptide transport by an ER luminal domain[132–136]. However, the peptide binding function of TAP is not impaired while ATP binding is blocked[134,136–138]. The blockage of ATP suggests an allosteric communication across the ER membrane, which arrests the transporter in a state unable to bind ATP[15]. Recent results indicate a dimerization of the NBDs, probably stabilizing TAP for structural analysis[139]. Despite distinct binding sites, ICP47 and US6 exclude the binding of each other, indicating that both inhibitors target different conformations of TAP[128,130]. Furthermore, it was discovered that viral PLC inhibition influences the composition of the PLC[140]. PLC purified by using ICP47 or US6 contained different ratios of the MHC I allomorphs HLA-A, HLA-B, and HLA-C.

1.3. Cryogenic electron microscopy

Structural biology has undergone a revolution in recent years. For many years, the field of structural biology has been dominated by crystallography and nuclear magnetic resonance (NMR), but cryogenic electron microscopy (cryo-EM) is catching up. Cryo-EM has itself undergone a "resolution revolution" with the introduction of direct electron detectors in the last decade and since is revolutionizing structural biology[141]. Improved cameras, microscopes, and algorithms for data evaluation have now pushed cryo-EM to unforeseen heights. In 2021 already almost 25% of the total number of structures deposited in the protein

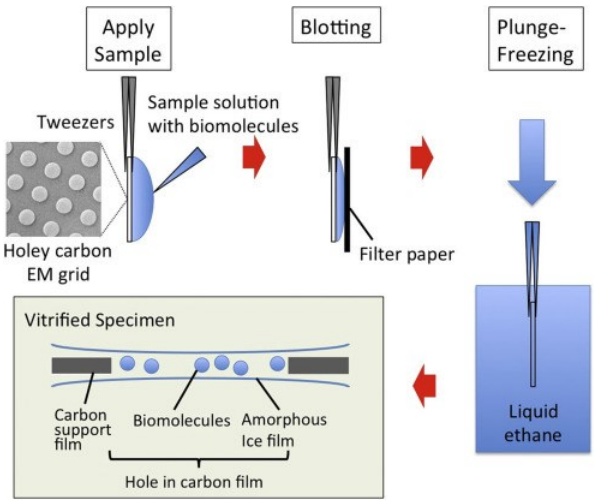

Figure 1.3-1: Sample preparation for single particle cryo-EM. Specimen preparation by plunge freezing. Aqueous solutions containing the protein of interest are applied onto a holy carbon film, supported by an EM-grid. Excess solution and specimen (>99%) is removed by a blotting paper to produce a thin film of sample. Subsequently, the sample is vitrified in liquid ethane (<160°C). Later, the proteins embedded in the thin ice layer can be imaged in the electron microscope. Figure from[246].

data base (PDB) were obtained by cryo-EM and numbers are still rising exponentially[142]. Many of these structures include proteins or assemblies that could not be resolved by other approaches.

EM uses electrons instead of light to image proteins. As they easily interact with almost all substances, imaging must be performed under very high vacuum, which is harmful for almost all biological samples. To conserve their properties, samples are embedded in thin (few µm) aqueous ice by cooling it rapidly below the vitrification temperature of water (-146° ± 4°C) in a process called plunge freezing, which prevents the formation of hexagonal ice (Figure 1.3-1)[(ref. 143)]. Sample preparation is often a major bottleneck in solving a structure by cryo-EM because the process is highly variable and requires optimization. Many factors can be altered and optimized (e.g., sample preparation, temperature, humidity, blotting conditions, grid material and geometry, buffer conditions, etc.) and the path towards good sample preparation is not necessarily straight forward. Ideally, the sample is embedded in ice only slightly thicker than the longest dimension of the sample itself to obtain maximal signal to noise levels[144,145]. Subsequently, the samples are imaged at low electron currents in the microscope. For small specimens (like proteins) usually several hundred to thousand images of the specimen are collected and analyzed by single-particle analysis (SPA)[(ref. 146,147)]. During this process, protein particles are identified on the images, extracted, corrected for imaging errors introduced by the microscope, and finally used to calculate an average 3D model of the protein or assembly of interest. If this structure is of sufficient quality and resolution it can serve as template to build an atomistic model.

1.4. Reconstitution of membrane proteins

Membrane proteins are naturally embedded in a lipid bilayer and their hydrophobic regions make them insoluble in aqueous solutions. Rendering them soluble is a prerequisite for purification and many biochemical assays, including structural analysis. Traditionally, membrane proteins are solubilized from their membrane utilizing detergents[148,149]. These amphiphilic molecules shield the hydrophobic region of a membrane protein and render them soluble due to their hydrophilic head groups. Many different detergents and derivates with a large variety of properties are commercially available. The final choice of detergent strongly depends on the individual properties of the target protein or complex and its interactions with the detergent as well as the desired application. The TAP1/2 heterodimer tolerates only solubilization by digitonin or the synthetically produced derivative glyco-diosgenin (GDN)[(ref. 1,150)]. In addition, some detergents mimic the properties of the membrane poorly, which can lead to drastic different biochemical behavior of solubilized proteins or an reduced stability[151–154]. Also structural analysis can be hampered by the background signal introduced by free detergent[148,149,155]. Therefore, alternatives for solubilization of membrane proteins for biochemical and structural analysis have been developed.

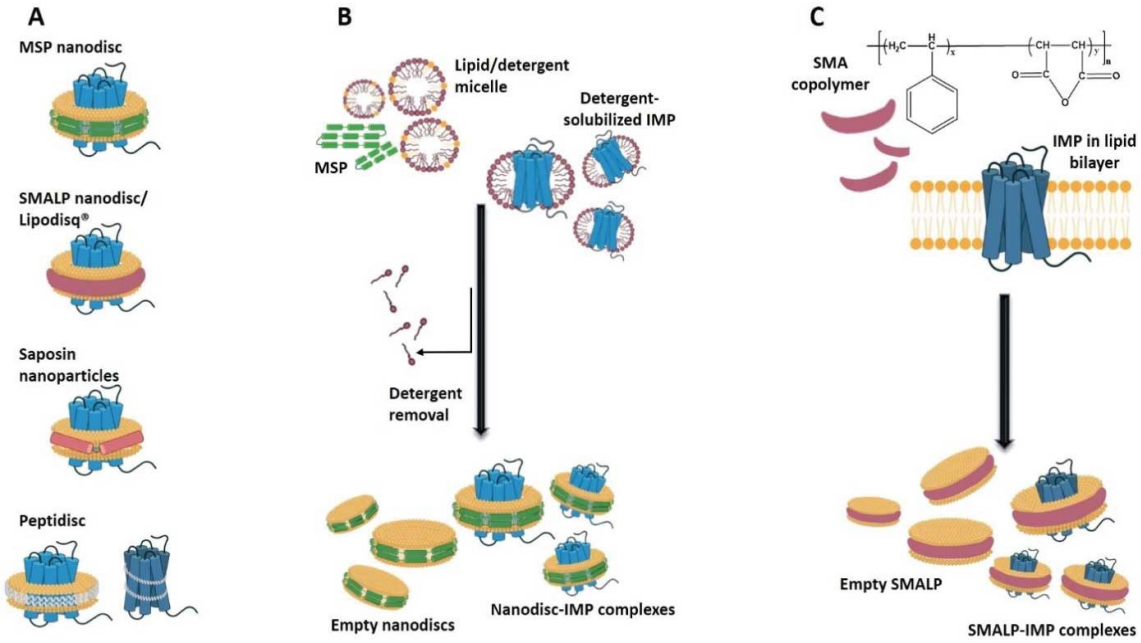

Figure 1.4-1: Membrane mimetic systems. (**A**) Schematic depiction of membrane proteins reconstituted in membrane scaffold proteins (MSP), styrene-maleic-acid copolymers (SMA) or di-isobutylene maleic acid copolymers (DIBMA), Saposin, or synthetic peptide derived discs (Peptidisc). (**B**) Membrane protein reconstitution procedure. After mixing of solubilized membrane protein with scaffold and lipids, the detergent is removed by dialysis or BioBeads. (**C**) Direct solubilization process by SMA into lipid particles (SMALPs). Figure from[149].

Detergents can be replaced for example by amphipols, which bind much stronger to membrane proteins and therefore also keep the protein in solution without free amphipol molecules in solution[156,157]. This benefits structural analysis where limited background signal is favorable. Unfortunately, the PLC does not tolerate amphipol reconstitution[158].

A set of different approaches tries to mimic the lipid bilayer of the membrane and thereby preserve membrane protein stability and function (Figure 1.4-1 A, B). The first of these systems was the nanodisc, which was developed by the Sligar laboratory[159,160]. Nanodiscs mimic the membrane by providing the membrane protein with a small patch of lipid bilayer, encapsulated by amphiphilic belt proteins called membrane scaffold protein (MSP)[(ref. 159–162)]. The MSPs are derivatives of the apolipoprotein A and encapsulate the lipid disc[163]. Nowadays, several variants of the original MSP have been developed to form nanodiscs with diameters from 8.4 to 17 nm[164,165]. Also in structural analysis by cryo-EM, nanodiscs have been established as valuable tool[166,167].

Several similar approaches have been developed in recent years. Saposin is also a belt protein, similar to the original nanodiscs[168]. In contrast, the system can flexibly adopt to the size of the protein or assembly that is reconstituted[169,170]. Therefore, one kind of scaffold protein can be used to reconstitute a variety of target proteins.

Membrane proteins can also be reconstituted in discs formed by small synthetic peptides (Peptidisc), which are also derived from the aa sequence of apoliprotein A[171]. Several amphiphilic peptides form a flexible disc and keep the reconstituted protein in solution. No additional lipids are used in this approach, minimizing the size of the disc, and retaining only essential lipids copurified with the protein of interest.

All methods require solubilization of the protein by detergent before they are reconstituted into the lipid discs. Thus, drawbacks of detergent solubilization (loss of interaction with cofactors, destabilization, loss of function, etc.) persist. This drawback was circumvented by solubilization and stabilization of membrane proteins using polymers. Two examples of polymers used in biochemistry are styrene-maleicacid copolymers (SMA) or di-isobutylene maleic acid copolymers (DIBMA)[(ref. 172,173)]. Both systems can readily extract proteins from their lipid environment and preserve a near native lipid environment (Figure 1.4-1 C)[(ref. 174)].

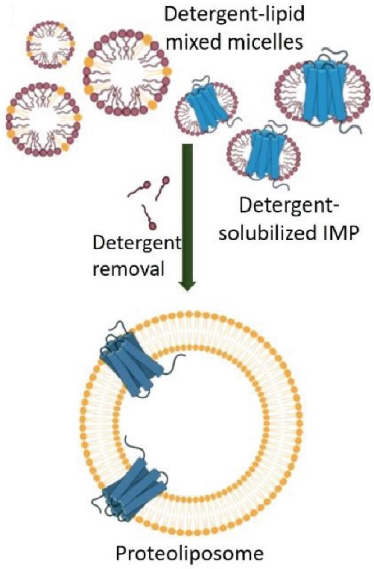

Figure 1.4-2: Reconstitution of membrane proteins in liposomes. Detergent solubilized membrane protein is incubated with destabilized liposomes. Gradually, the detergent is removed by addition of BioBeads finishing the reconstitution procedure. Figure is adapted from[149].

The lipid environment is dramatically reduced to a small patch during reconstitution of in membrane mimetic systems. Reconstitution into liposomes can be performed to obtain a full lipid environment (Figure 1.4-2). Here, purified protein is reconstituted into unilamellar lipid vesicles by incubation of solubilized protein with destabilized liposomes[175]. After removal of the detergent, the protein is stably reconstituted[176,177]. This system allows to study processes that require the presence of an intact lipid membrane (e.g., lateral diffusion, peptide transport). However, reconstitution of membrane proteins in liposomes remain challenging and requires optimization in each case[149].

2. Aims

The PLC is a central machinery in peptide loading and quality control of MHC I in the ER[16]. Despite this important function in the adaptive immune system, the structural and functional understanding of the PLC is limited. The main components, architecture, and general functions of this labile and heterogenous assembly have been solved[1,2]. However, detailed structural insights into the interactions and mechanisms are lacking. These include (i) the editing loop which is directly involved in peptide editing processes but was not resolved in tapasin structures but only in the tapasin homolog TAPBPR[1,28,60,62]. (ii) MHC I carries an N-linked glycan on Asn86, which is critically involved in the quality control of MHC I folding and peptide loading in the ER. The arrangement of the glycan within the PLC and its involvement in the quality control of MHC I within the PLC remains enigmatic. This work aims to answer these critical questions by providing a high-resolution structure of MHC I engaged in the PLC. Furthermore, the structural investigations were combined with the evaluation of the peptide-dependent glycan status of MHC I.

Given the central function of the PLC in MHC I loading, it has been speculated that several other factors are involved in the MHC I loading process and use the PLC as interaction hub. Namely, the zinc-metallopeptidases ERAP1 and ERAP2 have been suggested as putative interaction partners of the PLC[27]. Also the α-Glucosidase GluII which removes glucoses from N-linked glycans, could be structurally and functionally linked to the actions of the PLC. This PhD thesis aims to investigate the molecular sociology of the PLC and to unravel whether and how the named proteins perform their tasks in collaboration with the PLC.

Elegant purification strategies have been previously developed for the PLC[1,140]. However, these strategies rely on the use of viral inhibitors for TAP and thereby inhibit the peptide transport function of the PLC. In this work an evolved variant of a photocleavable TAP inhibitor ICP47 (pc-ICP47^{SBP}) will be evaluated for PLC purification and subsequent activation by light. Successful activation of TAP functions include peptide binding, peptide dependent ATP hydrolysis, and peptide transport. This work aims to study fully functional PLC in a sealed membrane environment (liposomes) to understand the functional interplay of TAP with the peptide editing modules as well as investigate release of MHC I after successful peptide loading and quality control.

3. Material and methods

3.1. Chemicals

General chemicals were purchased from Sigma-Aldrich or Roth. Special reagents are listed.

3.1.1. Antibodies

Table 1: Antibodies used in this study. IB = immunoblotting, FC = flow cytometry, SEC = size exclusion chromatography

Target protein	Antibody	Host	Application	Supplier	Dilution
TAP1	148.3 [178]	Mouse	IB FC	in house	1:20 20 µM
TAP2	483.3 [21]	Mouse	IB FC	in house	1:20 20 µM
tapasin	ab13518	Rabbit	IB	Abcam	1:1000
ERp57	ab10287 ab13506	Rabbit Mouse	IB FC	Abcam Abcam	1:1000 20 µM
HLA-A/B/C	HC10 AM33035PU-N	Mouse	IB FC	Acris Antibodies	1:300 20 µM
HLA-A	ab52922	Rabbit	IB	Abcam	1:1000
Loaded HLA	W6/32^{AF647} W6/32	Mouse Mouse	FC SEC	Biolegend Biolegend	20 µM 3x excess
calreticulin	C4606 ab22683	Rabbit Mouse	IB FC	Sigma-Aldrich Abcam	1:1000 660 µM
β_2m	HPA006361	Rabbit	IB	Novo Antibodies	1:1000
SBP	sc-101595	Mouse	IB	Santa Cruz	1:500
His6	H1029	Mouse	IB	Sigma-Aldrich	1:1000
IgG mouse	A-21235	Goat	FC	Thermo Fisher	80 nM
IgG rabbit	A-21244	Goat	FC	Thermo Fisher	80 nM

3.1.2. Chemicals and reagents

Chemical	Supplier
[γ-^{32}P]ATP	Hartmann Analytik
10x MOPS buffer	Thermo Fisher Scientific
^{3}H-ATP	Perkin-Elmer
4-12% Nu-PAGE Bis-Tris protein gel	Thermo Fisher Scientific
Alexa Fluor 647 C_2 maleimide	Thermo Fisher Scientific
Amersham Hybond P 0.2 µm PVDF membrane	Cytiva
Amicon Ultra 15 centrifugal filter (10 kDa)	Merck
Amicon Ultra 15 centrifugal filter (3 kDa)	Merck

Chemical	Supplier
Amicon Ultra centrifugal filter (100 kDa)	Merck
BioBeads SM-2 adsorbent media	Sigma Aldrich
Bovine brain lipids fraction V	Sigma Aldrich
C-Clip	FEI
C-Clip ring	FEI
Clarity Western ECL reagent	BioRad
DIBMA (Sokalan CP9)	BASF
DiD	Thermo Fisher Scientific
DOPC	Avanti polar lipids
E. coli polar lipid extract	Avanti polar lipids
Fetal calf serum	Capricorn
Glyco-diosgenin (GDN)	Anatrace
Gravity flow column	BioRad Laboratories Inc.
Hepes buffer (1 M)	Gibco
InstantBlue	Expedon
MicroBeta counter	Wallace
Ni-NTA agarose resin	Quiagen
NuPAGE 12% Bis-Tris	Thermo Fisher Scientific
PageRuler prestained protein ladder	Thermo Fisher Scientific
Pierce High Capacity Streptavidin Agarose	Thermo Fisher Scientific
PNGase F	NEB
Protease inhibitor mix	Serva
Quantifoil R0.6/1	Quantifoil MicroTools
Quantifoil R1.2/1.3	Quantifoil MicroTools
RPMI 1640	Gibco
Slide-A-Lyzer dialysis cassette (10 kDa)	Thermo Fisher Scientific
SMA 1:1,2 Xiran SL40005 P20	Polyscope
SMA 1:2 Xiran SL30010 P20	Polyscope
SMA 1:3 Xiran SL25010 P20	Polyscope
SCPA (SPA) beads	Perkin-Elmer
TLC PEI-Cellulose F	Merck
Trypsin Gold	Promega
UltrAuFoil R1.2/1.3	Quantifoil MicroTools
Whatman 595 filter papers	Cytiva
Zeba Spin desalting column (7 kDa MWCO)	Thermo Fisher Scientific

3.1.3. Devices and accessories

Device / Accessory	Manufacturer
ACQUITY UPLC Peptide BEH C_{18} column, 130 Å 1.7 µm, 2.1 mm x 100 mm	Waters
ACQUITY UPLC Protein BEH C_4 column, 300 Å 1.7 µm, 2.1 mm X 150 mm	Waters
Agilent, 1200 Series System	Agilent
Äkta Ettan	General Electric

Device / Accessory	Manufacturer
Äkta Go	General Electric
BD FACSMelody Cell Sorter	BD Biosciences
CLARIOstar,	BMG Labtech
LC-MS, BioAccord	Waters
Liberty Blue peptide synthesizer	CEM
Nanodrop spectrophotometer ND-1000	PEQLAB Biotechnologie GmbH
NanoSight LM10	Malvern
Pelco easiGlow glow discharge	TED Pella Inc.
PerfectSil 300 ODS C_{18} 5 µm 300 x10 mm	MZ-Analysentechnik
Personal molecular imager	BioRad
Scintillation reader	Wallac MicroBeta
Shimadzu HPLC	Shimadzu
Shodex KW404-4F	Shodex
Superdex 200 Increase 10/300 GL column	Cytiva
Superose 6 increase 3.2/300	Cytiva
TEM, F30	Thermo Fisher
TEM, KRIOS	Thermo Fisher
TEM, Tecnai Spirit	Thermo Fisher
Trans-Blot Turbo	BioRad
Ultima XE 90	Beckmann Coulter
Vilber Fusion X	Vilber
Vitrobot Mark IV	Thermo Fisher
WX-80 ultracentrifuge	Thermo Fisher
λ=365 nm diode M365L2, adjustable SM2 lens tube, powered and controlled by a DC2200	ThorLabs

3.1.4. Peptides

Table 2: Peptides used in this study. ^{F} indicates labelling with fluorescein, ^{AF647} indicates labelling with AF647. *indicates predicted affinities by NetMHCpan version 4.1b[179]. Ψ indicates hPhe(PO(OAd)-CH_2)-GlyOH.

Identifier	Sequence	Target protein	Affinity
CSN **C^{F}SN**	AIFCSNMTK AIFC^{F}SNMTK	HLA-A*03:01	20 nM*
HYC **HYC^{F}**	THYCAPRRL THYC^{F}APRRL	HLA-B*15:10	400 nM*

Identifier	Sequence	Target protein	Affinity
C4F	RRYC^{F}KSTEL	TAP1/2 HLA-A*03:01	146 nM[180] 20 µM*
R9L	RRYQKSTEL	TAP1/2 HLA-A*03:01	146 nM[180] 20 µM*
NST^{F}	RRYQNSTC^{AF647}L	TAP1/2 and ER glycosylation	high[181]
DG057	H-hFΨ(P(O)(OH)CH_2)GGSGSGSQFGGGSQY	ERAP1 ERAP2 HLA-A*03:01	25 nM[4] 15 nM[4] n.d.

3.2. Cell culture

3.2.1. Raji cell culture

Raji cells (Raji ATCC CCL-86) were cultivated at 37°C and 5-8% CO_2. The cells were maintained in RPMI 1640 (Gibco) supplemented with 10% FCS (Capricorn) and 3 mM Hepes-NaOH pH 7.2 – 7.5 (Gibco). For large scale culture the cells were grown under continuous shaking (125 rpm) in 1 L Erlenmeyer-flasks in a shaking incubator (Eppendorf). Cells were harvested by centrifugation (1000 xg, 3 min), snap frozen in liquid nitrogen and stored at -80°C until used.

For long term storage of viable cells, they were centrifuged (3 min, 400 xg) and resuspended in freezing medium (FCS + 10% (v/v) DMSO) and transferred in cryo-tubes. The cells were slowly frozen (1 K/min) at -80°C.

3.3. Protein biochemistry

3.3.1. Expression and purification of ICP47^{SBP}, ICP47^{His6}, and ICP47^{AF647}

The ICP47^{SBP} and ICP47^{His6} sequence were cloned into a pETM-11 (European Molecular Biology Laboratory, EMBL) using the NcoI and BamHI restriction sites. Both proteins were produced and purified in a similar way. The vector was transformed into competent *E. coli* One Shot BL21(DE3) cells (Thermo Fisher) and grown to OD_{600} = 0.6 at 37 °C, 125 rpm. Expression was induced with 0.2 mM isopropyl-β-D-thiogalactoside (IPTG) for 6 h at 22 °C. The cells were lysed by sonification in 50 mM Na_2HPO_4/NaH_2PO_4 pH 8.0, 150 mM NaCl, 20 mM imidazole, 0.2% (v/v) Tween 20, 2 mM DTT, supplemented with 2.5 mM PMSF, 3.75 mg/mL lysozyme, 6.25 mM benzamidine, 1.25 U/µL DNAse, and 0.75 µL benzonase (10 KU/mL). His_6-TEV-ICP47^{SBP} or His_6-TEV-ICP47^{His6} was separated from the lysate via reverse IMAC (Ni-NTA Agarose resin, QIAGEN). After washing with 50 mM NaH_2PO_4 pH 8.0, 150 mM NaCl, 20 mM imidazole, 0.2% (v/v) Tween 20, 10 mM DTT, ICP47^{SBP} was eluted supplementing the wash buffer with 500 mM imidazole. The His_6 tag was removed by overnight TEV protease (in house prepared) digestion. Finally, ICP47^{SBP} or ICP47^{His6} were

purified by reversed phase C_{18} HPLC (Agilent, 1200 Series System; PerfectSil 300 ODS C_{18} 5 µm 300 x10 mm) applying a linear water/acetonitrile gradient from 5-60% (v/v) supplemented with 0.1% (v/v) TFA.

$ICP47^{AF647}$ was purified and labeled by Christian Winter, Goethe University Frankfurt.

$ICP47^{V86C\text{-}SBP}$ was produced in the same way as $ICP47^{SBP}$. $ICP47^{V86C\text{-}SBP}$ was labeled with 1.2 molar excess of Alexa Fluor 647 C_2 maleimide (AF647, Thermo Fisher) in phosphate-buffered saline (PBS) pH 7.2 with 20% (v/v) DMF and 2.5 mM tris(2-carboxyethyl)phosphine (TCEP) for 4 h at RT. $ICP47^{AF647}$ was purified by reversed phase C_{18} HPLC applying a linear water/acetonitrile gradient from 5-60% (v/v) supplemented with 0.1% (v/v) TFA. The identity of $ICP47^{AF647}$ was confirmed by LC-MS analysis. M_{calc}: 15,938.55 Da, M_{obs}: 15,938.77 Da.

3.3.2. Production of pc-$ICP47^{SBP}$

$pc\text{-}ICP47^{SBP}$ was designed and produced by Christian Winter, Goethe University Frankfurt, from synthetically produced $pc\text{-}ICP47_{2\text{-}23}^{\text{-Hmp}}$ and $^{Cys}ICP47^{SBP}$ as described in [182].

$pc\text{-}ICP47_{2\text{-}23}^{\text{-Hmp}}$ synthesis: 0.2 mmol of Tentagel S RAM (0.22 mmol/g resin substitution; Rapp Polymere) were pre-swollen in dimethylformamide (DMF). The terminal fluorenylmethoxycarbonyl protecting group (Fmoc) was removed by treatment with 20% (v/v) piperidine in DMF for 15 min, at 22 °C with heavy agitation. Hmp(Trt)-OH was coupled to the resin two times, using a premixed solution of 6 mmol Hmp(Trt)-OH, 5 mmol N,N-diisopropylcarbodiimide (DIC, 0.5 M), and 5 mmol of hydroxybenzotriazole (HOBt, 0.5 M) in DMF for 60 min. The first amino acid (Tyr23) was coupled via Mitsunobu reaction dissolving 2 mmol Fmoc-Tyr(tBu)-OH in 2 mmol triphenylphosphine in 3.8 mL of THF. The solution was added to the resin and cooled to -20 °C. 2 mmol diisopropyl azodicarboxylate (DIAD, 40% (v/v) in toluene) were chilled to 20 °C and added slowly to the resin over a period of 20 min. After 2 h with heavy agitation at room temperature (RT), the reaction solution was removed. The remaining amino acids (Carbolution) were sequentially coupled to the Hmp(Trt)-Tyr(tBu)-loaded resin using standard Fmoc SPPS double coupling conditions on a Liberty Blue Peptide Synthesizer (CEM). (R)-3-(Fmoc-amino)-3-(2-nitrophenyl)propionic acid (Anp, Alfa Aesar) was coupled twice for 30 min at 50 °C. The peptide was protected from light and cleaved in 87.5% (v/v) trifluoroacetic acid (TFA), 5% (v/v) thioanisole, 2.5% H_2O, 2.5% triisopropylsilane (TIPS), 2.5% (v/v) 1,2-ethanethiol (EDT) for 2 h at RT. The product was precipitated in ether at -20 °C, dried over vacuum, and purified by C_{18} RP-HPLC. The identity was verified by LC-MS: $pc\text{-}ICP47_{2\text{-}23}$-Hmp: M_{calc}: 2,636.1788 Da, M_{obs}: 2,636.1753 Da.

^{Cys}ICP47^{SBP} production and purification: The His$_6$SUMO-^{Cys}ICP47^{SBP} sequence was cloned into a pETM 11 (European Molecular Biology Laboratory, EMBL) using the SapI restriction site. The vector was transformed into competent *E. coli* One Shot BL21(DE3) cells and grown to OD_{600} = 0.7 at 37 °C. Expression was induced with 0.2 mM IPTG for 4 h at 22 °C. The cells were lysed by sonification in Ni-NTA buffer, supplemented with 2.5 mM PMSF, 3.75 mg/mL lysozyme, 6.25 mM benzamidine, and 1 U/mL benzonase. His$_6$SUMO-^{Cys}ICP47^{SBP} was isolated from the lysate by reverse-IMAC. After washing thrice with Ni-NTA buffer (50 mM Na_2HPO_4/NaH_2PO_4 pH 8.0, 150 mM NaCl, 20 mM imidazole, 0.2% (v/v) Tween 20, 2 mM DTT), His$_6$SUMO-^{Cys}ICP47^{SBP} was eluted supplementing the wash buffer with 500 mM imidazole. The imidazole concentration was lowered to 20 mM by repetitive ultrafiltration (Amicon Ultra-15, 3 kDa MWCO). The His$_6$SUMO-tag was removed by overnight ULP1 protease digestion. ^{Cys}ICP47^{SBP} was purified by reversed phase C_{18} HPLC (Agilent, 1200 Series System; PerfectSil 300 ODS C_{18} 5 µm 300x10 mm) applying a linear water/acetonitrile gradient from 5-50% (v/v) supplemented with 0.1% (v/v) TFA. Degassed buffers were always used to prevent oxidation. The identity of ^{Cys}ICP47^{SBP} was confirmed by LC-MS analysis. M_{calc}: 12,514.57 Da, M_{obs}: 12,514.61 Da.

Native chemical ligation of pc-ICP47$^{23Cys\text{-}SBP}$: 1.0 molar equivalents (eq) of ^{Cys}ICP47^{SBP} (1 mM) were ligated to 1.2 eq pc-ICP47$_{2\text{-}23}$-Hmp. pc-ICP47$_{2\text{-}23}$-^{Hmp} was dissolved in a ligation solution containing 5 M guanidine hydrochlorid (GdmCl), 150 mM 4-mercaptophenyl-acetic acid (MPAA), 150 mM TCEP, 200 mM Na_2HPO_4 pH 7.0 and 20% (v/v) hexafluoroisopropanol (HFIP) were added to the solution. The pH was adjusted before dissolving pc-ICP47$_{2\text{-}23}$-Hmp, since high local concentrations of NaOH can destroy Hmp. The solution was flushed with argon and added to ^{Cys}ICP47^{SBP}. The ligation reaction was incubated for 5 h and monitored by LC-MS by acquiring 1 µL aliquots of the reaction mixture in an argon chamber. The samples were diluted with 19 µL 200 mM TCEP in H_2O + 0.1% (v/v) formic acid, pH 2.0. pc-ICP47$^{23Cys\text{-}SBP}$: M_{calc}: 15,031.31 Da, M_{obs}: 15,031.58 Da.

Desulfurization of pc-ICP47$^{23Cys\text{-}SBP}$: The ligation cocktail containing pc-ICP47$^{23Cys\text{-}SBP}$ was prepared for desulfurization by removal of excess MPAA by rapid-spin size exclusion chromatography purification, using a Zeba Spin Desalting Column (7 K MWCO, Thermo Fisher), equilibrated with desulfurization buffer (150 mM TCEP in 5 M GdmCl, pH 7.05). The solution was flushed with argon and 15% (v/v) 2-methylpropane-2-thiol (tBuSH) were added. The reaction was started by addition of 10 mM 2,2'-azobis-[2-(2-imidazolin-2-yl)propane]dihydro-chloride (VA-044). Complete desulfurization was achieved after 35 min at 42 °C. The exact matching of reaction time and temperature is essential for quantitative desulfurization since the radical desulfurization mechanism can also destroy the photolabile orthonitrobenzene on Anp. The reaction was monitored by LC-MS and purified by C_{18} RP-HPLC, applying a linear water/acetonitrile gradient from 5-50% (v/v) supplemented with 0.1% (v/v) TFA. pc-ICP47^{SBP} yield: 85%; M_{calc}: 14,999.24 Da, M_{obs}: 14,999.37 Da.

3.3.3. Expression and purification of MSP2N2

The plasmid pMSP2N2 was a gift from Stephen Sligar (Addgene plasmid #29520). Membrane scaffold protein MSP2N2 was expressed and purified as described (Grinkova et al., 2010). In brief, MSP2N2 was expressed in *E. coli* BL21(DE3) grown in LB media supplemented with 0.5% (w/v) glucose at 37 °C. At an OD_{600} = 0.8, expression was induced with 1 mM IPTG and cells were grown for 1 h at 37 °C. Subsequently, the temperature was lowered to 28 °C and cells were grown for 4 h. Cells were disrupted by sonication in lysis buffer (50 mM Tris-HCl pH 8.0, 500 mM NaCl, 1% (v/v) Triton X-100, 4% (w/v) Na-deoxycholate, protease inhibitor mix (Serva)). The protein was purified via its N-terminal His_7-tag by incubating the lysate with Ni-NTA Agarose resin (Quiagen) and eluted with imidazole (25 mM Hepes-NaOH pH 7.5, 500 mM NaCl, 300 mM imidazole). To remove imidazole, MSP2N2 was dialyzed against storage buffer (25 mM Hepes-NaOH pH 7.5, 250 mM NaCl, 10% (v/v) glycerol), aliquoted, snap-frozen in liquid nitrogen and stored at -80 °C.

3.3.4. Expression and purification of Saposin A

The Saposin A-encoding plasmid was kindly provided by Jens Frauenfeld (Salipro AB, Stockholm, Sweden) within the context of a material transfer agreement. Saposin A was expressed and purified as described[168]. In brief, Saposin A was expressed in *E. coli* Rosetta-gami 2(DE3) grown in TB medium supplemented with ampicillin (100 µg/mL) and kanamycin (30 µg/mL). Protein production was induced by the addition of 1 mM IPTG. Cells were resuspended in Saposin lysis buffer (20 mM Hepes-NaOH, pH 7.5, 150 mM NaCl, 20 mM imidazole), disrupted by sonication, and the lysate centrifuged for 30 min at 26,000 xg. The supernatant was heated to 85 °C for 10 min and again centrifuged for 30 min at 26,000 xg. Saposin A was purified via its N-terminal His6-tag by incubating the lysate with Ni-NTA Agarose resin (Quiagen). To remove imidazole, Saposin A was dialyzed overnight against Saposin SEC buffer (20 mM Hepes-NaOH, pH 7.5, 150 mM NaCl). Finally, Saposin A was purified via SEC (Superdex 200 Increase 10/300 GL, Cytiva). Peak fractions were concentrated using Amicon Ultra-15 mL centrifugal filters with a 3 kDa cut-off (Millipore), snap frozen in liquid nitrogen, and stored at -80 °C.

3.3.5. Expression and purification of ERAP1 and ERAP2

Expression and purification of ERAP1 and ERAP2 were performed by George Mavridis, supervised by Efstratos Stratikos from the National Centre for Scientific Research Democritos in Athens, Greece.

High-five (Hi5) insect cells were grown in Sf-900II culture medium (Thermo Fisher Scientific) at 27 °C. Infection with recombinant baculovirus was carried out in 50 mL flasks at a cell density of 1–1.5 x 10^6 cells/mL, and incubation was continued by gentle shaking at

27 °C for 72 h. The culture medium was centrifuged (4500 xg, 15 min, 4 °C), and the supernatant was dialyzed overnight against buffer containing 10 mM NaH_2PO_4, pH 8.0, 100 mM NaCl. Supernatant was then equilibrated to binding buffer (50 mM NaH_2PO_4, pH 8.0, 300 mM NaCl, 10 mM imidazole). Batch binding onto nickel-nitrilotriacetic acid–agarose beads (Thermo Fisher Scientific) was achieved by mild rotation at 4 °C for 2 h. Supernatant and beads were afterwards loaded to a nickel-nitrilotriacetic acid column and washed several times with buffer: 50 mM NaH_2PO_4, pH 8.0, 300 mM NaCl, 10-30 mM imidazole. Elution was performed by 50 mM NaH_2PO_4, pH 8.0, 300 mM NaCl, 150 mM imidazole. Final dialysis of elution fractions was conducted overnight against 10 mM Hepes-NaOH, pH 7.0, 100 mM NaCl. Protein aliquots were kept at -80 °C after the addition of 10% (v/v) glycerol.

3.3.6. Expression and purification of GluII

Expression and purification of GluII was performed by Mario Hensen supervised by Nicole Zitzmann from the Oxford Glycobiology Institute, Department of Biochemistry, University of Oxford, Great Britain.

The *M. musculus* GANAB (α-GluII α-subunit, Uniprot accession no.: Q8BHN3-2 with the amino acid substitution F724G) and *M. musculus* PRKCSH (α-GluII β-subunit, Uniprot accession no.: O08795 with the amino acid substitutions L88P_S90N) were cloned into the mammalian expression vector pHLsec carrying a C-terminal His_6- or a N-terminal FLAG-tag, respectively.
Co-transfection into the FreeStyle 293 Expression System (Life Technologies) took place following the manufactures protocol. Cells were maintained for four days at 37 ˚C, 8% CO_2, shaking at 135 rpm. Cells were pelleted by centrifugation at 3,000 ×g, 45 min. The supernatant was adjusted to 1x PBS (pH 7.4) and sterile filtered. The whole sample was applied to a HisTrap excel (GE LifeSciences) column pre-equilibrated with 1x PBS and subsequently washed with 5 mM imidazole, 1x PBS. Elution took place using 10 column volumes of 350 mM imidazole, 5% (w/v) glycerol, 1x PBS. The imidazole containing buffer of the eluate was exchanged with 5% (w/v) glycerol, 1x PBS using Ultra-15 spin concentrator (Amicon, 30 kDa MWCO) and the concentrated sample applied to a Superdex 200 16/600 column (GE Lifesciences) pre-equilibrated with 20 mM Hepes-NaOH, pH 7.5, 150 mM NaCl.

3.3.7. Processing of mammalian spleen for PLC purification

Fresh spleens were obtained from the slaughterhouse. Processing of the spleens was performed at 4 °C or on ice. Omitting connective tissue, the pulpa was removed from the spleen and coarsely homogenized by squeezing through a sieve. Homogenized spleen tissue was incubated in hemolysis buffer (5.6 mM NH_4Cl, 11.9 mM $NaHCO_3$, 0.137 mM EDTA) on ice for 1 min under gentle shaking and centrifuged for 5 minutes, 1000 xg, 4 °C. The

supernatant was discarded, and the procedure was repeated 3 to 5 times until a pale, pink pellet was obtained. Pellets were frozen in liquid nitrogen and stored at -80 °C until further use.

3.3.8. Purification of PLC

PLC was isolated from human Burkitt's lymphoma cells (Raji) or processed mammalian spleen. Frozen cells or spleen pellets were thawed and resuspended in 20 mM Hepes-NaOH pH 7.4, 150 mM NaCl, 10 mM $MgCl_2$, protease inhibitor mix (Serva) and incubated with $ICP47^{SBP}$ for 15 min. Membranes were mixed with 2% (w/v) glyco-diosgenin (GDN, Anatrace) by douncing and incubated for 2 h, 4 °C under agitation. Insoluble material was removed by centrifugation (45 min, 100,000 xg). $ICP47^{SBP}$ tagged PLC was bound to Streptavidin High-Capacity Agarose (Pierce) and washed extensively. Either PLC was directly eluted in elution buffer (20 mM Hepes-NaOH pH 7.4, 150 mM NaCl, 0.05% (w/v) GDN, 2.5 mM biotin) (PLC::GDN) or reconstituted in a membrane mimetic system.

3.3.9. PLC reconstitution in MSP2N2 (on beads)

PLC bound to Streptavidin High Capacity Agarose (Pierce) was reconstituted in MSP2N2 nanodiscs in a molar ratio of 1:40:500 (PLC:MSP2N2:lipids). First, PLC was incubated with bovine brain lipids (Sigma) for 15 min, 4 °C under constant agitation in buffer with reduced detergent content (20 mM Hepes-NaOH pH 7.4, 150 mM NaCl, 0.003% (w/v) GDN). Afterwards, MSP2N2 was added and incubated for further 30 min at 4 °C. To induce nanodisc formation, BioBeads (Bio-Rad) were added and incubated for 1 h at 4 °C under constant agitation. Additional BioBeads were added for 1 h, 4 °C. The agarose resin was washed extensively with buffer without detergent (20 mM Hepes-NaOH pH 7.4, 150 mM NaCl) and reconstituted PLC::MSP2N2 was eluted by biotin (20 mM Hepes-NaOH pH 7.4, 150 mM NaCl, 2.5 mM biotin). For subsequent experiments, PLC::MSP2N2 was concentrated using a 100 kDa MWCO filter concentrator (Amicon).

3.3.10. PLC reconstitution in Peptidisc (on beads)

Reconstitution of PLC in Peptidisc was performed similar to MPS2N2 reconstitution. PLC bound to Streptavidin High-Capacity Agarose (Pierce) was reconstituted in Peptidisc (Peptidisc biotech) by incubation 0.2 mg/mL Peptidiscs in low GDN buffer (20 mM Hepes-NaOH pH 7.4, 150 mM NaCl, 0.003% (w/v) GDN) for 1 h, 4 °C under agitation. Afterwards the beads were washed with detergent free buffer (20 mM Hepes-NaOH pH 7.4, 150 mM NaCl) and eluted with biotin (20 mM Hepes-NaOH pH 7.4, 150 mM NaCl, 2.5 mM biotin). For subsequent experiments, PLC::Peptidisc was concentrated using a 100 kDa MWCO filter concentrator (Amicon).

3.3.11. PLC reconstitution in Saposin A (on beads)

Reconstitution of PLC in Saposin A was performed similar to MPS2N2 reconstitution. PLC bound to Streptavidin High-Capacity Agarose (Pierce) was reconstituted in Saposin by incubation with Saposin solution (0.45 mg/mL Saposin A, and 0.25 mg/mL bovine brain lipids in low GDN buffer (20 mM Hepes-NaOH pH 7.4, 150 mM NaCl, 0.003% (w/v) GDN)) for 1 h, 4 °C, agitation. Afterwards the beads were washed with detergent free buffer (20 mM Hepes-NaOH pH 7.4, 150 mM NaCl) and eluted with biotin (20 mM Hepes-NaOH pH 7.4, 150 mM NaCl, 2.5 mM biotin). For subsequent experiments, PLC::Saposin was concentrated using a 100 kDa MWCO filter concentrator (Amicon).

3.3.12. PLC reconstitution in liposomes

Liposomes were generated from 70% *E. coli* polar lipids, 30% DOPC, and <1% DiD for fluorescence detection of liposomes in flow cytometry experiments. Lipids were solved in chloroform and dried by vacuum evaporation. Lipids were resolved in reconstitution buffer (20 mM MES-NaOH pH 6.8, 150 mM NaCl) with a final lipid concentration of 10 g/L. The liposomes were sonicated for 30 min and subjected to five freeze-thaw cycles. Before protein reconstitution, the liposomes were extruded using a 400 nm polycarbonate filter.

PLC was purified in detergent (PLC::GDN) and incubated with Triton X-100 destabilized liposomes[175]. Liposome sealing was induced by four consecutive BioBead additions at 4°C (1 h, overnight, 2 h, 2 h). Reconstituted liposomes were harvested by centrifugation at 270,000 xg, 30 min, 4 °C, and resuspended in reconstitution buffer (20 mM MES-NaOH pH 6.8, 150 mM NaCl) at a lipid concentration of 5 mg/mL.

3.3.13. PLC solubilization with SMA/DIBMA

PLC solubilization with SMA and DIBMA was performed like the purification in GDN. However, SMA or DIBMA were used instead of GDN for solubilization, and no additional detergent was used in any buffer. SMA (1:1,2; 1:2; 1:3) and DIBMA were used at a concentration of 2% (w/v) for solubilization. The purification was performed with ICP47^{SBP} as described in 3.3.8.

3.3.14. ERAP1/2 peptide loading complex pulldown assay

Purified PLC was bound on high-capacity streptavidin-agarose beads (Pierce) after purification from Raji cells and incubated for 30 min, 4 °C on an overhead rotor with a 4-fold molar excess of either DG057, ERAP1, ERAP2, or a mixture of ERAP1/ERAP2. In addition, ERAP1, ERAP2, or ERAP1/ERAP2 mixture was incubated for 30 min with equimolar ratios of the peptide DG057 before incubation with the PLC for 30 min, 4 °C on an overhead rotor. The supernatant was collected, and the beads were washed three times with buffer (20 mM Hepes-NaOH, pH 7.5, 150 mM NaCl, 0.02% (w/v) GDN, 1.25 mM benzamidine, 0.5 mM

PMSF). The PLC was eluted by boiling in 5x SDS-PAGE loading buffer. Protein pulldown was analyzed by SDS-PAGE (4–12% BisTris gels). A schematic description can be found in Figure 4.6-1 A.

3.3.15. Size exclusion chromatography

Size exclusion chromatography (SEC) was used for analysis and final purification step for proteins. PLC analysis was mainly performed on a Shimadzu HPLC system equipped with a KW404-4F (Shodex) or a Superose 6 increase 3.2/300 (Cytiva) equilibrated in running buffer dependent on protein purification (stated with each protein or experiment). Both columns were also used on a Äkta micro FPLC. For purification of larger amounts of proteins an Äkta pure system equipped with a Superdex 200 Increase 10/300 GL (Cytiva) was used. Signals were recorded at A_{280}, $F_{280/340}$, and when applicable at fluorophore dependent fluorescence channel indicated with the respective experiment.

3.3.16. Size exclusion analysis of ERAP1/2 – PLC interaction

3.5 pmol of purified PLC were incubated with ERAP1, ERAP2, or ERAP1/2 mixtures in the presence or absence of the peptide DG057 as described above (3.3.14) for 30 min at 4 °C, respectively. SEC analysis was performed with a Shimadzu HPLC system equipped with a KW404-4F column (Shodex) in running buffer (20 mM Hepes-NaOH, pH 7.5, 150 mM NaCl, 0.01% (w/v) GDN).

3.3.17. Peptide synthesis – DG057

Peptide synthesis of DG057 was performed by Angelos Lelis, supervised by Dimitris Georgiadis, National and Kapodistrian University of Athens, Greece.

The phosphinic peptide DG057 (H-hFΨ(P(O)(OH)CH_2)GGSGSGSQFGGGSQY-OH, Figure 4.6-1) was prepared by applying standard solid-phase peptide synthesis on trityl alcohol lanterns (15 µmol/pin) using an Fmoc based coupling chemistry. Trityl alcohol lanterns were converted to the corresponding trityl chloride by using a solution of acetyl chloride in dry dichloromethane (1:10, v/v) at RT. The first amino acid for the synthesis of DG057, Fmoc-Tyr(tBu)-OH, was coupled with a loading of 11.1 µmol/pin. Fmoc deprotection was achieved by soaking the lanterns into a solution of 20% (v/v) piperidine in N,N-dimethylformamide over 1 h for each cycle of the synthesis. Fmoc-protected amino acids (45 µmol/pin) were coupled to the developing peptide by using 1-hydroxybenzotriazole (45 µmol/pin), and N,N-diisopropylcarbodiimide (45 µmol/pin) in dichloromethane/N,N-dimethylformamide (6:1) (0.4 mL/pin), and each coupling reaction was allowed to proceed for 5 h. Side-chain protected amino acids used were as follows: Fmoc-Tyr(^{t}Bu)-OH, Fmoc-Gln(Trt)-OH, Fmoc-Ser(^{t}Bu)-OH, Fmoc-Trp(Boc)-OH, and Fmoc-Arg(Pbf)-OH. Coupling of the building block Boc-(R)-hPhe(PO(OAd)-CH_2)-GlyOH (23 µmol/pin) was performed using the coupling conditions described above (36 µmol/pin of each reagent). Deprotection and removal of the final

pseudopeptides from the polymer support was accomplished by using a solution of TFA/dichloromethane/triisopropylsilane/H_2O (39:58:2:1) for 3 h at RT. After concentration *in vacuo*, the crude products were precipitated in cold diethyl ether. DG057 was obtained after purification by analytical reverse-phase HPLC and characterized by MS. DG057: electrospray-MS m/z (z = 1): M_{cal} 1528.6; M_{obs}: 1528.5. Lyophilized peptide was solved in H_2O.

Synthesis of the building block Boc-(R)-hPhe(PO(OAd)-CH_2)-GlyOH is described in detail in[4].

3.3.18. Peptide binding assay

Binding of fluorescently labeled peptides C^FSN, HYC^F, or C4F was analyzed by fluorescence polarization. The initial polarization of 75 nM fluorescent peptide in buffer was analyzed at $\lambda_{ex/em}$ of 485/520 nm using a microplate reader (CLARIOstar, BMG LABTECH). Afterwards, PLC::MSP2N2 or PLC::GDN was added to a final concentration of 75 nM, and the sample was mixed by shaking 5 s before polarization recording (500 rpm, double orbital mode). 150 µM competitor peptide CSN, R9L, or HYC, were added and the measurement was continued. The fluorescence anisotropy was calculated using:

$$r = \frac{I_{\parallel} - I_{\perp}}{I_{\parallel} + 2 \times I_{\perp}}$$

Resulting curves were fitted using OriginPro 2020 by a linear fit for constant data (fitting function: y = a + b*x), exponential fitting with either one factor for binding and R9L competition (fitting function: $y = y_0 + A*\exp(R_0*x)$) or two factors for CSN competition (fitting function: $y = A_1*\exp(-x/t_1) + A_2*\exp(-x/t_2) + y_0$).

3.3.19. Thermostability assay

Thermostability of PLC::GDN and PLC::MSP2N2 was determined with SEC purified PLC. Purified PLC was aliquoted in 20 µL aliquots, incubated for 60 min in a gradient thermocycler (Biometra) in the temperature range from 4 °C to 70 °C. Samples were analyzed by SEC at $F_{280/340}$. The peak height was evaluated, and the resulting sigmoidal curve was fitted in OriginPro 2020 using a Boltzmann fit.

3.3.20. SDS-PAGE

Proteins were separated based on their molecular mass by sodium dodecyl sulfate-polyacrylamide gel electrophoresis (SDS-PAGE). For PLC samples, either NuPAGE 4-12% Bis-Tris gels (Thermo Fisher) or self-casted 11% gels (stacking gel: 6% (v/v) polyacrylamide, 190 mM TRIS-HCl pH 6.8, 0.12 % (w/v) APS, 0.01% (v/v) TEMED; separation gel: 11% (v/v) polyacrylamide, 380 mM TRIS-HCl pH 8.8, 0.1 % (w/v) APS, 0.01% (v/v) TEMED) were used. pc-$ICP47^{SBP}$ samples were analyzed with NuPAGE 12% Bis-Tris gels. Samples were incubated with 1x SDS sample buffer (2% (w/v) SDS, 50 mM

TRIS-HCl pH 7.5, 10% (v/v) glycerol, 1 mg/mL bromophenol blue, 1% (v/v) β-mercaptoethanol) for 5 min at 95 °C. For all gels shown in this thesis, a PageRuler prestained protein ladder (Thermo Scientific) was used. Gel electrophoresis was performed at 140 V for 1.5-2 h running in 1x MOPS buffer (Thermo Fisher) for NuPAGE gels or 1x Laemmli buffer (25 mM TRIS-HCl pH 7.0, 192 mM glycine, 0.1% (w/v) SDS) for self-casted gels. Directly after performing the SDS-PAGE, proteins were visualized either by a Coomassie staining, silver staining, or by immunoblotting

3.3.21. SDS-PAGE silver staining

For fixation of the proteins, polyacrylamide gels were incubated for 5 min at RT in 60 mL fixation solution (1.25% (w/v) trichloroacetic acid, 0.03% (v/v) formaldehyde, in acetone). After 3x 5 s rinsing the gel in H_2O, a wash step of 5 min at RT with H_2O was applied, followed by another rinsing step and pre-treatment with 60 mL acetone 50% (v/v) for 5 min at RT. Acetone was removed, and 60 mL of pre-treatment solution (0.03% (w/v) $Na_2S_2O_3$ pentahydrate in H_2O) was added and incubated for 1 min at RT. After a third rinsing in H_2O, the gel was incubated with impregnation solution (0.26% (w/v) $AgNO_3$, 0.37 % (v/v) formaldehyde in H_2O) for 8 min at RT. The impregnation solution was removed, the gel rinsed for a fourth time and protein bands detected by the addition of developing solution (2% (w/v) Na_2CO_3, 0.015% formaldehyde, 0.008% (w/v) $Na_2S_2O_3$ pentahydrate in H_2O) for 10-20 s. Depending on the intensity of the silver-stained protein bands, the developing solution was removed, and 1% (v/v) glacial acetic acid added to stop the reaction. Silver-stained gels were immediately documented.

3.3.22. SDS-PAGE Coomassie staining

The polyacrylamide gels were incubated with Instant Blue staining solution (Expedon) for 15-30 min at RT according to the manufacturer's instructions.

3.3.23. Immunoblotting

Proteins separated by SDS-PAGE were transferred onto PVDF membranes (Amersham Hybond-P, GE Healthcare) by using the semidry Trans-Blot Turbo (BioRad) system or WetBlot (Biorad) system. The membrane was activated by incubation in methanol. Afterwards, a Whatman paper and the membrane were soaked in transfer buffer (25 mM Tris-HCl, 192 mM glycine, 0.03% (w/v) SDS, 10% (v/v) methanol). The gel and an additional Whatman paper, soaked in transfer buffer, were put on the membrane. This packet was placed between a platinum coated titanium anode and a stainless-steel cathode of the Trans-Blot Turbo Electrophoretic Transfer Cell (semidry blot) or in the blotting chamber for wet-blot system. An electrical field (semidry: 30 min, 150 V, or wetblot: 15 h, 30 V) was applied to transfer the proteins to the membrane. Subsequently, the membrane was blocked for 1 h with 3% (w/v) milk powder in TBS-T (20 mM Tris-HCl, pH 7.6, 7.5 mM NaCl, 0.1% (w/v) Tween 20) to cover unspecific binding sites. After washing twice with TBS-T, the

membrane was incubated with the primary antibody (see Table 1) over night at 4 ºC or for 1 h at RT, before incubation with the secondary antibody (1 h, RT). Blots were incubated with Clarity Western ECL reagent (BioRad) and chemiluminescence was recorded with a Lumi-Imager (Roche) running LumiAnalyst software or recorded with a Vilber Fusion X running Fusion FX7 Edge software (Vilber). Signals were quantified with ImageJ[183].

3.3.24. ATP binding assay

ATP binding of PLC::GDN and PLC::MSP2N2 was measured by Erich Stefan, Goethe University Frankfurt.

ATP binding was examined by a scintillation proximity assay (SCPA) described in detail in (Stefan et al., 2020, 2021). 130 nM Purified PLC complexes were incubated with 2.8 µM ATP, 0.2 µM [2,5',8-^{3}H(N)]-ATP (^{3}H-ATP, PerkinElmer), and 1 mM $MgCl_2$ in Hepes buffer (20 mM Hepes-NaOH pH 7.5, 150 mM NaCl, 0.05% (w/v) GDN) for PLC::GDN or in Hepes buffer without GDN for PLC::MSP2N2 for 1 h at 4 °C. Copper-chelated SCPA beads (PerkinElmer) were added to a final concentration of 5 mg/mL for 30 min on ice. Total binding was determined at 20 °C in cpm mode (Wallac MicroBeta). Bound PLC complexes were eluted from the beads by addition of SDS (1% (w/v)) for 10 min at 20 °C, and background binding was examined.

3.3.25. ATP hydrolysis assay

500 nM (UV illuminated) PLC were mixed with ATPase buffer (20 mM Hepes-NaOH pH 7.4, 100 mM NaCl, 5 µM EGTA, 5 mM NaN_3, 1 mM Oubain, 0.01% (w/v) GDN) and supplemented with 10 mM $MgCl_2$ and 10 µM R9L and 0.5 mM Vanadate, depending on the stated sample condition. The reaction was started by addition of 5 mM ATP (containing trace amounts of [γ-^{32}P]ATP) for 20 min at 37 °C. Samples were set up in triplicates and spotted in duplicates on TLC PEI-Cellulose F plates (Merck). TLC plates were run in 0.8 M LiCl in acetic acid and developed for 12 h on a Personal Molecular Imager (PMI) System (BioRad) running Quantity One 4.6.9 (BioRad). Band intensities were quantified in ImageJ[183].

3.3.26. LC-MS analysis of intact proteins under denaturating conditions

LC-MS measurements and analysis was performed by Christian Winter, Goethe University Frankfurt am Main.

All LC-MS measurements were performed with a BioAccord System (Waters) running Unify 1.9.4 (Waters). Peptides were analyzed with an ACQUITY UPLC Peptide BEH C_{18} column, 130 Å, 1.7 µm, 2.1 mm x 100 mm (Waters), applying a linear water/acetonitrile gradient supplemented with 0.1% (v/v) formic acid at 60 °C, 30 V cone voltage, 0.8 kV capillary voltage, and 550 °C desolvation temperature. Mass spectra were recorded in positive mode at 5 Hz in MS^{e} mode at 50-2000 m/z. Intact protein LC-MS measurements were acquired on an

ACQUITY UPLC Protein BEH C_4 column, 300 Å, 1.7 µm, 2.1 mm X 150 mm (Waters) at 80 °C using a cone voltage of 60 V, 1.5 kV capillary voltage and 500 °C desolvation temperature. Mass spectra were recorded in positive polarity at 2 Hz in full scan mode at 400-7000 m/z. Masses of peptides and proteins were calculated and confirmed in Unify. Intact mass spectra were deconvoluted in Unify using the MaxEnt1 algorithm iterating to convergence. Spectra with high background noise were subjected to automatic baseline correction before deconvolution. Deconvoluted spectra were centroidized based on peak height, and mock spectra were extracted. Centroidized spectra were used for mass calculations. All intact protein mass spectra show the top 95% of signal intensity. UV spectra were recorded at 280 nm with 10 Hz.

3.3.27. LC-MS analysis for protein identification

LC-MS measurements and analysis of tapasin isoforms was performed by Christian Winter, Goethe University Frankfurt am Main.

12 µg PLC::GDN were separated on a NuPAGE 4-12%, Bis-Tris, Mini Protein Gel (Thermo Fisher), stained with InstantBlue (Abcam). All PLC protein bands as well as empty control bands of similar size were exercised. An in-gel trypsin digest was performed without iodoacetamide treatment using 3 µL of 1 µg/µL Trypsin Gold (Promega)[(ref. 184)]. Trypsin-digested samples were subjected to LC-MS analysis in a BioAccord system (Waters) and separated on ACQUITY UPLC Peptide BEH C_{18} column, 130 Å, 1.7 µm, 2.1 mm x 100 mm (Waters) and ACQUITY UPLC Peptide CSH C_{18} column, 130 Å, 1.7 µm, 2.1 mm x 150 mm (Waters). Mass spectra were recorded in positive polarity at 5 Hz in MS^e mode at 50-2000 m/z, 30 V cone voltage, 60-140 V fragmentation cone voltage, 1.2 kV capillary voltage and 550 °C desolvation temperature. Trypsin digest prediction, peptide identification and sequence coverage mapping were performed in Unify using the PeptideMap feature against a library of predicted tapasin variants. Peptide detection sensitivity was adjusted to detect no unspecific tapasin peptides in other components of the PLC and the empty control samples.

LC-MS measurements and analysis of ovine and bovine PLC were performed by Carla Schmidt and Susann Kostmann, Martin-Luther-University Halle-Wittenberg.

Gel electrophoresis was performed using 4–12% NuPAGE Bis-Tris gels according to the manufacturer's protocols (NuPAGE system, Thermo Fisher). Protein gel bands were excised, and the proteins were hydrolyzed as described previously[185]. Briefly, proteins were reduced with 10 mM DTT, alkylated with 55 mM iodoacetamide, and hydrolyzed with Trypsin (Roche).
Extracted peptides were dissolved in 2% (v/v) acetonitrile, 0.1% (v/v) formic acid, and separated using a DionexUltiMate 3000 RSLCnano System (Thermo Fisher Scientific). For this, the peptides were first loaded onto a reversed-phase C_{18} pre-column (µ-Precolumn C_{18}

PepMap 100, C_{18}, 300 µm I.D., particle size 5 µm pore size; Thermo Fisher Scientific). 0.1% formic acid (v/v) was used as mobile phase A and 80% (v/v) acetonitrile, 0.1% (v/v) formic acid, as mobile phase B. The peptides were then separated on a reversed-phase C_{18} analytical column (HPLC column Acclaim PepMap 100, 75 µm I.D., 50 cm, 3 µm pore size; Thermo Fisher Scientific) with a gradient of 4−90% (v/v) B over 70 min at a flow rate of 300 nL/min. Peptides were directly eluted into a Q Exactive Plus Hybrid Quadrupole-Orbitrap mass spectrometer (Thermo Fisher). Data acquisition was performed in data-dependent and positive ion modes. Mass spectrometric conditions: capillary voltage, 2.8 kV; capillary temperature, 275 °C; normalized collision energy, 30%; MS scan range in the Orbitrap, m/z 350–1600; MS resolution, 70,000; automatic gain control target, 3^6. The 20 most intense peaks were selected for fragmentation in the HCD cell at an AGC target of 1^5; MS/MS resolution, 17,500. Previously selected ions were dynamically excluded for 30 s and singly charged ions and ions with unrecognized charge states were also excluded. The 'lock mass option' was enabled using lock mass m/z 445.120025[ref. 186]. Obtained raw data were converted to .mgf files and were searched against the SwissProt database using the Mascot search engine 2.5.1 (Matrix Science). The mass accuracy filter was 10 ppm for precursor ions and 0.5 Da for MS/MS fragment ions. Peptides were defined to be tryptic with maximal two missed cleavage sites. Carbamidomethylation of cysteines and oxidation of methionine residues were allowed as variable modifications.

3.3.28. PNGase treatment

20 µL 0.5 mg/mL PLC in 20 mM Hepes-NaOH pH 7.4, 150 mM NaCl, 0.01% (w/v) GDN were heat-disintegrated for 15 min at 65 °C at 600 rpm. Subsequently the sample was incubated with 2 µL of PNGase F (NEB, 500 units/µL) at 37 °C, 200 rpm. After 2 h, 2 µL of PNGase F were added, and incubation was continued overnight. Deglycosylated samples were directly subjected to intact protein LC-MS analysis.

3.3.29. GluII treatment

1.2 µM PLC::MSP2N2 in 20 mM Hepes-NaOH pH 7.4, 150 mM NaCl were preincubated, depending on the respective condition, with 1 mM FC14, 20 µM of high-affinity peptide (CSN), or low-affinity peptide (R9L) for 30 min at 4 °C. Directly before deglucosylation at 37 °C for 5 min, 0.6 µM of GluII were added. The reaction was stopped by injection into the LC-MS system.

3.3.30. Liposome size determination

Liposomes were analyzed by dynamic light scattering to confirm their diameter using a NanoSight LM10 (Malvern). Liposomal size distribution was plotted in OriginPro 2022b.

3.3.31. Flow cytometry of liposomes

Flow cytometry analysis were performed by Christian Winter, Darja Cernova, and Jacqueline Patzsch, all Goethe University Frankfurt am Main.

PLC::liposomes were stained with antibodies and analysis by flow cytometry. First PLC::liposomes were incubated with the primary antibody (20 µM) for 30 min, 4 °C. Afterwards, liposomes were diluted with buffer (20 mM MES-NaOH pH 6.8, 150 mM NaCl) followed by pelleting of the liposomes (80,000 xg, 4 °C, 20 min) and resuspended in buffer. After the addition of the secondary antibody (30 min, 4 °C) and 10-fold dilution with buffer the liposomes were analyzed by flow cytometry.

3.3.32. Protease protection assay

The proteinase K protection assay to analyze PLC membrane topology in liposomes was performed by Christian Winter, Goethe University Frankfurt as described elsewhere[187].

Liposomes were incubated for 15 or 30 min at 37 °C with and without 400 µg/mL proteinase K (Thermo Scientific) in the presence or absence of SDS. The reaction was stopped by addition of 20 mM PMSF for 5 min on ice. Samples were precipitated in 10% (v/v) TCA for 30 min. After centrifugation (5 min, 12,000 xg), pellets were washed with acetone, dried, and analyzed by SDS-PAGE and immunoblotting.

3.3.33. Flow cytometry of microsomes

Flow cytometry analysis were performed by Christian Winter, Goethe University Frankfurt.

10 µg of microsomes (crude protein) in microsome buffer (10 mM Hepes-NaOH pH 7.4, 10 mM KCl, 6 mM $MgCl_2$, 1 mM DTT) were incubated with 650 nM of primary antibody for 30 min at 4 °C. Excess of primary antibody was removed by ultracentrifugation (180,000 xg, 15 min, 4 °C). The samples were resuspended in microsome buffer containing 80 nM of AF647-labeled secondary antibody and incubated for 30 min at 4 °C. Excess of secondary antibody was removed by ultracentrifugation (180,000 xg, 15 min, 4 °C). After resuspension in microsome buffer, samples were subjected to flow cytometric analysis.

3.3.34. Peptide transport assay – liposomes

The transport activity of PLC in liposomes was analyzed utilizing the fluorescent labeled reporter peptide C4F. 2 µL liposomes were added to 18 µL of transport buffer (MES-NaOH pH 6.5, 150 mM NaCl) containing 10 mM ATP or ADP, 10 mM $MgCl_2$, 10 mM creatine phosphate, 0.5 mg/mL creatine kinase. UV illuminated samples were exposed to UV_{365} for 180 s on ice. The transport was initiated by the addition of 10 µM C4F and performed for at 32 °C in a shaking incubator (300 rpm, Eppendorf). The sample was chilled on ice and

diluted to 200 µL with transport buffer. All samples were prepared in triplicates. Transported peptide was analyzed by flow cytometry.

3.3.35. Peptide transport assay – microsomes

The transport activity of PLC in microsomes was analyzed utilizing the fluorescent labeled reporter peptide NST^{AF647}. 20 µg (crude protein) of microsomes were added to 18 µL of transport buffer (20 mM MES-NaOH pH 6.5, 150 mM NaCl) containing 10 mM ATP, 10 mM $MgCl_2$, 10 mM creatine phosphate, 1 mg/mL creatine kinase. $ICP47^{SBP}$ inhibited samples were pre-incubated with 10 µM of $ICP47^{SBP}$ or pc-$ICP47^{SBP}$ for 20 min on ice. UV illuminated samples were exposed to UV_{365} for 180 s, on ice. The transport was initiated by the addition of 10 µM NST^{AF647} and performed for 5 min at 32 °C in a shaking incubator (300 rpm). The sample was chilled on ice and the mixture was layered on top of 180 µL transport buffer containing 0.5 M sucrose in a TLA-100 tube (Beckman). Non-transported NST^{AF647} was separated by centrifugation at 228,000 xg for 15 min at 4 °C. The supernatant was removed, and the microsomal pellet was resuspended in 200 µL of transport buffer. The sample was washed again at 228,000 xg for 15 min at 4 °C and resuspended in 200 µL of transport buffer. All samples were prepared in triplicates. Transport activity was analyzed by flow cytometry.

3.3.36. pc-ICP47 cleavage

UV illumination was performed in a self-assembled illumination setup. Samples were transferred into a 1.5 mL tube and placed in a chilled aluminum block on ice. A λ=365 nm diode (ThorLabs) was placed 1 cm above the opened tube and focused onto the bottom of the tube. Samples were illuminated for 180 s, 25% lamp intensity (~50 mW) and analyzed by SEC and immunoblot. For analysis of cleavage kinetics in the PLC, the intensity of *$ICP47^{SBP}$ band in immunoblot was quantified by ImageJ. Data points were fitted in OriginPro 2022b using the ExpDecay1 function.

3.3.37. $ICP47^{AF647}$ binding after pc-$ICP47^{SBP}$ cleavage

The native PLC (1 µM final) purified with pc-$ICP47^{SBP}$ or $ICP47^{SBP}$ was treated with standard UV illumination conditions and supplemented with 10 mM ATP, 15 mM $MgCl_2$ in 150 mM NaCl, 0.05% (w/v) GDN, 20 mM MES-NaOH, pH 6.5. After 10 min at 32 °C, 10 µM of $ICP47^{AF647}$ were added and incubated for 20 min at 4 °C. $ICP47^{AF647}$ rebinding was verified by SEC comigration with the running buffer containing 20 mM MES-NaOH, pH 6.5, 150 mM NaCl 0.01% (w/v) GDN. $ICP47^{AF647}$ comigration was recorded in the $\lambda_{ex/em}$ 650/665 nm channel, using PLC purified with $ICP47^{AF647}$ as reference for 100% binding.

3.4. Electron microscopy

3.4.1. Negative stain electron microscopy

2 µl of purified protein were applied to a glow-discharged carbon-coated copper grid (400 mesh) and stained with 2% (w/v) uranyl formate. Data was collected either (i) on a Tecnai-Spirit transmission electron microscope (Thermo Fisher), operated at 120 kV and equipped with a Gatan 4x4k CCD camera. Images were automatically collected using the Leginon software package[188] at a nominal magnification of 42,000x, corresponding to a pixel size of 2.68 Å or (ii) on a FEI F30 (Thermo Fisher) operated at 300 kV and equipped with a Gatan US4000 4x4k CCD camera at a nominal magnification of 39,000x corresponding to a pixel size of 2.5 Å. Images were automatically collected with the EPU software package (Thermo Fisher). All images were processed in the cisTEM software package[189].

3.4.2. Cryo-EM: Sample preparation and image collection

3 µL of PLC samples (1 to 2 mg/mL) sample were applied onto freshly glow-discharged cryo-EM grids and plunge-frozen in liquid ethane using a Vitrobot Mark IV (Thermo Fisher) equipped with filter paper (Whatman 595). Micrographs were recorded automatically (SerialEM) on a 300 kV FEI Titan Krios in energy-filtered transmission electron microscopy mode with a K2 direct detector (Gatan) and a Gatan GIF Quantum SE post-column energy filter at 130,000x magnification and a pixel size of 1.05 Å. Dose-fractionated movies were acquired at an electron flux of 5.1 e^- per pixel per s over 14 s with 0.35 s exposures per frame (40 frames in total), corresponding to a total electron dose of ~65 e^- $Å^2$. Movies were recorded in the defocus range from −1.5 to –2.5 µm.

3.4.3. Cryo-EM data analysis of PLC::MSP2N2

Cryo-EM data analysis was performed using CryoSPARC v2.15 - 3.2(ref. 146). A total of 2,341 movies were used for analysis. Motion correction was performed using patch motion correction implemented in CryoSPARC. The contrast transfer function (CTF) was estimated using patch CTF function of CryoSPARC. Initial particles were picked from a subset of data using a blob picker (minimum particle diameter 150 Å, maximum particle diameter 400 Å). The particles were extracted at a box size of 360 px and subjected to 2D classification to identify good particle picks. These picks were used to train Topaz (deep picker) on denoised images[190,191]. Subsequently, the trained picking model was utilized to pick particles in all images, yielding 613,746 particles picked and extracted at a box size of 360 px. 2D classification was used to identify good particles for *ab initio* model generation, which directly yielded maps for full PLC including the membrane region as well as a more focused map consisting of one editing module only. These maps were used as references to identify suitable particles for refinement in several rounds of 3D classification. The 3D classification resulted in two clean particle stacks for the full PLC (52,668 particles) and the editing module (97,952 particles). Each subset of particles was individually refined by homogeneous and

non-uniform refinement. Optimal results were obtained using non-uniform refinement utilizing a mask for the region of interest, enforced non-negativity, optimization of per particle defocus, and optimized per group CTF parameters enabled. For the focused editing submodule map, a resolution of 3.73 Å was estimated using the 0.143 cut-off criteria (Figure 4.4-3). For the full PLC, the highest resolution obtained was 4.01 Å (Figure 4.4-2). However, this map seemed to represent a consensus map of different PLC compositions of mainly one well resolved editing module; the second tapasin and MHC I were less represented. Separating the underlying states using ab initio model generation and/or heterogeneous refinement failed. Heterogeneous reconstruction with the same set of particles by deep learning using the neural network-based algorithm of CryoDRGN[192] (https://github.com/zhonge/cryodrgn) (version 0.3.1) revealed different assembly states of the PLC. CryoDRGN was run for 50 epochs with input image poses and CTF parameters from a consensus homogeneous reconstruction in cryoSPARC, encoder and decoder network architectures of 3 hidden layers with 256 nodes per layer, 8-dimensional latent space, and pose refinement. Selected maps generated by cryoDRGN representative of the latent space, as judged from a principal component analysis projection, were used as references in heterogeneous 3D refinement in CryoSPARC and resulted in five subsets of particles representing different assembly states of the PLC. Individual stacks were subjected to homogeneous and non-uniform refinements resulting in resolutions between 6 Å and 9 Å.

3.4.4. Model building

Model building of the PLC was performed in collaboration with Christoph Thomas, Goethe University Frankfurt.

The structure of a PLC editing module (PDB: 6ENY) was initially fitted into the cryo-EM map using bulk flexible fitting by ISOLDE[193] implemented for ChimeraX. Final model building was carried out in COOT[194], and real-space refinement was performed using Phenix[195]. The editing loop of tapasin was modeled *de novo*. Carbohydrates were validated using Privateer[196] of the CCP4 software suite. Refinement and validation statistics are summarized in Supplementary Table 6-4.

4. Results and Discussion

4.1. Isolation and characterization of PLC from primary mammalian tissue

To understand the interplay and functions of the PLC subunits detailed structural information is critical. In this PhD thesis different approaches were evaluated to improve the current resolution of the PLC editing module (5.8 Å)[1]. Generation of cells for PLC preparation from human Raji cells is an expensive and tedious task. Primary tissue from non-human mammals could be a source for structural and functional analysis of the PLC because it is available in large quantities. In addition, other multi-protein complexes (e.g. the complex I of the respiratory chain) have been structurally investigated from non-human sources before the structure of the human counterpart was solved, probably because of a higher intrinsic stability of the non-human complexes[197,198].

An ideal source for the purification of the PLC from primary tissue is the spleen. This organ combines immunogenic function with low content of connective tissue, allowing straightforward processing tissue for PLC isolation. The TAP inhibitor ICP47 from herpes simplex virus 1 (HSV1) was equipped with a streptavidin binding peptide (SBP) tag (ICP47^{SBP}) for the purification of the PLC from human cells[1]. Herpesviruses are strongly host specific and highly adapted, so the approach to use HSV1 ICP47 as TAP inhibitor in other mammalian species might not be straightforward. However, studies have shown that, although murine TAP is inhibited only at very low efficiency by HSV ICP47[123,199,200], porcine, bovine, and canine TAP are inhibited by HSV1 ICP47[201]. In addition, sheep was

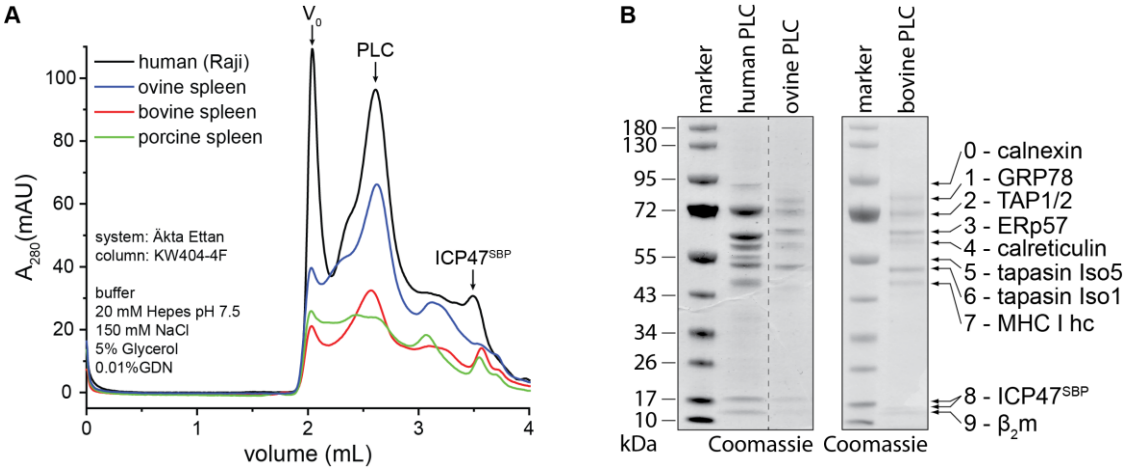

Figure 4.1-1: PLC purified from mammalian tissue. (**A**) PLC purified using ICP47^{SBP} from bovine (red) and ovine spleen (blue) has a similar SEC profile compared to human PLC from Raji cells (black). The profile of protein from porcine spleen (green) does not match human PLC and lacks a clear peak. (**B**) SDS-PAGE (reducing, 4-12%, Coomassie) of PLC purified from human cells, ovine, or bovine spleen. Bands were cut for mass spectrometry analysis. Bands are numbered and indicate the respective sample for MS-analysis (see Table 3and Table 4).

identified as candidate for PLC purification via HSV1 ICP47, based on high similarity to human TAP1 (Table 6-1).

Spleens from cow (*Bos taurus*), pig (*Sus scrofa*), sheep (*Ovis aries*), and lymph nodes from cow were evaluated for PLC purification via ICP47^{SBP} affinity purification. Bovine and ovine spleen yielded PLC with high purity after purification with ICP47^{SBP} (Figure 4.1-1). A peak in SEC was observed at a similar elution volume compared to human PLC from Raji cells. The protein composition in SDS-PAGE of bovine and ovine PLC matched the human PLC, which, together with similar SEC profiles, indicated successful purification of PLC from ovine and bovine spleen. However, differences in yield (Figure 4.1-1 A) and protein content (Figure 4.1-1 B) were apparent. The human PLC showed a sub-stoichiometric amount for calnexin which was not observed in ovine or bovine PLC. In addition, two variants of tapasin were identified in PLC from Raji cells (Iso1, Iso5, see chapter 4.3.3) while only one band was present for tapasin in sheep and cow. The PLC from bovine and ovine spleen showed an additional band at higher molecular weight than TAP1/2, which neither matched the molecular weight of TAP1/2 nor calnexin. Bovine lymph nodes also yielded PLC like bovine spleen. However, their high content of connective tissue and smaller size made them a less useful specimen. Pig spleen did not yield protein similar to human PLC. The SEC analysis

Table 3: Protein identification of ovine PLC by MS. Separated protein bands were cut from coomassie-stained SDS-PAGE (Figure 4.1-1 B (ovine)), as indicated. Extraction, in solution digestion, and protein identification by mass spectrometry was performed by Carla Schmidt and Susann Kostmann, Martin-Luther-University Halle-Wittenberg.

Band	Proposed protein	Protein score	Protein mass (Da)	Peptide sequences (#)	Sequence coverage (%)
1	TAP1	1524	87163	17	23.1
	PCCA	1480	79871	27	34.1
	GRP78	1223	72356	41	47.8
	HSP7C	450	71196	28	37.8
2	RPN1	779	68652	25	43.8
	TAP1	657	87163	14	19.3
	TAP2	621	75616	19	27.7
	ERp57	564	56894	24	43.0
3	**ERp57**	9217	56894	67	75.0
	PCCA	1172	58553	23	40.3
	RPN2	1047	69171	20	30.6
4	**calreticulin**	2705	48009	34	64.3
6	**tapasin**	446	47744	3	4.5
7	**HLA-A**	1148	40338	7	17.8
8	**ICP47**	1929	9787	11	71.6
	β_2m	131	13456	4	26.3
9	**β_2m**	820	13456	5	33.1
	ICP47	266	9787	6	61.4

lacked a clear peak and the protein pattern in SDS-PAGE also did not resemble human PLC (Appendix Figure 6.1-1). PLC from pig was therefore not further investigated.
Purification from processed spleen that had been stored at -80°C for prolonged time (>3-6 months) yielded only little to no PLC. Therefore, only fresh spleens were used for PLC purification. In addition, the amount and quality of PLC that was extracted from spleens varied and could not be predicted.

The established antibodies against the human PLC components predictably failed to detect PLC proteins from both sheep and bovine spleen, similar to few available antibodies available against bovine and ovine PLC components. Therefore, proteins were identified by mass spectrometry after tryptic digestion of the proteins separated by SDS-PAGE. Digestion and protein identification were performed in the lab of Carla Schmidt (Martin-Luther-University Halle-Wittenberg). The proteins identified in the sample from ovine PLC (Table 3) resemble the PLC composition found in the human counterpart. The proteins identified included the membrane transporter TAP1/2, the chaperones tapasin, and calreticulin, ERp57, and the MHC I heterodimer (MHC I hc, β_2m). All PLC components known from human PLC

Table 4: Protein identification of bovine PLC by MS. Separated protein bands were cut from coomassie-stained SDS-PAGE (Figure 4.1-1 B (bovine)), as indicated. Extraction, in solution digestion, and protein identification by mass spectrometry was performed by Carla Schmidt, Martin-Luther-University Halle-Wittenberg.

Band	Proposed protein	Protein score	Protein mass (Da)	Peptide sequences (#)	Sequence coverage (%)
1	**GRP78**	2955	72356	53	61.5
	TAP1	2070	79100	9	8.6
	ERp57	1203	56894	35	54.3
2	ERp57	2468	56894	52	73.3
	TAP1	1100	79100	7	7.3
3	**ERp57**	16891	56894	96	81.8
	calreticulin	2273	48009	38	66.7
4	**calreticulin**	5738	48009	52	73.6
	ERp57	3250	56894	59	78.4
6	**tapasin**	2151	47744	2	2.4
	HLA-B	1262	41487	15	42.9
	HLA-A	316	40338	4	10.3
7	**HLA-B**	5710	41487	24	57.7
	HLA-A	1579	40338	9	18.3
8	HLA-B	495	41487	8	28.3
	HLA-A	75	40338	2	6.7
	β_2m	455	13668	6	28.8
9	**β_2m**	1687	13668	11	48.3

were detected in the corresponding bands in ovine PLC with reasonable protein score and sequence coverage. The protein score is a relative score which indicates the probability that a certain protein is part of the analyzed sample. The higher the score, the more likely this protein is part of the sample. However, this score cannot be used to compare samples from different experiments. Many samples (e.g. band 3) contained proteins also identified in adjacent bands. Contaminations of adjacent bands by proteins with a similar molecular weight are plausible because of a marginal spatial separation of proteins with a mass range between 45-75 kDa in the SDS-PAGE used. Most PLC components appear in this region. However, the PLC components cover a large spread of molecular weight from the smallest PLC component β_2m (13.6 kDa) to TAP1 (~80 kDa) which requires the use of a gradient gel to separate all components. Protein detected in adjacent bands are reflected by a lower score (e.g. ERp57 in band 2, Table 3). For most of the proteins (6/9) the sequence coverage is higher than 30% indicating medium accuracy in determining the protein and species, which is in accordance with correct identification of the protein but not the species.

The proteins identified in bovine PLC are comparable to ovine PLC and human PLC (Table 4). However, some PLC proteins were not detected (TAP2, ICP47) or only with a very low sequence coverage (TAP1). These proteins were either membrane bound (TAP1/2) or very small (ICP47). This makes their extraction and digestion from the SDS-PAGE challenging. Additionally, the amount of bovine PLC available for the SDS-PAGE was lower than in the comparable experiment with ovine PLC (Figure 4.1-1 A) and therefore a lower number of peptides was detected in MS. Still, the proteins detected in bovine PLC align with the results from ovine PLC and SDS-PAGE and prove a similar PLC composition in all three species.

Interestingly, 78 kDa glucose-regulated protein (GRP78) was identified as protein in band 1 in bovine and ovine PLC. GRP78 is also known as immunoglobulin binding protein (BiP) and is an ER-located protein involved in chaperoning and stress reactions[202]. It has been shown to interact with MHC I and is also hijacked by viruses to degrade MHC I[10,203]. However, it has not been found in the human PLC[1,2]. Attempts to localize the binding site of GRP78 in the PLC by crosslink MS failed due to too low amounts of PLC.

To confirm structural integrity and to investigate the overall architecture of bovine and ovine PLC, PLC from both species were analyzed by negative-stain electron microscopy (Figure 4.1-2). Both samples of mammalian PLC were well distributed across the grid without larger aggregates. The size of single particles of approximately 15 x 25 nm matched the dimensions of the human PLC[1]. Overall appearance was comparable with human PLC investigated in negative-stain EM. Most prominent, the detergent micelle including TAP and the other membrane proteins was clearly visible. The NBDs of TAP were present but not as defined as the micelle, which has been observed similarly for human PLC[1]. Most likely, the orientation of TAP and the NBDs is flexible in the detergent micelle, and they were therefore not well

resolved. Furthermore, the editing modules were clearly visible in the ovine PLC, less defined in the bovine PLC. In the latter case this is due to the much smaller size of the data set. The negative-stain data additionally confirmed the purification of PLC from sheep and cow spleen.

Taken together, the presented data on bovine and ovine PLC showed a similar composition and appearance of the PLC compared to human PLC. While this study was restricted by primary tissue availability and PLCs which bound ICP47^{SBP}, it can be assumed that PLC composition and organization is a common feature in mammals.
The presence of GRP78 is an interesting finding, which was consistent in both evaluated species. Interactions of GRP78 with MHC I hc has been described outside of the PLC, before the MHC I hc associates with calreticulin, and on the cell surface[203,204]. However, it remains unclear whether in this case GRP78 is associated to the MHC I hc and the PLC because of a role in MHC I folding and quality control, or whether GRP78s presence indicates stress in the spleen induced by slaughtering the animal and subsequent hypoxia and lack of glucose supply[202].

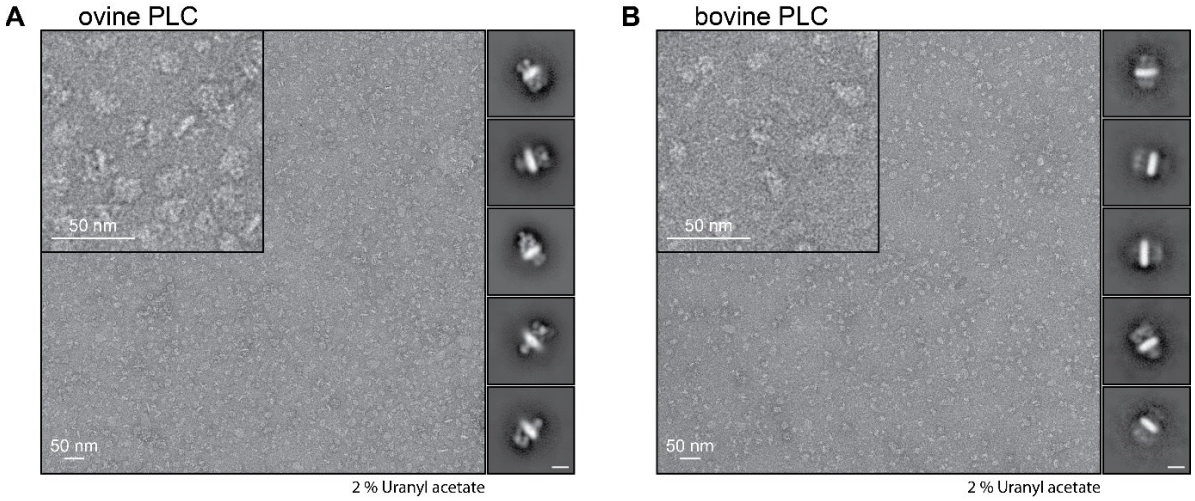

Figure 4.1-2: Negative stain analysis of PLC from cow and sheep spleen. (A) Micrograph of ovine PLC purified from sheep spleen, spotted on continuous carbon grids, and stained with 2% (w/v) uranyl formate solution. A total of 310 micrographs were imaged and processed yielding 231,074 particle picks. 125,001 particles were selected for reclassification (50 classes). Five representative classes are shown on the right side of the micrograph. The scale bar in the classes corresponds to 10 nm. **(B)** Micrograph of bovine PLC purified from cow spleen, spotted on continuous carbon grids, and stained with 2% (w/v) uranyl formate solution. A total of 60 micrographs were imaged and processed yielding 40,024 particle picks. 4,543 particles were selected for reclassification (10 classes). Five representative classes are shown on the right side of the micrograph. The scale bar in the classes corresponds to 10 nm.

4.2.Reconstitution of human PLC in membrane mimetics

Previous work demonstrated the isolation of the human PLC from Raji cells utilizing the viral inhibitor ICP47^{SBP} for structural analysis[1]. To purify and stabilize the PLC in a soluble form the detergents digitonin (PLC::digitonin) or its derivative glyco-diosgenin (GDN, PLC::GDN) had been used. Structural analysis of PLC::GDN by cryo-EM was possible but required stabilization of the PLC by chemical crosslinking with glutaraldehyde (GraFix)[(ref. 1,205)]. The chemical crosslinking can limit resolution and also detergents can introduce artefacts in structural studies[155]. Therefore, stabilizing the PLC in a detergent free state was necessary to omit chemical crosslinking for structural and functional analysis. Several approaches of stabilizing membrane proteins and complexes in solution without a requirement of detergent have been reported in the last years (see chapter 1.4) and were evaluated in this PhD thesis for the PLC.

4.2.1. Purification of human PLC after SMA/DIBMA solubilization not possible

Polymeric styrene-maleic acid (SMA) and diisobutylene-maleic acid (DIBMA) facilitate the direct solubilization of a membrane protein from its native membrane without the use of detergent. They also retain native lipids from the original membrane environment[206].

To evaluate SMA and DIBMA for PLC purification, both reagents were used to solubilize the PLC from human Raji cells and solubilization and purification were compared with the detergent GDN. The PLC was purified by affinity purification via ICP47^{SBP} (Figure 4.2-1). Using GDN, PLC was successfully isolated as indicated by the protein bands in the elution

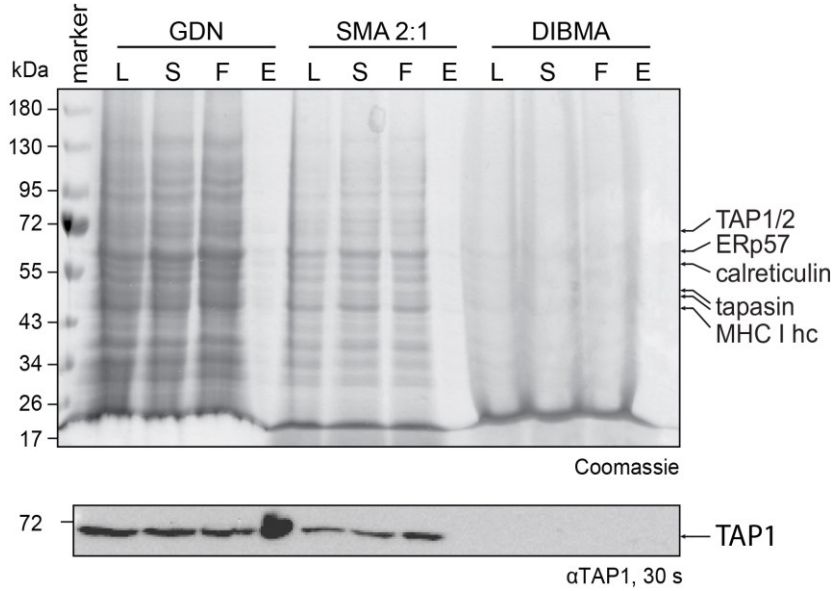

Figure 4.2-1: PLC cannot be purified using SMA 2:1 and DIBMA. Raji cells were incubated with ICP47^{SBP} and the membranes were solubilized with either 2% (w/v) GDN, 1.5% (w/v) SMA (2:1), or 1.5% (w/v) DIBMA. The samples were analyzed by SDS-PAGE (reducing, 11%, Coomassie) (top) and immunoblot (bottom). L = lysate, S = supernatant ultracentrifugation, F = flowthrough affinity purification, E = eluted protein.

sample in SDS-PAGE and the strong TAP1 signal in the corresponding immunoblot. However, no PLC was detected in the eluates from SMA 2:1 and DIBMA solubilization and purification. After SMA 2:1 solubilization, TAP1 was detected in the supernatant and in the flowthrough of the affinity purification by immunoblotting, indicating successful solubilization. However, no protein or TAP1 was detected in the eluate. This indicated an incompatibility of the streptavidin-based affinity purification with SMA 2:1 or disruption of PLC during solubilization by SMA 2:1. If the PLC was disrupted, it did not bind ICP47^{SBP} and was therefore not isolated during affinity purification. No TAP1 was detected in any of the DIBMA samples by immunoblotting. However, TAP1 was detected in SMA and GDN samples originating from the same batch of cells as the DIBMA sample. Therefore, TAP1 must have been present in the DIMBA sample, too. This indicated a problem with the immunoblotting in the presence of DIBMA. No protein was detected in the eluate fractions of DIBMA treated samples by SDS-PAGE, too. Therefore, PLC purification utilizing DIBMA was not further investigated.

SMA is a pH-sensitive compound. At low pH (<6) it becomes insoluble while at neutral or basic pH it is charged and will adopt a random coil conformation which is soluble in aqueous solutions[173,207]. In addition, the composition of the SMAs can affect the size of resulting SMA lipid discs (SMALPs) and SMA variant-dependent protein solubilization efficiency has been demonstrated[208]. Therefore, PLC purification was tested with three different SMAs which differ in their styrene to maleic acid ratio (1.2:1 = Xiran SL40005 P20, 2:1 = Xiran SL30010 P20, 3:1 = Xiran SL25010 P20) at pH of 8.1 which should promote solubility of the SMAs. The PLC purification and stability at pH 8.1 was evaluated with PLC::GDN.

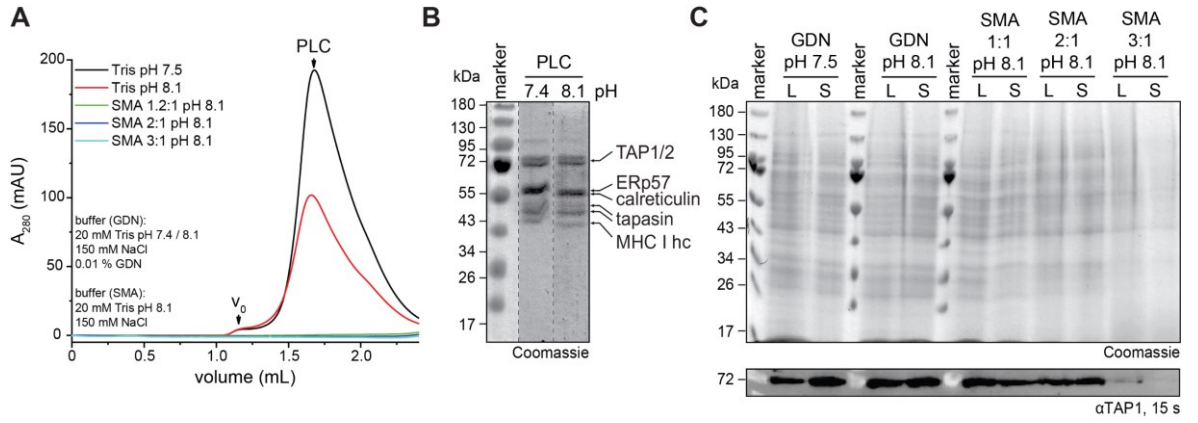

Figure 4.2-2: SMA solubilized the human PLC but purification was not possible. (**A**) SEC of PLC purified from Raji cells either by solubilization with GDN at pH 7.4 or 8.1 or different SMA variants at pH 8.1 on a Superose 6 increase 3.2/300. For GDN-solubilized PLC, the system was in 20 mM Tris-HCl pH 7.4 or 8.1, 150 mM NaCl, 0.01% (w/v) GDN. For SMA-solubilized samples, buffer without GDN at pH 8.1 was used. (**B**) SDS-PAGE (reducing, 11%, Coomassie) of PLC peak fractions from GDN-solubilized PLC from panel (A). (**C**) Analysis of the PLC solubilization by SDS-PAGE (reducing, 11%, Coomassie) and immunoblotting using an anti-TAP1 antibody (mAb 148.3). L = lysate, S = supernatant ultracentrifugation.

PLC purification with GDN was possible at pH 7.4 and pH 8.1 in TRIS-HCl buffer (Figure 4.2-2 A, B). After purification at both pH values, PLC was detected as single peak in SEC and all PLC components were present in SDS-PAGE. However, a higher yield was obtained at pH 7.5 than at pH 8.1. Additionally, both PLC preparations showed tailing in SEC, which was not observed with PLC purified in Hepes-NaOH buffer at pH 7.5[1]. TRIS-HCl might be a suboptimal buffer system for PLC, reducing the stability of the complex and inducing tailing.
Like previous results (Figure 4.2-1), no protein was detected after affinity purification for any of the SMA compounds (Figure 4.2-2 A). However, SMA 1.2:1 and SMA 2:1 were effective in solubilizing protein as indicated by the presence of TAP1 in both samples before (L) and after solubilization (S) (Figure 4.2-2 C). Probably, TAP1 and the other PLC components were solubilized by SMA 1.2:1 and SMA 2:1 but purification of PLC was unsuccessful. Either SMA disturbed the interaction of TAP with ICP47^{SBP} and thereby interfered with the purification of the PLC, or SMA shielded the SBP-tag and ICP47^{SBP} could not bind to streptavidin-beads. The results with SMA 3:1 were similar to the DIBMA test. The TAP1 signal in the immunoblot before solubilization (S) was much weaker than the signals in the samples from SMA 1.2:1 and SMA 2:1. No TAP1 was detected after the sample after solubilization (S).
Almost all purifications with SMA or DIBMA reported in literature were performed with His-tagged proteins and subsequent Ni-NTA purification. Therefore, ICP47 was exchanged by an His_8-tag (ICP47^{His8}) instead of the SBP-tag and evaluated in PLC purification (Figure 4.2-3). While pulldown of PLC::GDN with ICP47^{His8} was possible, the sample contained many impurities which hampered further use of this construct.

SMA and DIBMA were not compatible for PLC purification with the established ICP47^{SBP} purification strategy and not further investigated. Similarly, ICP47^{His8} cannot be used to obtain pure PLC. SMA, DIBMA or ICP47^{His8} were not further investigated.

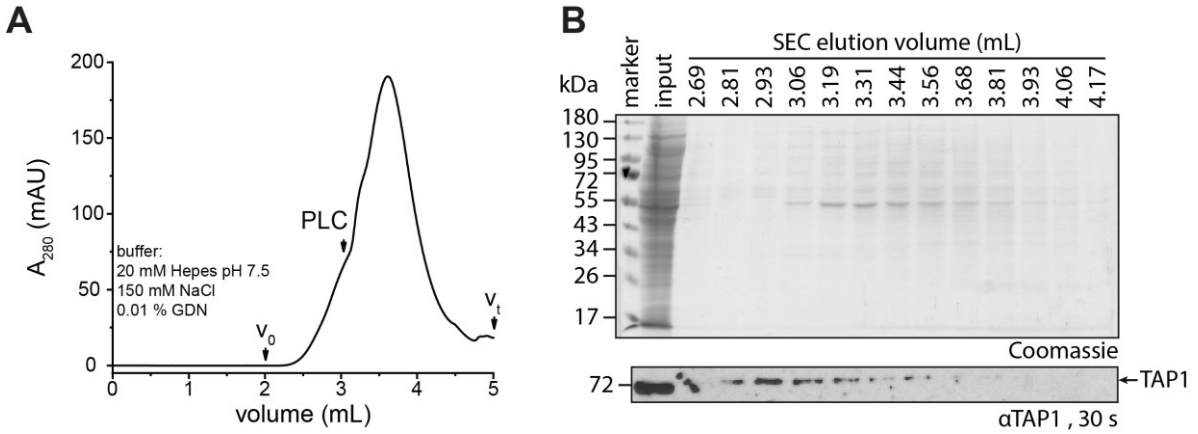

Figure 4.2-3: Impure purification of human PLC by ICP47^{His8}. (**A**) SEC analysis of PLC purified by ICP47^{His8} with a KW404-4F column. (**B**) Analysis of fractions from SEC in (A) by SDS-PAGE (reducing, 11%, Coomassie) and immunoblot using anti-TAP1 antibody (mAb 148.3).

4.2.2. Reconstitution in MSP2N2 nanodiscs

Nanodiscs were the first membrane reconstitution system developed to keep membrane proteins in solution without detergent[159]. Lipids and membrane proteins are encapsulated by a scaffold protein derived from apolipoprotein A. These membrane scaffold proteins (MSPs) are available in different sizes. The micelle of the PLC::GDN has a maximum diameter of 15 nm[1]. Therefore, the largest available nanodisc MSP2N2 with a diameter of 15-17 nm was chosen as scaffold for the PLC[165].

Using ICP47^{SBP} for affinity purification, PLC was purified from Raji cells after solubilization in GDN. Reconstitution was performed while PLC was bound to streptavidin agarose beads. Tethering of the PLC during the reconstitution allowed extensive washing of reconstituted PLC and removed contaminants, like free MSP2N2 or lipids. Therefore, the resulting PLC appeared without MSP2N2 contamination and monodisperse in SEC (Figure 4.2-4 A), and pure in SDS-PAGE (Figure 4.2-4 B). All previously identified PLC components were detected in reconstituted PLC in a similar ratio to PLC::GDN (Figure 4.2-4 B). ICP47^{SBP} blocks central functions of TAP. Therefore, peptide binding, peptide-dependent ATP hydrolysis, and peptide transport cannot be analyzed[123]. However, TAP still bound ATP (Figure 4.2-4 C) and there was no difference in ATP binding between PLC::GDN and PLC::MSP2N2 indicating successful reconstitution of the PLC in nanodiscs. The integrity of PLC::MSP2N2 was analyzed by negative-stain EM (see chapter 4.4.1).

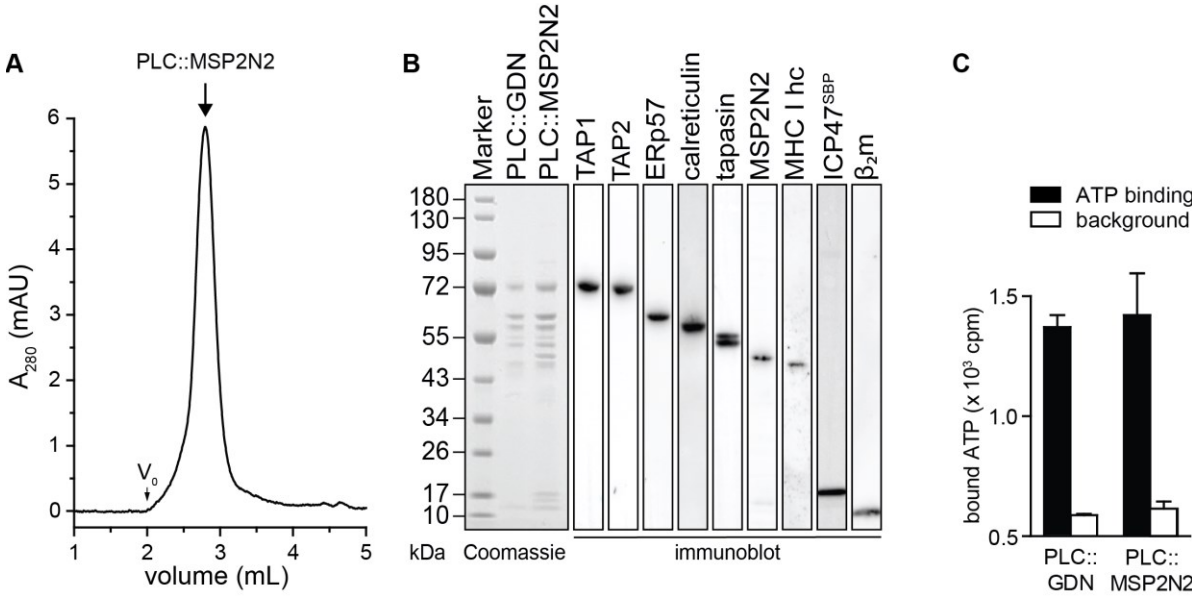

Figure 4.2-4: PLC reconstituted in large lipid nanodiscs is intact and binds ATP. (**A**) PLC reconstituted in large lipid nanodiscs (PLC::MSP2N2) is monodisperse in size-exclusion chromatography. (**B**) Compositional analysis of human PLC purified by ICP47^{SBP} in detergent (PLC::GDN) and reconstituted in lipid nanodiscs (PLC::MSP2N2). The composition of the reconstituted PLC is verified by SDS-PAGE (reducing, 4-12%, Coomassie) and immunoblotting. (**C**) PLC::GDN and PLC::MSP2N2 show the same ATP equilibrium binding as PLC::GDN, analyzed by scintillation proximity assays. ATP-binding analyses were performed by Erich Stefan, Goethe-University Frankfurt.

One major aim of nanodisc reconstitution of the PLC was to increase the stability and omitting chemical crosslinkers, which were necessary to study the assembly of the PLC::GDN by cryo-EM[1]. A classical approach to determine the thermal stability is recording melting curves utilizing fluorescent dyes which attach to hydrophobic patches on proteins when they become exposed after denaturation (e.g., cypro-orange). For membrane proteins, the thiol-reactive CPM is more often used to avoid binding of the dye to hydrophobic membrane regions of the proteins without any denaturation[209]. Both dyes have been checked with PLC::GDN and reconstituted variants but failed to provide reliable and reproducible results[210]. The PLC is a multi-protein assembly with a separate melting temperature for each component and an additional overall denaturation temperature for the assembly. Therefore, an assay directly evaluating the complex stability was established for the PLC, similar to an assay adapted to determine TAP stability[128]. PLC::MSP2N2 or PLC::GDN were purified and aliquots of the sample heated at different temperatures between 4 and 70 °C for 60 min. After removal of aggregates, the remaining PLC was analyzed by SEC and the peak height determined (Appendix Figure 6.1-2). The resulting data points were fitted with a sigmoidal curve and the half maximal value was determined (Figure 4.2-5). For PLC::GDN a T_m of 34.1 ± 3.2 °C and for the PLC::MSP2N2 a T_m of 37.2 ± 0.7 °C was determined. The increase of the melting temperature by 3.1 °C after MPS2N2 reconstitution indicated a stabilization of the PLC by the nanodisc reconstitution. However, the experiment has been performed only once and requires reproduction. Nevertheless, MSP2N2 reconstitution of the PLC allowed structural analysis of the PLC by cryo-EM without use of chemical crosslinkers (Chapter 4.4.2).

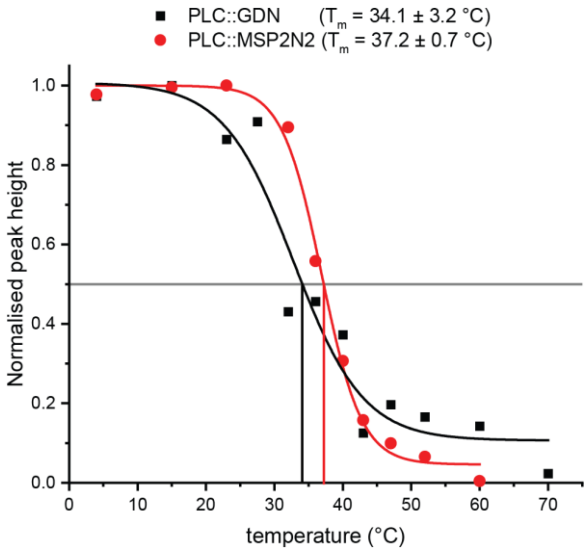

Figure 4.2-5: PLC stabilized in MSP2N2 nanodiscs. Purified PLC::GDN and PLC::MSP2N2 were aliquoted and heated for 1 h at the indicated temperature. The samples were subsequently analyzed by SEC and the amount of fully assembled PLC determined by $F_{280/315}$. The peak heights were normalized to the maximal height and plotted against the temperature. The curves were fitted with a sigmoidal fit to obtain half maximal values. The raw data are shown in Appendix Figure 6.1-2. n = 1.

Overall, the PLC was successfully reconstituted in MSP2N2 nanodiscs. The results indicated that the PLC is fully assembled, functional in ATP binding, and thermostabilized compared to PLC::GDN. Therefore, PLC::MSP2N2 was a promising sample for structural studies by cryo-EM (see chapter 4.4) and functional studies in a membrane environment.

4.2.3. Reconstitution in Saposin A and Peptidiscs

Similar to MSP2N2, Saposin A is an amphipathic membrane scaffold protein, which can form a disc around membrane proteins and keep them in solution without detergent[168]. Like nanodisc reconstituon, the reconstitution with Saposin A and peptidisc is usually performed in solution but has been adapted for on-bead reconstitution of the PLC. Reconstitution in small peptide detergent alternative Peptidisc[171] has been likewise performed with the PLC in this PhD thesis.

Both reconstitution systems were suitable to keep the PLC in solution without detergent as shown by PLC purification and reconstitution (Figure 4.2-6 A). The integrity of the reconstituted PLC was demonstrated by SEC analysis and compared to PLC::GDN (Figure 4.2-6 B). The PLC::Saposin appeared monodisperse and had a similar elution volume compared to the PLC::GDN, which indicated a similar size. Consequently, the hydrodynamic

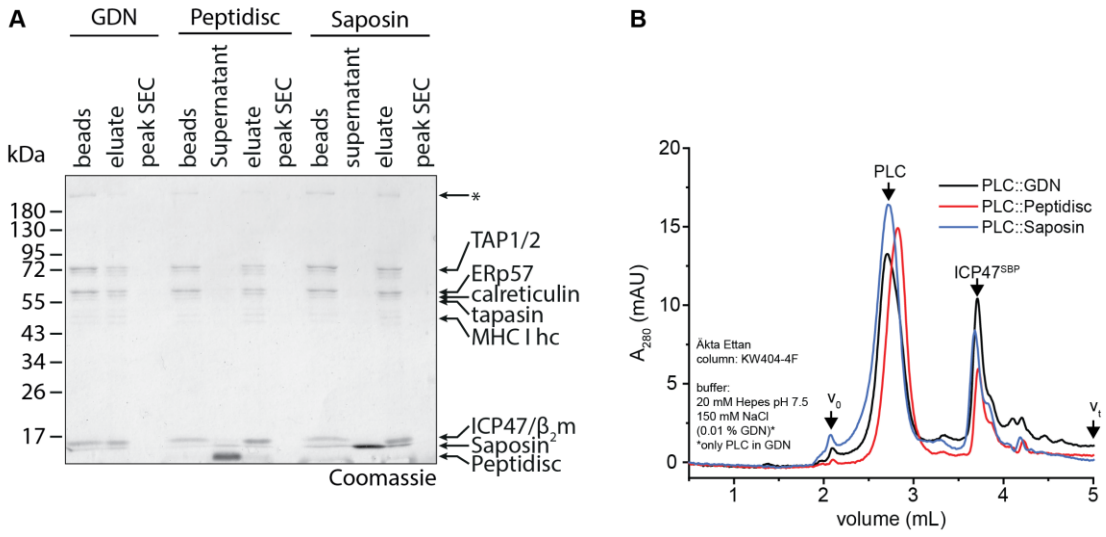

Figure 4.2-6: PLC reconstituted in Saposin A and Peptidisc. (**A**) SDS-PAGE (reducing, 11%, Coomassie) from PLC purifications and reconstitutions in different systems. GDN, PLC solubilized and purified using GDN. Peptidisc; PLC solubilized in GDN and reconstituted in Peptidisc on beads. Elution in buffer without detergent. Saposin; PLC solubilized in GDN and reconstituted in Saposin A on beads. Elution in buffer without detergent. (**B**) SEC from PLC reconstituted in Peptidisc (red), Saposin A (blue) and solubilized in GDN (black). The PLC appears monodisperse in all three samples.

radius of the membrane region stabilized by Saposin A is similar to what was observed in PLC::GDN. PLC reconstituted in Peptidisc appeared also monodisperse in SEC. However, the peak was shifted to a higher elution volume, which could be caused by a smaller hydrodynamic volume of the micelle. The SDS-PAGE (Figure 4.2-6 A) did not indicate loss of any PLC subunits, and because the Peptidisc likely replaces the detergent without additional lipids, this could result in a smaller assembly compared to the bulky micelle formed by GDN. Cryo-EM structures of the membrane proteins MsbA and MscS reconstituted in Peptidisc have a very small micelle and direct contact to the Peptidisc surrounding them[211], which supports the assumption of a smaller Peptidisc micelle surrounding the PLC.

PLC reconstituted in Saposin A and Peptidisc were analyzed by negative-stain EM to validate integrity after reconstitution (see chapter 4.4.1).

4.3. Mass spectrometric analysis of human PLC

Analyzing the function and interplay of the PLC requires a good description of the composition of the subunits in the PLC. Previous works have described the composition of the PLC[2,81] and the architecture of the complex[1,158]. These experiments also included the detection of components and their interaction by MS following crosslinking and trypsin digestion. Substoichiometric MHC I variants were also identified within the PLC by this method[1]. A more recent work focused on the MHC I content in the PLC depending on inhibition of TAP before the purification procedure[140]. However, none of the work mentioned above analyzed the PLC proteins at full length or delivered information about the glycans present on the two glycoproteins MHC I and tapasin.

Here, the PLC was analyzed by intact protein mass-spectrometry analysis under denaturating conditions (LC-MS). This method allows to study all components of a complex like the PLC separately at their full length. Using C_4 reverse phase chromatography, all components of PLC::MSP2N2 were separated and identified by TOF-MS (Figure 4.3-1**,** Figure 4.3-2, Appendix Table 6-2). The masses of the soluble PLC components β_2m, calreticulin, and ERp57 matched the expected masses (Appendix Table 6-2). Similarly, the additional components MSP2N2 and ICP47^{SBP} were detected with their full mass matching the expected mass. However, for ICP47^{SBP} an additional mass was detected. This second ICP47^{SBP} variant lacks the mass of the initial three amino acids GAM. Still, this variant can bind and inhibit TAP sufficiently for PLC purification.

Analysis of the two glycoproteins tapasin and hc is described in detail in chapters 4.3.1 and 4.3.2, respectively. Interestingly, tapasin showed two distinct peaks, which supplements the observation of two separated bands in SDS-PAGE and immunoblot (Figure 4.2-4 B). The identity of the second band is analyzed in more detail in chapter 4.3.3.

Two alternative isoforms have been reported for TAP1[ref. 212]. Isoform 1 is a short version comprised of 748 amino acids and a theoretical mass of 80,832 Da. The longer isoform 2 can be formed when an earlier initiator sequence is utilized and a larger TAP1 variant with 808 amino acids and a theoretical weight of 87,218 Da is produced. However, only isoform 1 was observed for TAP1 (M_{obs}: 80,832 Da), indicating that this is the relevant isoform in Raji cells. TAP2 (Uniprot Q03519) is more variable than TAP1 and two isoforms were observed. The TAP2 isoform 1 was detected, including the mutation A665T (M_{cal}: 77,724 Da, M_{obs}: 77,727 Da). This mutation has been reported in the African population[213], which correlates with the origin of the Raji cells which were isolated from an African lymphoma patient[214]. Additionally, the TAP2 isoform 3 was detected (M_{cal}: 75,662 Da, M_{obs}: 75,665 Da). This isoform results from a nucleotide exchange which leads to a premature stop codon causing a 17 amino acid shorter version.

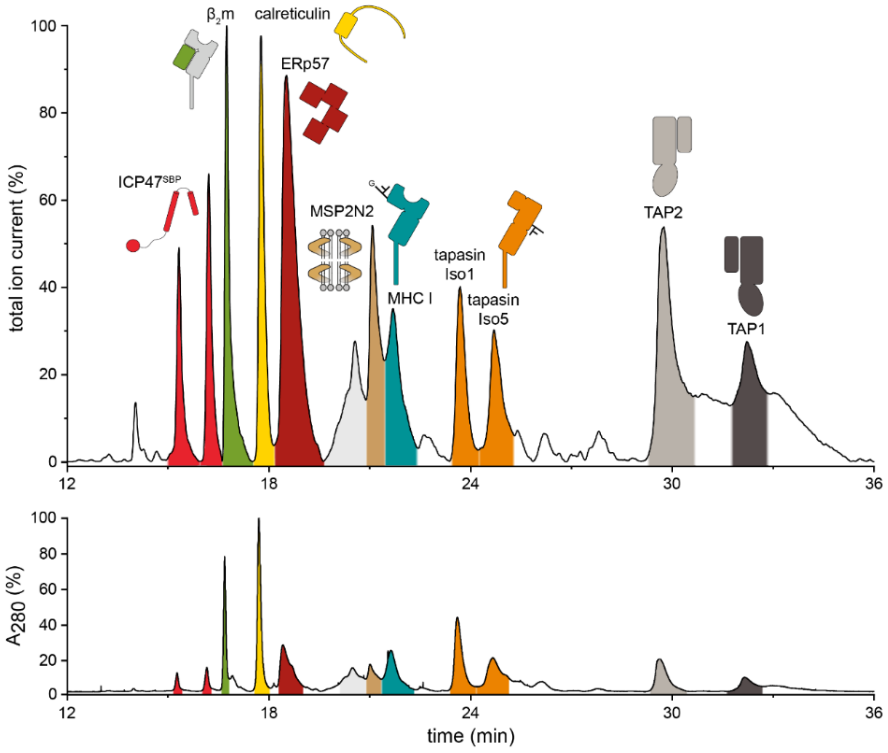

Figure 4.3-1: PLC subunits analyzed by LC-MS. The native, virally arrested PLC was reconstituted in large nanodiscs (MSP2N2) and subjected to LC-MS analysis. Separated PLC subunits were highlighted and assigned in their respective color in the total ion current and A_{280}. All components of the PLC were successfully identified by MS. The mass spectra and deconvoluted MS data for identified components are shown in Figure 4.3-4 and listed in Appendix Table 6-2. $ICP47^{SBP}$ is present in two variants, one of which contains the additional N-terminal sequence GAM. Tapasin appears in two isoforms in PLC from Raji cells. LC-MS and data analysis was performed by Christian Winter, Goethe University Frankfurt.

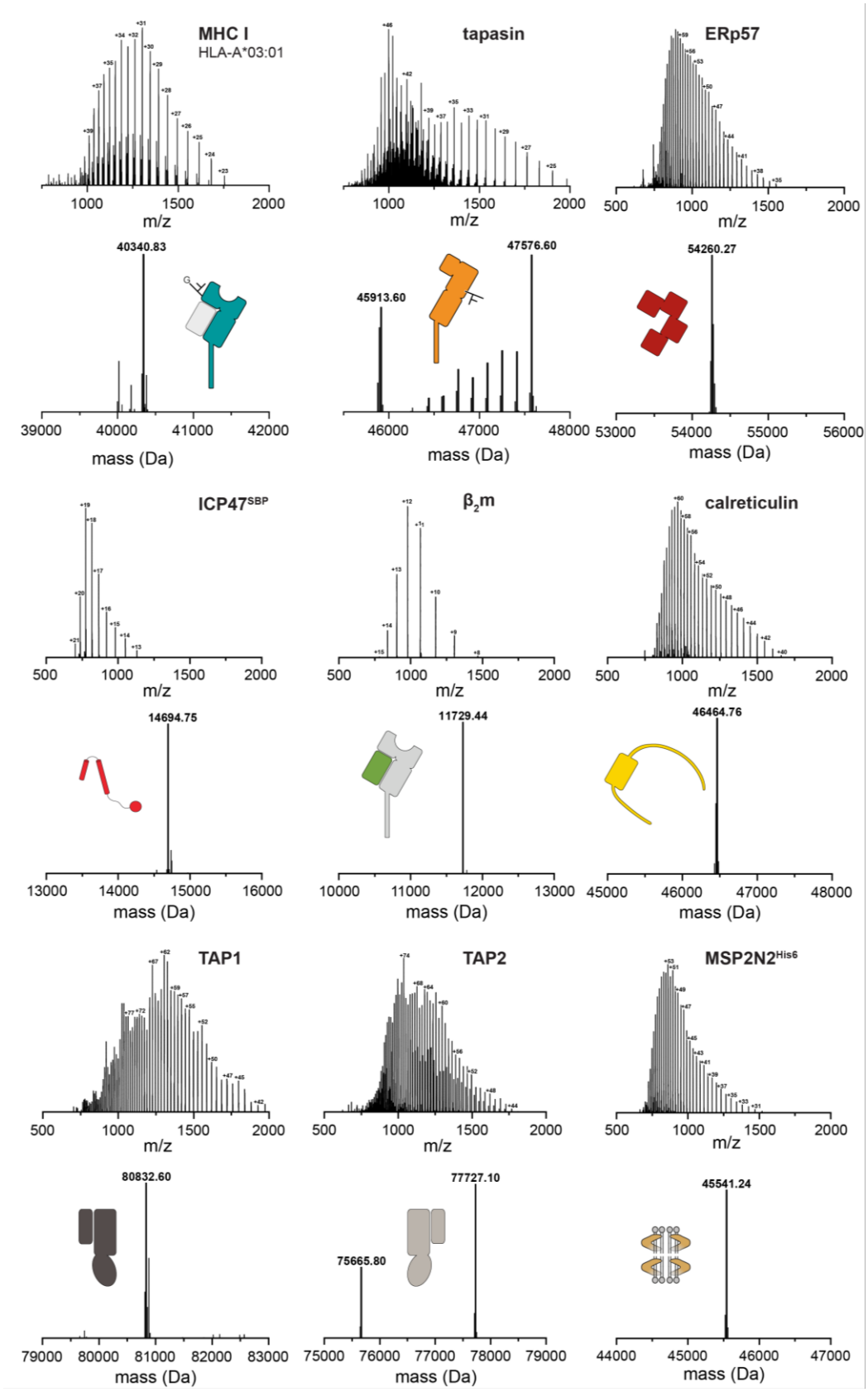

Figure 4.3-2: Identification of PLC subunits by intact protein LC-MS. Combined MS raw spectra (upper) and MaxEnt1 deconvoluted (lower) spectra of PLC components (Figure 4.3-2). The assignment of the sequences and theoretical masses of PLC components are shown in Table 6-2.

4.3.1. MHC I glycosylation

MHC I heavy chains carry a conserved N-linked glycan on Asn86[ref. 215]. The glycan serves as a marker for the folding, ERQC, and in the case of MHC I, also marks the peptide loading status. After expression, a $Glc_3Man_9GlcNAc_2$ is transferred to Asn86 which is subsequently trimmed by GluI and GluII to $Glc_1Man_9GlcNAc_2$. Calreticulin binds monoglucosylated MHC I molecules and recruits them into the PLC for peptide loading and quality control[16]. Once MHC I is loaded with a suitable peptide, MHC I is completely deglucosylated by GluII, and leaves the PLC towards the cell surface via the secretory pathway.

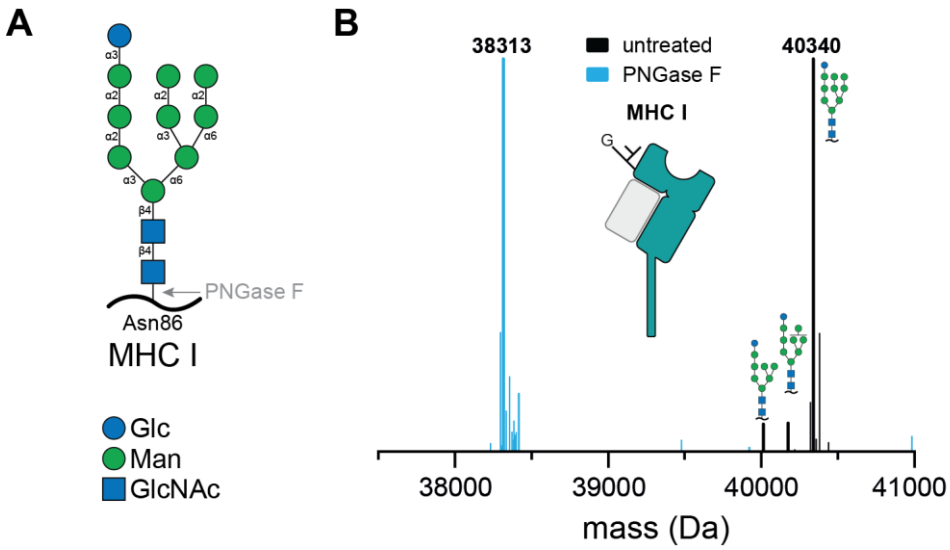

Figure 4.3-3: Glycosylation of MHC I heavy chain. (**A**) Schematic representation of N-linked glycan on MHC I heavy chain Asn86. The grey arrow indicates the PNGase F cleavage site. (**B**) Glycosylation pattern of MHC I allomorph HLA-A*03:01 associated with the PLC ($Glc_1Man_{9-7}GlcNAc_2$), analyzed by mass spectrometry (deconvoluted spectrum, black). The PNGase F-treated sample is shown as reference in cyan. HLA-A*03:01 is the predominate allomorph in LC-MS analysis. LC-MS and data analysis was performed by Christian Winter, Goethe University Frankfurt.

LC-MS allowed to analyze the mass of intact MHC I hc molecules. Raji cells express four different canonical HLA molecules (HLA-A*03:01, HLA-B*15:10, HLA-C*04:01, HLA-C*03:CD, genotyping by Halvard Bönig, Goethe University Frankfurt). However, only HLA-A*03:01 was detected by LC-MS with a sufficient signal to noise ratio for further experiments. As expected, HLA-A*03:01 was detected in the monoglucosylated form ($Glc_1Man_9GlcNAc_2$; M_{cal}: 40,340 Da, M_{obs}: 40,340 Da, Figure 4.3-3). Two alternative forms were observed with much lower intensity. The mass difference between the variants was 162 Da which equals the mass of one hexose, either mannose or glucose. For MHC I incorporated in the PLC the monoglucosylated form is required for the interaction with calreticulin. Therefore, loss of one or two mannoses, explains the lower intensity peaks. Mannoses are removed from N-linked glycans by the ER-α1,2-mannosidase I (ERmanI) in

the ER[216]. Their action flags molecules as defective and often leads to their degradation via the ERAD pathway. However, these MHC I molecules could also originate from retrograde transport from the Golgi apparatus where N-linked glycans can undergo heavy modifications which often include removal of several mannoses[217]. After full removal of the N-linked glycan by PNGase F, the expected molecular weight for HLA-A*03:01 was observed (M_{cal}: 38,312 Da, M_{obs}: 38,313 Da).

4.3.2. Tapasin glycosylation

Tapasin carries an N-linked glycan on Asn233 which faces the cavity in the PLC which is formed between the two tapasins in the PLC. To date, it is unclear whether this glycan has a function in MHC I recruitment or PLC assembly but it has been proposed to be involved in MHC I recruiting or sealing the cavity between both tapasins in the PLC[1,218].
Contrary to the defined glycosylation found on MHC I, the glycan on tapasin was very

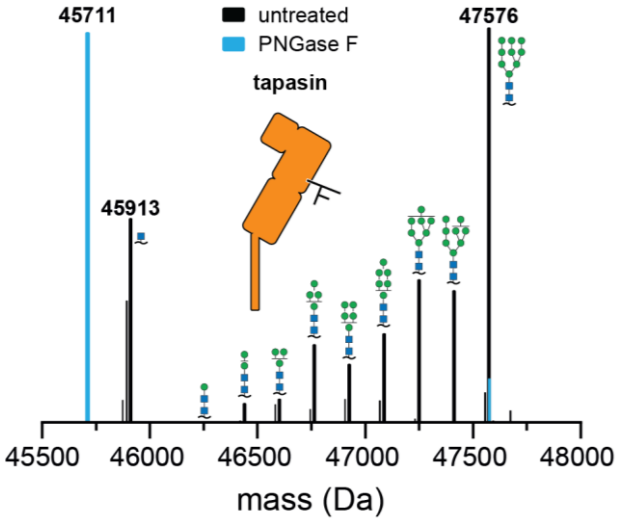

Figure 4.3-4: Complex glycosylation pattern of tapasin in the PLC. Glycosylation of tapasin in the PLC ($Man_{9\text{-}0}GlcNAc_{2\text{-}1}$), analyzed by MS (deconvoluted spectrum, black). PNGase F-treated sample is shown as reference in cyan. LC-MS and data analysis was performed by Christian Winter, Goethe University Frankfurt.

variable (Figure 4.3-4). The main species carried a $Man_9GlcNAc_2$ N-linked glycan without terminal glucose residues. The absence of glucose was confirmed because the glycan pattern did not change upon GluII treatment after PLC disruption in Fos-Choline-14 (Appendix Figure 6.1-5). A full range of mannose trimming was observed ($Man_{9\text{-}0}GlcNAc_2$), even down to a single GlcNAc as minimal N-linked glycan modification. This held true for the well-described canonical isoform 1 (Iso1) and a newly identified tapasin isoform 5 (Iso5, see chapter 4.3.3). Deglycosylation by PNGase F resulted in a single mass peak for both isoforms, excluding post-translational modifications other than N-linked glycosylation as being responsible for the difference in mass.

It is unclear in which order the mannoses are trimmed. Mannose trimming of N-glycans by ERmanI is linked to ERAD and involves the removal of three to four of the nine mannoses of the N-linked glycan[216]. However, such drastic modification as observed in this experiment are unusual for ER-resident proteins. Previously, tapasin glycan species trimmed down to $Man_6GlcNAc_2$ were reported[219]. However, even proteins modified in the Golgi apparatus usually retain at least their trimannosyl core ($Man_3GlcNAc_2$) during glycan trimming and subsequent modification to complex glycans[217]. One can hypothesize that tapasin undergoes iterative rounds of glycan trimming, but that glycan-trimmed tapasin might be constantly recycled into the PLC and are thereby protected from ERAD.

4.3.3. Identification of an alternative tapasin isoform in human PLC

PLC analyzed by SDS-PAGE, immunoblotting, and LC-MS showed a distinct double band for tapasin (Figure 4.2-4 B**,** Figure 4.3-1). The main band, representing ~63% of the total tapasin in the purified PLC, was detected at the expected molecular weight of 47.5 kDa, resembling the canonical tapasin isoform 1 (Iso1) (Uniprot ID: O15533-1, Figure 4.3-5 A). In addition, a second band at slightly higher molecular weight was detected in SDS-PAGE and immunoblot, representing ~37% of the total amount of tapasin. Subsequent LC-MS analysis of reconstituted PLC::MSP2N2 confirmed this result (Figure 4.3-1). Tapasin displays a complex glycosylation pattern (see chapter 4.3.2). However, for both detected forms of tapasin a mass difference of 1,077 Da is apparent (Figure 4.3-5 B). To eliminate the mass uncertainty introduced by the glycosylation, the sample was deglycosylated by PNGase F. Afterwards two distinct peaks were observed, one for each tapasin variant, with a consistent mass difference of 1,077 Da (Figure 4.3-5 B). Consequently, the N-linked glycan was excluded as cause of the mass difference. So far, no other post-translational modifications of tapasin have been reported. Thus, a difference in the primary structure was a likely cause of weight difference.

To identify isoforms of tapasin, both bands were extracted from SDS-PAGE and digested by trypsin. The resulting peptides were identified by MS and mapped onto the sequence of tapasin (Figure 4.3-5 C, Table 6-3). The lower band in SDS-PAGE represented the well-described Iso1 with 428 amino acids and an intact mass of 45,711 Da (deglycosylated), which is in accordance with the theoretical mass of 45,711 Da for the mature protein without signal peptide and glycan. However, the high molecular weight band represented a new tapasin isoform (Iso5) with an intact mass of 46,788 Da. The mass of this protein did not match with any of the previously described four isoforms. Comparative analysis of tryptic peptides revealed a long (2,120.2 Da), dominant peptide originating from the new isoform. In combination with a database analysis of predicted mRNA transcripts (NCBI reference sequence: XP_016866716.1), this peptide was assigned to the C terminus of tapasin Iso5. The observed intact mass of 46,788 Da was in accordance with the theoretic mass of 46,789 Da

for Iso5. The unique new C-terminal peptide indicated that exon 7 was skipped, leading to a frameshift in exon 8 and a new stop codon (Figure 4.3-5 D).

Effectively, Iso5 is very similar to Iso1 but carries a different cytosolic C-terminal tail. Since MHC I peptide proofreading and interactions with the second tapasin molecule in the PLC are mediated by the ER-lumenal domains, it is very likely that this isoform of tapasin is fully active as a chaperone within the PLC[55,220,221]. The interaction between tapasin and TAP in the ER membrane depends on a critical salt bridge between Lys428 of tapasin and Asp32 of TAP1/2[(ref. 17)]. The tapasin Lys428 is unaffected by the frameshift which occurs after amino acid 443. Thus, interaction with TAP1/2 was not affected. Yet, Iso5 lacks the C-terminal KKXX motif that is responsible for ER retention via COPI retrograde transport[222,223], suggesting that tapasin Iso5 might travel along the secretory route without retrograde transport. However, exon 7 skipping has not been observed in any other cell than Raji cells. Therefore, it could be a distinct property of Raji cells.

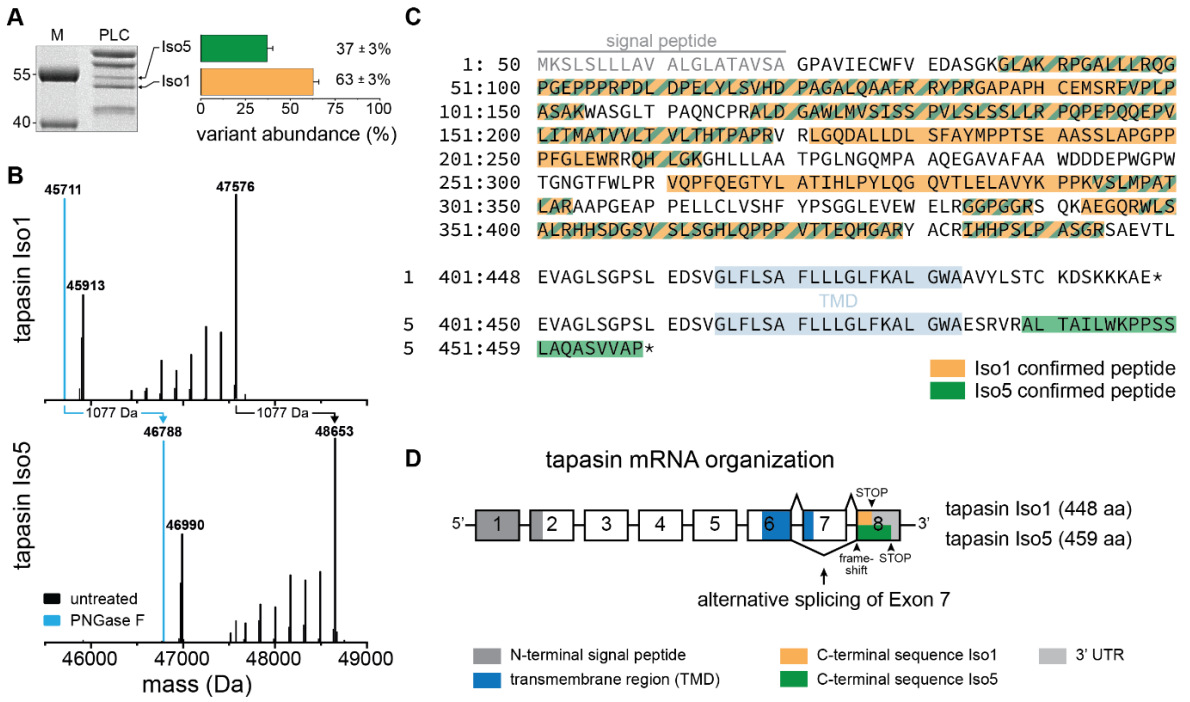

Figure 4.3-5: The PLC from Raji cells incorporates different splice variants of tapasin. (A) Two tapasin variants are recruited to the PLC in Raji cells, as demonstrated by SDS-PAGE. The abundance of isoform 1 (Iso1) and isoform 5 (Iso5) were quantified in PLC from Raji cells (n = 3). **(B)** Both tapasin variants showed a similar glycosylation pattern, as deconvoluted by mass spectra of tapasin Iso1 (top) and Iso5 (bottom). The masses of the two PNGase F-treated isoforms are shown in cyan. **(C)** Two tapasin isoforms were identified by tryptic digest and MS. Identified peptides of Iso1 and Iso5 are colored in orange and green, respectively. Peptide data is summarized in Table 6-3. **(D)** Schematic illustration of tapasin mRNA organization. The skipped exon 7 resulted in a frameshift in exon 8 and an extended C-terminal sequence (Iso5) compared to the canonical tapasin variant (Iso1). PNGase F treatment, trypsin digestion, LC-MS and data analysis were performed by Christian Winter, Goethe University Frankfurt.

4.4. Structural analysis of MHC I editing in the PLC

Structural information is often crucial to understand the function of proteins and their assemblies. The protein composition of the PLC has been determined and also the general architecture of the PLC was reported previously[1,2]. However, the intermediate resolution (5.8 Å) of the structure solved by cryo-EM was not sufficient to describe and understand the functional details of the PLC. Furthermore, it was necessary to stabilize PLC::GDN for cryo-EM by chemical crosslinking which could induce artefacts.

4.4.1. Negative-stain electron microscopy

The PLC was reconstituted in three different membrane mimetics to facilitate structural analysis without the need of detergent (see chapter 4.2). To verify the structural integrity of the PLC after the reconstitution process, the reconstituted PLCs were evaluated by negative-stain EM (Figure 4.4-1). PLC::MSP2N2 assemblies (particles) were distributed homogenously across the grid (Figure 4.4-1 A). The particles' size matched the reported size for the human PLC in GDN[1]. The 2D class averages showed features of the editing modules, the membrane region embedded in MSP2N2, as well as the NBDs. However, the position of the NBDs was blurry and varied between different views which indicated high flexibility of their position relative to the well resolved editing modules. The PLC samples reconstituted in Saposin A and Peptidisc were analyzed accordingly (Figure 4.4-1 B and C, respectively). Both reconstitution methods yielded evenly distributed PLC across the grid with low number

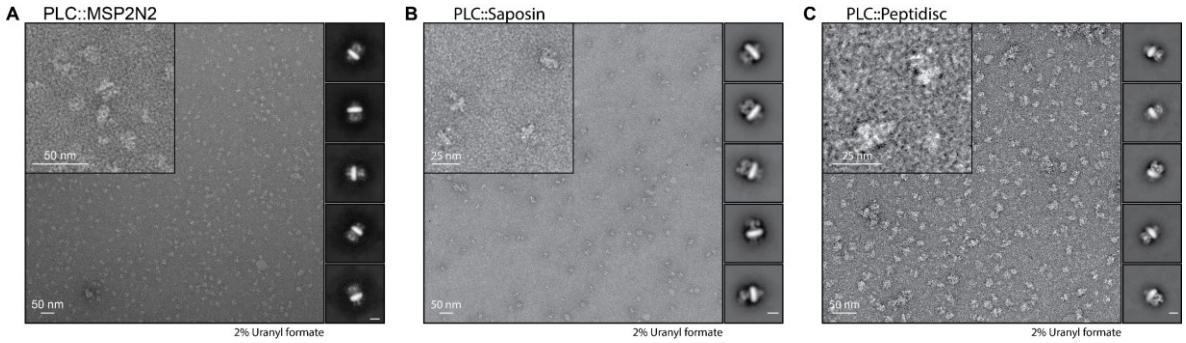

Figure 4.4-1: PLC is intact after reconstitution in membrane mimetics. All samples were spotted on continuous carbon grids and stained with 2% (w/v) uranyl formate solution. The scale bar in the classes corresponds to 10 nm. (**A**) Micrograph of PLC::MSP2N2. A total of 196 micrographs were imaged and processed yielding 94,109 particle picks. 18,600 particles were selected for reclassification (50 classes). Five representative 2D classes are shown on the right side of the micrograph. (**B**) Micrograph of PLC::Saposin. A total of 371 micrographs were imaged and processed yielding 144,162 particle picks. 28,314 particles were selected for reclassification (50 classes). Five representative 2D classes are shown on the right side of the micrograph. (**C**) Micrograph of PLC::Peptidisc. A total of 102 micrographs were imaged and processed yielding 29,150 particle picks. 11,256 particles were selected for reclassification (30 classes). Five representative classes are shown on the right side of the micrograph. An enlarged version of the image is depicted in Appendix Figure 6.1-3.

of aggregates. The 2D class averages indicated successful reconstitution of fully assembled PLC into the respective membrane mimetic system. Similar to PLC::MSP2N2, the features of PLC were conserved after reconstitution in Saposin A and Peptidisc and were visualized in negative-stain EM.

Due to the encouraging results in negative-stain EM for PLC reconstituted in all three membrane mimetic systems, subsequent cryo-EM experiments were performed. The results for the cryo-EM experiments with PLC::MSP2N2 are described in detail in chapter 4.4.2. PLC::Saposin and PLC::Peptidisc did not pass initial screenings. PLC::Peptidisc seemed to aggregate upon freezing for cryo-EM analysis and only a low number of particles were visible in suitable ice, as documented by the Master Thesis of Leon Hennecke[210]. Similar results were obtained with PLC reconstituted in Saposin A[210].

4.4.2. Cryo-EM analysis of PLC::MSP2N2

In the present work, PLC was reconstituted in MSP2N2 nanodiscs (chapter 4.2.2) resulting in sufficient stabilization of the PLC for cryo-EM sample preparation without need for chemical fixation (Appendix Figure 6.1-4). A sample of ~1.8 mg/mL PLC::MSP2N2 was frozen on Quantifoil Cu 300 1.2/1.3 grids and imaged in a Titan KRIOS cryo-TEM. The particles were well distributed and intact PLC molecules were visible. In total 2,341 micrographs were recorded and analyzed by cryoSPARC[146,224]. A subset of 100 micrographs was selected for training of the deep picker TOPAZ[190,191]. Reference-free classification of particles picked by blob picking from these 100 images showed already the known features of intact PLC, proving the stabilization of the PLC by MSP2N2 reconstitution. The trained TOPAZ picker identified 613,746 particles in the full set of micrographs. A selection was used to generate reference-free *ab-initio* reconstructions. Two resulting classes represented PLC assemblies and were used in several rounds of 2D classification, 3D classification, and subsequent refinement: (i) PLC including the membrane region (Figure 6.1-4, orange). One editing module was fully defined while the second editing module was not fully assembled. (ii) A single editing module (Figure 6.1-4, green). Map (i) (Figure 6.1-4, orange) refined to a resolution of 4.01 Å generated from 52,688 particles (Figure 4.4-2). The single editing module (ii) (Figure 6.1-4, green) refined to a higher resolution of 3.73 Å from 97,952 particles (Figure 4.4-3). Both maps contained one fully assembled editing module with all expected subunits present (tapasin, ERp57, calreticulin, MHC I hc, and β_2m). In the map of assembly (i) further density was visible for the second editing module and the membrane region. The resolution in the membrane region was low and no density for TAP or other transmembrane regions was observed. Probably TAP and the bound tapasin helices are very dynamic and/or flexible within the PLC and were therefore not resolved. Reconstituting the PLC in MSP2N2 alone was not sufficient to stop these movements. Maybe stabilization of TAP by usage of other inhibitors (e.g. US6[(ref. 139)]), ATP, or trapping of TAP by vanadate or ATP analogues like AMPPNP could help, as demonstrated for the TAP homolog TmrAB[5]. A strategy to generate inhibitor-free PLC for these experiments is discussed in chapter 4.8.

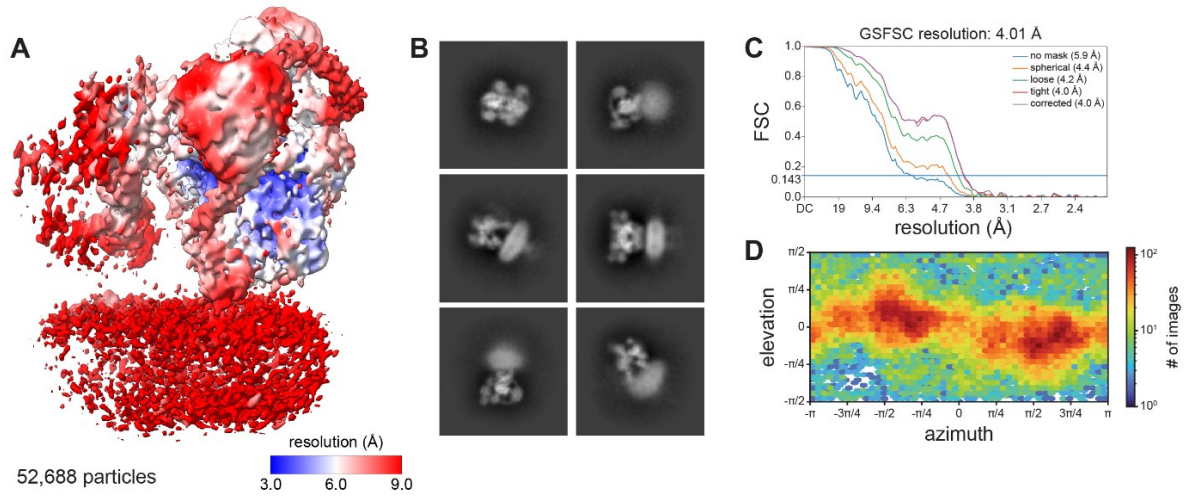

Figure 4.4-2: Cryo-EM analysis of PLC reconstituted in lipid nanodiscs. (**A**) 3D representation of the full PLC structure from 52,688 particles. (**B**) Representative 2D class averages from the final set of particles with defined density for ER-lumenal editing module regions and blurred signal for membrane associated regions. (**C**) Fourier shell correlation (FSC) curve of 3D reconstructions from two independently refined half datasets of the full PLC, generated by non-uniform refinement in cryoSPARC. An overall resolution of 3.73 Å was achieved as judged by the 0.143 threshold criteria. (**D**) Angular assignment of particles from the final dataset in respect to the 3D structure (A).

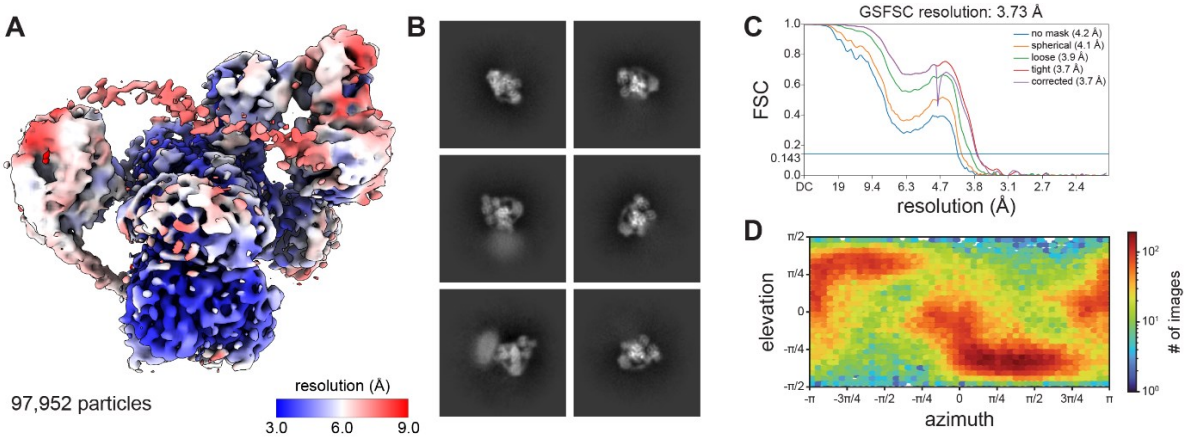

Figure 4.4-3: Cryo-EM analysis of the PLC editing module. (**A**) 3D representation of a single editing module structure from 97,952 particles. (**B**) Representative 2D class averages from the final set of particles with defined density for ER-lumenal editing module regions and blurred signal for all membrane associated regions. (**C**) Fourier shell correlation (FSC) curve of 3D reconstructions from two independently refined half datasets of the full PLC, generated by non-uniform refinement in cryoSPARC. An overall resolution of 3.73 Å was achieved as judged by the 0.143 threshold criteria. (**D**) Angular assignment of particles from the final dataset in respect to the 3D structure (A).

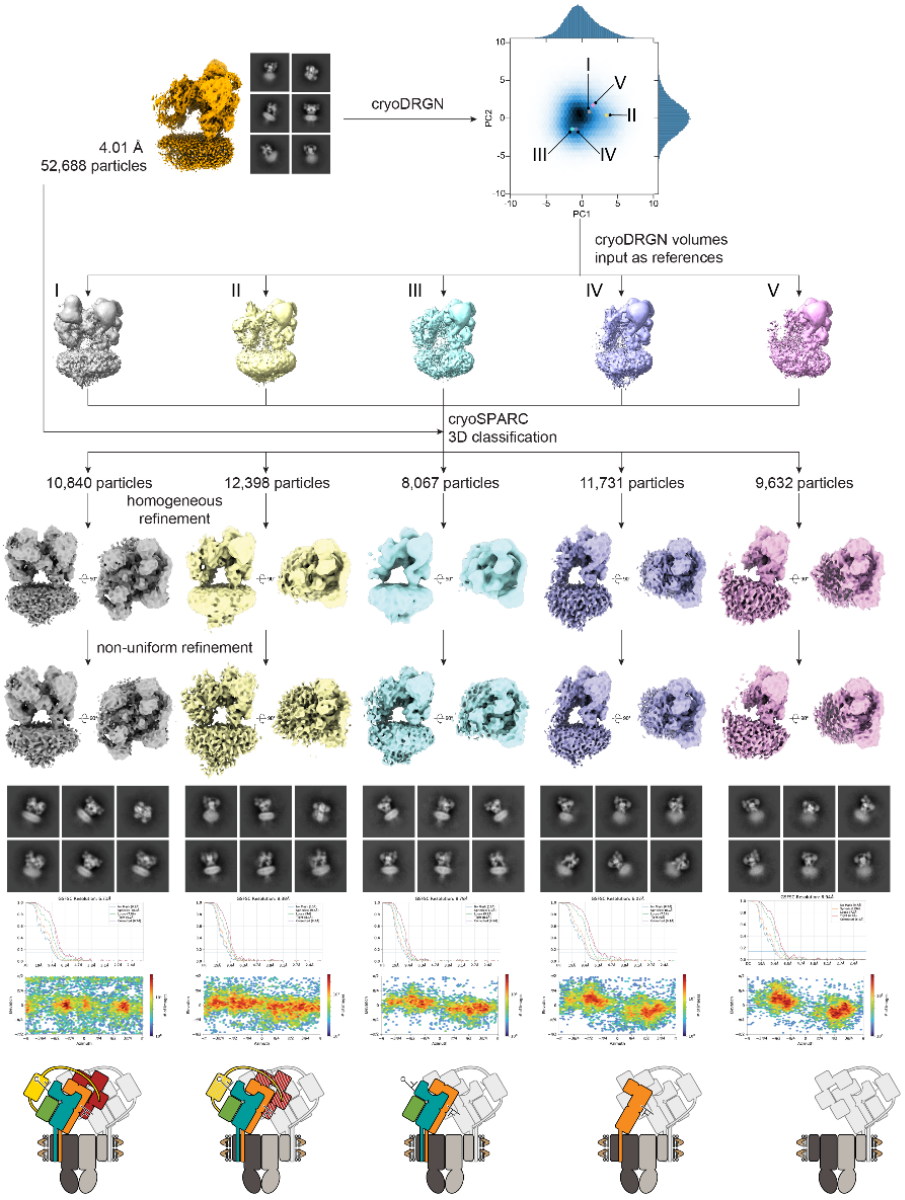

Figure 4.4-4: CryoDRGN analysis of different PLC assembly states. Particles of a single reconstruction from a homogeneous 3D refinement of the PLC (orange, "consensus map") were analyzed by deep learning using the neural network-based algorithm of cryoDRGN to reveal distinct PLC assemblies. Five different assembly states (I–V, colored tiles) were chosen from the principal component analysis projection of the 8-dimensional latent space (top right) for 3D classification, followed by homogeneous and non-uniform refinement in cryoSPARC. The chosen 3D reconstructions generated by cryoDRGN showed distinct PLC assembly intermediates. The fully assembled PLC (I, grey) with two complete editing modules. PLC reconstruction with a single editing module (V, pink). Densities representing reconstructions with intermediate assembly states of the second editing module (II – IV, yellow, blue, and purple). Depicted below each 3D map from non-uniform refinement are representative 2D class averages, Fourier shell correlation (FSC) curves of the 3D reconstructions from two independently refined half datasets, and angular assignments of particles from the final dataset with respect to the 3D structure above. Cartoons at the bottom depict the assembly state of the PLC by illustrating the subunits identified in each map. cryoDRGN analysis was performed by Christoph Thomas, Goethe University Frankfurt.

Reference-free 2D classification of the particles from partially assembled PLC indicated that fully assembled PLC with two complete editing modules was present within the sample (Figure 4.4-2 B). These different assembly states were not separated from the partial assembly (i) refined in cryoSPARC. Therefore, particles and their orientation from the partially assembled PLC were extracted from cryoSPARC and analyzed in cryoDRGN (Figure 4.4-4)[ref. 192]. Principal component analysis in cryoDRGN showed a single peak. However, manual inspection yielded five maps reflecting distinct PLC compositions present in the data (Figure 4.4-4 I-V) which were not separated previously in cryoSPARC. These maps served as references I-V for 3D classification and refinement in cryoSPARC. Approximately 20% of the particles were fully assembled PLC molecules (I, grey) proving the purification of intact PLC from Raji cells. ~18% of the particles were classified and refined to a PLC model consisting of only one editing module attached to the membrane region (V, pink). This state has been modeled *in silico* and showed a high degree of flexibility between editing module and membrane[225]. This flexibility is reflected in the less defined and displaced membrane density below the editing module. The states II, III, and IV represent PLCs with different assembly states of the second editing module while one editing module is always fully assembled. In state II (yellow) calreticulin and ERp57 are less defined. In state III (cyan) both proteins are completely missing in the second editing module, and in state IV (purple) tapasin is the only remaining PLC component in the second editing module. Similar intermediates have been found in the previous structure analysis of PLC[1]. Most likely, the state I represents the native state of fully assembled PLC with two MHC I molecules before loading. Similarly, state V could be an equivalent state, however in a PLC where only one editing module is present. For states II, III, and IV, it remains unclear whether these represent naturally occurring states or whether these are generated during cryo-EM sample preparation.

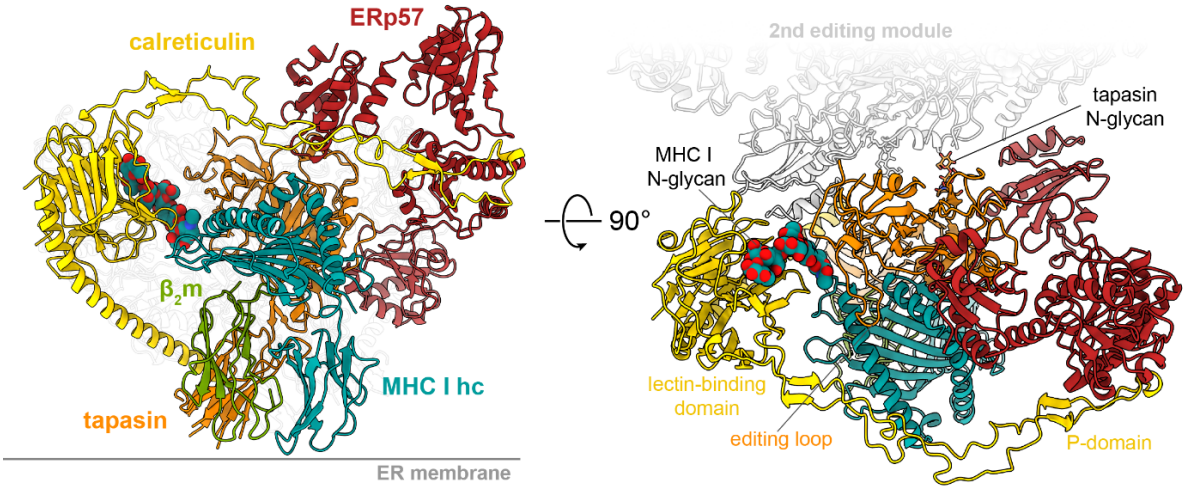

Figure 4.4-5: Structure of the PLC editing module. Structure of the peptide-receptive MHC I stabilized by a multivalent chaperone network in the editing module (side and top view). The glycan of MHC I and tapasin is shown as space-filling model and stick model, respectively. The proposed position of the second editing module is indicated in light grey. The model was generated in cooperation with Christoph Thomas, Goethe University Frankfurt.

The vitrification process is harsh and many air-water-surface contacts can occur which can harm and destroy proteins or complexes[226–229]. Especially, the fact that ERp57 is not present in all states is a strong indication for particle damage, since tapasin and ERp57 appear almost always as heterodimer in the ER lumen and are linked by a covalent disulfide bond in the PLC[59].

Despite the confinement in large lipid nanodiscs, the two editing modules and the transport complex TAP remained flexible relative to each other, limiting the overall resolution of the entire PLC. Focused refinement on the fully assembled editing module resulted in a cryo-EM map with an average resolution of 3.7 Å. The resolution of the single editing module was significantly improved from previously 5.8 Å to 3.7 Å[1]. This allowed to model the PLC in detail (Figure 4.4-5). The previous model (PDB: 6ENY) was docked into the new density and flexibly adapted by using ISOLDE integrated in ChimeraX[193]. Afterwards the structure was further refined in COOT and Phenix[194,195]. The density of the A-branch of the MHC I glycan was build *de novo* and validated in Privateer (Figure 4.4-6 A)[(ref. 196)]. Similarly, the editing loop of tapasin (residues 11-20) was modeled *de novo* (Figure 4.4-6 B). The refinement of the model has been performed by Christoph Thomas, Goethe University Frankfurt.

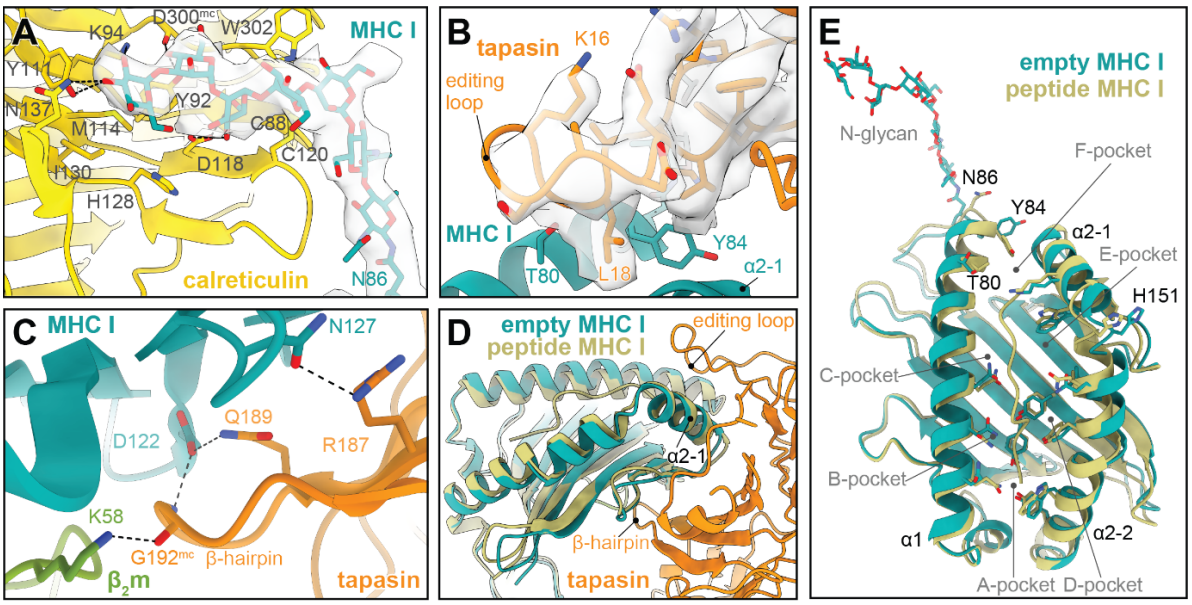

Figure 4.4-6: MHC I interactions in the PLC. (**A**) Interaction of the MHC I glycan with the lectin domain of calreticulin. The cryo-EM map of the glycan is depicted as a transparent isosurface (contour level 0.19, light grey). (**B**) Tapasin editing loop and its interactions with the MHC I hc molecule. The cryo-EM map of the editing loop is depicted as a transparent isosurface (contour level 0.19, light grey). (**C**) β-hairpin of tapasin and its interactions with β_2m and MHC I hc. (**D**) Superposition of peptide-loaded MHC I (PDB: 3RL1) with empty MHC I in the PLC (side view, including the interface with tapasin). (**E**) Peptide-receptive MHC I are stabilized in a widened conformation as highlighted by superposition of peptide-loaded MHC I (PDB: 3RL1) with the PLC-associated MHC I.

The model of the PLC editing module proves findings from the previous PLC structure where chemical crosslinking was applied to stabilize the PLC[1]. As major interaction hub, tapasin contacts all other PLC subunits (Figure 4.4-5). In addition to the non-covalent interactions, tapasin is disulfide-linked via Cys95 to Cys33 of ERp57. The high-resolution structure allowed to build an atomic model of the surprisingly well resolved N-linked glycan bridging the lectin domain of calreticulin to Asn86 of MHC I hc. The terminal glucose on the MHC I glycan is coordinated by Lys94, Asn137, and Tyr111 of calreticulin, consistent with the structure of the isolated lectin domain bound to a Glc_1Man_3 tetrasaccharide[30]. Whereas Met114 and Ile130 of calreticulin shape the glucose-binding pocket, further contacts to the N-glycan are established by Asp118, $Asp300^{mc}$ (main chain), Tyr92, and Trp302. Additional calreticulin residues involved in glycan binding are His128 and the disulfide bond between Cys88 and Cys120 (Figure 4.4-6 A). The mannoses in the B/C-branch of the glycan were too flexible to be resolved at high resolution. In contrast to the N-glycan of MHC I, only the trisaccharide $Man_1GlcNAc_2$ stem of the Asn233-linked glycan in tapasin was defined by the cryo-EM map, suggesting that the remaining sugar moieties of the tapasin-linked glycan are flexible.

Besides the structurally defined N-linked glycan of MHC I, the reconstruction revealed crucial features of the tapasin-MHC I multi-chaperone complex which have not been elucidated so far. A well-resolved loop of tapasin (residue 11-20), referred to as editing loop, is positioned on top of the F-pocket of the empty MHC I peptide-binding groove (Figure 4.4-6 B, Figure 4.4-7). Leu18 of the editing loop contacts MHC I in a position that would clash with Tyr84 of peptide-bound MHC I Figure 4.4-6 B). Thus, the structure suggests that Leu18 disrupts the contact of Tyr84 with the C terminus of cargo peptides and thereby contributes to peptide exchange catalysis[62]. This arrangement resembles the position of the scoop loop in TAPBPR, which is larger (16 amino acids vs. 10 amino acids in tapasin) but is similarly positioned and disturbs the interaction between Tyr84 in MHC I and the C terminus of the cargo peptide by inserting residues 34-36 into the MHC I peptide binding groove

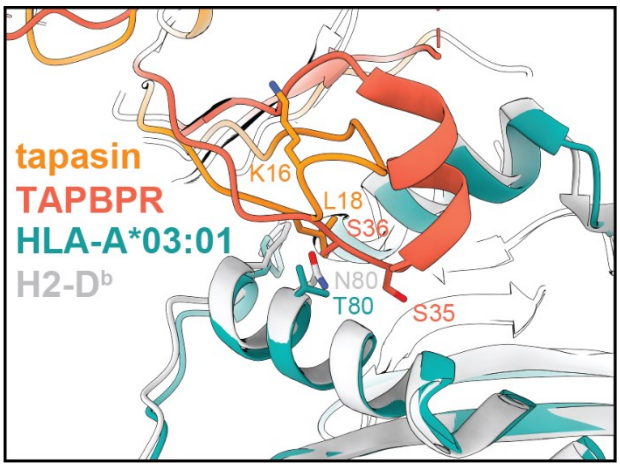

Figure 4.4-7: Editing loop comparison between tapasin and TAPBPR. Superposition of the tapasin editing loop in the PLC (orange/teal, PDB: 7QPD) with the TAPBPR scoop loop in the TAPBPR-H2-D^b chaperone complex (light red/light grey, PDB: 5OPI).

(Figure 4.4-7)[ref. 28]. The displacement of Tyr84 is stabilized by the interaction with Glu72 of tapasin, consistent with TAPBPR-MHC I crystal structures[28,73]. Leu18 of the editing loop also supports the open MHC I conformation by pushing away Thr80 and Leu81 in the α1 helix, as well as Ala139 and Ile142 in the α2-1 helix of MHC I. HLA-A*03:01, the predominant allomorph in the isolated PLC, harbors an acidic F-pocket, and it was hypothesized that this acidic F-pocket is stabilized by Lys16 of the editing loop[62]. However, this was not observed in this structure. On the contrary, the side chain of Lys16 is flexible in the structure and points away from the MHC I peptide-binding groove, which is consistent with previous simulations[230]. Notably, rat and mouse tapasin do not contain any basic residue in the editing loop, rendering the proposed F-pocket stabilization as a general accessory catalytic principle unlikely. Consistent with the structure of TAPBPR-MHC I chaperone complexes[28,73], the floor of the peptide-binding groove is acted upon by a β-hairpin of tapasin (Figure 4.4-6 C). Direct contacts in this region include Arg187 and Gln189 of tapasin, as well as Asn127 and Asp122 of MHC I. The latter residue also forms a hydrogen bond with the main-chain of Gly192 at the tip of the tapasin β-hairpin, which additionally interacts with Lys58 of β_2m. The contact of Arg187 in tapasin with the MHC I hc might contribute to substrate specificity of the peptide editor, as the interacting MHC I residue (Asn127 in HLA-A*03:01) is not conserved between allomorphs (Appendix Table 6-5). However, the allomorph specificity of tapasin cannot be reduced to this interaction alone, but instead it also is dependent on the intrinsic flexibility of each allomorph[231].

A superimposition of the chaperone-stabilized empty MHC I onto the X-ray structure of soluble, non-glycosylated peptide-loaded HLA-A*03:01 highlights the open conformation of PLC-bound MHC I[232] (Figure 4.4-6 D, E). The rearrangement of the α1 and α2 helices results in a widening of the peptide-binding groove, facilitating peptide exchange. The α1 helix (residues 57-85) displays Cα shifts which are most pronounced at the F-pocket (residues 79-85), with a root mean square deviation (RMSD) of 1.8 Å. Interaction with tapasin leads to a lateral shift of the α2 helix which is most pronounced in the hinge region (residues 149-153), with an RMSD of 2.0 Å. In contrast to TAPBPR-MHC I complexes[16,28,73], the empty peptide-binding groove of the PLC-bound MHC I is in its widened conformation stabilized on both helices, not only by multivalent protein-protein interactions with tapasin, but also by glycan-protein contacts via calreticulin. Based on the shift of the α1 helix, one can hypothesize that the closing of the peptide-binding groove after successful peptide loading results in a release of the glycan from the lectin domain of calreticulin.

4.5. Allosteric coupling of peptide loading and MHC I glycan processing

Peptide proofreading by tapasin ensures that only kinetically stable pMHC I loaded with high-affinity peptides are released to the cell surface, whereas suboptimal, low-affinity peptides are discharged and eventually replaced by high-affinity epitopes[16,54,55,220,233]. Once MHC I molecules are loaded with an optimal epitope, they leave the PLC to present the peptide cargo on the cell surface. Additionally, the terminal glucose of the Asn86-linked (p)MHC I glycan must be removed by GluII to pass ERQC. To understand the loading, proofreading and glycan processing of MHC I in more detail, the first step was to investigate MHC I peptide binding in the context of purified, nanodisc reconstitute PLC.

The peptide proofreading activity of lipid-embedded PLC was analyzed by fluorescence polarization using the fluorescein (^{F})-labeled peptide C^{F}SN (AIFC^{F}SNMTK). This HIV-Nef73-derived epitope binds with high affinity to HLA-A*03:01, the predominant MHC I allomorph in PLC isolated from Burkitt's lymphoma cells. Within 15 min, binding of C^{F}SN was observed upon its addition to PLC-bound MHC I (Figure 4.5-1). In contrast, the suboptimal peptide C4F (RRYC^{F}KSTEL) did not interact with the PLC under these conditions. Importantly, bound C^{F}SN peptides were rapidly displaced by an excess of unlabeled CSN peptide, while a similar excess of the unfavored peptide R9L (RRYQKSTEL) did not trigger substantial peptide exchange. Thus, the reconstituted PLC was fully functional in catalyzing peptide proofreading.

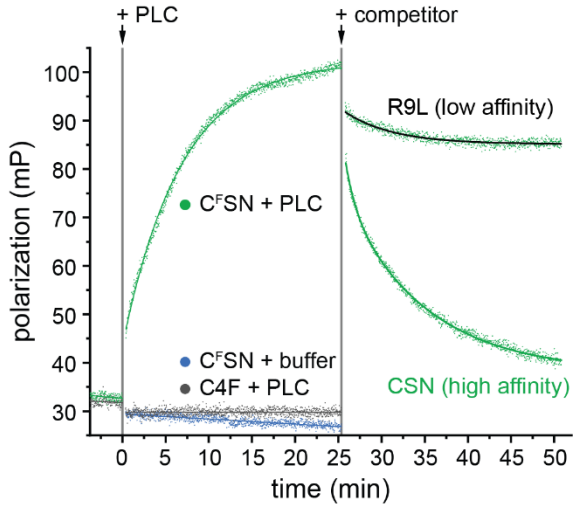

Figure 4.5-1: Peptide binding and editing of PLC chaperoned MHC I. Peptide binding and proofreading of the PLC reconstituted in lipid nanodiscs (75 nM) was monitored by fluorescence polarization using equal concentration of fluorescent reporter peptides. PLC-associated HLA-A*03:01 bound the high-affinity epitope C^{F}SN (AIFC^{F}SNMTK; $K_d \approx 10$ nM). In contrast, the low-affinity HLA-B*27:01-restricted epitope C4F (RRYC^{F}KSTEL; $K_d \approx 20$ µM) did not interact with PLC-associated MHC I. For peptide editing, a 2000-fold molar excess of unlabeled high-affinity peptide (150 µM CSN, AIFCSNMTK; $K_d \approx 10$ nM) displaced the reporter peptide (green trace), while the same excess of low-affinity peptides (150 µM R9L, RRYQKSTEL, $K_d \approx 20$ µM, black trace) did not outcompete the bound reporter peptide C^{F}SN.

To monitor the glycosylation status of HLA-A*03:01 during peptide proofreading, HLA-A*03:01 was analyzed by LC-MS after GluII trimming in the presence and absence of the high-affinity peptide CSN, or in the presence of the non-binding peptide R9L (Figure 4.5-2). In the absence of peptides, the addition of GluII did not change the glycan of MHC I ($Glc_1Man_9GlcNAc_2$, 40,340 Da), demonstrating that the terminal glucose is protected from processing by GluII. However, in the presence of the high-affinity peptide CSN, a single glucose moiety was removed by GluII, reflected by a mass shift of 162 Da ($Man_9GlcNAc_2$-MHC I, 40,178 Da) (Figure 4.5-2, Appendix Figure 6.1-7). Mannose and glucose are epimers, meaning that the determination of the leaving group directly by MS is not possible. However, since GluII exclusively cleaves terminal glucose residues at the A-branch, with flexibility in the number of mannoses at the B- and C-branches[37], Glucose is the only plausible leaving group. The structure of the glycans described is supported by previous experiments, where arm-specific isomers were distinguished[219].

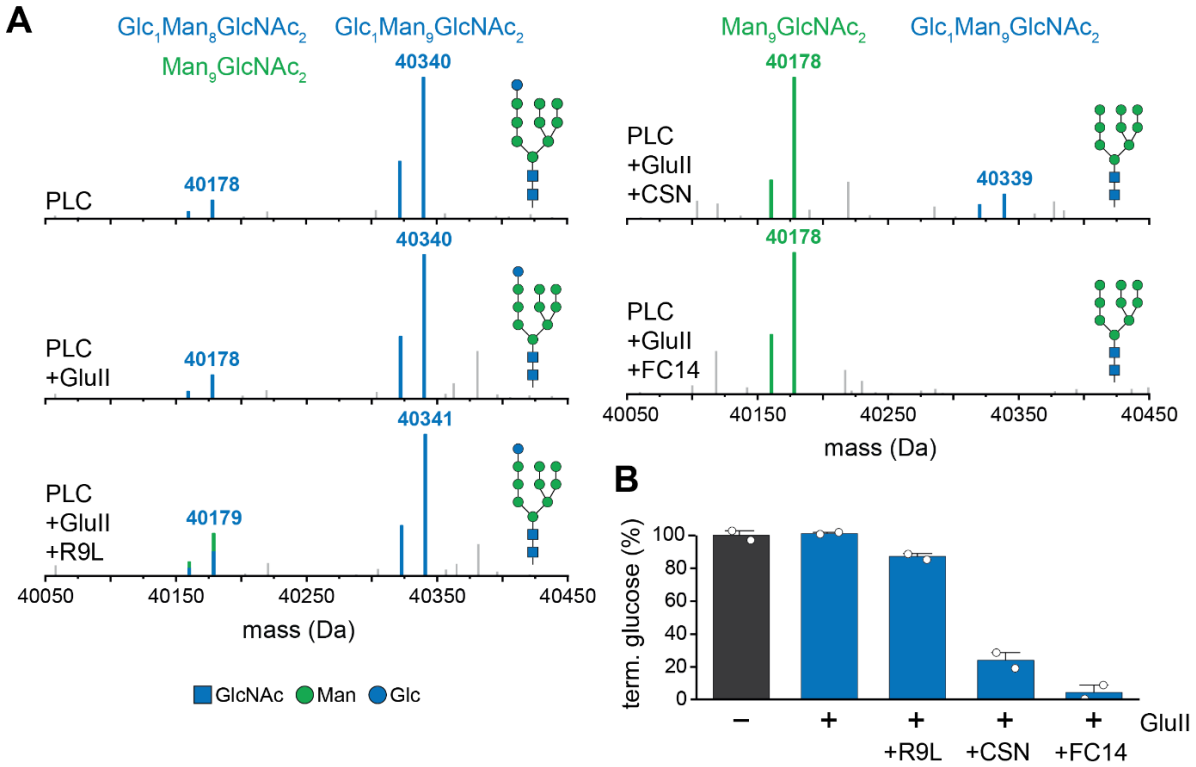

Figure 4.5-2: Peptide editing is coupled to MHC I glycan processing by GluII. (**A**) Peptide loading is allosterically coupled to N-glycan deglucosylation of MHC I by GluII. The terminal glucose on HLA-A*03:01 is removed by GluII only when an optimal peptide epitope (CSN) is loaded onto MHC I, or if the PLC is disintegrated by detergent (FC14), which leaves the glycan accessible for GluII trimming. GluII is not observed in presence of a low affinity HLA-A*03:01 peptide (R9L). (**B**) Quantification of the glucose trimming. The percentage of the $Glc_1Man_9GlcNAc_2$- and $Man_9GlcNAc_2$-modified HLA-A*03:01 after GluII treatment. Mean ± SEM (n=2) is shown. LC-MS analysis was performed by Christian Winter, Goethe University Frankfurt.

In contrast, processing of the MHC I glycan by GluII was not induced by addition of the unfavored peptide R9L. To verify peptide-independent deglucosylation of MHC I, the PLC was disintegrated by the detergent Fos-Choline-14 (FC14) which allows free access of the GluII to MHC I (Appendix Figure 6.1-6). Notably, the MHC I glycan was completely deglucosylated after disassembly of the PLC (Figure 4.5-2). These observations indicate that GluII-mediated glycosidic bond cleavage of the innermost glucose residue on the MHC I glycan is allosterically coupled to peptide editing.

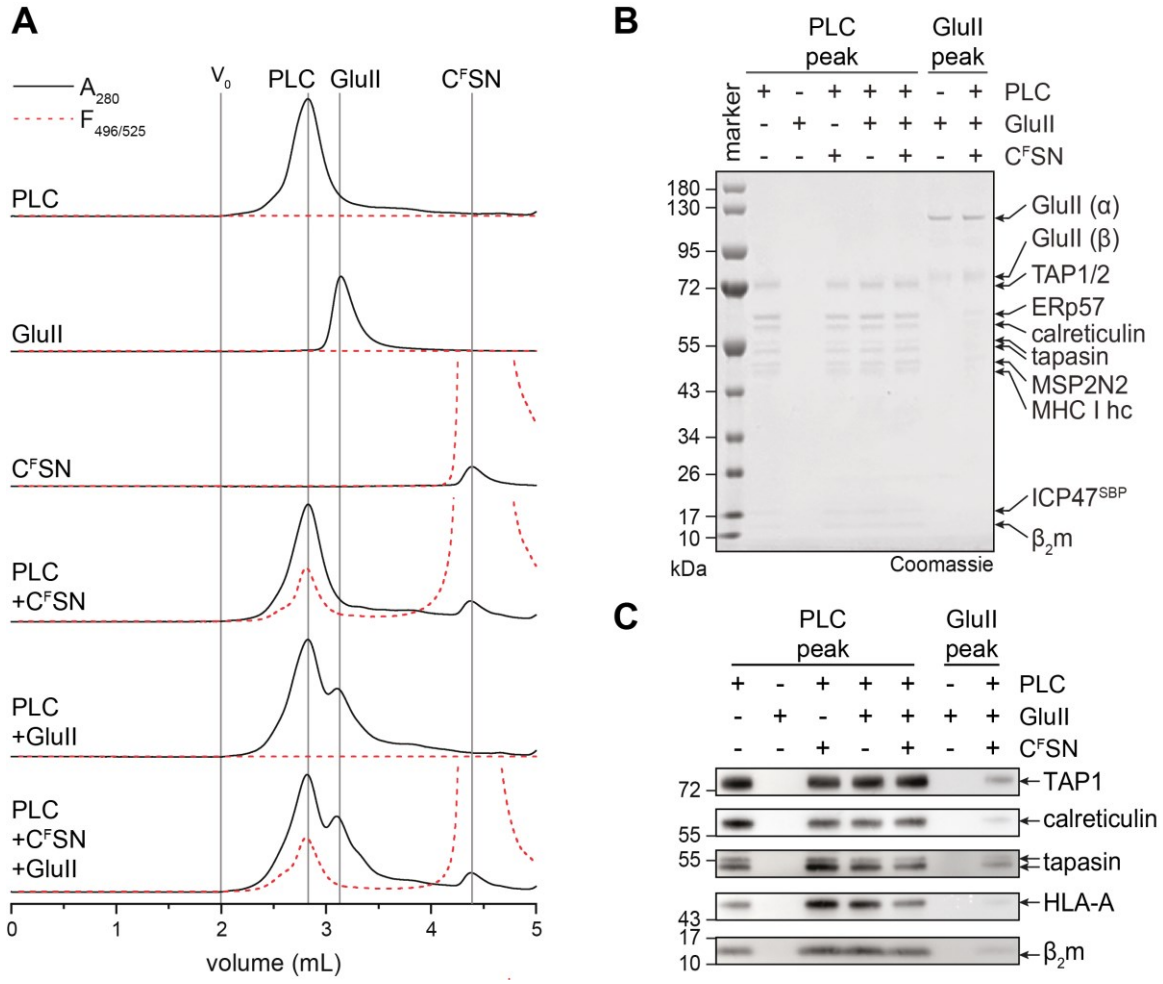

Figure 4.5-3: PLC remains fully assembled during peptide loading and deglucosylation. (**A**) The size of the nanodisc reconstituted PLC remained unchanged after peptide binding and GluII trimming as demonstrated by SEC. Peptide loading and glycan trimming by GluII did not change the overall composition and stoichiometry of the PLC. (**B**, **C**) The PLC remained fully assembled after MHC I loading with high-affinity peptide epitope (CSN) and GluII-catalyzed deglucosylation of MHC I as demonstrated by SDS-PAGE (reducing, 4-12%, Coomassie) (B) and immunoblotting (C) of SEC fractions corresponding to the PLC and GluII peak

The previous model of the sequential loading and disassembly of the PLC after MHC I loading with a high-affinity peptide suggested that calreticulin would leave and allow access of GluII to the MHC I glycan. This is further supported by current working models of ERQC[15,234,235]. The PLC composition was analyzed before and after peptide loading and

glycan trimming by SEC, SDS-PAGE, and immunoblotting. Using the high-affinity fluorescent peptide $C^{F}SN$ as reporter, we followed peptide loading of MHC I in parallel by fluorescence-detection SEC. No change in size and overall composition of the PLC upon peptide loading of MHC I and glycan trimming by GluII was observed (Figure 4.5-3 A). This indicates that MHC I glycan processing by GluII occurs upon loading of optimal epitopes in the fully assembled PLC containing calreticulin (Figure 4.5-3 B, C). This implies that the supramolecular organization of the PLC is characterized by a significant degree of plasticity. Taken together, the finding of an allosteric coupling between peptide editing and glycan processing during MHC I quality control suggests that GluII is a transient component of the PLC providing additional layers of complexity in the organization and function of the PLC.

In conclusion, the glycan processing studies demonstrated that, as far as the nanodisc reconstituted PLC is concerned, the status of the MHC I glycan is coupled to the peptide-loading status. Based on the structural data (chapter 4.4) and the identification of context-sensitive MHC I glycan processing, the following model for peptide loading and quality control of MHC I was proposed (Figure 4.5-4): After recruitment of peptide-receptive MHC I in complex with calreticulin into the PLC, MHC I complexes acquire high-affinity peptide epitopes through tapasin-catalyzed proofreading and peptide exchange. Binding of an optimal epitope weakens the interaction between MHC I and tapasin, but also leads to a rearrangement of the MHC I glycan. This rearrangement loosens the connection between the A-branch of the glycan and the lectin domain of calreticulin and allows deglucosylation by

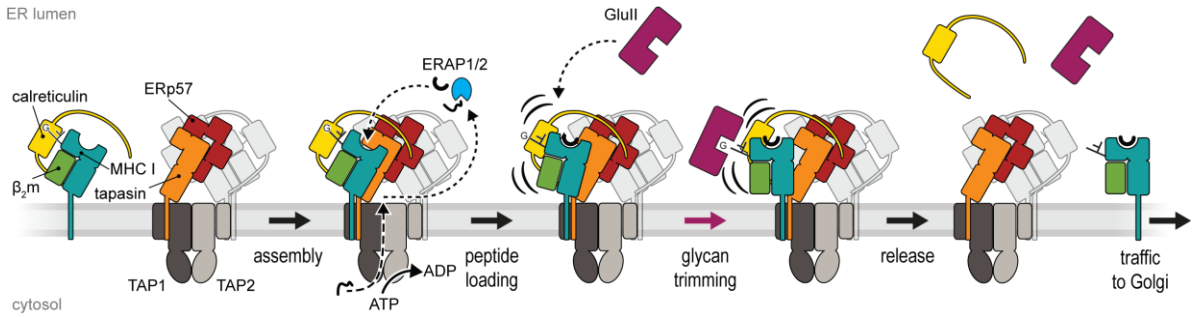

Figure 4.5-4: Mechanism of MHC I assembly, peptide editing, and quality control. Peptide-receptive MHC I heterodimers are recruited by calreticulin to the PLC and form the fully assembled PLC, which is composed of two editing modules. The peptide transporter TAP shuttles peptides from the cytosol into a molecular basket formed by the editing modules. Two lateral windows allow peptides to diffuse into the ER lumen to be edited by the ER-resident aminopeptidase ERAP1/2 and subsequently loaded onto MHC I molecules. After tapasin-facilitated peptide loading and proofreading of pMHC I, the MHC I glycan becomes accessible for trimming by GluII in the presence of calreticulin. Thus, calreticulin is not required to leave the PLC for N-glycan editing when MHC I release is restricted. Glucose-trimmed pMHC I complexes are released from the PLC and traffic via the Golgi compartment to the cell surface. The remaining asymmetric PLC resides in the membrane awaiting the next calreticulin associated MHC I heterodimers.

GluII as a prerequisite for pMHC I trafficking to the cell surface. This model entails that peptide loading and proofreading of MHC I molecules can be coupled to glycan trimming by GluII in a fully assembled PLC, establishing the role of the MHC I glycan as allosteric sensor in quality control. A limitation of these experiments is that the diffusion of membrane-bound PLC components, including the client (p)MHC I, is restricted by the membrane scaffold. Consequently, MHC I molecules are always tethered to the PLC, and it cannot not be determined whether pMHC I leaves the PLC before or after GluII trimming. Reconstitution of the pure PLC in continuous membranes that allow free diffusion of the PLC and its components is necessary to answer this question.

The structural and mechanistic data also provide the molecular basis of the specificity for glycosylated MHC I in the case of the PLC as opposed to the glycan-independent TAPBPR-MHC I interaction[236]. The observation that GluII-mediated glycan trimming of pMHC I takes place within the calreticulin-containing PLC establishes the notion that the PLC is a highly dynamic and malleable system, able to accommodate large transient components. Thus, the PLC emerges as a supramolecular assembly that is more complex than previously anticipated, and which might function as an interaction hub for additional ERQC factors beyond GluII.

4.6.No kinetically stable interaction between human PLC and ERAP1/2

Several proteins are involved in the loading process of MHC I. However, only few proteins are stably associated with the PLC or MHC I. The aminopeptidases ERAP1 and ERAP2 are accessory proteins present in the ER which trim peptides to an appropriate length for MHC I loading[24,86]. It has been speculated that ERAP1 and/or ERAP2 transiently interact with the PLC but they have not been observed as permanent interaction partners in PLC purifications[1,2]. We hypothesized that loading of MHC I in the PLC with a trap peptide for ERAP1/2 might allow to study the putative interaction between ERAP1/2 and the PLC. The peptide DG057 is a 15mer peptide based on the epitope SQFGGGSQY from eukaryotic translation initiation factor 3 subunit D. This epitope is a high-affinity binder of MHC I allele A*03:01 which is the main MHC I allele in PLC isolated from Raji cells. To trap ERAP1 or ERAP2 after peptide binding, DG057 carries a non-hydrolyzable phosphinic group between amino acid 1 and 2 and thereby acts as high-affinity inhibitor of the transition state of both enzymes (H-hFΨ(P(O)(OH)CH_2)GGSGSGSQFGGGSQY, structure shown in Figure 4.6-1 A). DG057 can bind ERAP1 and ERAP2 and is a potent inhibitor *in vitro* with an IC_{50} of 25 nM and 15 nM for ERAP1 and ERAP2, respectively (Figure 4.6-1 B, C).

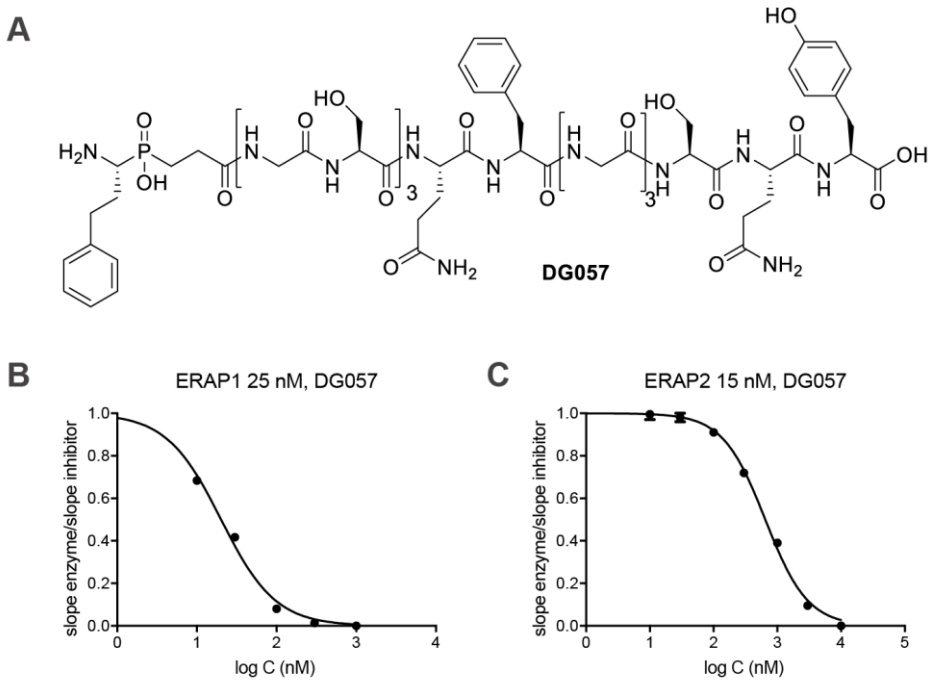

Figure 4.6-1: DG057 is active as ERAP1/2 inhibitor. (A) Schematic depiction of the 15mer DG057 peptide. **(B)** Inhibition of ERAP 1 and (**C**) ERAP2 activity by DG057. IC_{50} was determined after fitting data to a logarithmic dose-response model. Peptide and ERAP1/2 preparations, and inhibition experiments were performed by George Mavridis, National Centre for Scientific Research Democritos**,** Athens.

To investigate the interactions between PLC and ERAP1/2, purified PLC was incubated with ERAP1, ERAP2, or a mixture of both proteins while the PLC was immobilized on streptavidin-coated agarose beads. In addition, either PLC or ERAP1/2 were premixed and incubated with DG057 (Figure 4.6-2 A). This setup allowed a stringent washing scheme to remove unbound proteins and prevented false positive results. Bound proteins were eluted by SDS and analyzed by SDS-PAGE (Figure 4.6-2 B). All PLC components were bound to the affinity resin but the two putative PLC interaction partner ERAP1 and ERAP2 were not detected. In contrast, both proteins were found in the wash fraction (supernatant). The addition of DG057 did not affect the outcome of the experiment.

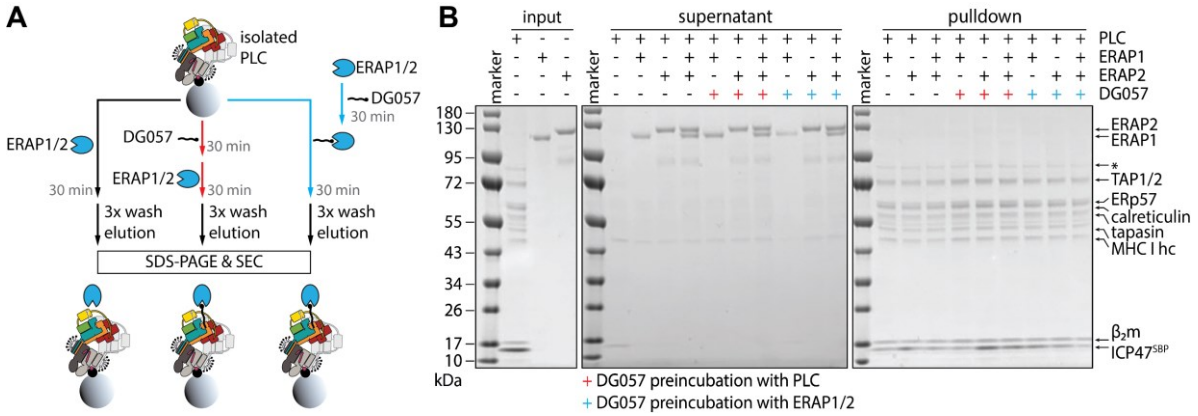

Figure 4.6-2: ERAP1 and ERAP2 do not interact with immobilized PLC. (A) Schematic depiction of ERAP1/2 pulldown experiment with PLC bound to streptavidin beads. Binding of ERAP1/2 was evaluated either in the absence of peptide (left), PLC preincubated with DG057 (middle), or ERAP1/2 preincubated with DG057. **(B)** SDS-PAGE (reducing, 4-12%, Coomassie) analysis of PLC bound onto streptavidin beads incubated with ERAP1, ERAP2, and ERAP1/ERAP2 mixture in the absence or presence of peptide DG057.

To verify the result, the same experiment was performed in solution and analyzed by SEC (Figure 4.6-3). The PLC eluted as monodisperse peak at 2.85 mL. ERAP1 (3.58 mL), ERAP2 (3.53 mL), and the mixture of ERAP1 and ERAP2 (3.55 mL) also eluted as monodisperse peaks. However, incubation of the PLC with ERAP1, ERAP2 or ERAP1 and ERAP2 mixture did not affect the elution of the PLC nor ERAP1/2 (Figure 4.6-3). Also, preincubation of either PLC or ERAP1/2 with the ERAP trap peptide DG057 did not affect the elution volume of either component. Thus, the SEC analysis confirmed the result of the ERAP pulldown experiment. No kinetically stable interaction between the PLC and ERAP1/2 was observed.

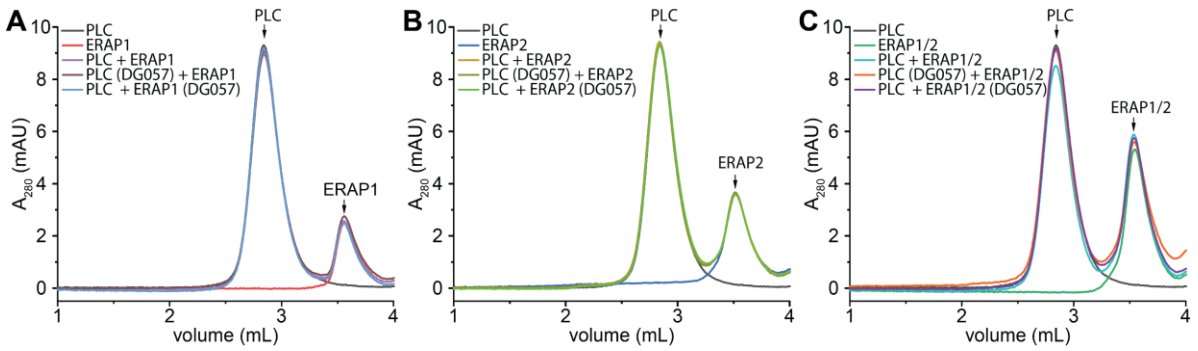

Figure 4.6-3: ERAP1 and ERAP2 do not interact kinetically stable with PLC. Overlay of chromatograms from size-exclusion analysis of mixtures of PLC and (**A**) ERAP1, (**B**) ERAP2, and (**C**) ERAP1/ERAP2 mixture in the presence or absence of peptide DG057. PLC elutes as a single monodisperse peak at 2.85 mL and ERAP1 and ERAP2 elute as single peaks at 3.58 and 3.53 mL, respectively. ERAP1/ERAP2 mixture elutes at 3.55 mL. Premixing PLC with ERAP1 and/or ERAP2 does not significantly change the migration of the PLC or ERAP1 or ERAP2. The addition of peptide DG057 to ERAP1 or ERAP2 and/or the PLC does not significantly change the migration of the proteins.

The presented results indicate that ERAP1 and ERAP2 were no stable binding partners of the PLC. Neither the pulldown with PLC immobilized on beads nor analysis in solution by SEC suggested a kinetically stable interaction. Also, addition of the peptide DG057 to either PLC or ERAP1/2 did not alter the interaction. Previous results suggested that ERAP1 might be able to cleave a 16 aa long peptide which was covalently bound to MHC I at its C terminus[100]. Thus, the N terminus of the peptide can dissociate and allow ERAP1 trimming[101]. However, recent data suggests that a cleavage of suboptimal MHC I binders is only possible when these peptides are completely dissociated from MHC I and are trimmed in solution which also supports the hypothesis that the PLC and ERAP1 and ERAP2 perform their tasks independently[4].

4.7.Reconstitution of human PLC in liposomes

It is necessary to provide a functional lipid environment for the PLC to examine MHC I recruitment, peptide transport and subsequent MHC I loading by the PLC, as well as pMHC I release from the PLC. Nanodiscs encapsulate lipids together with the protein of interest, but lateral diffusion is restricted. Therefore, nanodisc cannot sufficiently model assembly and disassembly processes occurring in the membrane during the MHC I loading and quality control process. Liposomes provide a platform to study functional properties of membrane proteins in 'unlimited' lipid environment, allowing lateral diffusion as well as providing a sealed volume to study peptide transport processes. Reconstitution of ABC transporters in liposomes has been demonstrated for TAP and homologs[49,150,175], but not for the assembled PLC.

Liposomes were generated from mixtures of ~70% *E. coli* polar lipids, ~30% 1,2-dioleoyl-sn-glycero-3-phosphocholine (DOPC), and <1% 1,1'-dioctadecyl-3,3,3',3'-tetramethyl-indodicarbocyanine (DiD) and destabilized with Triton X-100 as previously described[49,175]. After 30 min incubation of the destabilized liposomes with purified PLC::GDN, the detergent was gradually removed overnight by BioBeads. Finally, the liposomes were harvested by ultracentrifugation and resuspended in detergent-free buffer. SDS-PAGE indicated the successful reconstitution of PLC in the liposomes (Figure 4.7-1 A). All PLC components were equally well reconstituted and with a total efficiency of 54 ± 5% demonstrated by the intensity of TAP1/2 in the SDS-PAGE (n = 3, Figure 4.7-1 B). The mean diameter of

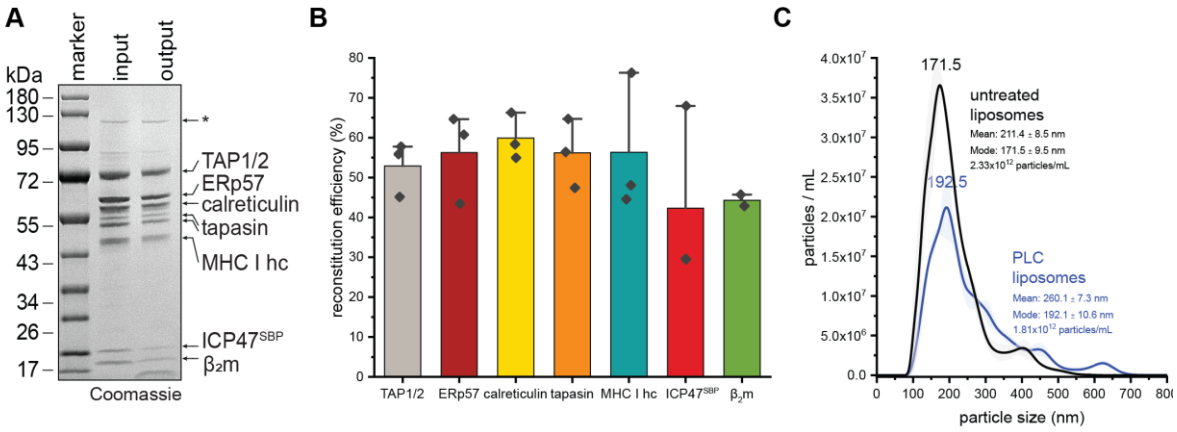

Figure 4.7-1: PLC reconstituted in liposomes. (**A**) PLC is reconstituted in liposomes. All components are visible SDS-PAGE (reducing, 4-12%, Coomassie) of PLC::GDN (input) and PLC::liposomes (output). The bands were quantified, and the reconstitution efficiency was determined by TAP1/2 intensity to 54 ± 5%. (**B**) Analysis of reconstitution efficiency for each PLC component. All components are reconstituted in liposomes with similar efficiency. (**C**) Size analysis of PLC::liposomes compared to empty liposomes. Based on the liposomes counted after reconstitution ~25 PLCs are estimated per liposome. Size analysis of liposomes was performed by Christian Winter, Goethe University Frankfurt.

PLC::liposomes was larger than untreated liposomes (260 ± 7 nm and 211 ± 9 nm, respectively). The concentration of proteoliposomes was approximately 1.8 x 10^{12} liposomes/mL (protein content ~0.8 mg/mL, Figure 4.7-1 C). Based on these liposome counts and protein concentration, approximately 25 PLCs per liposome are estimated. Liposome measurements analzyed the size distribution of the liposomes. Consequently, particle picking was set up to account for well-focused particles for optimal tracking which can result in a misleading low number of liposomes. Therefore, the settings were not optimal for determination of liposome concentration and the actual number of liposomes present in the solution might be underestimated, resulting in an overestimation of the number of PLCs per liposome.

The accessibility of several PLC components in liposome-reconstituted PLC was demonstrated by antibody staining and detection by flow cytometry (Appendix Figure 6.1-8). Antibodies against each of TAP1, ERp57, calreticulin, and MHC I bound PLC::liposomes specifically. The antibodies targeting ERp57, calreticulin, and MHC I are targeting epitopes which are located inside the ER. In contrast, the TAP1 antibody binds to the NBD of TAP1 in the cytosol[21]. Detecting all antibodies indicates that the PLC is reconstituted in both possible orientations in the liposomes. First, the right-side-out orientation with the editing modules (tapasin, ERp57, calreticulin, MHC I hc, β_2m) enclosed in the liposomes and the NBDs of TAP1/2 facing the outside. Second, the inside-out orientation with the editing modules facing the outside of the liposomes while TAP NBDs are facing the lumen of the liposomes. The orientation of the PLC in the liposomes was further characterized by limited proteolysis (Figure 4.7-2). 75% of the PLC editing module components ERp57 and calreticulin were protected from protease K treatment and therefore oriented right-side-out with the editing

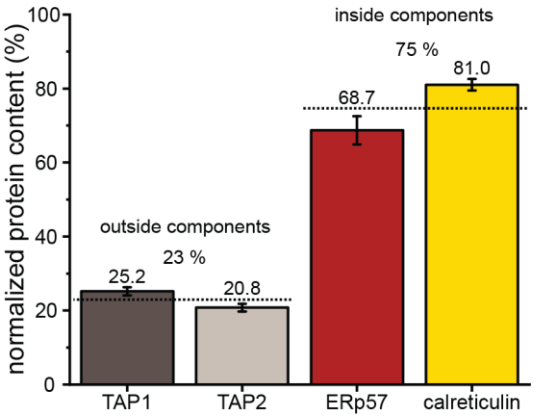

Figure 4.7-2: PLC orientation in liposomes. The orientation of the PLC was analyzed by limited protease K proteolysis and immunoblotting. The quantification of TAP1, TAP2, ERp57, and calreticulin after protease digestion indicates that 75% of the PLCs are oriented with the editing modules facing the lumen of the liposomes while 23% are oriented with the editing modules facing the outside of the liposomes. The blots are depicted in Appendix Figure 6.1-9. The limited proteolysis assay was performed by Christian Winter, Goethe University Frankfurt.

modules facing the inside of the liposomes. 23% of PLCs were oriented inside-out with the editing modules facing the outside and TAP1/2 remaining detectable after protease K treatment. The presence of calreticulin, the only soluble PLC component besides the MHC I-bound β_2m, is an indication for the reconstitution of assembled PLC. A formal proof of the a fully intact PLC after reconstitution was not possible, because the liposomes could not be resolubilized by the ultra-mild detergents GDN and digitonin[210]. Harsher detergents like Triton X-100 and Brij 96 were able to solubilize the liposomes but disassembling or aggregating the PLC[210].

As demonstrated with PLC::MSP2N2 (see chapter 4.5), the PLC facilitates MHC I peptide loading. Similarly, MHC I should be loaded with peptides if the PLC is reconstituted in an active form in the liposomes. To prove this, peptide binding to HLA-A*03:01 was evaluated with the high-affinity binder C^{F}SN (Figure 4.7-3). Like detergent-solubilized PLC, HLA-A*03:01 in the PLC::liposomes bound the high-affinity peptide specifically. Peptide-editing function was demonstrated after addition of CSN, reflected by the reduced C^{F}SN polarization. Interaction of the TAP-binding peptide C4F with PLC::liposomes or unspecific binding of C^{F}SN to empty liposomes was not observed.

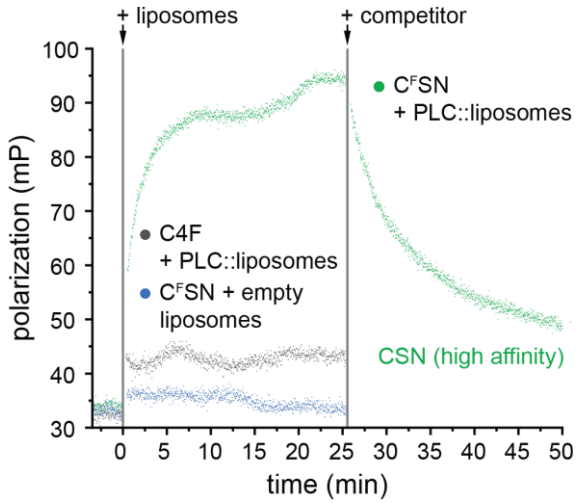

Figure 4.7-3: Peptide binding and editing of PLC chaperoned MHC I in liposomes. Peptide binding and proofreading of the PLC reconstituted in liposomes (65 nM) was monitored by fluorescence polarization fluorescent reporter peptides (75 nM). PLC-associated HLA-A*03:01 bound the high-affinity epitope C^{F}SN (AIFC^{F}SNMTK; $K_d \approx 10$ nM). In contrast, the low-affinity HLA-B*27:01-restricted epitope C4F (RRYC^{F}KSTEL; $K_d \approx 20$ µM) did not interact with PLC-associated MHC I. For peptide editing, a 2000-fold molar excess of unlabeled high-affinity peptide (150 µM CSN, AIFCSNMTK; $K_d \approx 10$ nM) displaced the reporter peptide.

Liposomes provide space for lateral diffusion of membrane proteins and complexes. Therefore, liposomes are the perfect system to study the dissociation process of pMHC I after peptide loading which is hindered in nanodisc-reconstituted PLC (see chapter 4.5). The

monoclonal antibody W6/32 specifically detects pMHC I molecules[237,238]. No structure of this antibody in complex with its epitope is available, but several amino acids have been identified that are involved in the interaction[239]. Based on these reports, two binding interfaces for W6/32 on MHC I are proposed: (i) the hinge region of the α2-helix of the MHC I hc and (ii) an interaction interface between the MHC I hc and the N terminus of β_2m below the F-pocket. Both possible epitopes are likely shielded when MHC I is engaged in the PLC. Shielding of both epitopes by the PLC was verified with PLC::GDN (Figure 4.7-4 A). The peak shape and elution volume of the PLC remained unchanged after addition of 3x molar excess of W6/32 monoclonal antibody, proving that MHC I was not accessible for W6/32 in the PLC. Afterwards, the accessibility of pMHC I in liposomes was analyzed by flow cytometry after addition of W6/32 to peptide treated PLC::liposomes (Figure 4.7-4 B, C). In the absence of high-affinity binders for MHC I, low background of W6/32^{AF647} was observed. Once the PLC was incubated with high-affinity peptides for HLA-A*03:01 (CSN) and HLA-B*15:10 (HYC), the fluorescence signal intensity increased, indicating binding of W6/32^{AF647}. Consequently, pMHC I dissociated from the PLC and was accessible for W6/32^{AF647}.

The allosteric coupling between peptide loading and deglucosylation of pMHC I by GluII suggest that GluII promotes pMHC I release from the PLC (see chapter 4.4 and 4.5)[(ref. 240)]. This coupling was not necessary to release pMHC I from PLC reconstituted in liposomes. Further experiments should reveal whether GluII acts concerted with the PLC or whether pMHC I release and full deglucosylation are independent processes.

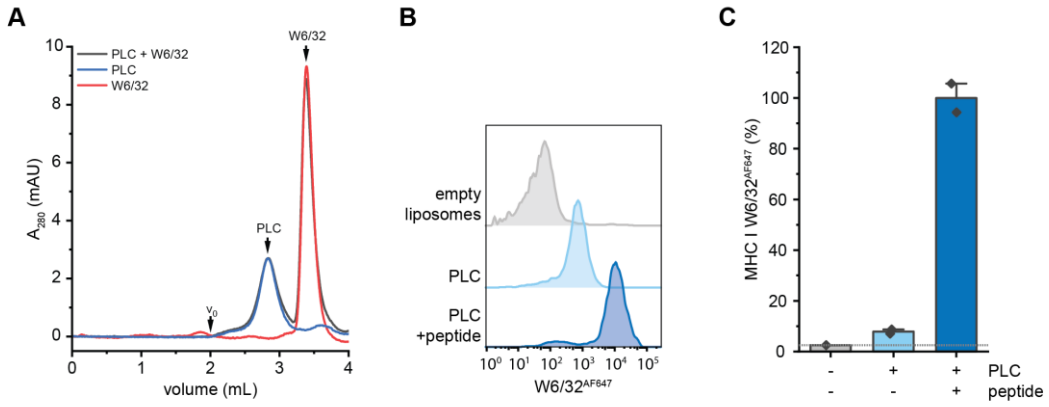

Figure 4.7-4: Peptide-dependent dissociation of MHC I from the PLC. (**A**) Binding analysis of W6/32 to unloaded PLC::GDN. The elution volume and peak shape of PLC::GDN (blue) is not altered in presence of W6/32 (grey). Also the signal intensity and peak shape of W6/32 remains unchanged (red). (**B**) Flow cytometry analysis of W6/32 binding to PLC in liposomes in presence (dark blue) and absence (light blue) of high-affinity HLA-A*03:01 (CSN) and HLA-B*15:10 (HYC) binding peptides. (**C**) Bar diagram of flow cytometry analysis of W6/32 binding to PLC in liposomes from (B). n = 2. W6/32 binding analysis and flow cytometry measurements were perfomed by Darja Cernova and Jacqueline Patzsch, Goethe University Frankfurt.

4.8. Photocleavable ICP47^{SBP} as tool for functional and structural studies

PLC can be purified with the viral TAP inhibitor ICP47^{SBP} which allowed structural analysis of endogenous PLC. However, the viral inhibitor inhibits TAP main function – peptide transport – by blocking peptide binding and peptide-induced ATP hydrolysis. Therefore, functional and structural analysis of fully assembled PLC remains limited and does not include TAP engagement or manipulation. ICP47 has been previously engineered with a photocleavable amino acid at position 15, replacing a Met by the photolabile beta-amino acid 3-amino-3-(2-nitrophenyl)-propanoic acid (Anp) (pc-ICP47$_{2-55}$)[ref. 241]. This tool has been used to control TAP activity in the cellular context. However, the tool was limited to 54 aa because it was produced completely by solid phase peptide synthesis and lacked an affinity tag to be used for PLC purification. Christian Winter successfully evolved the tool and synthesis strategy to produce a semi-synthetic pc-ICP47^{SBP} at full length of ICP47$_{2-88}$, the photocleavable Anp at position 15, and a C-terminal SBP tag that allows PLC purification (Figure 4.8-1). After successful cleavage experiments of pc-ICP47^{SBP}, pc-ICP47^{SBP} was evaluated for PLC purification and subsequent reactivation. Acidic pH is crucial for ideal cleavage conditions of orthonitrobenzole-based photocages like Anp in pc-ICP47^{SBP} [ref. 242,243]. Therefore, the pH stability of the PLC was evaluated in acidic conditions (Appendix Figure 6.1-10). Human PLC was stable in the range from pH 7.4 to 6.5, while aggregation occurred at a pH value of 6.2. Therefore, the experiments with pc-ICP47^{SBP} and the PLC were performed at pH 6.5.

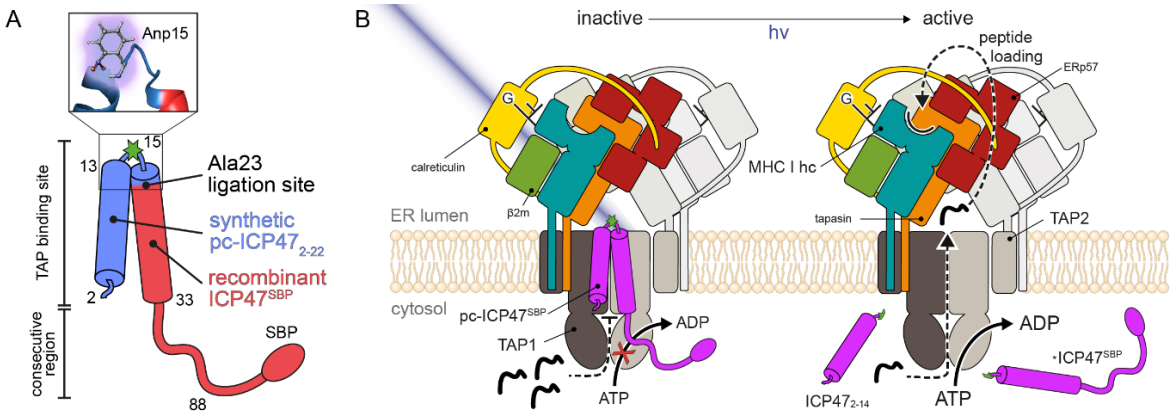

Figure 4.8-1: Photocleavable ICP47^{SBP}. (**A**) Schematic depiction of the semi-synthetically produced pc-ICP47^{SBP}. Amino acids 2-33 form a helix-turn-helix motif and inhibit TAP function. The consecutive region comprising amino acids 34-55 increase the binding stability to TAP[128]. The N-terminal region of the semisynthetic inhibitor (blue) can be split by light due to incorporation of the photocleavable beta-amino acid Anp. The recombinant part (aa 23-140) of the pc-ICP47^{SBP} has a C-terminal SBP affinity tag. Both parts are fused by native chemical ligation at position 23. Anp has been modeled into the three-dimensional structure of the loop region for visualization (zoom-in, PDB: 5U1D). (**B**) The PLC in the ER membrane. Two editing modules are assembled around the transporter associated with peptide transport (one is colored light grey). TAP is inhibited by pc-ICP47^{SBP} (purple), antigenic peptides cannot be bound and translocated. Upon light illumination (hν), peptide transport activity is restored, recovering peptide binding and transport.

PLC was purified utilizing pc-ICP47^{SBP} (Figure 4.8-2 A) and illuminating pc-ICP47^{SBP} bound to PLC for 180 s with UV_{365} was optimal for cleavage of the pc-ICP47^{SBP} (Figure 4.8-2 B, C). The composition and hydrodynamic radius of the PLC were not affected by UV_{365} illumination. Immunoblotting against the SBP-tag confirmed the photocleavage of pc-ICP47^{SBP} by an almost complete shift of pc-ICP47^{SBP} towards lower molecular weight (*ICP47^{SBP}, Figure 4.8-2 B).

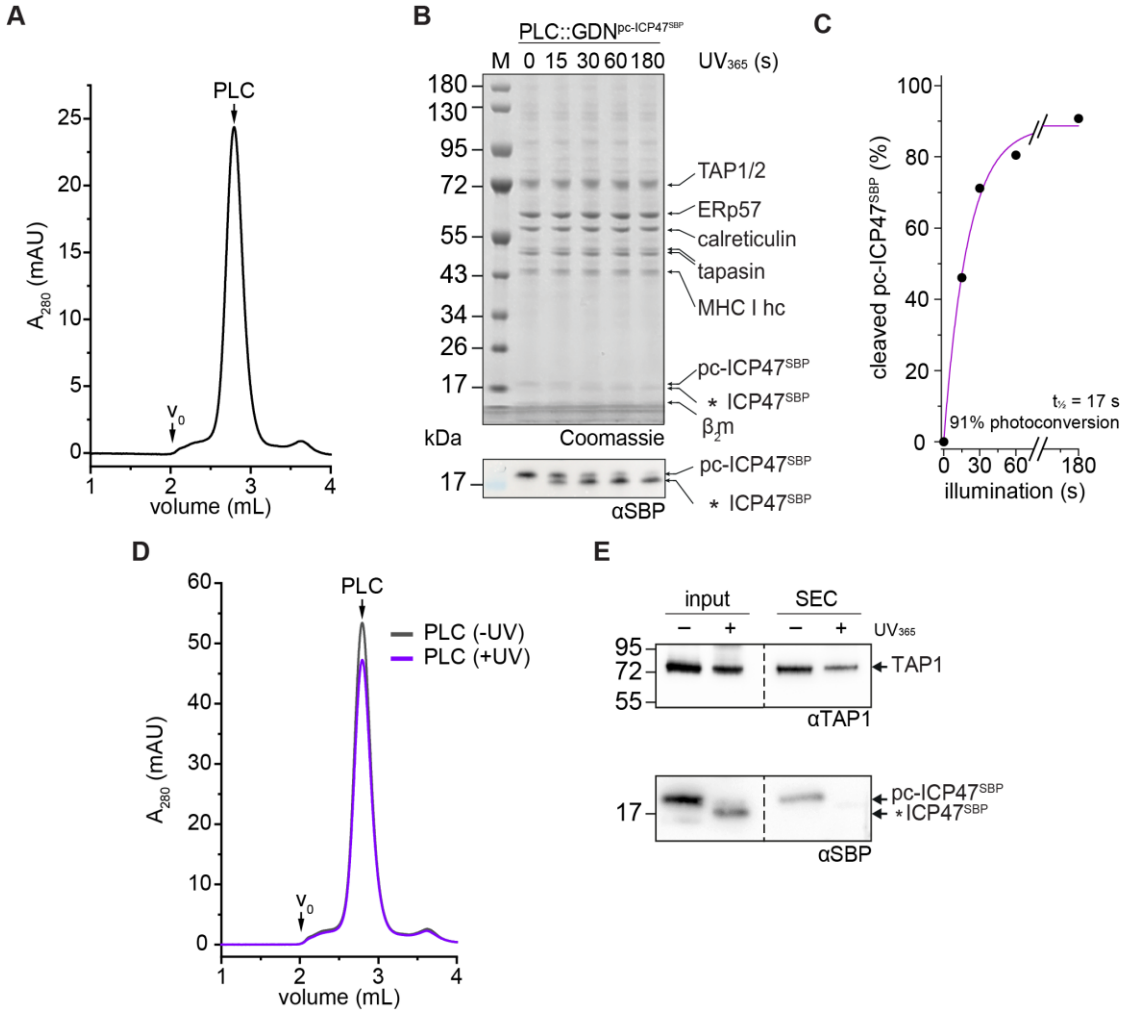

Figure 4.8-2: PLC purification by pc-ICP47 and PLC reactivation. (**A**) Monodisperse PLC purified from Raji cells by pc-ICP47^{SBP}. (**B**) SDS-PAGE (reducing, 4-12%, Coomassie) of PLC purified via pc-ICP47^{SBP} before and after UV illumination. PLC subunit composition is unaffected by UV illumination. PLC bound pc-ICP47^{SBP} cleavage analyzed by SDS-PAGE and subsequent immunoblotting (αSBP). *ICP47^{SBP} = C-terminal cleavage fragment. (**C**) pc-ICP47^{SBP} cleavage kinetic based on band intensities from immunoblot (αSBP) from (B). (**D**) PLC purified by pc-ICP47^{SBP} remained fully assembled after UV_{365} illumination. (**E**) Before and after photocleavage of pc-ICP47^{SBP}, the native PLC was analyzed by SEC, SDS-PAGE, and subsequent immunoblotting (αSBP). Photofragments of pc-ICP47^{SBP} were efficiently removed by SEC from the PLC after photocleavage.

Further analysis of the cleavage reaction indicated a quantitative cleavage of pc-ICP47^{SBP} engaged in the PLC after 180 s with $t_{½}$ = 17 s (Figure 4.8-2 B, C). Upon illumination, the hydrodynamic shape of the PLC did not change, demonstrating that the macromolecular assembly of the PLC was unaffected by the photocleavage of the viral inhibitor (Figure 4.8-2 D). SEC analysis and immunoblotting demonstrated that the *ICP47^{SBP} fragment no longer co-migrated with the PLC after light-induced cleavage and that the PLC was free of pc-ICP47^{SBP} (Figure 4.8-2 E). The free peptide-binding site in TAP was probed with fluorophore labeled ICP47^{AF647} which can bind TAP like other ICP47 variants and can also be used to purify PLC via an SBP tag (Appendix Figure 6.1-11). Probing of UV_{365}-illuminated PLC purified by pc-ICP47^{SBP} demonstrated that the fluorophore-labeled ICP47^{AF647} bound specifically to PLC treated with UV_{365}, which indicated that TAP function was restored (Figure 4.8-3 A, Appendix Figure 6.1-11). However, only 25% PLC bound ICP47^{AF647}. The low binding efficiency is likely caused by the membrane dependency of ICP47. ICP47 requires a membrane to fold and gain high affinity to TAP (~50 nM)[ref. 127,199]. In a membrane-free solution the affinity to TAP is reduced (~5 µM)[ref. 125], which could explain the low occupancy of PLC::GDN with labeled ICP47^{AF647}.

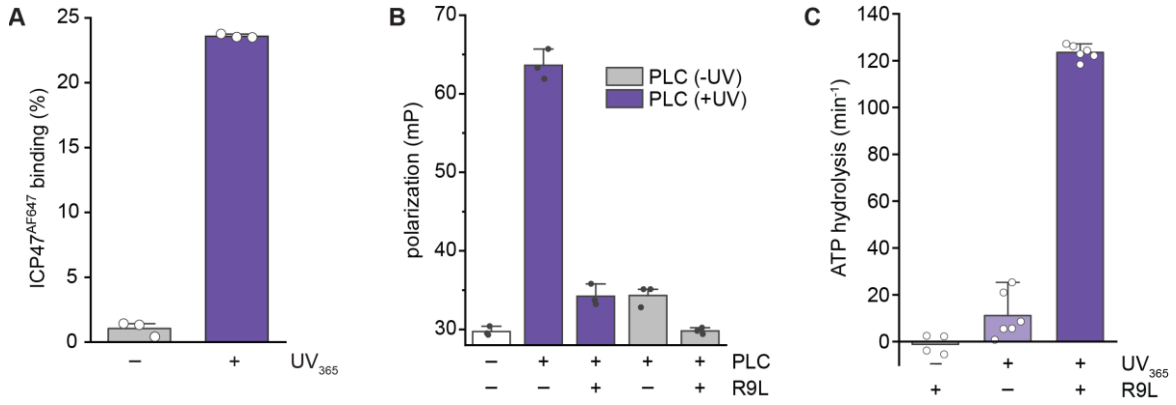

Figure 4.8-3: Photoactivation of PLC purified by pc-ICP47^{SBP}. (**A**) ICP47^{AF647} re-binding after photocleavage of pc-ICP47^{SBP}, analyzed by fluorescence-based SEC. After illumination, the TAP-binding pocket is free for ICP47^{AF647} binding (purple). See Appendix Figure 6.1-11 for SEC chromatograms. (**B**) Peptide binding to TAP within the native PLC analyzed by fluorescence anisotropy. The PLC (150 nM final) was added to the fluorescent reporter peptide C4F (50 nM). C4F cannot bind to pc-ICP47^{SBP} arrested PLC (grey). After UV_{365} illumination, peptide binding was restored and was specific, as demonstrated by competition with excess unlabeled antigenic peptide R9L (purple). Peptide binding kinetics are shown in Appendix Figure 6.1-12. (**C**) Vanadate sensitive ATP hydrolysis of TAP in the PLC is restored after UV_{365} illumination and R9L addition.

Binding of the high-affinity TAP binder C4F to native PLC before and after photorelease of pc-ICP47^{SBP} was analyzed by fluorescence polarization (Figure 4.8-3 B). Illumination with UV_{365} triggered C4F binding to TAP comparable to previously published results[150]. Without light activation, only minimal binding of C4F to the pc-ICP47^{SBP}-arrested PLC was observed.

Peptide binding was specific as indicated by competition to background level with an excess of unlabeled high-affinity TAP binder (R9L). The binding kinetics were rapid, showing association of C4F or R9L competition within 5 min upon peptide addition at room temperature (Appendix Figure 6.1-12). Upon binding of R9L peptide-dependent ATPase, activity of TAP was detected after UV_{365} activation of the PLC (Figure 4.8-3 C). In summary, the native PLC stabilized and purified by pc-ICP47^{SBP} was activated by UV-light for further functional and structural analyses.

Final experiments with pc-ICP47^{SPB} demonstrated peptide transport activity after UV_{365}-dependent splitting of pc-ICP47^{SBP} with PLC::liposomes or PLC in microsomes (Figure 4.8-4). In liposomes, time-dependent accumulation of C4F was observed while not-illuminated liposomes or illuminated liposomes in presence of ADP did not show similar peptide accumulation. However, due to the low PLC content in the liposomes, the accumulation of peptide inside the liposomes was low. Consequently, bound, but not transported, peptides resulted in the background signal visible in the ADP sample after UV_{365}-illumination. In microsomes, >90% of transport activity of untreated microsomes was restored after illumination of pc-ICP47^{SBP} treated liposomes. Remarkably, the transport was not influenced by UV light. However, both ICP47^{SBP} and pc-ICP47^{SBP} were able to completely inhibit TAP-dependent peptide transport.

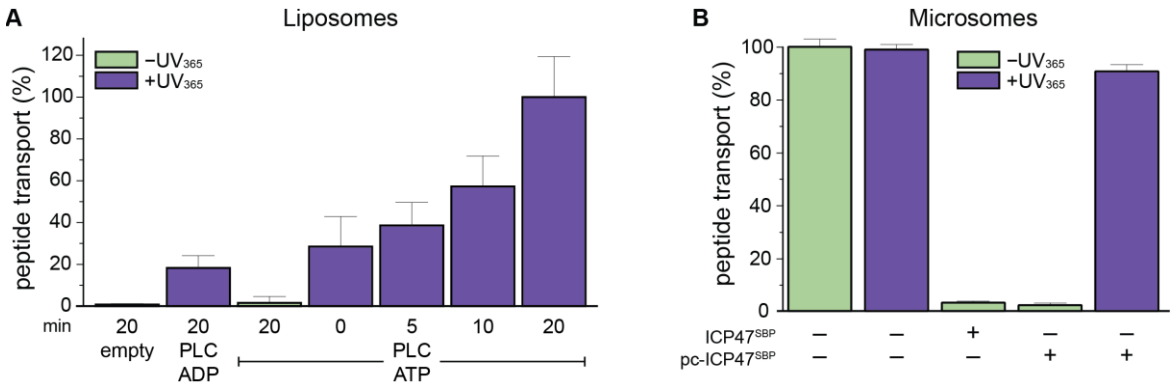

Figure 4.8-4: Peptide transport restored after pc-ICP47^{SBP} photocleavage. (**A**) PLC mediated peptide translocation assay in liposomes, analyzed by flow cytometry. The C4F peptide accumulation in liposomes was triggered by UV_{365} illumination and increased over 15 min. (**B**) PLC mediated peptide translocation assay in microsomes, analyzed by flow cytometry. Peptide translocation in microsomes was not affected by UV_{365} illumination. Binding of pc-ICP47^{SBP} inhibited peptide translocation to the same extend as ICP47^{SBP}. Upon photocleavage of pc-ICP47^{SBP}, PLC mediated NST^{AF647} peptide translocation activity was fully restored. Experimental setup and gating strategies are visualized in Appendix Figure 6.1-13. Microsome preparation and transport experiments were performed by Christian Winter, Goethe University Frankfurt.

pc-ICP47^{SBP} is a valuable tool that allows PLC purification as well as specific and effective activation of TAP functions in solution and membrane environments. These features will enable studying the functional connection of the peptide transporter TAP with peptide loading and quality control of MHC I in the editing modules. Furthermore, functional TAP allows to utilize additional stabilization strategies for structural analysis. Variations in the inhibitor stall TAP in a different conformations[139] and different inhibition strategies allowed to decipher various states in the transport cycle of the TAP homolog TmrAB[5]. Purification of the PLC with pc-ICP47^{SBP} and subsequent activation will enable verification of these strategies on fully assembled PLC.

5. Conclusion

This PhD thesis succeeded in advancing the understanding of the inner mechanics of the PLC by obtaining detailed structural and functional information about the PLC. Analysis of PLC derived from *bos taurus* and *ovis aries* demonstrated that the general construction principle of the PLC is similar in mammalian species. The components already known from human PLC (TAP1/2, tapasin, ERp57, calreticulin, MHC I hc, and β_2m) were identified and similarly organized in both investigated mammalian species. Additional to the known proteins, GRP78 was found in PLC from both species, contrary to results from human PLC. Future work should determine whether GRP78 is a stoichiometric component of the PLC in these species or whether association of GRP78 with the PLC is a reaction to hypoxia and energy shortage in the cells. However, due to low PLC yields from cow and sheep spleen, high resolution structural analysis was not feasible within the scope of this work.

Stabilization of human PLC in membrane mimetics allowed to advance structural analysis to molecular details and interactions within the PLC. For the first time, two important functional elements in the PLC were resolved: The editing loop of tapasin has been captured during interaction with the F-pocket of MHC I, facilitating peptide exchange by widening the peptide binding groove and disturbing interactions between cargo peptides and the binding groove. Additionally, part of the MHC I N-linked glycan on Asn86 was resolved. The A-branch of this glycan is stretched between MHC I Asn86 and the lectin domain of calreticulin. For the glycan, being a crucial quality marker for the folding and loading status of MHC I, this PhD thesis demonstrated the allosteric linkage between peptide loading of MHC I and full deglucosylation by GluII. The deglucosylation was performed while calreticulin remained present in the PLC. Based on these findings, MHC I deglucosylation by GluII was included in the MHC I loading and quality control scheme performed by the PLC. Furthermore, this PhD thesis identified GluII as transient component of the PLC, linking ERQC with loading control of MHC I. However, the results must be further validated in a membrane-reconstituted system, which allows lateral diffusion of membrane proteins and pMHC I dissociation from the PLC. Liposomes would be a suitable reconstitution system for this analysis. The nanodisc used in this thesis prevented dissociation of pMHC I and other PLC components from the assembly because of the limited size and restriction by the MSP.

In addition, to include GluII in the list of (transient) PLC interaction partners, further analysis of the molecular sociology of the PLC was performed in this PhD thesis. Interaction studies excluded the zinc-metallopeptidases ERAP1 and ERAP2 as kinetically stable PLC interaction partners. Neither ERAP1, ERAP2, nor a mixture of ERAP1 and ERAP2 interacted kinetically stable with the PLC. In contrast, these aminopeptidases act independently of the PLC on free peptides in the ER[4].

Finally, this PhD thesis established two crucial methods for further advancing functional and structural investigations of the PLC. Purified human PLC was successfully reconstituted in liposomes. In this reconstitution system, pMHC I dissociation from the PLC has been demonstrated by detection of free pMHC I, which dissociated from PLC. Liposomes will allow detailed functional studies on pMHC I release from the PLC, dependent on presence of high-affinity peptide binders/cargos, glycosylation status, or even peptide transport. Additionally, the photocleavable tool pc-ICP47^{SBP} provided the ability to purify, reconstitute, and activate TAP within isolated and reconstituted PLC. In this PhD thesis, peptide binding, peptide-stimulated ATP hydrolysis, and transport activity of TAP after pc-ICP47^{SPB}-dependent PLC purification and subsequent activation were demonstrated. pc-ICP47^{SBP} will facilitate the use of different TAP stabilization strategies to PLC samples, which were not accessible because of TAP inhibition by ICP47^{SBP}. Stabilization of ABC transporters in different transport states was crucial for the analysis of the transport cycle of the functional TAP homolog TmrAB[5], and will likewise facilitate structural and functional TAP and PLC investigations. The tools of liposome reconstitution together with activation of PLC after purification with pc-ICP47^{SBP} will facilitate to explore the interplay of TAP with the editing modules.

6. References

1. Blees, A., Januliene, D., Hofmann, T., Koller, N., Schmidt, C., Trowitzsch, S., Moeller, A. & Tampé, R. Structure of the human MHC-I peptide-loading complex. *Nature* **551**, 525–528 (2017).
2. Hulpke, S., Baldauf, C. & Tampé, R. Molecular architecture of the MHC I peptide-loading complex: one tapasin molecule is essential and sufficient for antigen processing. *FASEB J.* **26**, 5071–5080 (2012).
3. Blum, J. S., Wearsch, P. A. & Cresswell, P. Pathways of antigen processing. *Annu. Rev. Immunol.* **31**, 443–473 (2013).
4. Mavridis, G. *et al.* A systematic re-examination of processing of MHCI-bound antigenic peptide precursors by endoplasmic reticulum aminopeptidase 1. *J. Biol. Chem.* **295**, 7193–7210 (2020).
5. Hofmann, S. *et al.* Conformation space of a heterodimeric ABC exporter under turnover conditions. *Nature* **571**, 580–583 (2019).
6. Ljunggren, H.-G. & Kärre, K. In search of the 'missing self': MHC molecules and NK cell recognition. *Immunol. Today* **11**, 237–244 (1990).
7. Cruz-Muñoz, M. E., Valenzuela-Vázquez, L., Sánchez-Herrera, J. & Santa-Olalla Tapia, J. From the 'missing self' hypothesis to adaptive NK cells: Insights of NK cell-mediated effector functions in immune surveillance. *J. Leukoc. Biol.* **105**, 955–971 (2019).
8. Madden, D. R., Gorga, J. C., Strominger, J. L. & Wiley, D. C. The three-dimensional structure of HLA-B27 at 2.1 Å resolution suggests a general mechanism for tight peptide binding to MHC. *Cell* **70**, 1035–1048 (1992).
9. Springer, S. Transport and quality control of MHC class I molecules in the early secretory pathway. *Curr. Opin. Immunol.* **34**, 83–90 (2015).
10. Hegde, N. R., Chevalier, M. S., Wisner, T. W., Denton, M. C., Shire, K., Frappier, L. & Johnson, D. C. The role of BiP in endoplasmic reticulum-associated degradation of major histocompatibility complex class I heavy chain induced by cytomegalovirus proteins. *J. Biol. Chem.* **281**, 20910–20919 (2006).
11. Prevosto, C., Usmani, M. F., McDonald, S., Gumienny, A. M., Key, T., Goodman, R. S., Gaston, J. S. H., Deery, M. J. & Busch, R. Allele-independent turnover of human leukocyte antigen (HLA) class Ia molecules. *PLoS One* **11**, e0161011 (2016).
12. Pishesha, N., Harmand, T. J. & Ploegh, H. L. A guide to antigen processing and presentation. *Nat. Rev. Immunol.* **22**, 751–764 (2022).
13. Truong, H. V. & Sgourakis, N. G. Dynamics of MHC-I molecules in the antigen processing and presentation pathway. *Curr. Opin. Immunol.* **70**, 122–128 (2021).
14. Neefjes, J., M Jongsma, M. L. & Paul, P. Towards a systems understanding of MHC class I and MHC class II antigen presentation. *Nat. Rev. Immunol.* **11**, 823–836 (2011).
15. Trowitzsch, S. & Tampé, R. Multifunctional chaperone and quality control complexes in adaptive immunity. *Annu. Rev. Biophys.* **49**, 135–161 (2020).
16. Thomas, C. & Tampé, R. MHC I assembly and peptide editing — chaperones, clients, and molecular plasticity in immunity. *Curr. Opin. Immunol.* **70**, 48–56 (2021).
17. Blees, A., Reichel, K., Trowitzsch, S., Fisette, O., Bock, C., Abele, R., Hummer, G., Schäfer, L. V. & Tampé, R. Assembly of the MHC I peptide-loading complex determined by a conserved ionic lock-switch. *Sci. Rep.* **5**, 17341 (2015).
18. Rock, K. L. & Goldberg, A. L. Degradation of cell proteins and the generation of MHC class I-presented peptides. *Annu. Rev. Immunol.* **17**, 739–779 (1999).
19. Yewdell, J. W. DRiPs solidify: Progress in understanding endogenous MHC class I antigen processing. *Trends Immunol.* **32**, 548–558 (2011).

20. Dolan, B. P., Li, L., Veltri, C. A., Ireland, C. M., Bennink, J. R. & Yewdell, J. W. Distinct pathways generate peptides from defective ribosomal products for CD8+ T cell immunosurveillance. *J. Immunol.* **186**, 2065–2072 (2011).
21. van Endert, P. M., Tampé, R., Meyer, T. H., Tisch, R., Bach, J. F. & McDevitt, H. O. A sequential model for peptide binding and transport by the transporters associated with antigen processing. *Immunity* **1**, 491–500 (1994).
22. Androlewicz, M. J., Anderson, K. S. & Cresswell, P. Evidence that transporters associated with antigen processing translocate a major histocompatibility complex class I-binding peptide into the endoplasmic reticulum in an ATP-dependent manner. *Proc. Natl. Acad. Sci.* **90**, 9130–4 (1993).
23. Neefjes, J. J., Momburg, F. & Hämmerling, G. J. Selective and ATP-dependent translocation of peptides by the MHC-encoded transporter. *Science* **261**, 769–71 (1993).
24. Chang, S.-C., Momburg, F., Bhutani, N. & Goldberg, A. L. The ER aminopeptidase, ERAP1, trims precursors to lengths of MHC class I peptides by a "molecular ruler" mechanism. *Proc. Natl. Acad. Sci.* **102**, 17107–17112 (2005).
25. Serwold, T., Gonzalez, F., Kim, J., Jacob, R. & Shastri, N. ERAAP customizes peptides for MHC class I molecules in the endoplasmic reticulum. *Nature* **419**, 480–483 (2002).
26. York, I. A., Chang, S.-C., Saric, T., Keys, J. A., Favreau, J. M., Goldberg, A. L. & Rock, K. L. The ER aminopeptidase ERAP1 enhances or limits antigen presentation by trimming epitopes to 8–9 residues. *Nat. Immunol.* **3**, 1177–1184 (2002).
27. Mpakali, A., Maben, Z., Stern, L. J. & Stratikos, E. Molecular pathways for antigenic peptide generation by ER aminopeptidase 1. *Mol. Immunol.* **113**, 50–57 (2019).
28. Thomas, C. & Tampé, R. Structure of the TAPBPR–MHC I complex defines the mechanism of peptide loading and editing. *Science* **358**, 1060–1064 (2017).
29. Ruiz-Canada, C., Kelleher, D. J. & Gilmore, R. Cotranslational and posttranslational N-Glycosylation of polypeptides by distinct mammalian OST isoforms. *Cell* **136**, 272–283 (2009).
30. Kozlov, G., Pocanschi, C. L., Rosenauer, A., Bastos-Aristizabal, S., Gorelik, A., Williams, D. B. & Gehring, K. Structural basis of carbohydrate recognition by calreticulin. *J. Biol. Chem.* **285**, 38612–20 (2010).
31. Zhang, W., Wearsch, P. A., Zhu, Y., Leonhardt, R. M. & Cresswell, P. A role for UDP-glucose glycoprotein glucosyltransferase in expression and quality control of MHC class I molecules. *Proc. Natl. Acad. Sci.* **108**, 4956–4961 (2011).
32. Tannous, A., Pisoni, G. B., Hebert, D. N. & Molinari, M. N-linked sugar-regulated protein folding and quality control in the ER. *Semin. Cell Dev. Biol.* **41**, 79–89 (2015).
33. Avezov, E., Frenkel, Z., Ehrlich, M., Herscovics, A. & Lederkremer, G. Z. Endoplasmic reticulum (ER) mannosidase I is compartmentalized and required for N-glycan trimming to Man5-6GlcNAc2 in glycoprotein ER-associated degradation. *Mol. Biol. Cell* **19**, 216–25 (2008).
34. Peaper, D. R. & Cresswell, P. The redox activity of ERp57 is not essential for its functions in MHC class I peptide loading. *Proc. Natl. Acad. Sci.* **105**, 10477–10482 (2008).
35. Caputo, A. T., Alonzi, D. S., Kiappes, J. L., Struwe, W. B., Cross, A., Basu, S., Darlot, B., Roversi, P. & Zitzmann, N. Structural insights into the broad-spectrum antiviral target endoplasmic reticulum alpha-glucosidase II. *Adv. Exp. Med. Biol.* **1062**, 265–276 (2018).

36. Pelletier, M. F., Marcil, A., Sevigny, G., Jakob, C. A., Tessier, D. C., Chevet, E., Menard, R., Bergeron, J. J. M. & Thomas, D. Y. The heterodimeric structure of glucosidase II is required for its activity, solubility, and localization in vivo. *Glycobiology* **10**, 815–27 (2000).
37. Totani, K., Ihara, Y., Matsuo, I. & Ito, Y. Substrate specificity analysis of endoplasmic reticulum glucosidase II using synthetic high mannose-type glycans. *J. Biol. Chem.* **281**, 31502–31508 (2006).
38. Uebel, S., Meyer, T. H., Kraas, W., Kienle, S., Jung, G., Wiesmller, K.-H. & Tamp, R. Requirements for peptide binding to the human transporter associated with antigen processing revealed by peptide scans and complex peptide libraries. *J. Biol. Chem.* **270**, 18512–18516 (1995).
39. Androlewicz, M. J. & Cresswell, P. Human transporters associated with antigen processing possess a promiscuous peptide-binding site. *Immunity* **1**, 7–14 (1994).
40. Corradi, V., Singh, G. & Tieleman, D. P. The human transporter associated with antigen processing. *J. Biol. Chem.* **287**, 28099–28111 (2012).
41. Seyffer, F. & Tampé, R. ABC transporters in adaptive immunity. *Biochim. Biophys. Acta - Gen. Subj.* **1850**, 449–460 (2015).
42. Parcej, D. & Tampé, R. ABC proteins in antigen translocation and viral inhibition. *Nat. Chem. Biol.* **6**, 572–580 (2010).
43. Kaer, L. Van, Ashton-Rickardt, P. G., Ploegh, H. L. & Tonegawa, S. TAP1 mutant mice are deficient in antigen presentation, surface class I molecules, and CD4−8+ T cells. *Cell* **71**, 1205–1214 (1992).
44. Koch, J., Guntrum, R., Heintke, S., Kyritsis, C. & Tampé, R. Functional dissection of the transmembrane domains of the transporter associated with antigen processing (TAP). *J. Biol. Chem.* **279**, 10142–10147 (2004).
45. Momburg, F., Roelse, J., Howard, J. C., Butcher, G. W., Hämmerling, G. J. & Neefjes, J. J. Selectivity of MHC-encoded peptide transporters from human, mouse and rat. *Nature* **367**, 648–651 (1994).
46. Koopmann, J. O., Post, M., Neefjes, J. J., Hämmerling, G. J. & Momburg, F. Translocation of long peptides by transporters associated with antigen processing (TAP). *Eur. J. Immunol.* **26**, 1720–8 (1996).
47. Gorbulev, S., Abele, R. & Tampé, R. Allosteric crosstalk between peptide-binding, transport, and ATP hydrolysis of the ABC transporter TAP. *Proc. Natl. Acad. Sci.* **98**, 3732–3737 (2001).
48. Herget, M., Oancea, G., Schrodt, S., Karas, M., Tampé, R. & Abele, R. Mechanism of substrate sensing and signal transmission within an ABC transporter. *J. Biol. Chem.* **282**, 3871–3880 (2007).
49. Stefan, E., Hofmann, S. & Tampé, R. A single power stroke by ATP binding drives substrate translocation in a heterodimeric ABC transporter. *eLife* **9:e55943**, (2020).
50. Chen, M., Abele, R. & Tampé, R. Peptides induce ATP hydrolysis at both subunits of the transporter associated with antigen processing. *J. Biol. Chem.* **278**, 29686–29692 (2003).
51. Ernst, R., Koch, J., Horn, C., Tampé, R. & Schmitt, L. Engineering ATPase activity in the isolated ABC cassette of human TAP1. *J. Biol. Chem.* **281**, 27471–27480 (2006).
52. Oldham, M. L., Hite, R. K., Steffen, A. M., Damko, E., Li, Z., Walz, T. & Chen, J. A mechanism of viral immune evasion revealed by cryo-EM analysis of the TAP transporter. *Nature* **529**, 537–540 (2016).
53. Oldham, M. L., Grigorieff, N. & Chen, J. Structure of the transporter associated with antigen processing trapped by herpes simplex virus. *eLife* **5**, e21829 (2016).

54. Ortmann, B. *et al.* A critical role for tapasin in the assembly and function of multimeric MHC class I-TAP complexes. *Science* **277**, 1306–9 (1997).
55. Fleischmann, G., Fisette, O., Thomas, C., Wieneke, R., Tumulka, F., Schneeweiss, C., Springer, S., Schäfer, L. V. & Tampé, R. Mechanistic basis for epitope proofreading in the peptide-loading complex. *J. Immunol.* **195**, 4503–4513 (2015).
56. Tan, P., Kropshofer, H., Mandelboim, O., Bulbuc, N., Hämmerling, G. J. & Momburg, F. Recruitment of MHC class I molecules by tapasin into the transporter associated with antigen processing-associated complex is essential for optimal peptide loading. *J. Immunol.* **168**, 1950–1960 (2002).
57. Frickel, E.-M., Frei, P., Bouvier, M., Stafford, W. F., Helenius, A., Glockshuber, R. & Ellgaard, L. ERp57 is a multifunctional thiol-disulfide oxidoreductase. *J. Biol. Chem.* **279**, 18277–18287 (2004).
58. Harris, M. R., Yu, Y. Y. L., Kindle, C. S., Hansen, T. H. & Solheim, J. C. Calreticulin and calnexin interact with different protein and glycan determinants during the Assembly of MHC class I. *J. Immunol.* **160**, 5404–5409 (1998).
59. Peaper, D. R., Wearsch, P. A. & Cresswell, P. Tapasin and ERp57 form a stable disulfide-linked dimer within the MHC class I peptide-loading complex. *EMBO J.* **24**, 3613–3623 (2005).
60. Dong, G., Wearsch, P. A., Peaper, D. R., Cresswell, P. & Reinisch, K. M. Insights into MHC class I peptide loading from the structure of the tapasin-ERp57 thiol oxidoreductase heterodimer. *Immunity* **30**, 21–32 (2009).
61. Wieczorek, M., Abualrous, E. T., Sticht, J., Álvaro-Benito, M., Stolzenberg, S., Noé, F. & Freund, C. Major histocompatibility complex (MHC) class I and MHC class II proteins: Conformational plasticity in antigen presentation. *Front. Immunol.* **8**, 292 (2017).
62. Lan, H. *et al.* Exchange catalysis by tapasin exploits conserved and allele-specific features of MHC-I molecules. *Nat. Commun.* **12**, 4236 (2021).
63. Williams, A. P., Peh, C. A., Purcell, A. W., McCluskey, J. & Elliott, T. Optimization of the MHC Class I peptide cargo is dependent on tapasin. *Immunity* **16**, 509–520 (2002).
64. Neefjes, J. J., Hämmerling, G. J. & Momburg, F. Folding and assembly of major histocompatibility complex class I heterodimers in the endoplasmic reticulum of intact cells precedes the binding of peptide. *J. Exp. Med.* **178**, 1971–1980 (1993).
65. Bai, L., Wang, T., Zhao, G., Kovach, A. & Li, H. The atomic structure of a eukaryotic oligosaccharyltransferase complex. *Nature* **555**, 328–333 (2018).
66. Wild, R., Kowal, J., Eyring, J., Ngwa, E. M., Aebi, M. & Locher, K. P. Structure of the yeast oligosaccharyltransferase complex gives insight into eukaryotic N-glycosylation. *Science* **359**, 545–550 (2018).
67. Williams, D. B. Beyond lectins: the calnexin/calreticulin chaperone system of the endoplasmic reticulum. *J. Cell Sci.* **119**, 615–623 (2006).
68. Ortmann, B., Androlewicz, M. J. & Cresswell, P. MHC class l/β2-microglobulin complexes associate with TAP transporters before peptide binding. *Nature* **368**, 864–867 (1994).
69. Garrett, T. P. J., Saper, M. A., Bjorkman, P. J., Strominger, J. L. & Wiley, D. C. Specificity pockets for the side chains of peptide antigens in HLA-Aw68. *Nature* **342**, 692–696 (1989).
70. Elliott, T. & van Hateren, A. Protein plasticity and peptide editing in the MHC I antigen processing pathway. *Biochemistry* **57**, 1423–1425 (2018).

71. van Hateren, A., Bailey, A., Werner, J. M. & Elliott, T. Plasticity of empty major histocompatibility complex class I molecules determines peptide-selector function. *Mol. Immunol.* **68**, 98–101 (2015).
72. Müller, I. K., Winter, C., Thomas, C., Spaapen, R. M., Trowitzsch, S. & Tampé, R. Structure of an MHC I–tapasin–ERp57 editing complex defines chaperone promiscuity. *Nat. Commun.* **13**, 5383 (2022).
73. Jiang, J., Natarajan, K., Boyd, L. F., Morozov, G. I., Mage, M. G. & Margulies, D. H. Crystal structure of a TAPBPR–MHC I complex reveals the mechanism of peptide editing in antigen presentation. *Science* **358**, 1064–1068 (2017).
74. Beerbaum, M., Ballaschk, M., Erdmann, N., Schnick, C., Diehl, A., Uchanska-Ziegler, B., Ziegler, A. & Schmieder, P. NMR spectroscopy reveals unexpected structural variation at the protein–protein interface in MHC class I molecules. *J. Biomol. NMR* **57**, 167–178 (2013).
75. Hee, C.-S., Beerbaum, M., Loll, B., Ballaschk, M., Schmieder, P., Uchanska-Ziegler, B. & Ziegler, A. Dynamics of free versus complexed β2-microglobulin and the evolution of interfaces in MHC class I molecules. *Immunogenetics* **65**, 157–172 (2013).
76. Nakamura, K. *et al.* Functional specialization of calreticulin domains. *J. Cell Biol.* **154**, 961–972 (2001).
77. Michalak, M., Corbett, E. F., Mesaeli, N., Nakamura, K. & Opas, M. Calreticulin: one protein, one gene, many functions. *Biochem. J.* **344**, 281 (1999).
78. Varricchio, L., Falchi, M., Dall'Ora, M., De Benedittis, C., Ruggeri, A., Uversky, V. N. & Migliaccio, A. R. Calreticulin: Challenges posed by the intrinsically disordered nature of calreticulin to the study of its function. *Front. Cell Dev. Biol.* **5**, 96 (2017).
79. Kielbik, M., Szulc-Kielbik, I. & Klink, M. Calreticulin—Multifunctional chaperone in immunogenic cell death: Potential significance as a prognostic biomarker in ovarian cancer patients. *Cells* **10**, 130 (2021).
80. Panaretakis, T. *et al.* The co-translocation of ERp57 and calreticulin determines the immunogenicity of cell death. *Cell Death Differ.* **15**, 1499–1509 (2008).
81. Hulpke, S. & Tampé, R. The MHC I loading complex: a multitasking machinery in adaptive immunity. *Trends Biochem. Sci.* **38**, 412–420 (2013).
82. Frickel, E.-M., Riek, R., Jelesarov, I., Helenius, A., Wüthrich, K. & Ellgaard, L. TROSY-NMR reveals interaction between ERp57 and the tip of the calreticulin P-domain. *Proc. Natl. Acad. Sci.* **99**, 1954–1959 (2002).
83. Michalak, M., Groenendyk, J., Szabo, E., Gold, L. I. & Opas, M. Calreticulin, a multi-process calcium-buffering chaperone of the endoplasmic reticulum. *Biochem. J.* **417**, 651–666 (2009).
84. Cascio, P. 26S proteasomes and immunoproteasomes produce mainly N-extended versions of an antigenic peptide. *EMBO J.* **20**, 2357–2366 (2001).
85. Blanchard, N. *et al.* Endoplasmic reticulum aminopeptidase associated with antigen processing defines the composition and structure of MHC class I peptide repertoire in normal and virus-infected cells. *J. Immunol.* **184**, 3033–3042 (2010).
86. Saveanu, L. *et al.* Concerted peptide trimming by human ERAP1 and ERAP2 aminopeptidase complexes in the endoplasmic reticulum. *Nat. Immunol.* **6**, 689–697 (2005).
87. Mpakali, A., Giastas, P., Mathioudakis, N., Mavridis, I. M., Saridakis, E. & Stratikos, E. Structural basis for antigenic peptide recognition and processing by endoplasmic reticulum (ER) aminopeptidase 2. *J. Biol. Chem.* **290**, 26021–26032 (2015).
88. Georgiadou, D. & Stratikos, E. Cellular mechanisms that edit the immunopeptidome. *Curr. Proteomics* **6**, 13–24 (2009).

89. Alvarez-Navarro, C. & López de Castro, J. A. ERAP1 structure, function and pathogenetic role in ankylosing spondylitis and other MHC-associated diseases. *Mol. Immunol.* **57**, 12–21 (2014).
90. Hammer, G. E., Gonzalez, F., James, E., Nolla, H. & Shastri, N. In the absence of aminopeptidase ERAAP, MHC class I molecules present many unstable and highly immunogenic peptides. *Nat. Immunol.* **8**, 101–8 (2007).
91. Barnea, E. *et al.* The human leukocyte antigen (HLA)-B27 peptidome in vivo, in spondyloarthritis-susceptible HLA-B27 transgenic rats and the effect of ERAP1 deletion. *Mol. Cell. Proteomics* **16**, 642–662 (2017).
92. Hammer, G. E., Gonzalez, F., Champsaur, M., Cado, D. & Shastri, N. The aminopeptidase ERAAP shapes the peptide repertoire displayed by major histocompatibility complex class I molecules. *Nat. Immunol.* **7**, 103–112 (2006).
93. York, I. A., Brehm, M. A., Zendzian, S., Towne, C. F. & Rock, K. L. Endoplasmic reticulum aminopeptidase 1 (ERAP1) trims MHC class I-presented peptides in vivo and plays an important role in immunodominance. *Proc. Natl. Acad. Sci.* **103**, 9202–9207 (2006).
94. Nagarajan, N. A., de Verteuil, D. A., Sriranganadane, D., Yahyaoui, W., Thibault, P., Perreault, C. & Shastri, N. ERAAP shapes the peptidome associated with classical and nonclassical MHC class I molecules. *J. Immunol.* **197**, 1035–1043 (2016).
95. Zervoudi, E. *et al.* Probing the S1 specificity pocket of the aminopeptidases that generate antigenic peptides. *Biochem. J.* **435**, 411–420 (2011).
96. Lorente, E., Barriga, A., Johnstone, C., Mir, C., Jiménez, M. & López, D. Concerted In vitro trimming of viral HLA-B27-restricted ligands by human ERAP1 and ERAP2 aminopeptidases. *PLoS One* **8**, e79596 (2013).
97. Papakyriakou, A., Mpakali, A. & Stratikos, E. Can ERAP1 and ERAP2 form functional heterodimers? A structural dynamics investigation. *Front. Immunol.* **13**, 1358 (2022).
98. Evnouchidou, I., Weimershaus, M., Saveanu, L. & van Endert, P. ERAP1–ERAP2 dimerization increases peptide-trimming efficiency. *J. Immunol.* **193**, 901–908 (2014).
99. Nguyen, T. T., Chang, S.-C., Evnouchidou, I., York, I. A., Zikos, C., Rock, K. L., Goldberg, A. L., Stratikos, E. & Stern, L. J. Structural basis for antigenic peptide precursor processing by the endoplasmic reticulum aminopeptidase ERAP1. *Nat. Struct. Mol. Biol.* **18**, 604–613 (2011).
100. Chen, H., Li, L., Weimershaus, M., Evnouchidou, I., van Endert, P. & Bouvier, M. ERAP1-ERAP2 dimers trim MHC I-bound precursor peptides; implications for understanding peptide editing. *Sci. Rep.* **6**, 28902 (2016).
101. Papakyriakou, A., Reeves, E., Beton, M., Mikolajek, H., Douglas, L., Cooper, G., Elliott, T., Werner, J. M. & James, E. The partial dissociation of MHC class I–bound peptides exposes their N terminus to trimming by endoplasmic reticulum aminopeptidase 1. *J. Biol. Chem.* **293**, 7538–7548 (2018).
102. Ito, Y., Kajihara, Y. & Takeda, Y. Chemical-synthesis-based approach to glycoprotein functions in the endoplasmic reticulum. *Chemistry* **26**, 15461–15470 (2020).
103. Kuribara, T. & Totani, K. Structural insights into N-linked glycan-mediated protein folding from chemical and biological perspectives. *Curr. Opin. Struct. Biol.* **68**, 41–47 (2021).
104. Adams, B. M., Oster, M. E. & Hebert, D. N. Protein quality control in the endoplasmic reticulum. *Protein J.* **38**, 317–329 (2019).
105. Ninagawa, S., George, G. & Mori, K. Mechanisms of productive folding and endoplasmic reticulum-associated degradation of glycoproteins and non-glycoproteins. *Biochim. Biophys. Acta - Gen. Subj.* **1865**, 129812 (2021).

106. De Praeter, C. M. *et al.* A novel disorder caused by defective biosynthesis of N-Linked oligosaccharides due to glucosidase I deficiency. *Am. J. Hum. Genet.* **66**, 1744–1756 (2000).
107. Gallo, G. L., Valko, A., Aramburu, S. I., Etchegaray, E., Völker, C., Parodi, A. J. & D'Alessio, C. Abrogation of glucosidase I–mediated glycoprotein deglucosylation results in a sick phenotype in fission yeasts: Model for the human MOGS-CDG disorder. *J. Biol. Chem.* **293**, 19957–19973 (2018).
108. Hammond, C., Braakman, I. & Helenius, A. Role of N-linked oligosaccharide recognition, glucose trimming, and calnexin in glycoprotein folding and quality control. *Proc. Natl. Acad. Sci.* **91**, 913–917 (1994).
109. Hettkamp, H., Legler, G. & Bause, E. Purification by affinity chromatography of glucosidase I, an endoplasmic reticulum hydrolase involved in the processing of asparagine-linked oligosaccharides. *Eur. J. Biochem.* **142**, 85–90 (1984).
110. Lucocq, J. M., Brada, D. & Roth, J. Immunolocalization of the oligosaccharide trimming enzyme glucosidase II. *J. Cell Biol.* **102**, 2137–2146 (1986).
111. Caputo, A. T. *et al.* Structures of mammalian ER α-glucosidase II capture the binding modes of broad-spectrum iminosugar antivirals. *Proc. Natl. Acad. Sci.* **113**, E4630–E4638 (2016).
112. D'Alessio, C., Caramelo, J. J. & Parodi, A. J. UDP-GlC:glycoprotein glucosyltransferase-glucosidase II, the ying-yang of the ER quality control. *Semin. Cell Dev. Biol.* **21**, 491–499 (2010).
113. Trombetta, E. S., Simons, J. F. & Helenius, A. Endoplasmic reticulum glucosidase II is composed of a catalytic subunit, conserved from yeast to mammals, and a tightly bound noncatalytic HDEL-containing subunit. *J. Biol. Chem.* **271**, 27509–27516 (1996).
114. Ware, F. E., Vassilakos, A., Peterson, P. A., Jackson, M. R., Lehrman, M. A. & Williams, D. B. The molecular chaperone calnexin binds Glc1Man9GlcNAc2 oligosaccharide as an initial step in recognizing unfolded glycoproteins. *J. Biol. Chem.* **270**, 4697–4704 (1995).
115. Michalak, M., Milner, R. E., Burns, K. & Opas, M. Calreticulin. *Biochem. J.* **285**, 681–692 (1992).
116. Mayerhofer, P. U. & Tampé, R. Antigen translocation machineries in adaptive immunity and viral immune evasion. *J. Mol. Biol.* **427**, 1102–1118 (2015).
117. Lankat-Buttgereit, B. & Tampé, R. The transporter associated with antigen processing: function and implications in human diseases. *Physiol. Rev.* **82**, 187–204 (2002).
118. Ritz, U. & Seliger, B. The transporter associated with antigen processing (TAP): structural integrity, expression, function, and its clinical relevance. *Mol. Med.* **7**, 149–158 (2001).
119. Seliger, B., Harders, C., Lohmann, S., Momburg, F., Urlinger, S., Tampé, R. & Huber, C. Down-regulation of the MHC class I antigen-processing machinery after oncogenic transformation of murine fibroblasts. *Eur. J. Immunol.* **28**, 122–133 (1998).
120. York, I. A., Roop, C., Andrews, D. W., Riddell, S. R., Graham, F. L. & Johnson, D. C. A cytosolic herpes simplex virus protein inhibits antigen presentation to CD8+ T lymphocytes. *Cell* **77**, 525–535 (1994).
121. Hill, A., Jugovic, P., York, L., Russ, G., Bennink, J., Yewdell, J., Ploegh, H. & Johnson, D. Herpes simplex virus turns off the TAP to evade host immunity. *Nature* **375**, 411–415 (1995).
122. Früh, K., Ahn, K., Djaballah, H., Sempé, P., van Endert, P. M., Tampé, R., Peterson, P. A. & Yang, Y. A viral inhibitor of peptide transporters for antigen presentation. *Nature* **375**, 415–8 (1995).

123. Ahn, K., Meyer, T. H., Uebel, S., Sempé, P., Djaballah, H., Yang, Y., Peterson, P. A., Früh, K. & Tampé, R. Molecular mechanism and species specificity of TAP inhibition by herpes simplex virus ICP47. *EMBO J.* **15**, 3247–55 (1996).
124. Neumann, L., Kraas, W., Uebel, S., Jung, G. & Tampé, R. The active domain of the herpes simplex virus protein ICP47: A potent inhibitor of the transporter associated with antigen processing (TAP). *J. Mol. Biol.* **272**, 484–492 (1997).
125. Aisenbrey, C., Sizun, C., Koch, J., Herget, M., Abele, R., Bechinger, B. & Tampé, R. Structure and dynamics of membrane-associated ICP47, a viral inhibitor of the MHC I antigen-processing machinery. *J. Biol. Chem.* **281**, 30365–30372 (2006).
126. Beinert, D., Neumann, L., Uebel, S. & Tampé, R. Structure of the viral TAP-inhibitor ICP47 induced by membrane association. *Biochemistry* **36**, 4694–4700 (1997).
127. Pfänder, R., Neumann, L., Zweckstetter, M., Seger, C., Holak, T. A. & Tampé, R. Structure of the active domain of the herpes simplex virus protein ICP47 in water/sodium dodecyl sulfate solution determined by nuclear magnetic resonance spectroscopy. *Biochemistry* **38**, 13692–8 (1999).
128. Herbring, V., Bäucker, A., Trowitzsch, S. & Tampé, R. A dual inhibition mechanism of herpesviral ICP47 arresting a conformationally thermostable TAP complex. *Sci. Rep.* **6**, 36907 (2016).
129. Galocha, B., Hill, A., Barnett, B. C., Dolan, A., Raimondi, A., Cook, R. F., Brunner, J., McGeoch, D. J. & Ploegh, H. L. The active site of ICP47, a herpes simplex virus-encoded inhibitor of the major histocompatibility complex (MHC)-encoded peptide transporter associated with antigen processing (TAP), maps to the NH2-terminal 35 residues. *J. Exp. Med.* **185**, 1565–72 (1997).
130. Matschulla, T. *et al.* A highly conserved sequence of the viral TAP inhibitor ICP47 is required for freezing of the peptide transport cycle. *Sci. Rep.* **7**, 2933 (2017).
131. Keefe, A. D., Wilson, D. S., Seelig, B. & Szostak, J. W. One-step purification of recombinant proteins using a nanomolar-affinity streptavidin-binding peptide, the SBP-Tag. *Protein Expr. Purif.* **23**, 440–6 (2001).
132. Dugan, G. E. & Hewitt, E. W. Structural and Functional Dissection of the Human Cytomegalovirus Immune Evasion Protein US6. *J. Virol.* **82**, 3271–82 (2008).
133. Ahn, K., Gruhler, A., Galocha, B., Jones, T. R., Wiertz, E. J. H. J., Ploegh, H. L., Peterson, P. A., Yang, Y. & Früh, K. The ER-luminal domain of the HCMV glycoprotein US6 inhibits peptide translocation by TAP. *Immunity* **6**, 613–21 (1997).
134. Lehner, P. J., Karttunen, J. T., Wilkinson, G. W. G. & Cresswell, P. The human cytomegalovirus US6 glycoprotein inhibits transporter associated with antigen processing-dependent peptide translocation. *Proc. Natl. Acad. Sci.* **94**, 6904–9 (1997).
135. Halenius, A., Momburg, F., Reinhard, H., Bauer, D., Lobigs, M. & Hengel, H. Physical and functional interactions of the cytomegalovirus US6 glycoprotein with the transporter associated with antigen processing. *J. Biol. Chem.* **281**, 5383–90 (2006).
136. Hengel, H., Koopmann, J. O., Flohr, T., Muranyi, W., Goulmy, E., Hämmerling, G. J., Koszinowski, U. H. & Momburg, F. A viral ER-resident glycoprotein inactivates the MHC-encoded peptide transporter. *Immunity* **6**, 623–32 (1997).
137. Hewitt, E. W., Gupta, S. S. & Lehner, P. J. The human cytomegalovirus gene product US6 inhibits ATP binding by TAP. *EMBO J.* **20**, 387–96 (2001).
138. Kyritsis, C., Gorbulev, S., Hutschenreiter, S., Pawlitschko, K., Abele, R. & Tampé, R. Molecular mechanism and structural aspects of transporter associated with antigen processing inhibition by the cytomegalovirus protein US6. *J. Biol. Chem.* **276**, 48031–9 (2001).
139. Sethumadhavan, S. PhD Thesis: Structural and functional characterisation of human cytomegalovirus encoded glycoprotein US6. (Goethe University Frankfurt, 2021).

140. Sethumadhavan, S., Barth, M., Spaapen, R. M., Schmidt, C., Trowitzsch, S. & Tampé, R. Viral immune evasins impact antigen presentation by allele-specific trapping of MHC I at the peptide-loading complex. *Sci. Rep.* **12**, 1516 (2022).
141. Kühlbrandt, W. The Resolution Revolution. *Science* **343**, 1443–1444 (2014).
142. Wu, M. & Lander, G. C. Present and emerging methodologies in cryo-EM single-particle analysis. *Biophys. J.* **119**, 1281–1289 (2020).
143. Dubochet, J., Adrian, M., Chang, J. J., Homo, J. C., Lepault, J., McDowall, A. W. & Schultz, P. Cryo-electron microscopy of vitrified specimens. *Q. Rev. Biophys.* **21**, 129–228 (1988).
144. Kim, L. Y. *et al.* Benchmarking cryo-EM single particle analysis workflow. *Front. Mol. Biosci.* **5**, 50 (2018).
145. Rice, W. J., Cheng, A., Noble, A. J., Eng, E. T., Kim, L. Y., Carragher, B. & Potter, C. S. Routine determination of ice thickness for cryo-EM grids. *J. Struct. Biol.* **204**, 38–44 (2018).
146. Punjani, A., Rubinstein, J. L., Fleet, D. J. & Brubaker, M. A. cryoSPARC: algorithms for rapid unsupervised cryo-EM structure determination. *Nat. Methods* **14**, 290–296 (2017).
147. Cheng, Y., Grigorieff, N., Penczek, P. A. & Walz, T. A primer to single-particle cryo-electron microscopy. *Cell* **161**, 438–449 (2015).
148. Autzen, H. E., Julius, D. & Cheng, Y. Membrane mimetic systems in CryoEM: keeping membrane proteins in their native environment. *Curr. Opin. Struct. Biol.* **58**, 259–268 (2019).
149. Majeed, S., Ahmad, A. B., Sehar, U. & Georgieva, E. R. Lipid membrane mimetics in functional and structural Ssudies of integral membrane proteins. *Membranes (Basel).* **11**, 685 (2021).
150. Herget, M., Kreiβig, N., Kolbe, C., Schölz, C., Tampé, R. & Abele, R. Purification and reconstitution of the antigen transport complex TAP. *J. Biol. Chem.* **284**, 33740–33749 (2009).
151. Lorsch, J. Laboratory methods in enzymology: Protein part C. *Methods Enzymol.* 296 (2014).
152. Thoma, J. & Burmann, B. M. Fake it ‘till you make it—the pursuit of suitable membrane mimetics for membrane protein biophysics. *Int. J. Mol. Sci.* **22**, 50 (2020).
153. Zhou, H.-X. & Cross, T. A. Influences of membrane mimetic environments on membrane protein structures. *Annu. Rev. Biophys.* **42**, 361–92 (2013).
154. Lee, S., Mao, A., Bhattacharya, S., Robertson, N., Grisshammer, R., Tate, C. G. & Vaidehi, N. How do short chain nonionic detergents destabilize G-protein-coupled receptors? *J. Am. Chem. Soc.* **138**, 15425–15433 (2016).
155. Gewering, T., Januliene, D., Ries, A. B. & Moeller, A. Know your detergents: A case study on detergent background in negative stain electron microscopy. *J. Struct. Biol.* **203**, 242–246 (2018).
156. Popot, J.-L. *et al.* Amphipols from A to Z. *Annu. Rev. Biophys.* **40**, 379–408 (2011).
157. Popot, J.-L. *et al.* Amphipols: polymeric surfactants for membrane biology research. *Cell. Mol. Life Sci.* **60**, 1559–1574 (2003).
158. Blees, A. PhD Thesis: Structural and functional analysis of the MHC I peptide-loading complex. (Goethe University Frankfurt, 2017).
159. Denisov, I. G. & Sligar, S. G. Nanodiscs in membrane biochemistry and biophysics. *Chem. Rev.* **117**, 4669–4713 (2017).
160. Denisov, I. G., Grinkova, Y. V., Lazarides, A. A. & Sligar, S. G. Directed self-assembly of monodisperse phospholipid bilayer nanodiscs with controlled size. *J. Am. Chem. Soc.* **126**, 3477–87 (2004).

161. Bayburt, T. H., Carlson, J. W. & Sligar, S. G. Reconstitution and imaging of a membrane protein in a nanometer-size phospholipid bilayer. *J. Struct. Biol.* **123**, 37–44 (1998).
162. Civjan, N. R., Bayburt, T. H., Schuler, M. A. & Sligar, S. G. Direct solubilization of heterologously expressed membrane proteins by incorporation into nanoscale lipid bilayers. *Biotechniques* **35**, 556–563 (2003).
163. Bibow, S. *et al.* Solution structure of discoidal high-density lipoprotein particles with a shortened apolipoprotein A-I. *Nat. Struct. Mol. Biol.* **24**, 187–193 (2017).
164. Hagn, F., Etzkorn, M., Raschle, T. & Wagner, G. Optimized phospholipid bilayer nanodiscs facilitate high-resolution structure determination of membrane proteins. *J. Am. Chem. Soc.* **135**, 1919–25 (2013).
165. Grinkova, Y. V., Denisov, I. G. & Sligar, S. G. Engineering extended membrane scaffold proteins for self-assembly of soluble nanoscale lipid bilayers. *Protein Eng. Des. Sel.* **23**, 843–8 (2010).
166. Efremov, R. G., Gatsogiannis, C. & Raunser, S. Lipid nanodiscs as a tool for high-resolution structure determination of membrane proteins by single-particle cryo-EM. *Methods Enzymol.* **594**, 1–30 (2017).
167. Mio, K. & Sato, C. Lipid environment of membrane proteins in cryo-EM based structural analysis. *Biophys. Rev.* **10**, 307–316 (2018).
168. Frauenfeld, J. *et al.* A saposin-lipoprotein nanoparticle system for membrane proteins. *Nat. Methods* **13**, 345–351 (2016).
169. Flayhan, A., Mertens, H. D. T., Ural-Blimke, Y., Martinez Molledo, M., Svergun, D. I. & Löw, C. Saposin lipid nanoparticles: A highly versatile and modular tool for membrane protein research. *Structure* **26**, 345-355.e5 (2018).
170. Lyons, J. A., Bøggild, A., Nissen, P. & Frauenfeld, J. Saposin-lipoprotein scaffolds for structure determination of membrane transporters. *Methods Enzymol.* **594**, 85–99 (2017).
171. Carlson, M. L. *et al.* The Peptidisc, a simple method for stabilizing membrane proteins in detergent-free solution. *eLife* **7**, e34085 (2018).
172. Oluwole, A. O., Danielczak, B., Meister, A., Babalola, J. O., Vargas, C. & Keller, S. Solubilization of membrane proteins into functional lipid-bilayer nanodiscs using a diisobutylene/maleic acid copolymer. *Angew. Chemie Int. Ed.* **56**, 1919–1924 (2017).
173. Dörr, J. M., Scheidelaar, S., Koorengevel, M. C., Dominguez, J. J., Schäfer, M., van Walree, C. A. & Killian, J. A. The styrene-maleic acid copolymer: a versatile tool in membrane research. *Eur. Biophys. J.* **45**, 3–21 (2016).
174. Jeong, C., Franklin, R., Edler, K. J., Vanommeslaeghe, K., Krueger, S. & Curtis, J. E. Styrene–maleic acid copolymer nanodiscs to determine the shape of membrane proteins. *J. Phys. Chem. B* **126**, 1034–1044 (2022).
175. Geertsma, E. R., Nik Mahmood, N. A. B., Schuurman-Wolters, G. K. & Poolman, B. Membrane reconstitution of ABC transporters and assays of translocator function. *Nat. Protoc.* **3**, 256–266 (2008).
176. Akbarzadeh, A., Rezaei-Sadabady, R., Davaran, S., Joo, S. W., Zarghami, N., Hanifehpour, Y., Samiei, M., Kouhi, M. & Nejati-Koshki, K. Liposome: classification, preparation, and applications. *Nanoscale Res. Lett.* **8**, 102 (2013).
177. Parmar, M. M., Edwards, K. & Madden, T. D. Incorporation of bacterial membrane proteins into liposomes: factors influencing protein reconstitution. *Biochim. Biophys. Acta* **1421**, 77–90 (1999).
178. Meyer, T. H., van Endert, P. M., Uebel, S., Ehring, B. & Tampé, R. Functional expression and purification of the ABC transporter complex associated with antigen processing (TAP) in insect cells. *FEBS Lett.* **351**, 443–7 (1994).

179. Reynisson, B., Alvarez, B., Paul, S., Peters, B. & Nielsen, M. NetMHCpan-4.1 and NetMHCIIpan-4.0: improved predictions of MHC antigen presentation by concurrent motif deconvolution and integration of MS MHC eluted ligand data. *Nucleic Acids Res.* **48**, W449–W454 (2020).
180. Uebel, S., Kraas, W., Kienle, S., Wiesmüller, K. H., Jung, G. & Tampé, R. Recognition principle of the TAP transporter disclosed by combinatorial peptide libraries. *Proc. Natl. Acad. Sci.* **94**, 8976–81 (1997).
181. Fischbach, H., Döring, M., Nikles, D., Lehnert, E., Baldauf, C., Kalinke, U. & Tampé, R. Ultrasensitive quantification of TAP-dependent antigen compartmentalization in scarce primary immune cell subsets. *Nat. Commun.* **6**, 6199 (2015).
182. Winter, C., Domnick, A., Cernova, D. & Tampé, R. Semisynthetic viral inhibitor for light control of the MHC I peptide loading complex. *Angew. Chemie Int. Ed.* **61**, e202211826 (2022).
183. Schneider, C. A., Rasband, W. S. & Eliceiri, K. W. NIH Image to ImageJ: 25 years of image analysis. *Nat. Methods* **9**, 671–5 (2012).
184. Link, A. J. & Labaer, J. In-gel trypsin digest of gel-fractionated proteins. *Cold Spring Harb. Protoc.* **2009**, pdb.prot5110 (2009).
185. Shevchenko, A., Tomas, H., Havlis, J., Olsen, J. V. & Mann, M. In-gel digestion for mass spectrometric characterization of proteins and proteomes. *Nat. Protoc.* **1**, 2856–60 (2006).
186. Olsen, J. V. *et al.* Parts per million mass accuracy on an Orbitrap mass spectrometer via lock mass injection into a C-trap. *Mol. Cell. Proteomics* **4**, 2010–21 (2005).
187. Luquet, E., Biesemann, C., Munier, A. & Herzog, E. Purification of synaptosome populations using fluorescence-activated synaptosome sorting. *Methods Mol. Biol.* **1538**, 121–134 (2017).
188. Suloway, C., Pulokas, J., Fellmann, D., Cheng, A., Guerra, F., Quispe, J., Stagg, S., Potter, C. S. & Carragher, B. Automated molecular microscopy: the new Leginon system. *J. Struct. Biol.* **151**, 41–60 (2005).
189. Grant, T., Rohou, A. & Grigorieff, N. cisTEM, user-friendly software for single-particle image processing. *eLife* **7**, (2018).
190. Bepler, T., Morin, A., Rapp, M., Brasch, J., Shapiro, L., Noble, A. J. & Berger, B. Positive-unlabeled convolutional neural networks for particle picking in cryo-electron micrographs. *Nat. Methods* **16**, 1153–1160 (2019).
191. Bepler, T., Kelley, K., Noble, A. J. & Berger, B. Topaz-denoise: general deep denoising models for cryoEM and cryoET. *Nat. Commun.* **11**, 5208 (2020).
192. Zhong, E. D., Bepler, T., Berger, B. & Davis, J. H. CryoDRGN: reconstruction of heterogeneous cryo-EM structures using neural networks. *Nat. Methods* **18**, 176–185 (2021).
193. Croll, T. I. ISOLDE: a physically realistic environment for model building into low-resolution electron-density maps. *Acta Crystallogr. Sect. D, Struct. Biol.* **74**, 519–530 (2018).
194. Emsley, P. & Cowtan, K. Coot: model-building tools for molecular graphics. *Acta Crystallogr. D. Biol. Crystallogr.* **60**, 2126–32 (2004).
195. Liebschner, D. *et al.* Macromolecular structure determination using X-rays, neutrons and electrons: recent developments in Phenix. *Acta Crystallogr. Sect. D, Struct. Biol.* **75**, 861–877 (2019).
196. Agirre, J., Iglesias-Fernández, J., Rovira, C., Davies, G. J., Wilson, K. S. & Cowtan, K. D. Privateer: software for the conformational validation of carbohydrate structures. *Nat. Struct. Mol. Biol.* **22**, 833–4 (2015).

197. Vinothkumar, K. R., Zhu, J. & Hirst, J. Architecture of mammalian respiratory complex I. *Nature* **515**, 80–84 (2014).
198. Zhu, J., Vinothkumar, K. R. & Hirst, J. Structure of mammalian respiratory complex I. *Nature* **536**, 354–358 (2016).
199. Tomazin, R., Hill, A. B., Jugovic, P., York, I., van Endert, P., Ploegh, H. L., Andrews, D. W. & Johnson, D. C. Stable binding of the herpes simplex virus ICP47 protein to the peptide binding site of TAP. *EMBO J.* **15**, 3256–66 (1996).
200. Verweij, M. C. *et al.* Inhibition of mouse TAP by immune evasion molecules encoded by non-murine herpesviruses. *Mol. Immunol.* **48**, 835–45 (2011).
201. Jugovic, P., Hill, A. M., Tomazin, R., Ploegh, H. & Johnson, D. C. Inhibition of major histocompatibility complex class I antigen presentation in pig and primate cells by herpes simplex virus type 1 and 2 ICP47. *J. Virol.* **72**, 5076–84 (1998).
202. Ibrahim, I. M., Abdelmalek, D. H. & Elfiky, A. A. GRP78: A cell's response to stress. *Life Sci.* **226**, 156–163 (2019).
203. Triantafilou, M., Fradelizi, D. & Triantafilou, K. Major histocompatibility class one molecule associates with glucose regulated protein (GRP) 78 on the cell surface. *Hum. Immunol.* **62**, 764–70 (2001).
204. Paulsson, K. M., Wang, P., Anderson, P. O., Chen, S., Pettersson, R. F. & Li, S. Distinct differences in association of MHC class I with endoplasmic reticulum proteins in wild-type, and beta 2-microglobulin- and TAP-deficient cell lines. *Int. Immunol.* **13**, 1063–73 (2001).
205. Stark, H. GraFix: stabilization of fragile macromolecular complexes for single particle cryo-EM. *Methods Enzymol.* **481**, 109–26 (2010).
206. Pollock, N. L., Lee, S. C., Patel, J. H., Gulamhussein, A. A. & Rothnie, A. J. Structure and function of membrane proteins encapsulated in a polymer-bound lipid bilayer. *Biochim. Biophys. acta Biomembr.* **1860**, 809–817 (2018).
207. Scheidelaar, S., Koorengevel, M. C., van Walree, C. A., Dominguez, J. J., Dörr, J. M. & Killian, J. A. Effect of polymer composition and pH on membrane solubilization by styrene-maleic acid copolymers. *Biophys. J.* **111**, 1974–1986 (2016).
208. Swainsbury, D. J. K., Scheidelaar, S., Foster, N., van Grondelle, R., Killian, J. A. & Jones, M. R. The effectiveness of styrene-maleic acid (SMA) copolymers for solubilisation of integral membrane proteins from SMA-accessible and SMA-resistant membranes. *Biochim. Biophys. acta. Biomembr.* **1859**, 2133–2143 (2017).
209. Alexandrov, A. I., Mileni, M., Chien, E. Y. T., Hanson, M. A. & Stevens, R. C. Microscale fluorescent thermal stability assay for membrane proteins. *Structure* **16**, 351–9 (2008).
210. Hennecke, L. K. Master Thesis: Mechanistic aspects of the MHC I peptide-loading complex. (Goethe University Frankfurt am Main, 2021).
211. Angiulli, G., Dhupar, H. S., Suzuki, H., Wason, I. S., Duong Van Hoa, F. & Walz, T. New approach for membrane protein reconstitution into peptidiscs and basis for their adaptability to different proteins. *eLife* **9**, (2020).
212. Abele, R. & Tampé, R. Moving the cellular peptidome by transporters. *Front. Cell Dev. Biol.* **6**, 43 (2018).
213. Tang, J., Freedman, D. O., Allen, S., Karita, E., Musonda, R., Braga, C., Jamieson, B. D., Louie, L. & Kaslow, R. A. Genotyping TAP2 variants in north american caucasians, brazilians, and africans. *Genes Immun.* **2**, 32–40 (2001).
214. Pulvertaft, R. J. V. A study of malignant tumours in Nigeria by short-term tissue culture. *J. Clin. Pathol.* **18**, 261–273 (1965).

215. Parham, P., Alpert, B. N., Orr, H. T. & Strominger, J. L. Carbohydrate moiety of HLA antigens. Antigenic properties and amino acid sequences around the site of glycosylation. *J. Biol. Chem.* **252**, 7555–67 (1977).
216. Roth, J. & Zuber, C. Quality control of glycoprotein folding and ERAD: the role of N-glycan handling, EDEM1 and OS-9. *Histochem. Cell Biol.* **147**, 269–284 (2017).
217. Stanley, P. Golgi glycosylation. *Cold Spring Harb. Perspect. Biol.* **3**, a005199–a005199 (2011).
218. Rizvi, S. M., Del Cid, N., Lybarger, L. & Raghavan, M. Distinct functions for the glycans of tapasin and heavy chains in the assembly of MHC class I molecules. *J. Immunol.* **186**, 2309–20 (2011).
219. Radcliffe, C. M., Diedrich, G., Harvey, D. J., Dwek, R. A., Cresswell, P. & Rudd, P. M. Identification of specific glycoforms of major histocompatibility complex class I heavy chains suggests that class I peptide loading is an adaptation of the quality control pathway involving calreticulin and ERp57. *J. Biol. Chem.* **277**, 46415–23 (2002).
220. Chen, M. & Bouvier, M. Analysis of interactions in a tapasin/class I complex provides a mechanism for peptide selection. *EMBO J.* **26**, 1681–90 (2007).
221. Lehner, P. J., Surman, M. J. & Cresswell, P. Soluble tapasin restores MHC class I expression and function in the tapasin-negative cell line .220. *Immunity* **8**, 221–31 (1998).
222. Jackson, L. P., Lewis, M., Kent, H. M., Edeling, M. A., Evans, P. R., Duden, R. & Owen, D. J. Molecular basis for recognition of dilysine trafficking motifs by COPI. *Dev. Cell* **23**, 1255–62 (2012).
223. Letourneur, F., Gaynor, E. C., Hennecke, S., Démollière, C., Duden, R., Emr, S. D., Riezman, H. & Cosson, P. Coatomer is essential for retrieval of dilysine-tagged proteins to the endoplasmic reticulum. *Cell* **79**, 1199–207 (1994).
224. Punjani, A., Zhang, H. & Fleet, D. J. Non-uniform refinement: adaptive regularization improves single-particle cryo-EM reconstruction. *Nat. Methods* **17**, 1214–1221 (2020).
225. Fisette, O., Schröder, G. F. & Schäfer, L. V. Atomistic structure and dynamics of the human MHC-I peptide-loading complex. *Proc. Natl. Acad. Sci.* **117**, 20597–20606 (2020).
226. Glaeser, R. M. Proteins, interfaces, and cryo-EM grids. *Curr. Opin. Colloid Interface Sci.* **34**, 1–8 (2018).
227. Glaeser, R. M. & Han, B.-G. Opinion: hazards faced by macromolecules when confined to thin aqueous films. *Biophys. rep.* **3**, 1–7 (2017).
228. Glaeser, R. M. How good can single-particle cryo-EM become? What remains before it approaches its physical limits? *Annu. Rev. Biophys.* **48**, 45–61 (2019).
229. Noble, A. J. *et al.* Routine single particle CryoEM sample and grid characterization by tomography. *eLife* **7**, e34257 (2018).
230. McShan, A. C., Devlin, C. A., Morozov, G. I., Overall, S. A., Moschidi, D., Akella, N., Procko, E. & Sgourakis, N. G. TAPBPR promotes antigen loading on MHC-I molecules using a peptide trap. *Nat. Commun.* **12**, 3174 (2021).
231. Abualrous, E. T., Fritzsche, S., Hein, Z., Al-Balushi, M. S., Reinink, P., Boyle, L. H., Wellbrock, U., Antoniou, A. N. & Springer, S. F pocket flexibility influences the tapasin dependence of two differentially disease-associated MHC class I proteins. *Eur. J. Immunol.* **45**, 1248–57 (2015).
232. Zhang, S., Liu, J., Cheng, H., Tan, S., Qi, J., Yan, J. & Gao, G. F. Structural basis of cross-allele presentation by HLA-A*0301 and HLA-A*1101 revealed by two HIV-derived peptide complexes. *Mol. Immunol.* **49**, 395–401 (2011).

233. Wearsch, P. A. & Cresswell, P. Selective loading of high-affinity peptides onto major histocompatibility complex class I molecules by the tapasin-ERp57 heterodimer. *Nat. Immunol.* **8**, 873–81 (2007).
234. Chapman, D. C. & Williams, D. B. ER quality control in the biogenesis of MHC class I molecules. *Semin. Cell Dev. Biol.* **21**, 512–9 (2010).
235. Peaper, D. R. & Cresswell, P. Regulation of MHC class I assembly and peptide binding. *Annu. Rev. Cell Dev. Biol.* **24**, 343–68 (2008).
236. Neerincx, A. & Boyle, L. H. Preferential interaction of MHC class I with TAPBPR in the absence of glycosylation. *Mol. Immunol.* **113**, 58–66 (2019).
237. Barnstable, C. J., Bodmer, W. F., Brown, G., Galfre, G., Milstein, C., Williams, A. F. & Ziegler, A. Production of monoclonal antibodies to group A erythrocytes, HLA and other human cell surface antigens-new tools for genetic analysis. *Cell* **14**, 9–20 (1978).
238. Brodsky, F. M. & Parham, P. Monomorphic anti-HLA-A,B,C monoclonal antibodies detecting molecular subunits and combinatorial determinants. *J. Immunol.* **128**, 129–35 (1982).
239. Tran, T. M., Ivanyi, P., Hilgert, I., Brdicka, T., Pla, M., Breur, B., Flieger, M., Ivasková, E. & Horejsí, V. The epitope recognized by pan-HLA class I-reactive monoclonal antibody W6/32 and its relationship to unusual stability of the HLA-B27/beta2-microglobulin complex. *Immunogenetics* **53**, 440–6 (2001).
240. Domnick, A., Winter, C., Sušac, L., Hennecke, L., Hensen, M., Zitzmann, N., Trowitzsch, S., Thomas, C. & Tampé, R. Molecular basis of MHC I quality control in the peptide loading complex. *Nat. Commun.* **13**, 4701 (2022).
241. Braner, M., Koller, N., Knauer, J., Herbring, V., Hank, S., Wieneke, R. & Tampé, R. Optical control of the antigen translocation by synthetic photo-conditional viral inhibitors. *Chem. Sci.* **10**, 2001–2005 (2019).
242. Klán, P., Šolomek, T., Bochet, C. G., Blanc, A., Givens, R., Rubina, M., Popik, V., Kostikov, A. & Wirz, J. Photoremovable protecting groups in chemistry and biology: Reaction mechanisms and efficacy. *Chem. Rev.* **113**, 119–91 (2013).
243. Schmierer, T., Laimgruber, S., Haiser, K., Kiewisch, K., Neugebauer, J. & Gilch, P. Femtosecond spectroscopy on the photochemistry of ortho-nitrotoluene. *Phys. Chem. Chem. Phys.* **12**, 15653–64 (2010).
244. Liu, C., Topchiy, E., Lehmann, T. & Basile, F. Characterization of the dehydration products due to thermal decomposition of peptides by liquid chromatography-tandem mass spectrometry. *J. mass Spectrom.* **50**, 625–32 (2015).
245. Bashirova, A. A. *et al.* HLA tapasin independence: broader peptide repertoire and HIV control. *Proc. Natl. Acad. Sci.* **117**, 28232–28238 (2020).
246. Murata, K. & Wolf, M. Cryo-electron microscopy for structural analysis of dynamic biological macromolecules. *Biochim. Biophys. acta. Gen. Subj.* **1862**, 324–334 (2018).

IV. Appendix

6.1. Figures

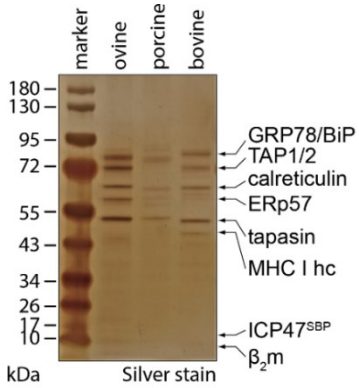

Figure 6.1-1: PLC purified from ovine and bovine spleen, but not from porcine. PLC from spleen was purified by using ICP47^{SBP} and polished by SEC. PLC peak fractions (ovine, bovine) analyzed by SDS-PAGE (reducing, 4-12%, silver stain). The protein pattern of ovine and bovine PLC resembles human PLC composition. However, it additionally contains GRP78. Porcine protein isolated from spleen by ICP47^{SBP} is different from the other PLC samples in protein composition and SEC profile (Figure 4.1-1).

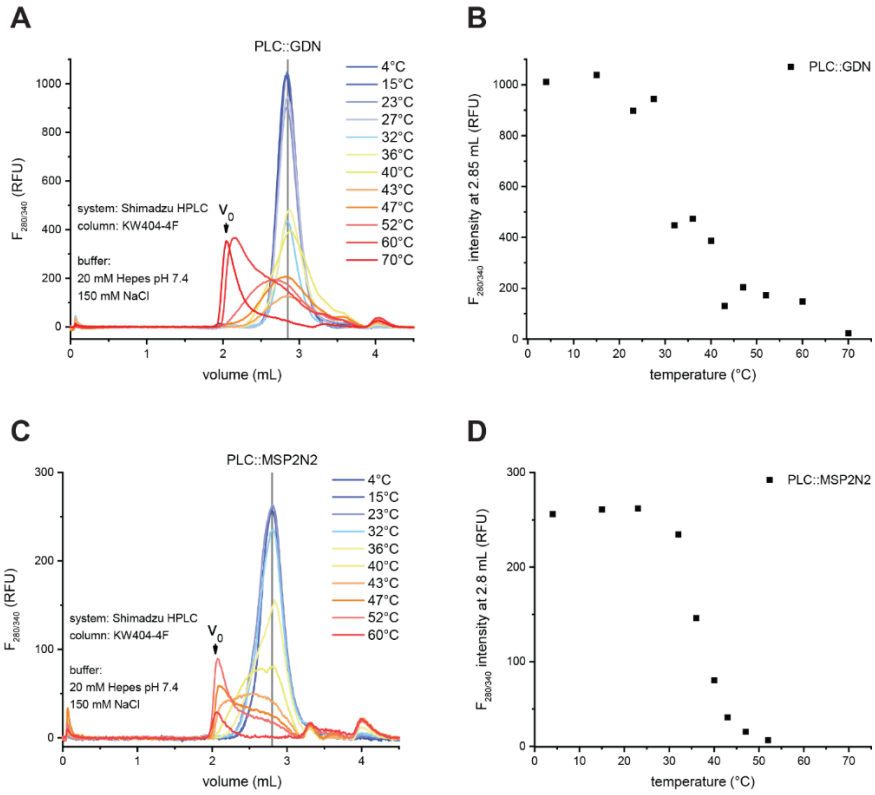

Figure 6.1-2: PLC stabilized by reconstitution in MSP2N2 nanodiscs. Purified PLC::GDN (**A**) and PLC::MSP2N2 (**C**) was aliquoted and heated for 1 h at the indicated temperature and analyzed by SEC. The intensity of intact PLC was determined by $F_{280/315}$. (**B**, **D**). Normalized results were fitted and are displayed in Figure 4.2-5

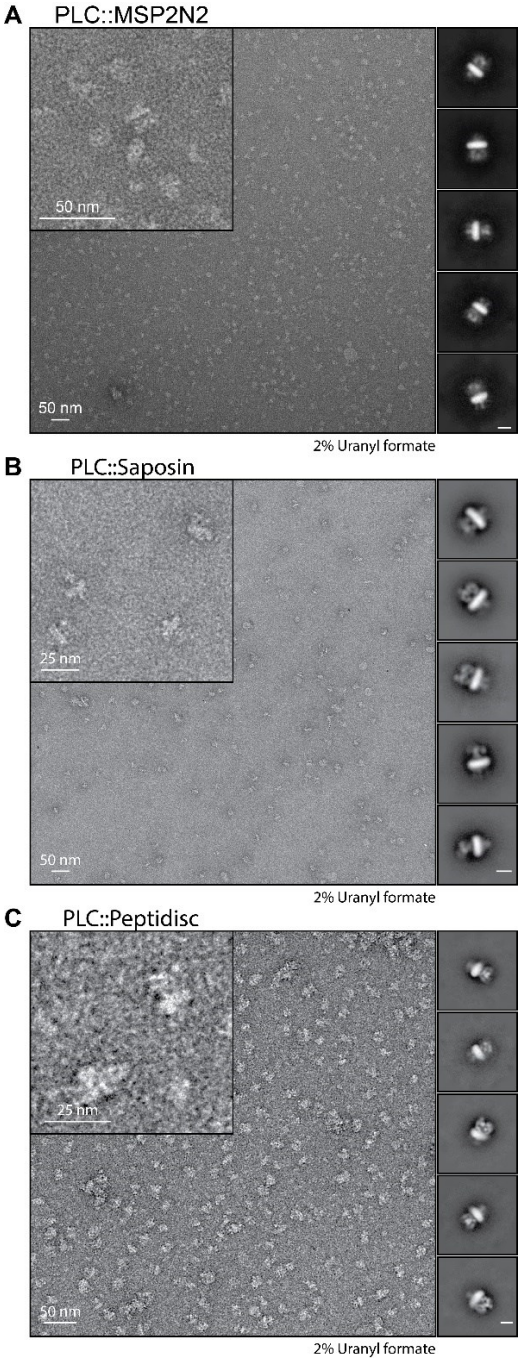

Figure 6.1-3: PLC is intact after reconstitution in membrane mimetics. All samples were spotted on continuous carbon grids and stained with 2% (w/v) uranyl formate solution. The scale bar in the classes corresponds to 10 nm. (**A**) Micrograph of PLC::MSP2N2. A total of 196 micrographs were imaged and processed yielding 94,109 particle picks. 18,600 particles were selected for reclassification (50 classes). Five representative 2D classes are shown on the right side of the micrograph. (**B**) Micrograph of PLC::Saposin. A total of 371 micrographs were imaged and processed yielding 144,162 particle picks. 28,314 particles were selected for reclassification (50 classes). Five representative 2D classes are shown on the right side of the micrograph. (**C**) Micrograph of PLC::Peptidisc. A total of 102 micrographs were imaged and processed yielding 29,150 particle picks. 11,256 particles were selected for reclassification (30 classes). Five representative classes are shown on the right side of the micrograph.

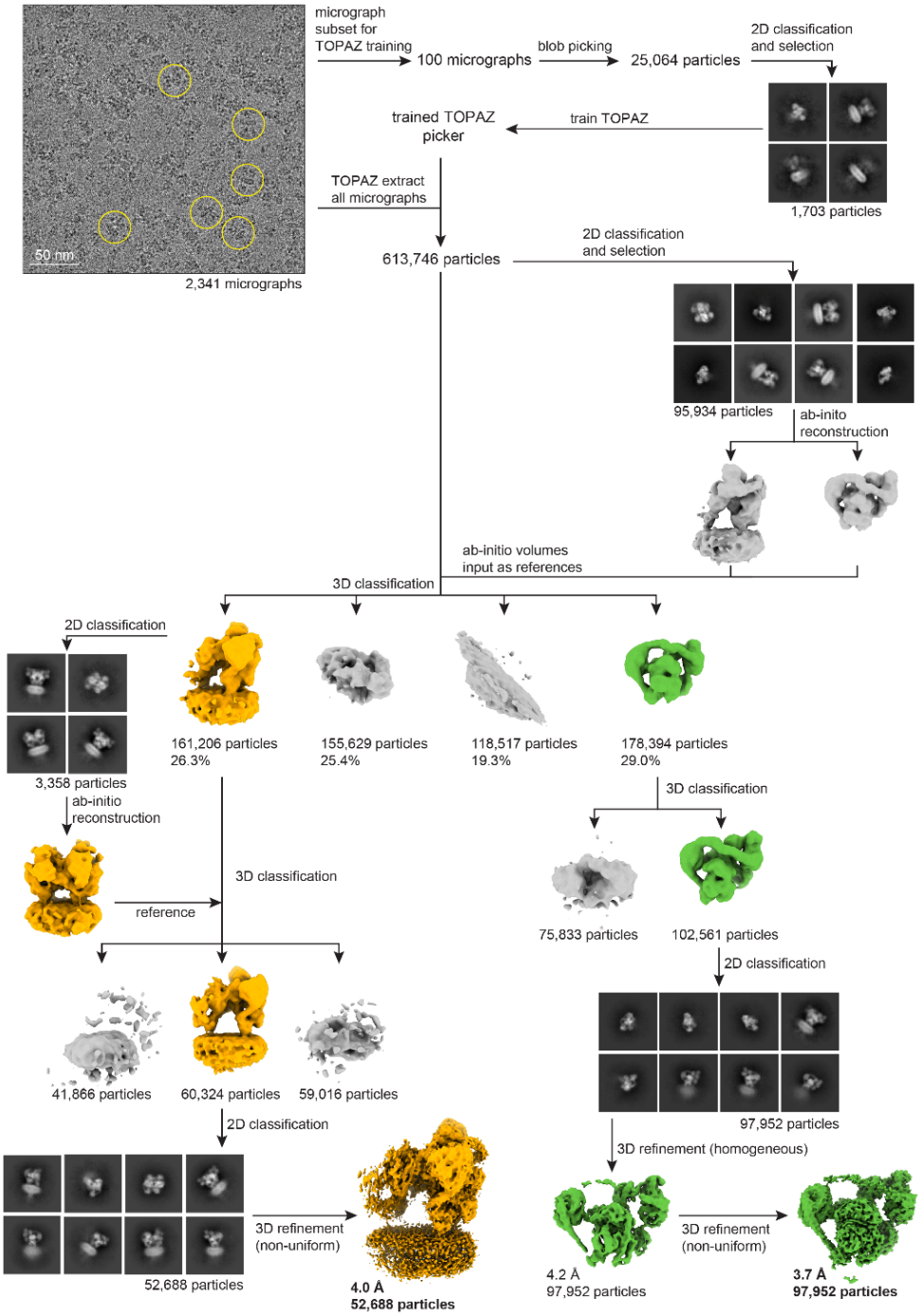

Figure 6.1-4: Cryo-EM data processing workflow. The full set of micrograph movies was corrected for motion and contrast transfer function in cryoSPARC. A subset of 100 micrographs was subjected to blob picking followed by 2D classification to obtain a training dataset of PLC particles for the deep picker TOPAZ. Subsequently, the trained TOPAZ instance was used to particle pick the entire set of micrographs. Initial 2D classification was then performed to select particles for *ab-initio* 3D reconstruction. The resulting *ab-initio* maps were used to classify the full dataset in 3D. 3D assemblies resembling PLC with density for the membrane region (orange, left) and a single editing module (green, right) were further sub-classified in 3D and 2D, and individually refined using homogenous and finally non-uniform refinement. All processing was performed using cryoSPARC.

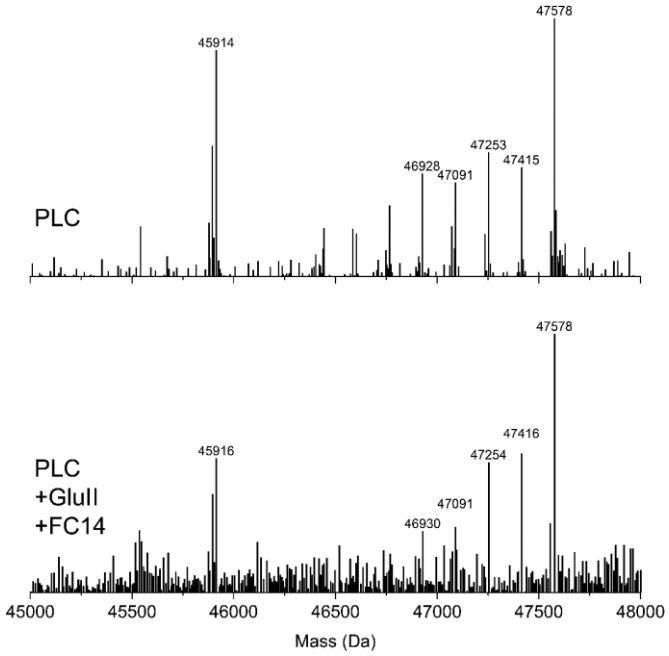

Figure 6.1-5: Tapasin glycan does not carry a glucose. Deconvoluted MS spectra of tapasin (Iso1) in the presence and absence of GluII and FC14. No change is observed upon PLC disintegration by FC14 and GluII treatment indicating that the N-linked glycan of tapasin does not carry a terminal glucose.

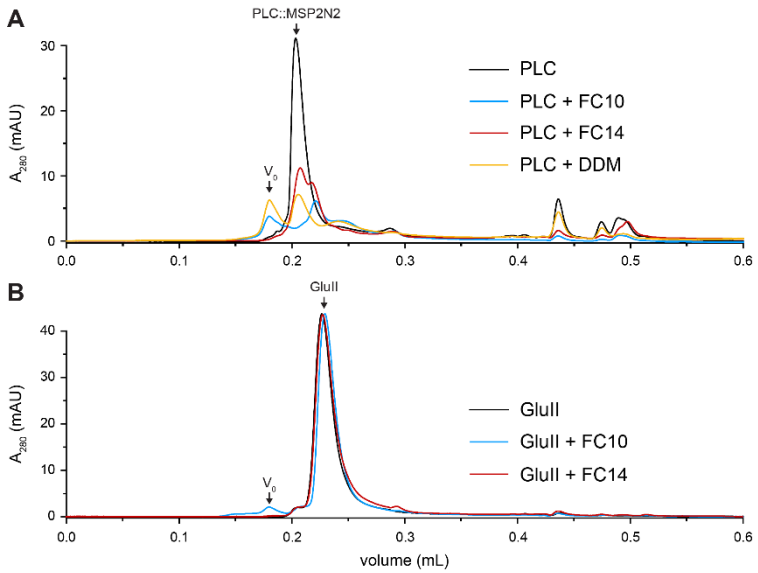

Figure 6.1-6: PLC and GluII detergent stability. **(A)** PLC::MSP2N2 and GluII were subjected to different detergents in size exclusion chromatography to evaluate specific disintegration of the PLC for GluII treatment and to retain GluII functional. For all detergents 2x CMC was used. The PLC disintegrated by the addition of FC10, FC14 and DDM. FC14 disintegrated the PLC to smaller entities while PLC destabilization by FC10 and DDM resulted in aggregates and disintegrated particles. (**B**) GluII integrity was not affected by the addition of either FC10 or FC14. SEC runs were performed by Christian Winter, Goethe University Frankfurt.

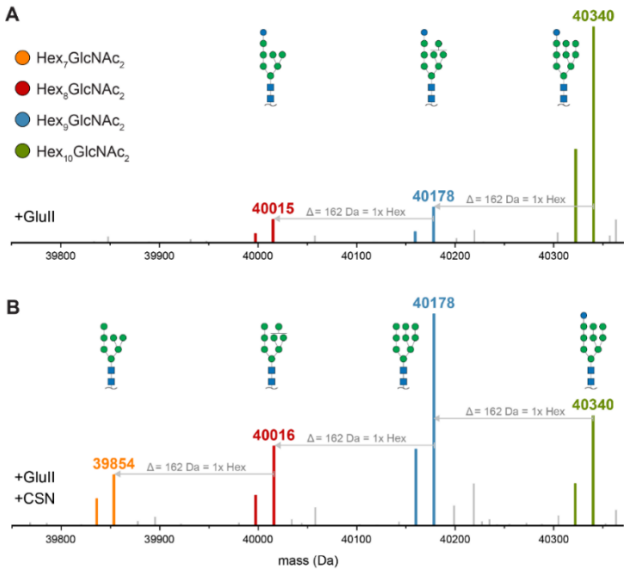

Figure 6.1-7: PLC-associated MHC I carries a terminal glucose in the A-branch. (**A**) Deconvoluted MS spectra of HLA-A*03:01 in the presence of GluII but absence of peptides. The full $Glc_1Man_9GlcNAc_2$ glycan on HLA-A*03:01 is depicted in green. A minor fraction of HLA-A*03:01 species harbor glycans with only nine (blue) or eight hexoses (red). (**B**) In the presence of high-affinity peptides, the pattern is shifted to lower MW and a new species with seven hexoses (orange) appears. The lower intensity mass peaks, lacking 18 Da in comparison to the labeled mass peaks, are a common artifact of rapid thermal decomposition inside the ESI-MS source[244] which appeared to be more pronounced in glycoproteins. LC-MS analysis was performed by Christian Winter, Goethe University Frankfurt.

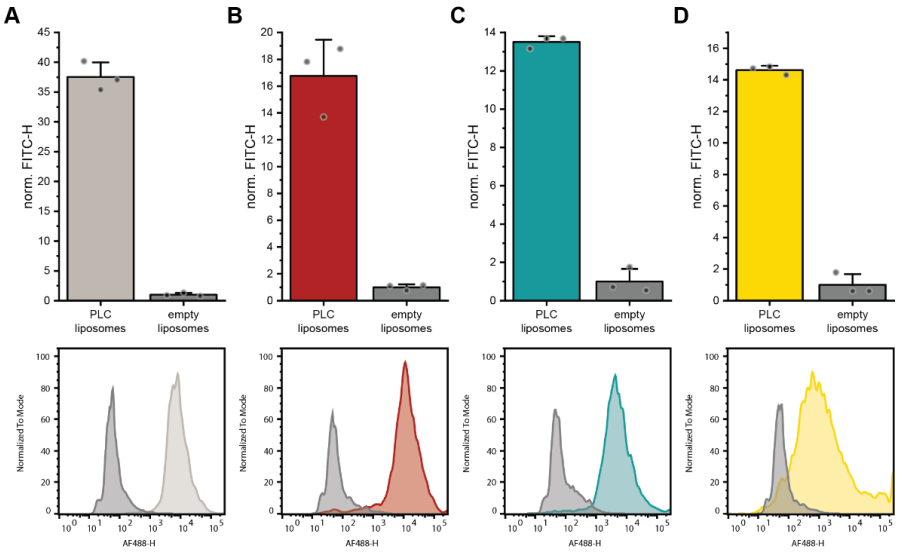

Figure 6.1-8: PLC components in PLC::liposomes. Liposomes and empty liposomes were stained with antibodies and analyzed by flow cytometry: (**A**) TAP1, (**B**) ERp57, (**C**) MHC I, and (**D**) calreticulin. Flow cytometry was performed by Christian Winter, Goethe University Frankfurt am Main

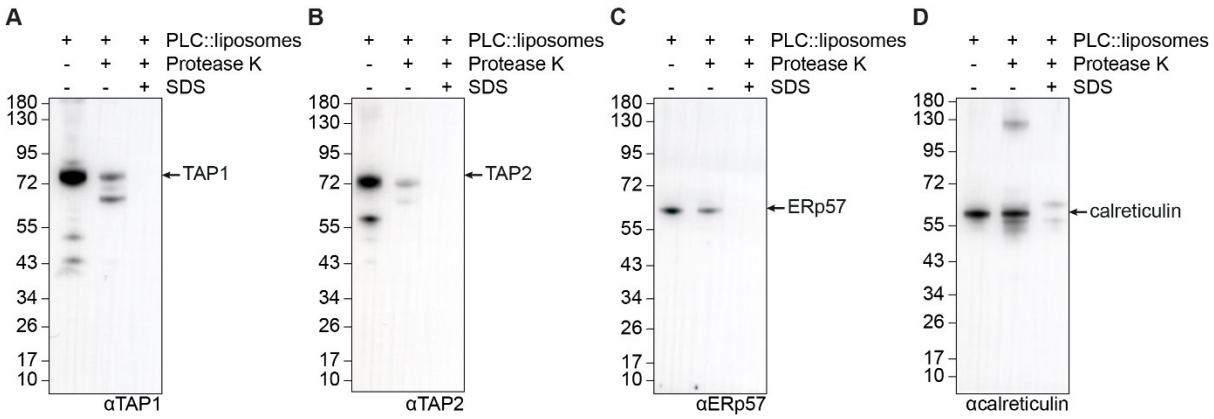

Figure 6.1-9: PLC orientation in liposomes – immunoblot analysis. The orientation of the PLC was analyzed by limited protease K proteolysis, SDS-PAGE and subsequent immunoblotting. The PLC components TAP1 (**A**), TAP2 (**B**), ERp57 (**C**), and calreticulin (**D**) were detected by immunoblotting after protease K treatment of PLC::liposomes. To verify full digestion of all proteins, the liposomes were disrupted with SDS before protease K treatment. Band intensities were quantified using ImageJ and are depicted in Figure 4.7-2. The limited proteolysis assay was performed by Christian Winter, Goethe University Frankfurt.

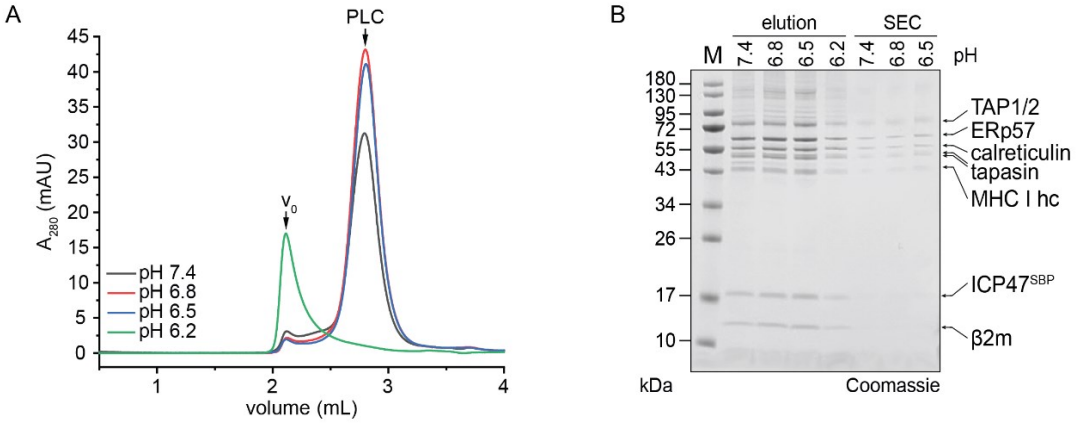

Figure 6.1-10: PLC pH stability evaluation. (**A**) PLC pH stability analyzed by SEC. PLC prepared in different pH conditions. For pH 6.8 and 6.5, elution volume and peak shape did not change in comparison to pH 7.4. At pH 6.2 the PLC aggregates as it eluted close to V_0 of the SEC column. (**B**) PLC preparations at different pH values analyzed by Coomassie stained SDS-PAGE (reducing, 4-12%, Coomassie), directly after preparation (elution) and after SEC purification (SEC). No changes in PLC subunit composition were evident at pH values between 7.4 and 6.5, while the yield was reduced at pH 6.2.

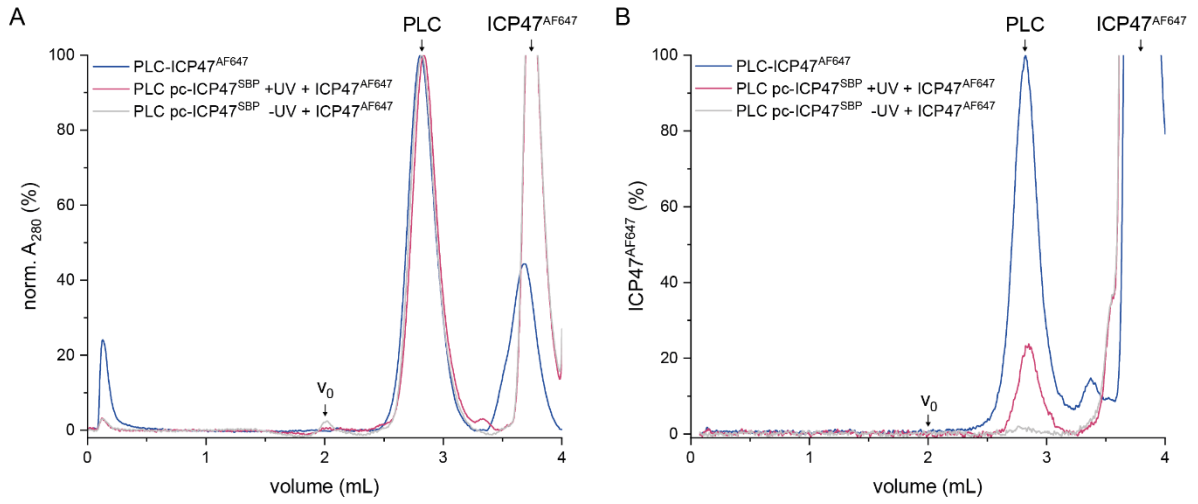

Figure 6.1-11: ICP47^{AF647} rebinding to PLC after pc-ICP47^{SBP} cleavage. (**A**) PLC purified with ICP47^{AF647} (blue) exhibited the same peak shape in SEC as PLC purified with pc-ICP47^{SBP}. ICP47^{AF647} rebinding was analyzed by addition of ICP47^{AF647} to PLC purified with pc-ICP47^{SBP}. To compensate for concentration differences after preparation, PLC peaks were normalized. AF647 fluorescence in (B) was normalized with the same factors. (**B**) $F_{647/670}$ chromatogram of SEC analyses shown in (A). PLC purified with ICP47^{AF647} was used as reference for full ICP47^{AF647} occupancy (blue). PLC purified with pc-ICP47^{SBP} did not show ICP47^{AF647} fluorescence. After UV_{365} illumination a quarter of the PLC was able to bind ICP47^{AF647}.

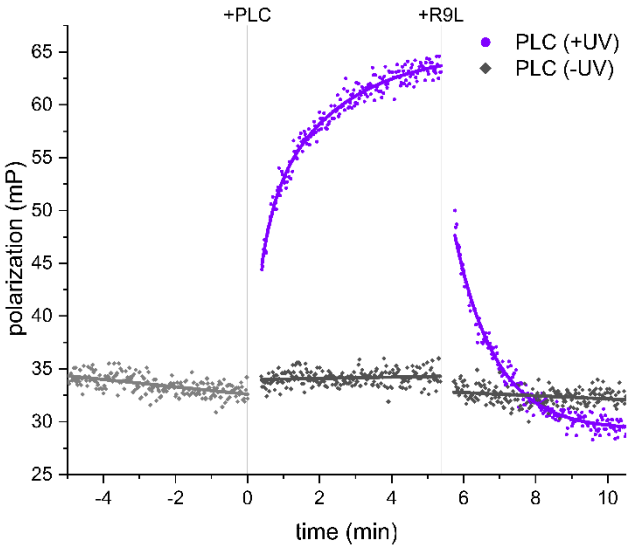

Figure 6.1-12: Binding kinetics of C4F after UV activation of TAP. Peptide binding of the high-affinity TAP binder C4F to the PLC monitored by fluorescence polarization. PLC (150 nM) was either untreated (black) or UV illuminated (purple) and to C4F (50 nM). Specific binding was confirmed by addition of 3000-fold molar excess of competitor peptide (R9L).

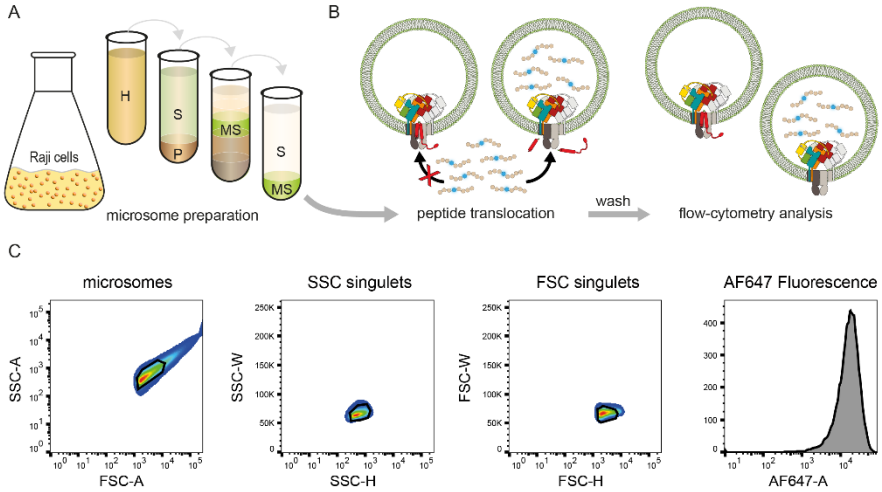

Figure 6.1-13: Microsome preparation and peptide transport after UV_{365} activation. (**A**) PLC-containing microsomes were prepared from Raji cells using differential and sucrose gradient centrifugation. H, homogenate; S, supernatant; P, Pellet; MS, microsomes. (**B**) Fluorescent reporter peptides were transported into the microsomal lumen upon light induced removal of pc-ICP47^{SBP}, leading to peptide accumulation and signal amplification. After peptide transport, microsomes were analyzed by flow cytometry. (**C**) Flow cytometric gating strategy for analysis of microsomes. The microsomes revealed a characteristic population that is best gated with tight gates around the population center. Fluorescence was analyzed after SSC-H/SSC-W and FSC-H/SSC-W doublet discrimination. Flow cytometry results of PLC mediated peptide translocation assay in microsomes depicted in Figure 4.8-4 B.

6.2. Tables

Table 6-1: Similarity of mammalian TAP1 protein sequences. Uniprot reference of the sequence and the species are stated. Similarity 60-70% is colored red,70-90% is colored orange, above 90% is colored green. Sequences were aligned by MUSCLE algorithm implemented in UGENE v.1.31.1

TAP1	Q03518 human	A6QPZ6 cow	W5PCZ7 pig	A5D9J3 sheep	1PTN5 dog	A0A3Q2HTF4 horse	P36370 rat	P21958 mouse
Q03518 human	100%	79%	77%	82%	79%	84%	72%	73%
A6QPZ6 cow	78%	100%	94%	80%	77%	80%	69%	70%
W5PCZ7 pig	77%	94%	100%	79%	77%	79%	69%	70%
A5D9J3 sheep	82%	81%	80%	100%	80%	85%	69%	70%
1PTN5 dog	79%	77%	77%	80%	100%	83%	69%	68%
A0A3Q2HTF4 horse	78%	75%	74%	79%	77%	100%	66%	67%
P36370 rat	72%	69%	69%	69%	69%	71%	100%	89%
P21958 mouse	73%	70%	70%	70%	68%	72%	89%	100%

Table 6-2: Subunits of the PLC identified by LC-MS

Component (reference)	aa sequence (mature protein)	M_{cal} (Da)	M_{obs} (Da)
β_2m (Uniprot: P61769)	IQRTPKIQVY SRHPAENGKS NFLNCYVSGF HPSDIEVDLL KNGERIEKVE HSDLSFSKDW SFYLLYYTEF TPTEKDEYAC RVNHVTLSQP KIVKWDRDM	11,729.01	11,729.44
calreticulin (Uniprot: P27797)	EPAVYFKEQF LDGDGWTSRW IESKHKSDFG KFVLSSGKFY GDEEKDKGLQ TSQDARFYAL SASFEPFSNK GQTLVVQFTV KHEQNIDCGG GYVKLFPNSL DQTDMHGDSE YNIMFGPDIC GPGTKKVHVI FNYKGKNVLI NKDIRCKDDE FTHLYTLIVR PDNTYEVKID NSQVESGSLE DDWDFLPPKK IKDPDASKPE DWDERAKIDD PTDSKPEDWD KPEHIPDPDA KKPEDWDEEM DGEWEPPVIQ NPEYKGEWKP RQIDNPDYKG TWIHPEIDNP EYSPDPSIYA YDNFGVLGLD LWQVKSGTIF DNFLITNDEA YAEEFGNETW GVTKAAEKQM KDKQDEEQRL KEEEEDKKRK EEEEAEDKED DEDKDEDEED EEDKEEDEEE DVPGQAKDEL	46,463.77	46,464.76
ERp57 (Uniprot: P30101)	SDVLELTDDN FESRISDTGS AGLMLVEFFA PWCGHCKRLA PEYEAAATRL KGIVPLAKVD CTANTNTCNK YGVSGYPTLK IFRDGEEAGA YDGPRTADGI VSHLKKQAGP ASVPLRTEEE FKKFISDKDA SIVGFFDDSF SEAHSEFLKA ASNLRDNYRF AHTNVESLVN EYDDNGEGII LFRPSHLTNK FEDKTVAYTE QKMTSGKIKK FIQENIFGIC PHMTEDNKDL IQGKDLLIAY YDVDYEKNAK GSNYWRNRVM MVAKKFLDAG HKLNFAVASR KTFSHELSDF GLESTAGEIP VVAIRTAKGE KFVMQEEFSR DGKALERFLQ DYFDGNLKRY LKSEPIPESN DGPVKVVVAE NFDEIVNNEN KDVLIEFYAP WCGHCKNLEP KYKELGEKLS KDPNIVIAKM DATANDVPSP YEVRGFPTIY FSPANKKLNP KKYEGGRELS DFISYLQREA TNPPVIQEEK PKKKKKAQED L	54,260.53	54,260.27
HLA-A*03:01 (NCBI: NP_002107.3)	GSHSMRYFFT SVSRPGRGEP RFIAVGYVDD TQFVRFDSDA ASQRMEPRAP WIEQEGPEYW DQETRNVKAQ SQTDRVDLGT LRGYYNQSEA GSHTIQIMYG CDVGSDGRFL RGYRQDAYDG KDYIALNEDL RSWTAADMAA QITKRKWEAA HEAEQLRAYL DGTCVEWLRR YLENGKETLQ RTDPPKTHMT HHPISDHEAT LRCWALGFYP AEITLTWQRD GEDQTQDTEL VETRPAGDGT FQKWAAVVVP SGEEQRYTCH VQHEGLPKPL TLRWELSSQP TIPIVGIIAG LVLLGAVITG AVVAAVMWRR KSSDRKGGSY TQAASSDSAQ GSDVSLTACK V	38,312.12	38,313.27

tapasin Iso1 (Uniprot: O15533)	GPAVIECWFV EDASGKGLAK RPGALLLRQG PGEPPPRPDL DPELYLSVHD PAGALQAAFR RYPRGAPAPH CEMSRFVPLP ASAKWASGLT PAQNCPRALD GAWLMVSISS PVLSLSSLLR PQPEPQQEPV LITMATVVLT VLTHTPAPRV RLGQDALLDL SFAYMPPTSE AASSLAPGPP PFGLEWRRQH LGKGHLLLAA TPGLNGQMPA AQEGAVAFAA WDDDEPWGPW TGNGTFWLPR VQPFQEGTYL ATIHLPYLQG QVTLELAVYK PPKVSLMPAT LARAAPGEAP PELLCLVSHF YPSGGLEVEW ELRGGPGGRS QKAEGQRWLS ALRHHSDGSV SLSGHLQPPP VTTEQHGARY ACRIHHPSLP ASGRSAEVTL EVAGLSGPSL EDSVGLFLSA FLLLGLFKAL GWAAVYLSTC KDSKKKAE	45,711.82	45,710.70
TAP2 – Iso1 A665T[1] (NCBI: NP_000535.3)	MRLPDLRPWT SLLLVDAALL WLLQGPLGTL LPQGLPGLWL EGTLRLGGLW GLLKLRGLLG FVGTLLLPLC LATPLTVSLR ALVAGASRAP PARVASAPWS WLLVGYGAAG LSWSLWAVLS PPGAQEKEQD QVNNKVLMWR LLKLSRPDLP LLVAAFFFLV LAVLGETLIP HYSGRVIDIL GGDFDPHAFA SAIFFMCLFS FGSSLSAGCR GGCFTYTMSR INLRIREQLF SSLLRQDLGF FQETKTGELN SRLSSDTTLM SNWLPLNANV LLRSLVKVVG LYGFMLSISP RLTLLSLLHM PFTIAAEKVY NTRHQEVLRE IQDAVARAGQ VVREAVGGLQ TVRSFGAEEH EVCRYKEALE QCRQLYWRRD LERALYLLVR RVLHLGVQML MLSCGLQQMQ DGELTQGSLL SFMIYQESVG SYVQTLVYIY GDMLSNVGAA EKVFSYMDRQ PNLPSPGTLA PTTLQGVVKF QDVSFAYPNR PDRPVLKGLT FTLRPGEVTA LVGPNGSGKS TVAALLQNLY QPTGGQVLLD EKPISQYEHC YLHSQVVSVG QEPVLFSGSV RNNIAYGLQS CEDDKVMAAA QAAHADDFIQ EMEHGIYTDV GEKGSQLAAG QKQRLAIARA LVRDPRVLIL DEATSALDVQ CEQALQDWNS RGDRTVLVIA HRLQTVQRAH QILVLQEGKL QKLAQLQEGQ DLYSRLVQQR LMD	77,724.23	77,727.10
TAP2 – Iso3 (NCBI: NP_ 001276972.1)	MRLPDLRPWT SLLLVDAALL WLLQGPLGTL LPQGLPGLWL EGTLRLGGLW GLLKLRGLLG FVGTLLLPLC LATPLTVSLR ALVAGASRAP PARVASAPWS WLLVGYGAAG LSWSLWAVLS PPGAQEKEQD QVNNKVLMWR LLKLSRPDLP LLVAAFFFLV LAVLGETLIP HYSGRVIDIL GGDFDPHAFA SAIFFMCLFS FGSSLSAGCR GGCFTYTMSR INLRIREQLF SSLLRQDLGF FQETKTGELN SRLSSDTTLM SNWLPLNANV LLRSLVKVVG LYGFMLSISP RLTLLSLLHM PFTIAAEKVY NTRHQEVLRE IQDAVARAGQ VVREAVGGLQ TVRSFGAEEH EVCRYKEALE QCRQLYWRRD LERALYLLVR RVLHLGVQML MLSCGLQQMQ DGELTQGSLL SFMIYQESVG SYVQTLVYIY GDMLSNVGAA EKVFSYMDRQ PNLPSPGTLA PTTLQGVVKF QDVSFAYPNR PDRPVLKGLT FTLRPGEVTA LVGPNGSGKS TVAALLQNLY QPTGGQVLLD EKPISQYEHC YLHSQVVSVG QEPVLFSGSV RNNIAYGLQS CEDDKVMAAA QAAHADDFIQ EMEHGIYTDV GEKGSQLAAG QKQRLAIARA LVRDPRVLIL DEATSALDVQ CEQALQDWNS RGDRTVLVIA HRLQTVQRAH QILVLQEGKL QKLAQL	75,662.95	75,665.80

TAP1 - Iso1 (NCBI: NP_ 000584)	ASSRCPAPRG CRCLPGASLA WLGTVLLLLA DWVLLRTALP RIFSLLVPTA LPLLRVWAVG LSRWAVLWLG ACGVLRATVG SKSENAGAQG WLAALKPLAA ALGLALPGLA LFRELISWGA PGSADSTRLL HWGSHPTAFV VSYAAALPAA ALWHKLGSLW VPGGQGGSGN PVRRLLGCLG SETRRLSLFL VLVVLSSLGE MAIPFFTGRL TDWILQDGSA DTFTRNLTLM SILTIASAVL EFVGDGIYNN TMGHVHSHLQ GEVFGAVLRQ ETEFFQQNQT GNIMSRVTED TSTLSDSLSE NLSLFLWYLV RGLCLLGIML WGSVSLTMVT LITLPLLFLL PKKVGKWYQL LEVQVRESLA KSSQVAIEAL SAMPTVRSFA NEEGEAQKFR EKLQEIKTLN QKEAVAYAVN SWTTSISGML LKVGILYIGG QLVTSGAVSS GNLVTFVLYQ MQFTQAVEVL LSIYPRVQKA VGSSEKIFEY LDRTPRCPPS GLLTPLHLEG LVQFQDVSFA YPNRPDVLVL QGLTFTLRPG EVTALVGPNG SGKSTVAALL QNLYQPTGGQ LLLDGKPLPQ YEHRYLHRQV AAVGQEPQVF GRSLQENIAY GLTQKPTMEE ITAAAVKSGA HSFISGLPQG YDTEVDEAGS QLSGGQRQAV ALARALIRKP CVLILDDATS ALDANSQLQV EQLLYESPER YSRSVLLITQ HLSLVEQADH ILFLEGGAIR EGGTHQQLME KKGCYWAMVQ APADAPE	80,832.50	80,832.60
ICP47^{SBP}	GAMASWALEM ADTFLDNMRV GPRTYADVRD EINKRGREDR	14,953.39	14,953.80
^{GAM}ICP47^{SBP}	EAARTAVHDP ERPLLRSPGL LPEIAPNASL GVAHRRTGGT VTDSPRNPVT RGSGGGSGGG SMDEKTTGWR GGHVVEGLAG ELEQLRARLE HHPQGQREP	14,694.07	14,694.75
MSP2N2	GHHHHHHHDY DIPTTENLYF QGSTFSKLRE QLGPVTQEFW DNLEKETEGL RQEMSKDLEE VKAKVQPYLD DFQKKWQEEM ELYRQKVEPL RAELQEGARQ KLHELQEKLS PLGEEMRDRA RAHVDALRTH LAPYSDELRQ RLAARLEALK ENGGARLAEY HAKATEHLST LSEKAKPALE DLRQGLLPVL ESFKVSFLSA LEEYTKKLNT QGTPVTQEFW DNLEKETEGL RQEMSKDLEE VKAKVQPYLD DFQKKWQEEM ELYRQKVEPL RAELQEGARQ KLHELQEKLS PLGEEMRDRA RAHVDALRTH LAPYSDELRQ RLAARLEALK ENGGARLAEY HAKATEHLST LSEKAKPALE DLRQGLLPVL ESFKVSFLSA LEEYTKKLNT Q	45,540.70	45,541.24

Table 6-3: Tapasin variant identification peptide hitlist.

	start	end	peptide	modifiers	mass (Da)	Δ (ppm)	response
tapasin Iso1	17	20	GLAK		388.254	-3.8	275918
	21	28	RPGALLLR		895.5814	-2.5	3068032
	29	60	QGPGEPPPRP DLDPELYLSV HDPAGALQAA FR		3410.7143	0.4	2765311
	61	64	RYPR		591.3332	-5	306098
	76	84	FVPLPASAK		929.5444	-1.2	6246995
	78	84	PLPASAK		683.4084	-0.4	527864
	98	149	ALDGAWLMVS ISSPVLSLSS LLRPQPEPQQ EPVLITMATV VLTVLTHTPA PR		5559.8815	-27.1	91060
	152	187	LGQDALLDLS FAYMPPTSEA ASSLAPGPPP FGLEWR	Ox M [14]	3817.8932	3.9	207048
	152	187	LGQDALLDLS FAYMPPTSEA ASSLAPGPPP FGLEWR		3801.8983	3.9	212356
	189	193	QHLGK		582.3352	-1.1	368091
	241	273	VQPFQEGTYL ATIHLPYLQG QVTLELAVYK PPK		3742.0351	2.6	184826
	274	283	VSLMPATLAR	Ox M [4]	1074.5974	-0.2	1367736
	274	283	VSLMPATLAR		1058.6022	-0.5	1850788
	314	319	GGPGGR		500.2562	-2.7	770414
	323	327	AEGQR		560.2766	-3.7	60435
	328	333	WLSALR		745.4337	-2.4	4444735
	334	359	HHSDGSVSLS GHLQPPPVTT EQHGAR		2731.3368	2.6	1942260
	364	374	IHHPSLPASG R		1171.6307	-2	3010338
tapasin Iso5	17	20	GLAK		388.2544	-2.6	103783
	21	28	RPGALLLR		895.5817	-2.1	1849609
	29	60	QGPGEPPPRP DLDPELYLSV HDPAGALQAA FR		3410.7244	3.4	1366241
	61	64	RYPR		591.3342	-3.3	112022
	65	75	GAPAPHCEMS R	Ox M [9]	1171.4978	-0.4	54388
	65	75	GAPAPHCEMS R		1155.5028	-0.5	170529
	76	84	FVPLPASAK		929.5448	-0.7	3364544
	98	149	ALDGAWLMVS ISSPVLSLSS LLRPQPEPQQ EPVLITMATV VLTVLTHTPA PR		5559.8861	-26.3	159761
	189	193	QHLGK		582.3361	0.4	124356
	274	283	VSLMPATLAR	Ox M [4]	1074.5988	1.2	651603
	274	283	VSLMPATLAR		1058.6029	0.2	938614
	314	319	GGPGGR		500.2575	-0.1	293087
	328	333	WLSALR		745.4345	-1.4	2487992
	334	359	HHSDGSVSLS GHLQPPPVTT EQHGAR		2731.336	2.4	1533672
	364	374	IHHPSLPASG R		1171.633	0	1702249
	419	439	ALTAILWKPP SSLAQASVVA P		2120.2157	2	1015612

Table 6-4: Cryo-EM data collection, refinement, and validation statistics

	PLC Editing Module **calreticulin-tapasin-ERp57-MHC I hc-β_2m** (EMDB-14119) (PDB: 7QPD)
Data collection and processing	
Microscope	TITAN-Krios
Camera	Gatan K2 Summit
Magnification	130,000
Voltage (kV)	300
Electron exposure (e–/Å^2)	68
Defocus range (μm)	-1.0 to -2.5
Pixel size (Å)	1.05
Symmetry imposed	C1
Initial particle images (no.)	613,746
Final particle images (no.)	97,952
Map resolution (Å)	3.73
FSC threshold	0.143
Refinement	
Map sharpening *B* factor (Å^2)	-81.1
Model composition	
Non-hydrogen atoms	11,521
Protein residues	1544
Carbohydrate	10
B factors (Å^2)	
Protein	63.89
Carbohydrate	87.35
R.m.s. deviations	
Bond lengths (Å)	0.0047
Bond angles (°)	0.78
Validation	
MolProbity score	1.85
Clashscore	9.50
Poor rotamers (%)	0.09
Carbohydrates[1]	
Stereochemical problems	0
Unphysical puckering amplitude	0
In unlikely ring conformation	0
Ramachandran plot	
Favored (%)	95.01
Allowed (%)	4.92
Disallowed (%)	0.07

[1]As reported by the Privateer software package

Table 6-5: Sequence alignments of different HLA-A allomorphs. Primary sequence of HLA-A allomorphs region adjacent to Asn127 (bold). Tapasin Arg187 interacts with HLA-A*03:01 Asn127 (Figure 4.4-6 C). Asn127 is not conserved between tapasin dependent (HLA-A*03:01, *01:01, *02:01, *80:01) and tapasin independent HLA-A allomorphs (HLA-A*02:01, *02:02, *02:05, *68:01)[ref. 245].

aa Pos.	110	120	130	140	150
A*03:01:01:01	CDVGSDGRFL	RGYRQDAYDG	KDYIAL**N**EDL	RSWTAADMAA	QITKRKWEAA
A*01:01:01:01	----P-----	----------	-------**-**---	----------	---------V
A*01:02:01:01	----P-----	----------	-------**-**---	----------	---------V
A*02:01:01:01	------W---	---H-Y----	------**K**---	----------	-T--H-----
A*02:02:01:01	------W---	---H-Y----	------**K**---	----------	-T--H-----
A*02:05:01:01	------W---	---H-Y----	------**K**---	----------	-T--H-----
A*68:01:01:01	----------	----------	------**K**---	----------	-T--H-----
A*80:01:01:01	----------	----------	-------**-**---	----------	----------

V. Abbreviations

Abbreviation	Full name
*ICP47^{SBP}	long fragment of pc-ICP47^{SBP} after photocleavage
2D	two dimensional
3D	three dimensional
aa	amino acid(s)
Å	Ångström
ABC transporter	ATP-binding cassette transporter
ADP	adenosine diphosphate
AF647	Alexa Fluor 647
AMPPNP	adenylyl-imidodiphosphate
Anp	3-amino-3-(2-nitrophenyl)-propanoic acid
APS	ammonium persulfate
ATP	adenosine triphosphate
BiP	immunoglobulin binding protein
β_2m	β-2-microglobulin
CCD	charge-coupled device
CD8$^+$	cluster of differentiation 8 positive
CMV	cytomegalovirus
Cryo-EM	cryogenic electron microscopy
CTF	contrast transfer function
Da	Dalton
DIAD	diisopropyl azodicarboxylate
DIBMA	diisobutylene maleic acid copolymers
DIBMALPs	DIBMA lipid particles
DIC	N,N-diisopropylcarbodiimide
DiD	1,1'-dioctadecyl-3,3,3',3'-tetramethylindodicarbocyanine
DMF	dimethylformamide
DNA	deoxyribonucleic acid
DNAse	deoxyribonuklease
DOPC	1,2-dioleoyl-sn-glycero-3-phosphocholine
DRiPs	defective ribosomal products
DTT	dithiothreitol
EBV	Epstein-Barr virus
EDT	1,2-ethanethiol
EDTA	ethylenediaminetetraacetic acid
EM	electron microscopy
eq	molar equivalents
ER	endoplasmic reticulum

ERAD	ER-associated protein degradation
ERAP1	ER aminopeptidase 1
ERAP2	ER aminopeptidase 2
ERmanI	ER-α1,2-mannosidase I
ERp57	ER protein 57
ERQC	ER glycoprotein quality control
FA	formic acid
FC14	Fos-Choline-14
Fmoc	fluorenylmethoxycarbonyl
GDN	glyco-diosgenin
Glc	glucose
GlcNAc	N-acetylglucosamine
GluII	α-1,2-glucosidase II
GraFix	gradient fixation
GRP78	78-kDa glucose regulated protein
H2-D^{b}	mouse MHC I homolog allele H2-D^{b}
hc	MHC I heavy chain
HCMV	human cytomegalovirus
HFIP	hexafluoroisopropanol
HIV	human immune deficiency virus
HLA	human leucocyte antigen
Hmp	2-hydroxy-3-mercaptopropionic acid
HOBt	hydroxybenzotriazole
HPLC	high pressure liquid chromatography
HSV	Herpes simplex virus
Hz	Hertz
IC_{50}	inhibitory concentration 50%
ICP47	infected cell protein 47
ICP47^{AF647}	ICP47 derivate equipped with an AF647 fluorophore
ICP47^{SBP}	ICP47 derivate equipped with an SBP-tag
Ig	immunoglobulin
IMAC	immobilized metal affinity chromatography
IPTG	isopropyl-β-D-thiogalactoside
Iso1	tapasin isoform 1
Iso5	tapasin isoform 5
K_d	dissociation constant
kDa	kilo Dalton
kV	kilo volt
LC-MS	liquid chromatography coupled mass spectrometry
m	meter

Man	mannose
M_{cal}	mass calculated
MES	2-(*N*-morpholino)ethanesulfonic acid
MHC I	Major Histocompatibility Complex Class I
min	minute
mM	millimolar
M_{obs}	mass observed
MPAA	4-mercaptophenyl-acetic acid
mRNA	messenger RNA
MS	mass spectrometry
MSP	membrane scaffold protein
MSP2N2	membrane scaffold protein variant 2N2
MWCO	molecular weight cutoff
NBD	nucleotide binding domain
Ni-NTA	Nickel-loaded nitrilotriacetic acid
n.d.	not determined
NMR	nuclear magnetic resonance
OD_{600}	optical density at 600 nm wavelength
OST	oligosaccharyltransferase
pc-ICP47^{SBP}	photocleavable ICP47^{SBP} derivate
PDB	protein database
PDI	protease disulfate isomerases
PLC	MHC I peptide loading complex
PLC::liposomes	liposome-reconstituted PLC
PLC::MSP2N2	MSP2N2-reconstituted PLC
PLC::Peptidisc	Peptidisc-reconstituted PLC
PLC::Saposin	Saposin A-reconstituted PLC
pMHC I	Peptide-loaded major histocompatibility complex I
PMSF	phenylmethylsulfonyl fluoride
PNGase	Peptide:N-glycosidase F
px	pixel
RMSD	root mean square deviation
RNA	ribonucleic acid
RP-HPLC	reverse phase HPLC
RT	room temperature
s	second
SBP	streptavidin-binding peptide
SDS	sodium dodecyl sulfate
SDS-PAGE	sodium dodecyl sulfate polyacrylamide gel electrophoresis
SEC	size exclusion chromatography

SEM	standard error of the mean
SMA	styrene-maleic-acid copolymers
SMALPs	SMA lipid particles
SPA	single particle analysis
SCPA	scintillation proximity assay
SPPS	solid phase peptide synthesis
TAP	transporter associated with antigen processing
TAPBPR	TAP-binding protein related
tBuSH	2-methylpropane-2-thiol
TCEP	tris(2-carboxyethyl)phosphine
TEMED	tetramethylethylenediamine
TEV	tobacco etch virus
TFA	trifluoroacetic acid
TIPS	triisopropylsilane
T_m	melting temperature
TMD0	transmembrane domains 0 of TAP
TmrAB	*Thermus thermophilus* multidrug resistance transporter A and B
TOF-MS	Time-of-flight mass spectrometry
UGGT1	UDP-glucose:glycoprotein glucosyltransferase 1
US6	unique short sequence six, viral TAP inhibitor. Origin CMV
UV	ultraviolet light
v/v	volume per volume
VA-044	2,2'-azobis-[2-(2-imidazolin-2-yl)propane] dihydro-chloride
w/v	weight per volume

VI. List of figures

Figure 1.1-1: MHC I loading and quality control. 17
Figure 1.1-2: Schematic overview of N-linked glycan processing in the ER and Golgi. 18
Figure 1.2-1: Schematic depiction of the PLC 19
Figure 1.2-2: Structure of the tapasin and ERp57 heterodimer in the PLC 21
Figure 1.2-3: Structure of the peptide loaded MHC I dimer 22
Figure 1.2-4: MHC I peptide binding groove and editing by tapasin/TAPBPR 23
Figure 1.2-5: Structure and interactions of calreticulin in the PLC 24
Figure 1.2-6: Viral immune evasins 27
Figure 1.3-1: Sample preparation for single particle cryo-EM. 28
Figure 1.4-1: Membrane mimetic systems 30
Figure 1.4-2: Reconstitution of membrane proteins in liposomes 31
Figure 4.1-1: PLC purified from mammalian tissue 53
Figure 4.1-2: Negative stain analysis of PLC from cow and sheep spleen 57
Figure 4.2-1: PLC cannot be purified using SMA 2:1 and DIBMA. 58
Figure 4.2-2: SMA solubilized the human PLC but purification was not possible 59
Figure 4.2-3: Impure purification of human PLC by ICP47^{His8} 60
Figure 4.2-4: PLC reconstituted in large lipid nanodiscs is intact and binds ATP 61
Figure 4.2-5: PLC stabilized in MSP2N2 nanodiscs 62
Figure 4.2-6: PLC reconstituted in Saposin A and Peptidisc 63
Figure 4.3-1: PLC subunits analyzed by LC-MS 65
Figure 4.3-2: Identification of PLC subunits by intact protein LC-MS 66
Figure 4.3-3: Glycosylation of MHC I heavy chain 67
Figure 4.3-4: Complex glycosylation pattern of tapasin in the PLC 68
Figure 4.3-5: The PLC from Raji cells incorporates different splice variants of tapasin 70
Figure 4.4-1: PLC is intact after reconstitution in membrane mimetics 71
Figure 4.4-2: Cryo-EM analysis of PLC reconstituted in lipid nanodiscs. 73
Figure 4.4-3: Cryo-EM analysis of the PLC editing module. 73
Figure 4.4-4: CryoDRGN analysis of different PLC assembly states. 74
Figure 4.4-5: Structure of the PLC editing module. 75
Figure 4.4-6: MHC I interactions in the PLC 76
Figure 4.4-7: Editing loop comparison between tapasin and TAPBPR 77
Figure 4.5-1: Peptide binding and editing of PLC chaperoned MHC I 79
Figure 4.5-2: Peptide editing is coupled to MHC I glycan processing by GluII 80
Figure 4.5-3: PLC remains fully assembled during peptide loading and deglucosylation 81
Figure 4.5-4: Mechanism of MHC I assembly, peptide editing, and quality control 82
Figure 4.6-1: DG057 is active as ERAP1/2 inhibitor 84
Figure 4.6-2: ERAP1 and ERAP2 do not interact with immobilized PLC 85
Figure 4.6-3: ERAP1 and ERAP2 do not interact kinetically stable with PLC 86

Figure 4.7-1: PLC reconstituted in liposomes 87
Figure 4.7-2: PLC orientation in liposomes 88
Figure 4.7-3: Peptide binding and editing of PLC chaperoned MHC I in liposomes 89
Figure 4.7-4: Peptide-dependent dissociation of MHC I from the PLC 90
Figure 4.8-1: Photocleavable ICP47^{SBP} 91
Figure 4.8-2: PLC purification by pc-ICP47 and PLC reactivation 92
Figure 4.8-3: Photoactivation of PLC purified by pc-ICP47^{SBP} 93
Figure 4.8-4: Peptide transport restored after pc-ICP47^{SBP} photocleavage 94
Figure 6.1-1: PLC purified from ovine and bovine spleen, but not from porcine 112
Figure 6.1-2: PLC stabilized by reconstitution in MSP2N2 nanodiscs 112
Figure 6.1-3: PLC is intact after reconstitution in membrane mimetics 113
Figure 6.1-4: Cryo-EM data processing workflow 114
Figure 6.1-5: Tapasin glycan does not carry a glucose 115
Figure 6.1-6: PLC and GluII detergent stability 115
Figure 6.1-7: PLC-associated MHC I carries a terminal glucose in the A-branch 116
Figure 6.1-8: PLC components in PLC::liposomes 116
Figure 6.1-9: PLC orientation in liposomes – immunoblot analysis 117
Figure 6.1-10: PLC pH stability evaluation 117
Figure 6.1-11: ICP47^{AF647} rebinding to PLC after pc-ICP47^{SBP} cleavage 118
Figure 6.1-12: Binding kinetics of C4F after UV activation of TAP 118
Figure 6.1-13: Microsome preparation and peptide transport after UV_{365} activation 119

VII. List of tables

Table 1: Antibodies used in this study 33
Table 2: Peptides used in this study 35
Table 3: Protein identification of ovine PLC by MS 54
Table 4: Protein identification of bovine PLC by MS 55
Table 6-1: Similarity of mammalian TAP1 protein sequences 120
Table 6-2: Subunits of the PLC identified by LC-MS 121
Table 6-3: Tapasin variant identification peptide hitlist. 124
Table 6-4: Cryo-EM data collection, refinement, and validation statistics 125
Table 6-5: Sequence alignments of different HLA-A allomorphs 126